EFFECT OF REFLOW TIME ON WETTING KINETICS, MICROSTRUCTURE AND JOINT STRENGTH OF Sn-Cu AND Sn-Ag-Cu SOLDERS

Thesis

Submitted in partial fulfillment of the requirements for the degree of

DOCTOR OF PHILOSOPHY

by

MRUNALI SONA

DEPARTMENT OF METALLURGICAL AND MATERIALS ENGINEERING

NATIONAL INSTITUTE OF TECHNOLOGY KARNATAKA,
SURATHKAL, MANGALURU – 575025

FEBRUARY, 2017

DECLARATION

by the

Ph. D. RESEARCH SCHOLAR

I hereby *declare* that the Research Thesis entitled **"Effect of reflow time on wetting kinetics, microstructure and joint strength of Sn-Cu and Sn-Ag-Cu solders"** which is being submitted to the **National Institute of Technology Karnataka, Surathkal** in partial fulfillment of the requirements for the award of the Degree of **Doctor of Philosophy** in Metallurgical and Materials Engineering is a *bonafide report of the research work carried out by me*. The material contained in this Research Thesis has not been submitted to any University or Institution for the award of any degree.

MRUNALI SONA

Register No. **121192MT12F06**
Department of Metallurgical and Materials Engineering

Place: NITK Surathkal, Srinivasnagar

Date:

CERTIFICATE

This is to *certify* that the Research Thesis entitled **“Effect of reflow time on wetting kinetics, microstructure and joint strength of Sn-Cu and Sn-Ag-Cu solders”** submitted by **MRUNALI SONA** (Register Number: **121192MT12F06**) as the record of the research work carried out by her, is *accepted as the Research Thesis* submission in partial fulfillment of the requirements for the award of degree of **Doctor of Philosophy**.

Research Guide
Dr. K. Narayan Prabhu
Professor
Dept. of Metallurgical and Materials Engineering
NITK, Surathkal

Chairman-DRPC
(Signature with Date and Seal)

ACKNOWLEDGEMENT

I would like to express my sincere and deep sense of gratitude to my research guide, Prof. K. Narayan Prabhu for his constant help, guidance and support throughout the research work. I am deeply indebted to him for his infinite patience, unfaltering encouragement and cheerfulness that kept me on track and helped me to finish this thesis. I also thank him for providing me excellent experimental facilities during the project work.

I profusely thank my RPAC members Dr. Mervin Herbert, Department of Mechanical Engineering and Dr. Kasturi V Bangera, Department of Physics for their insightful comments and valuable suggestions during the research work.

I am grateful to Dr. Uday Bhat, Associate Professor and the Head, Department of Metallurgical and Materials for allowing me use the XRD facility. I also express my gratitude to Prof. K. Rajendra Udupa, Department of Metallurgical and Materials Engineering, NITK, Surathkal for allowing me to use the scanning electron microscope.

I am grateful to Defence Research and Development Organization (DRDO), Govt. of India, for awarding me the Senior Research Fellowship during 5-01-2012 to 15-12-2014.

Heartfelt gratitude to Dr. Jagannath Nayak, former HOD and Faculty of the Department of Metallurgical and Materials Engineering, NITK-Surathkal for their timely support.

I am also deeply grateful for the companionship of the fellow researchers in the Casting Research Center, Department of Metallurgical and Materials Engineering, NITK. I am very much thankful to Dr. Satyanaryan, for his kind help during experimental analysis in the initial stages of the work. I sincerely thank Mr. Kiran Bhat, for training me and providing very fine technical details at an early stage of the research. Many thanks to Mr. Sanjay, for the time spent together during the experiments and for the infinite ways he helped me. I would like to thank my seniors Dr. Ramesh and Dr. Vijeesh for their help and suggestions. I extend my thanks Mr. Vignesh Nayak, Mr. Sudheer, and Mr. Pranesh for their timely help and cooperation.

My heartfelt thanks to lab technicians Mr. Satish, Mr. Dinesh, Mr. Yashwanth, Mr. Sundar Shettigara for helping me during sample preparation. I am also obliged to Mr. Vasant, Mrs. Sharmila, Mrs. Vinaya, and Mr. Giriyappa, all technical and non-technical staff of the Department of Metallurgical and Materials Engineering for their whole hearted help during the course of my work. Special thanks to Ms. Rashmi Banjan in connection with usage of scanning electron microscope.

I wish to thank Mr.Amarnadh, Mr. Srinivasa and Mr. Abu Bakar Siddique, M. Tech students for their support and cooperation during the research work.

I also thank my friends Mr. Vignesh, Mrs. Rashmi, Mr. Karthik, research scholars, Dept. of Mechanical Engineering, NITK and Dr. Shobha for their encouragement and support during my stay in the Institute.

I sincerely acknowledge the support extended to me by my parents and brother. They have been a constant source of love, concern and strength all these years.

Finally, I thank all those who directly / indirectly helped me to complete the research work successfully.

MRUNALI SONA

ABSTRACT

In the present study, the effect of reflow time on wetting behaviour, microstructure and shear strength of the Sn–0.7Cu, Sn-0.3Ag-0.7Cu and Sn-2.5Ag-0.5Cu lead-free solders on bare and nickel coated copper substrates was investigated. The solder alloys were reflowed at 270 °C for various reflow times of 10-10000 s. Furnace and quench cooling methods were adopted to assess the effect of varying cooling environment on solder/substrate systems. Final contact angle (θ_f) decreased with increase in reflow time. The spreading behaviour of the solder was categorized into capillary, gravity (diffusion), and viscous zones. Intermetallic compound (IMC) thickness initially increased with increase in reflow time up to 500 s in all solder/substrate systems. Furnace cooled solder/Cu substrate systems showed a drop in IMC thickness for the reflow time above 500 s due to spalling effect. IMC thickness increased with further increase in reflow time above 1000 s. Similarly, Sn-0.3Ag-07Cu and Sn-2.5Ag-0.5Cu solder alloys reflowed for 500 s on Ni coated Cu substrates showed a drop in IMC thickness. IMC thickness was fitted to a growth model to study the growth kinetics. The period corresponding to the end of gravity zone (T_{gz}) was measured from the relaxation curve obtained from wetting studies. T_{gz} was found to be 25 s for Sn–0.7Cu and 40 s for Sn-0.3Ag-0.7Cu and Sn-2.5Ag-0.5Cu solder alloy spreading on bare Cu substrate. The corresponding values were 50, 70 and 80 s respectively for the same alloys on Ni coated Cu substrate. Solder alloys were once again reflowed for the period corresponding to the end of gravity zone. Ball and single lap shear tests were performed to assess the joint strength as a function of reflow time. The joint strengths were found to be maximum at reflow times corresponding to the end of gravity regime for all solder/substrate systems.

Ball and single lap shear tests were also carried out for eutectic Sn-Pb solder alloy on bare and Ni coated Cu substrate to compare the results obtained with those of lead free alloys. Joint and yield strengths of all lead based samples were also found to be maximum at T_{gz}. Ball shear strength of Sn-Pb was found to be lower than lead free alloys. Yield strength of Sn-Pb solidified on bare Cu plate was comparable with Sn-0.7Cu solidified on Ni coated Cu plate. A dynamic contact angle at the end of gravity zone (θ_{gz}) was found to be a better wetting parameter compared to the final contact angle (θ_f) and the time to reach this value was used to assess the effect of wettability of liquid solder on microstructure and joint strength. The present investigation revealed the significance of gravity zone in the assessment of optimum reflow time for lead free solder alloys.

Keywords: Contact angle, wettability, IMC, joint shear strength

CONTENTS

LIST OF FIGURES

LIST OF TABLES

NOMENCLATURE

Symbols

T	Temperature (°C)
D	Base diameter (mm)
R_a	Average surface roughness (μm)
T_{gz}	Time corresponding to the end of gravity regime (s)
γ_{gs}	Interfacial energy between the solid surface and gas (J)
γ_{ls}	Interfacial energy between the solid and the liquid (J)
γ_{gl}	Interfacial energy between the gas and liquid (J)
θ_f	Final contact angle (°)
θ_{gz}	Contact angle corresponding to the end of gravity zone (°)

CHAPTER 1.

INTRODUCTION

In advanced designs, solder is an electrical inter-connect, a mechanical bond, and often serves as a thermal conduit to remove heat from joined devices. Soldering is a low temperature joining technique, carried out at temperatures below 400 °C. Solder alloy melts at a temperature well below the metals to be joined. Solder is an important part of electronic packaging and helps to achieve a durable and reliable electronic connection. Sn–Pb solders have been the traditional materials for the assembly of electronic devices. They still constitute to be the most prominent material for this purpose. The widespread use of lead-tin solders is mainly due to a combined merit of low cost, good soldering properties, adequate melting temperature range, good wettability and proper physical, mechanical, metallurgical, and fatigue resistance properties. However, lead (Pb) and Pb bearing compounds have been cited by the Environmental Protection Agency (EPA) as one of the top 17 toxic chemicals hazardous to human life and the environment [McCormack and Jin 1994]. Nowadays most of the electronic gadgets are proliferating and becoming obsolete at breathtaking speed. The obsolete electronic equipment's enter landfill. The main environmental issue is lead leaching into drinking water or watersheds due to improper disposal of electronic devices. Several European countries, U.S., and Japan have banned the use of Pb from electronic solders for sustaining green environment. A drop-in substitute for Pb should emulate various desirable properties in terms of melting temperature, electrical and thermal conductivity, wettability, thermal expansion coefficient, mechanical strength, ductility, thermal fatigue resistance, creep resistance, manufacturability, workability, joint reliability and cost. Potential lead-free solders developed so far are mostly Sn-based with different additives, such as Ag, Cu, Bi, In, Sb, Au, and Ni. Among them, the binary Sn-Cu and ternary Sn-Ag-Cu (SAC) alloys are considered to be attractive and reliable Pb-free solder alloys, due to their good mechanical and acceptable wetting properties when compared to Sn-Pb solder alloys [Wu et al. 2004, Sharma et al. 2016].

The reliability of solder joint is crucial in electronic industry. Solder joint reliability is the ability of joint to sustain its stability during its course of operation. Therefore, it can be practically assessed by the combination of service environment and system design. The service environment includes the temperature extremes that the product must withstand, possible mechanical and vibrational shocks the product may undergo and the frequency of power on/off cycling. Further from system design side, physical properties of the component and substrate, geometry of solder joint, the nature of intermetallic compound (IMC) formed and their structure, and mechanical properties of bulk solder alloy exert a significant effect on solder joint reliability. The formation of a strong and reliable solder joint is based on the ability of the liquid solder to uniformly and rapidly wet the substrate surface finish and interact with it to form a consistent intermetallic layer at the interface [Sona and Prabhu 2013]. It is well established that wetting plays a major role in the formation of a metallurgical bond at the solder/substrate interface and describes the degree of intimate contact between a liquid and a solid [Satyanarayan and Prabhu 2011]. The extent of wetting is measured by the contact angle formed at the the triple point between the three phases namely solid, liquid and vapor, and the substrate surface [Silva et al. 2015]. The rate of wetting specifies how fast the liquid wets the surface and spreads over the same. Thermal conditions of the system, viscosity of the liquid and chemical reactions occurring at the interface are the major factors which affect the spreading of liquid solder on the solid substrate [Satyanarayan and Prabhu 2011]. Chemical reaction at the interface results in the formation of intermetallic compounds. The intermetallic layer is a critical part of a solder joint because it facilitates bonding between the solder and the substrate. At low levels, they have a strengthening effect on the joint; but at higher levels, they tend to make the solder joints more brittle [Minna Arra et al. 2002]. Hence, the formation and growth of the IMC layer and the microstructure of the bulk solder are considered to have a paramount impact on the solder joint reliability as it reflects the strength of solder joints [Park et al. 2012].

A knowledge of the solder/conductor metal interactions and phase evolution in the solder interconnections is therefore important for the understanding of the reliability of the solder interconnections from the metallurgical viewpoint and for the optimization of the soldering process.

1.1 CONTENTS OF THE THESIS

A detailed review of the available literature on soldering, lead free solders, wetting behaviour of lead free solders, factors affecting the strength of solder joints, scope and objectives are presented in Chapter 2. The experimental set-up and methodology, materials used are given in Chapter 3. The results of the experiments carried out are presented in Chapter 4. A detailed interpretation of the experimental results, analysis and related discussion are presented in Chapter 5. The conclusions drawn based on the results and discussion are enlisted in Chapter 6.

CHAPTER 2

LITERATURE REVIEW

2.1 SOLDERING

Soldering is a process of making a sound electrical, thermal and mechanical joint between certain metals by joining them using fusible filler called solder. During soldering, adequate heat is applied to the parts to be joined to melt the solder and the molten solder gets drawn into the joint by capillary action. The actual joining is achieved by wetting action. Soldering has been the key assembly and interconnection technology for electronic products since the dawn of the electronic age, and will remain so in the foreseeable future. Solder joints have long been recognized as the weak links in electronic products. The performance and quality of the solder are crucial to the integrity of a solder joint, and the reliability of each individual joint can control the overall lifespan of an electronic product [Abtew and Selvaduray 2000, Ho et al. 2006]

2.2 CONVENTIONAL SOLDERS

Sn–Pb solders are the conventional materials used in the electronic devices. This alloy family consists of three basic compositions that have melting points in the 180 °C (355°F) region:

- 63Sn/37Pb: the eutectic composition with a melting point of 183°C (361°F). The term “eutectic” indicates that the composition produces an alloy with a distinct melting point, versus a melting range.
- 60Sn/40Pb: a variation from the eutectic, with a melting range of 183 to 188°C (361 to 370°F)

- 62Sn/36Pb/2Ag: a composition that is often chosen for silver metallization, with a melting point of 179°C (354°F) [Bastow 2003].

Pb in solders gives outstanding properties to the overall reliability of the Sn–Pb solder. It reduces the surface tension of pure tin and improves the wettability of solder alloy, Pb promotes the reaction between tin and substrate material and allows the rapid formation of inter metallic compounds (IMC), improves ductility of the alloy, and prevents the transformation of β-tin (white tin) to α-tin (gray tin). If the transformation occurs, it will cause dramatic volume increase (about 26 %) and loss of structural integrity and hence loss of reliability. Low melting temperature of eutectic Sn–Pb (183 °C) solder, allows the use of a low reflow temperature in the electronic packaging process and ensures the reliability of the packages. Fig. 2.1 shows the phase diagram of Sn-Pb system. As Pb is abundantly available in nature, it is economical to use in soldering alloys [Abtew and Selvaduray 2000, Ma and Suhling 2009, Kumar et al. 2010].

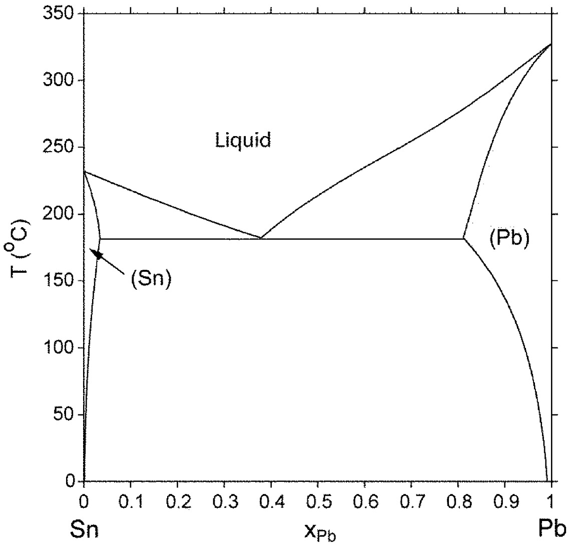

Fig. 2.1 Phase diagram of Sn-Pb system [Kattner 2002]

Microelectronics has made significant strides resulting in widespread utilization and disposal of components containing leaded solders. End-of-life disposal has been cited as a driving factor for the elimination of lead. One of the main concerns regarding lead-solder has been the leaching of this heavy metal from electronics in landfill. Such disposals result in lead entering the food chain and affecting human health. Lead binds strongly to proteins in the body and hinders normal function of the human body. Nervous and reproductive system disorders, delays in neurological and physical development, cognitive and behavioural changes, reduced production of hemoglobin resulting in anemia and hypertension are some of the adverse effects of lead on human health.

To mitigate these problems several European countries, U.S., and Japan have enacted new environmental legislations on the usage of hazardous substances. A lead level equal or less than 0.1%wt in each individual and homogeneous material is considered to be a lead free system [Hwang 2005]. Under the European Parliament and the Council of European Union, three directives namely WEEE (Waste Electrical and Electronic Equipment), RoHS (Restriction of use of Hazardous Substances) and ELV (End of Life Vehicle) have been initiated by the European Commission for restriction of use of Pb in electronic applications. The U.S. Environmental Protection Agency (EPA) has banned the use of lead in paints since 1978. Japan passed 'Home Electronics Recycle Law' in 1998 [Hwang 2005, Turbini et al. 2001] With the body of evidence pointing to serious adverse health effects of lead, a surge in the development of Pb-free alloy has begun over past few decades in the electronics industry and in universities. Several lead free solders have been already developed in past few years but most of the compositions cannot be readily utilized for commercial purpose.

Knowledge of the phase equilibria of solder-alloy and solder/substrate systems provides the basic roadmap for the initial selection of candidate solders and contributes to the understanding of solder wetting and spreading [Wu et al. 2004]. Virtually all of the lead-free solder alternatives developed so far utilize tin as one of the primary constituents and potential substitutes for Pb include, but not limited to, Bi, Cd, In, Zn, Au, Tl, Ga, Cu, Sb, and Ag. Among the numerous lead free solder alloys available, few families are of particular interest and prevailing choices of industry. Generally, lead free solder alloys with melting temperature approximately below 230 °C are opted since they do not require any changes in process, boards or components that are used with conventional Sn–Pb solder. Eutectic or near eutectic compositions are preferred most, for having the lowest and single melting temperature [Zeng and Tu 2002, Sona and Prabhu 2013]

2.3 LEAD FREE SOLDERS

Ever since the commencement of the research and development of Pb-free solder alloys, a large number of Pb-free solder alloys have been proposed and summarized. List of candidate lead free solders is given in Table 2.1. At present binary eutectic Sn-0.7Cu, Sn-3.5Ag and ternary eutectic, hypo or hyper eutectic Sn-Ag-Cu alloys are considered as potential alternatives for lead bearing solders. Table 2.2 lists the advantages and disadvantages of few major alloys.

Table 2.1: Lead free candidate alloys [Lee 1997]

Alloy category	Composition	Solidus (°C)	Liquidus (°C)	Note	Density (g/cm^3)	Manufacture /investigator
Sn-Pb	63Sn-37Pb	183	183	Eutectic	8.40	(Control)
Au-Sn	80Au-20Sn	280	280	Eutectic	14.51	
Bi-Cd	60Bi-40Cd	144	144	Eutectic	9.31	Indium
Bi-In	67Bi-33In	109	109	Eutectic	8.81	Indium
Bi-In-Sn	57Bi-26In-17Sn	79	79	Eutectic		
Bi-Sn	58Bi-42Sn	138	138	Eutectic	8.56	
	95Bi-5Sn	134	251		9.64	Indium
Bi-Sn-Fe	54.5Bi-43Sn-2.5Fe		137			AT&T
Bi-Sn-In	56Bi-42Sn-2In		138			IBM

Bi-Sb	95Bi-5Sb	~275	~308			Ford
In-Ag	97In-3Ag	143	143	Eutectic	7.38	Indium
	90In-10Ag	141	237		7.54	Indium
In-Bi-Sn	48.8In-31.6Bi-19.6Sn	59	59	Eutectic		
	51.0In-32.5Bi-16.5Sn	60	60	Eutectic	7.88	Indium
In-Sn	60In-40Sn	118	~127			
	52In-48Sn	118	118	Eutectic	7.30	Indium
	50In-50Sn	118	125		7.30	Indium
Sn	100Sn	232	232		7.28	Indium
Sn-Ag	96.5Sn-3.5Ag	221	221	Eutectic	7.36	Indium
	95Sn-5Ag	221	~250			
Sn-Ag-Cu	93.6Sn-4.7Ag-1.7Cu	216	216	Eutectic		Iowa State University
Sn-Ag-Cu-Sb	96.2Sn-2.5Ag-0.8Cu-0.5Sb	210	217			AIM (CASTIN)
Sn-Ag-Sb	65Sn-25Ag-10Sb		233			Motorola
Sn-Ag-Zn	95.5Sn-3.5Ag-1.0Zn		217			AT&T
Sn-Ag-Zn-Cu	95Sn-3.5Ag-1.0Zn-0.5Cu					AT&T
Sn-Bi-Ag	91.8Sn-4.8Bi-3.4Ag		211			Sandia
Sn-Bi-Ag-Cu	91.0Sn-4.5Bi-3.5Ag-1.0Cu		210			Senju
Sn-Bi-Cu-Ag	48Sn-46Bi-4Cu-2Ag					IBM

Sn-Bi-Cu-Ag-P	Bi 0.08-20%, Cu 0.02-1.5, Ag 0.01-1.5, P 0-0.20, rare earth mixture 0-0.20. balance Sn					Cookson
Sn-Cd	67.8Sn-32.2Cd	177	177	Eutectic	7.68	Indium
Sn-Cu	99.3Sn-0.7Cu	227	227	Eutectic		
	99Sn-1Cu	227	227			
	97Sn-3Cu	227	~330			Ford
Sn-Cu-Ag	95.5Sn-4Cu-0.5Ag	225	349 (260)			Engelhard (Silvabrite 100)
Sn-Cu-Sb-Ag	95.5Sn-3Cu-1Sb-0.5Ag		256			Motorola
Sn-In	70Sn-30In	120	~175			
	58Sn-42In	118	145		7.30	Indium
Sn-In-Ag	77.2Sn-20.0In-2.8Ag	175	187		7.25	Indium
Sn-In-Ag-Sb	88.5Sn-10.0In-1.0Ag-0.5Sb		211			Qualitek
Sn-In-Bi	90Sn-8In-2Bi					IBM
	80Sn-10In-10Bi	153	199			IBM
Sn-In-Bi-Ag	78.4Sn-9.8In-9.8Bi-2Ag					
	80Sn-10In-9.5Bi-0.5Ag	179	201			Ford
Sn-Sb	95Sn-5Sb	~234	240			Motorola
Sn-Sb-	Sn approx 90-					Willard

Bi-Ag	95%. Sb 3-5%, Bi 1-4.5, Ag 0.1-0.5					industries
Sn-Zn	91Sn-9Zn	199	199	Eutectic	7.27	Indium
Sn-Zn-In	87Sn-8Zn-5In	175	188			AT&T
Sn-Zn-In-Ag	87Sn-8Zn-5In-0.1Ag					AT&T
Sn-Zn-In-Cu	87Sn-8Zn-5In-0.1Cu					AT&T

Table 2.2: Advantages and disadvantages of few major alloys [Lee 1997, Efzan et al. 2012]

Composition	Advantages	Disadvantages
Sn-58Bi	1. Relatively inexpensive and used in wave soldering of printed circuit assemblies. 2. It has acceptable wettability on both bare Cu and Ni-Au plated substrate.	1. Suffers from rapid microstructural coarsening 2. Poor creep resistance 3. Bi is not very ductile; it causes the soldered area to peel off.
Sn-Bi-Fe	1. Addition of magnetically distributed insoluble Fe particles to Sn-Bi eutectic retards both high-temperature deformation and microstructural coarsening, thus widening the useful service range of Bi-Sn eutectic alloys to much higher homologous temperature.	

	2. In addition it improves the creep resistance at 100 °C by an order of 5X. Elements other than Fe also can be used to create fine precipitates	
In-48Sn	1. Commonly used for SMT applications. 52In-48Sn is considered as the lowest melting point practical solder and it is often used for soldering to metallizations on temperature sensitive components. 2. Eutectic In-48Sn shows a fair to acceptable wettability with an aid of relatively active flux on Cu, Ni-Sn, and pre tinned Kovar (53Fe-17Co-29Ni)	1. Eutectic In-48Sn shows a sluggish and poor wetting on Au. 2. It has poor fatigue and poor mechanical properties.
Sn-3.5Ag	1. It is used in both wave and reflow soldering. 2. Excellent mechanical properties due to the dispersion of Ag_3Sn precipitates within a β-Sn matrix. 3. Sn-3.5Ag has hiher strength and superior resistance to creep and thermal fatigue.	1.Soldering temperature is significantly more than conventional solders and they are poorly compatible with general PWB finishes. Sn-Ag solder microstructure is unstable at high temperature. 2. Poor wetting. The poor wettability of 96.5Sn-3.5Ag is caused by high interfacial tension between solder and flux that is probably related to the high surface tension of Ag. 3. It shows poor isothermal fatigue at

		low strain.
Sn-Ag-Bi	1. Good thermal fatigue resistance 2.Better wettability and low melting than the Sn-Ag-Cu group of alloys	1. If Pb is present on component terminations a low melting (96 °C) Sn-Pb-Bi phase forms. Hence this alloy cannot be used until lead is completely removed from component terminations or board pads.
Sn-Ag-Zn	1. Addition of 1% Zn to Sn-Ag eutectic improves mechanical strength by 48% while maintaining same level of ductility. 2. Addition of Zn suppresses the melting point of eutectic Sn-Ag alloy.	1. Addition of Zn >1% deteriorates the mechanical properties
Sn-Ag-Zn-Cu	1. Addition of small amount (<1%) of Cu to Sn-3.5Ag-1Zn improves the ductility of the solder alloy by refining the effective grain size and retaining uniform distribution of Ag_3Sn precipitates in the solidification microstructure. 2. Improves the mechanical properties.	1. Addition of Cu >1% is not desirable. It causes precipitates of additional IMC phases, which disturbs the finely dispersed precipitates in the surrounding matrix and weakens the mechanical properties.
Sn-0.7Cu	1. It is used in both wave and reflow soldering processes. 2. It has good fatigue resistance	1. Higher eutectic temperature (227 °C) causes the deterioration of board material in wave soldering.

		2. Poor wettability, low resistance to thermal stress, poor creep resistance 3. This alloy may corrode iron containing solder pots. Addition of trace amounts of Ni, Ge, P improves the oxidation resistance
Sn-9Zn	1. Low cost alternative and good mechanical properties 2. Low melting temperature.	1. Zinc alloys are difficult to use, need special fluxes and a nitrogen gas atmosphere is certainly required. Solder paste incorporating this alloy has a poor shelf life due to attack on the metal spheres by the organic acids or bases present in the flux vehicle. 2. This alloy drosses excessively when used in a wave soldering operation. 3.Poor corrosion resistance and susceptible oxidation 4. Poor wettability and poor compatibility with a Cu substrate under high temperature conditions
Sn-Zn-Bi	1. Additional of Bi improves the wettability	1. Bi is brittle in nature and has a strong tendency to segregation
Sn-Ag-Cu	1. Good thermal fatigue and creep resistance 2. Acceptable strength and wettability 3. Relatively good solderability.	1. High melting temperature (36 °C more than Sn-Pb solder) 2. Price is dependent on the spot price of silver

2.3.1 Sn-Ag-Cu solders

A survey by European lead free technology roadmap says that the near eutectic SAC alloys with a composition of 3-4 % Ag and 0.5-1 % Cu are the most popular and widely accepted solder alloy [Shnawah et al. 2012b]. Sn–Ag–Cu ternary alloy has the advantage of acceptable wetting ability, good interfacial properties, high creep resistance, low coarsening rate and also relatively low melting temperatures compared to 96.5Sn–3.5Ag binary eutectic alloy. Addition of Cu lowers the melting temperature and improves the wettability of SAC solder alloys. Ternary phase diagram of Sn–Ag–Cu is shown in Fig. 2.2

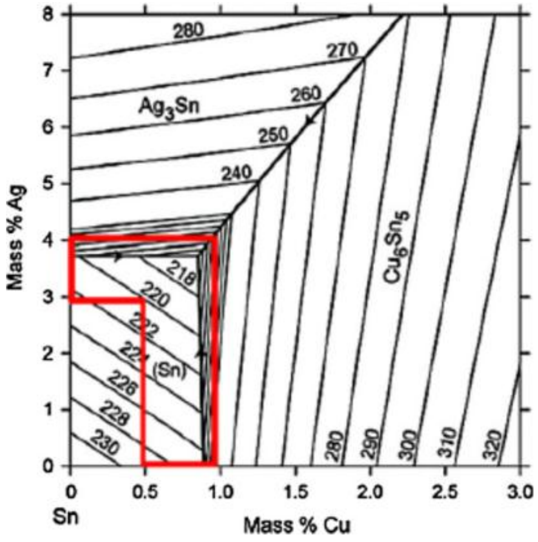

Fig. 2.2 Ternary phase diagram of Sn–Ag–Cu [Moon et al. 2000, Shnawah et al. 2012a]

The area indicated in the red box shows the near eutectic region. Most of the commercially available SAC alloy compositions are within this region [Ma and Suhling 2009]. The eutectic reaction takes place at a temperature of 217.2°C. Under equilibrium solidification conditions, the microstructure of near-eutectic SAC solders consist three phase ternary eutectic micro constituent, most likely consisting of a high volume fraction of β-Sn matrix containing small, needle, or disc-shaped particles of Ag_3Sn and Cu_6Sn_5 [Lewis et al. Kattner 2002, LaLonde et al. 2004] However, many researchers have observed a substantial deviation from uniform eutectic microstructure. The equilibrium ternary eutectic phase transformation is suppressed in Sn–Ag–Cu alloys, due to a typically large undercooling of about 10–50 °C associated with the nucleation of the β-Sn phase. Hence the Ag_3Sn and Cu_6Sn_5 intermetallic precipitates sometimes can grow to large sizes before the whole joint solidifies. These are said to be primary precipitates and the remaining fine intermetallic precipitates between the β-Sn dendrites are referred to as secondary precipitates [Yin et al. 2011]. In the absence of the eutectic transformation, liquid alloys traverse metastable portions of the primary Ag_3Sn or Cu_6Sn_5 phase fields, yielding primary-like intermetallic phases and reducing the Ag and Cu contents of the remaining liquid far below equilibrium values. Once β-Sn nucleation commences, the liquid alloy composition resides within the primary β-Sn region under conditions of large constitutional supercooling. This makes the β-Sn to adopt a dendritic morphology, and during dendrite growth interdendritic regions become enriched in Ag and Cu and eventually solidify as monovariant or invariant eutectic micro constituents, depending on local composition [LaLonde et al. 2004]. Microstructure of SAC bulk solder is shown in Fig. 2.3.

To enhance the reliability of micro solder joints, understanding the interfacial microstructure is required. The formation of interfacial IMCs indicates good wetting and bonding properties, however massive IMCs present at the interface may decrease the mechanical properties of the entire joint [Huang et al. 2006, Berthou et al. 2009]. Reaction between Sn and Cu yields Cu_6Sn_5. Reaction between Sn and Ag results in the formation of Ag_3Sn but Cu_3Sn will not be found at the eutectic point until the Cu content is high enough for the formation of Cu_3Sn at higher temperatures, so Cu_3Sn is absent in bulk specimens. There exists no reaction between Ag and Cu to form any intermetallic [Ma and Suhling 2009, Shnawah et al. 2012a]. Ag_3Sn and Cu_6Sn_5 are said to possess much higher strength than the bulk solder material in SAC alloys whereas primary β-Sn phase has the lowest elastic modulus and yield strength among the bulk constituent phases in SAC alloys. Hence presence of large amount of Ag_3Sn and Cu phases result in a stiff bulk solder whereas high fraction of the primary β-Sn phase yields a soft and highly compliant bulk solder. Ag_3Sn is the only Ag bearing phase present in the SAC solder. An increase in the amount of Ag content in SAC solders results in a quantitative increase of Ag_3Sn IMC particles formed [Kariya et al. 2004, M. Reid et al. 2008, Shnawah et al. 2012a]

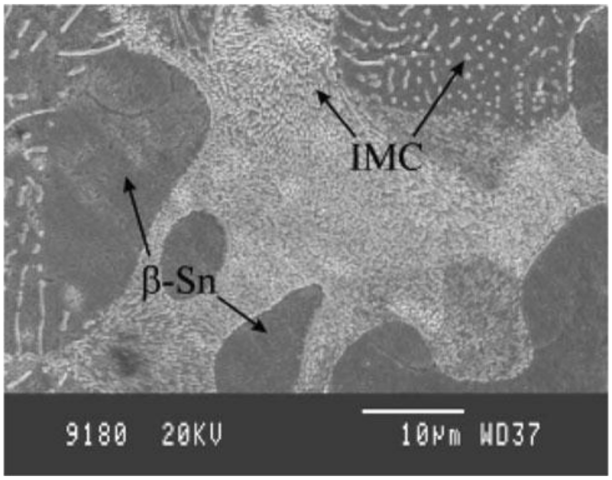

Fig. 2.3 Microstructure of SAC bulk solder [Wu et al. 2004]

2.4 WETTING BEHAVIOUR OF SOLDERS

The most important property for selecting lead free solder material is wettability. Wettability describes the ability of a molten solder to wet and spread spontaneously over an open surface. A metric of wettability is the contact angle, θ, formed at the edge of the spreading solder. The contact angle is defined as the angle formed by the intersection of the liquid-solid interface and the liquid-vapor interface (geometrically acquired by applying a tangent line from the contact point along the liquid-vapor interface in the droplet profile). The interface where solid, liquid, and vapor co-exist is referred as "three phase contact line". The lower the value of θ, better is the wettability [Yuan and Lee 2013].

Table 2.3: Contact angle of few solder alloys on Cu substrate (measured by wetting balance method) [Vinaco 2000, Wu et al. 2004, Matsumoto and Nogi 2008]

Solder alloy	Soldering temperature (°C)	Flux	Contact Angle (θ)
Sn-37Pb	215	RMA	22
	215	WS	12
	215	NC	31
	220	RMA	12
	260	RMA	17
Sn–3.5Ag	245	RMA	41
	245	WS	63
	245	NC	39
	254	RMA	27
Sn–0.7Cu	260	RMA	49
Sn–9Zn	245	RA	83
	260	RA	77
	290	RA	72
Sn-5Sb	268	RMA	42±7
Sn-50Sn	215	RMA	63±3
Sn-2.5Ag-0.7Cu	250	RMA	53
Sn-3.5Ag-0.7Cu	250	RMA	49
Sn-0.7Cu-0.3Ni	255	NC	47

RMA: rosin mildly activated, RA: rosin activated, WS: water soluble and NC: no-clean.

The value of θ can be measured directly by sessile drop experiment or computed from experimental data obtained by the meniscometer/ wetting balance technique [Awasthi et al. 1996 Vianco 2000]. However, the measurement of the contact angle involves the control of a number of parameters that can affect the results, namely, surface roughness, flux, reflow time, and reflow temperature [Arenas and Acoff 2004]. The driving force of wetting on substrates is mainly the interfacial energy that results from the imbalance of the surface and interface energies. Young's equation gives the balance of surface and interfacial tensions at equilibrium:

$$\gamma_{gs} = \gamma_{ls} + \gamma_{gl}\cos\theta \qquad (1)$$

where γ_{gs} is the surface tension of the solid surface/gas interface, γ_{ls} is the interfacial energy between the solid and the liquid and γ_{gl} is the surface tension of the gas/liquid interface, and θ is the equilibrium contact angle. Wettability is optimized by minimizing the value of the contact angle, which corresponds to lower surface-interfacial energy. Therefore, the measurement of the contact angle between the solder and the substrate is used to determine the extent of wetting, which, in turn, is a very important issue in the reliability of electronic packaging [Arenas and Acoff 2004]. Table 2.3 gives the contact angle of few solder alloys. It is clear from the literature that the wettability of the Pb-free solders is not as good as that of the traditional 63Sn-37Pb alloy; however, numerous prototyping experiments have confirmed that the Pb-free solders have adequate wettability (i.e., sufficiently low contact angles) to support cost-effective assembly processes for electronic components and printed circuit boards. In all previous research, wettability was assessed by measuring the equilibrium contact angle.

2.4.1 Factors affecting the wettability in soldering process

Solder flux, is made to assist soldering task by wiping off the oxide layer. Fluxes react with any oxide or tarnish present on the substrate surface and form a continuous film over the surface that inhibits access of oxygen to the substrate. A number of chemical substances such as ZnCl or HCl are used effectively to remove oxide contamination but these acidic materials are quite corrosive to the metal itself. For this reason, rosin fluxes have been used extensively which, although less acidic in character, do not afford as good fluxing action [Efzan and Marini 2012]. Majority of Sn-Pb solders are used with Rosin fluxes. ‘No Clean’ flux can cause reliability problems in the field due to aggressive residues, which may be electrical conducting or corrosive in humid environments [Hansen et al. 2009]. Sn-Ag, Sn-Cu eutectic alloys and Sn-3.8Ag-0.7Cu ternary eutectic alloys show good wetting with RMA (Mildly Activated Rosin) and RA (Activated Rosin), but poor wetting with R (Rosin) flux [Arenas et al. 2006]. Table 2.3 shows the effect of various fluxes on contact angle. Fluxes also affect the different interfacial tension forces present during wetting because of the change of the environment at the solder/substrate interface. In the presence of a flux, the classical Young-Dupre equation for the balance of surface tensions at the interface takes the following form,

$$\gamma_{fs} = \gamma_{ls} + \gamma_{fl} \cos\theta \tag{2}$$

An increase in the flux-substrate surface energy, or decrease in flux-solder surface energy will decrease the contact angle, thus increasing wettability. A flux addition that promotes those changes will result in improved wettability [Arenas and Acoff 2004].

Temperature is another important factor that affects spreading of solder. Decrease in surface tension and viscosity with the increase in temperature results in good spreading of solder alloy on the substrate [Kumar et al. 2010]. It was expected that in all cases the increase in reflow temperature would result in greater spreading; however, it is possible that for some fluxes, higher temperatures will increase the flux solder surface tension because of chemical reaction and decreases the wettability [Arenas and Acoff 2004]. Similarly, an increase in reflow time at a particular reflow temperature decreases the viscosity of solder and results in good spreading [Sona and Prabhu 2015].

An increase in substrate surface roughness improves the wettability of the substrate [Wenzel 1936]. The asperities of a rough surface act like capillary tubes and help in better spreading of solder alloy [Manko 1964]. Kumar et al. (2010), Satyanarayan and

Prabhu (2013) reported that contact angle decreases with increasing surface roughness. They also have concluded that increase in surface roughness decreases the solder joint reliability as more number of IMCs nucleate and grow on a rough surface.

2.5 NUMERICAL MODELING OF GROWTH BEHAVIOUR OF IMCS

The intermetallic layer thickness depends on solder composition, reflow temperature, duration and the substrate pad finishes. Researchers have put forward a number of modelling techniques to describe the growth behaviour of interfacial IMCs during soldering. Various thermal cycling aging profiles such as isothermal aging, accelerated thermal cycling and thermal shock affect the IMC growth rate. It is also found that IMC growth rate is higher during thermal shock and thermal cycling than isothermal aging [Pang et al. 2004]. IMCs grow during aging and strength of the solder joint decreases with the increase of IMCs size. Coarsening of microstructure is the main reason for the reduction in strength after aging of solder alloys. Based on experimental data, Hall and Petch found that the yield strength of a polycrystalline material is inversely proportional to its grain size as shown in the equation,

$$\sigma_y = \sigma_i + kd^{-0.5} \tag{3}$$

where σ_y is the yield strength of the polycrystalline material; σ_i is a constant for the material and gives the overall resistance of the lattice to dislocation movement; k is a constant which measures the contribution of hardening due to grain boundaries; and d is the grain size. The Hall-Petch theory states that the strength of materials reduces with increasing grain size. The increasing grain size brings down the amount of grain boundaries. Therefore, only fewer grain boundaries will be available to block the dislocation movement. Hence the material strength will be lost. The grain and phase structure coarsening is promoted by the self-diffusion of atoms, interstitials and vacancies.

According to the diffusion equation,

$$D = D_0 exp\left(-\frac{Q}{RT}\right) \tag{4}$$

where D is diffusivity, D_0 is a constant that is independent of temperature, R is the Boltzmann constant, Q is the activation energy, and T is the absolute temperature. Higher temperatures will increase the diffusivity of the atoms, interstitials and vacancies, leading to grain growth [Ma and Suhling 2009].

Generally, the thickness of the IMC layer can be determined using a simple growth model,

$$x = (Dt)^n \tag{5}$$

where x is the IMC layer thickness at time t, D is the diffusion coefficient of the diffusing atomic species which determine the growth of the IMC layer and n is the time exponent. It can be assumed that the value of n is 0.5 when the reaction is mainly controlled by the diffusion mechanism. The thickness of the IMC layer (x) is plotted against $t^{0.5}$, to analyze the growth rate. D is determined from a linear regression analysis of x versus $t^{0.5}$, where the slope of the graph is $D^{0.5}$ [Law et al. 2006 Yu and Wang 2008].

More precisely IMC layer thickness is measured using a relation [Berthou et al. 2009]

$$x = x_0 + kt^n \tag{6}$$

where x represents the thickness at time t, x_0 is the IMC thickness for the as-soldered condition, t is the aging time, n is the power law exponent. The common form of this equation used to model the IMC growth is used with n=0.5, corresponding to $D=k^{0.5}$. D is the usual diffusion coefficient; expressed in m^2s^{-1}.

$$x = x_0 + \sqrt{Dt} \tag{7}$$

D varies with the temperature according to Arrhenius law. Layer growth is faster at higher aging temperature with the diffusion coefficient being given by Arrhenius equation represented by equation (4) [Choubey et al. 2008 Yu and Wang 2008 Zeng et al. 2010]. Activation energy can be estimated and effect of temperature on growth rate can be evaluated by converting the equation (4) into the following form and by drawing Arrhenius plot of $ln(D)$ versus $1/kT$.

$$ln(D) = ln(D_0) + \left(-\frac{Q}{kT}\right) \tag{8}$$

where k is the Boltzmann constant.

Therefore, overall IMC layer growth kinetics is given by

$$x = x_0 + A_0 t^n exp\left(-\frac{\Delta H}{RT}\right) \tag{9}$$

where A_0 is the pre exponential diffusion factor, ΔH is the apparent activation energy for the growth. The growth kinetic parameters of the IMC layer such as *n, A,* ΔH were determined by plotting the measured IMC layer thickness against the exposure time, at any given temperature. The data are fitted using a power law relationship given by equation 9 [Vianco et al., Yoon and Jung 2004 Xu et al. 2005, Xu and Pang 2006] . Equation 9 can be used only for isothermal conditions.

Experimental study of IMC layer growth between Sn3.8Ag0.7Cu and Ni/Au surface finish by isothermal aging versus thermal cycling (TC) aging was investigated by Xu et al (2005) to develop a framework for correlating IMC layer growth behaviour. An integrated model for IMC growth was derived to describe the Ni-Cu-Sn IMC growth behaviour subject to TC aging. Temperature variation is a function of time for TC, and IMC thickness should be the accumulation of the interfacial reaction for different temperatures over accumulated time. The layer growth rate, *v*, is a function of both temperature and time. ν is given by the following relationship.

$$\nu = \frac{dx}{dt} = \frac{1}{x^m} A' \exp\left(-\frac{\Delta H'}{RT}\right) \tag{10}$$

or,

$$x^m dx = A' \exp\left(-\frac{\Delta H'}{RT}\right) dt \tag{11}$$

Integration of equation 10, over the thickness x_0 to x_1 and time interval *0* to *t* gives,

$$\int_{x_0}^{x_1} x^m dx = \int_0^t A' \exp\left(-\frac{\Delta H'}{RT}\right) dt \tag{12}$$

Since equation 11 is applicable for any temperature profile T(t), to find the co-efficient *m*, *A'* and $\Delta H'$, let *T* be a constant, and the integral formula is expressed as

$$x_t = x_0 + [(m+1)A']^{\frac{1}{m+1}} \exp\left(-\frac{\Delta \mathrm{H}'}{(1+\mathrm{m})\mathrm{RT}}\right)^{\frac{1}{\mathrm{t}^{\mathrm{m}+1}}} \tag{13}$$

Equation 13 and 9 are identical. Comparing these two equations, relationship between A_0 and *A'*, ΔH and $\Delta H'$, time exponents *n* and *m* can be found out. By substituting the values of A, ΔH and n in equation 10, the IMC growth corresponding to any temperature profile after any aging time can be predicted by,

$$x_t = x_0 + \left[\frac{1}{n^2} A_0^n \int_0^t A' \exp\left(-\frac{\Delta H'}{RT}\right) dt\right]^n \tag{14}$$

Equation 12 can be used to calculate the IMC layer growth for any TC aging profile since n, A_0 and ΔH can be easily found out through isothermal annealing. A simple approximation could be used to calculate the IMC thickness by numerical analysis,

$$x = x_0 + A_0 t_{eff}^n \exp\left(-\frac{\Delta H}{RT}\right) \tag{15}$$

where t_{eff} is the effective time and for most of the commonly used aging profiles, it is the total time at upper soak temperature [Xu and Pang 2006].

Pang et al (2004) studied the morphology and growth of interfacial IMCs formed between 95.5Sn-3.8Ag-0.7Cu and nickel/gold (Ni/Au) surface finish on BGA solder joint specimen. The growth behaviour of IMCs subjected to isothermal aging at 125°C, thermal cycling (TC), and thermal shock(TS) with upper soak temperatures of 125°C were compared. In order to simplify the comparison, the IMC growth was assumed to be volume diffusion controlled, i.e., the growth rate is proportional to the square root of time. They found that the effect of TS aging on IMC growth rate is more than TC aging. The TC aging has comparatively longer cycle time and soak period than TS aging and hence the stress relaxation at the solder joint is more pronounced in TC aging than TS aging. To quantify the acceleration effect of TC and TS aging, Pang et al used another parameter, "equivalent isothermal aging time," t_{eq}, which is the time required by isothermal aging to obtain the same IMC thickness compared with TC or TS aging, and it is given by,

$$t_{eq} = \frac{1}{D_{iso}^2}(x_t - x_0)^2 \tag{16}$$

TC and TS are the most common tests used in checking the reliability electronic packaging. An acceleration factor, K is defined to relate the accelerated test (under TC and TS aging) compared to isothermal aging. It is the ratio of TC and TS, IMC growth to isothermal aging IMC growth. It is expressed as,

$$K = \frac{t_{eq}}{t_{eff}} \tag{17}$$

or,

$$K = \frac{1}{D_{iso}^{2} t_{eff}} (x_t - x_0)^2 \tag{18}$$

The acceleration factor K is useful in reliability studies for correlating the IMC growth during TC, TS, and isothermal aging.

2.6 EFFECT OF VARIOUS PARAMETERS ON SOLDER JOINT RELIABILITY

2.6.1 Effect of Ag content on IMC formation at the solder substrate interface

One of the highly focused areas of research is the effect of Ag content of the Sn-Ag-Cu alloy on the interfacial microstructure and macro mechanical behaviour of the solder interconnects due to reliability concerns. The main concern is the existence of the large Ag_3Sn plates, which possess inherent in-compatible geometry to the surrounding microstructure, i.e. bulk solder and substrate. Cu is the most common conductor metal, which is utilized as substrate due to its good solderability characteristic and excellent thermal conductivity performance [Liu et al. 2000]. The Ag_3Sn appears at the interface between substrate and solder alloy when the Ag content is above 0.1 mass% [Liu et al. 2006]

[Keller et al (2011) studied the mechanical properties of Sn-xAg-0.4cu/Cu joints by varying Ag content from 0 to 5 wt.%. Shear tests were performed with four hypoeutectic (0–3 wt.% Ag), a eutectic (3.7 wt.% Ag) and two hypereutectic (4.5 and 5 wt.% Ag) solder compositions. Specimen without containing any Ag content (Sn–0.4 wt % Cu) showed the lowest shear strength value (<20 MPa). Shear strength increased initially with the Ag content and showed a maximum (32.5 MPa) at 3 wt.% Ag and later declined slightly for eutectic (30MPa) and hypereutectic compositions (<28 MPa). Solder without any Ag content showed the maximum ductility. Vicker hardness values also showed a similar trend. There was increase in hardness values up to addition of 3 wt.% Ag, later decreased with the increase of Ag content. A maximum of 17 HV was observed at 3 wt.% Ag where Sn-0.4Cu showed a Vicker hardness of 12.5 HV. The ideal soldering temperature leading to the maximum joint strength was found to be around 300˚C. After reflow at about 300˚C the microstructure of SnAgCu alloys consisted of sparse, huge primary precipitations, large areas of β-Sn dendrites and interdendritic regions, in which fine intermetallic particles were dispersed in a Sn matrix. The mechanical properties of the solder were mainly affected by the finer Ag_3Sn particles (≈140nm diameter) than the coarser Cu_6Sn_5 particles (≈ lμm diameter) and were controlled by particle hardening within the interdendritic zones. Dislocation interaction with the small Ag_3Sn precipitates within the interdendritic zones plays the dominant role in solder strengthening. (i) particle shearing or (ii) by-passing by bowing of dislocations (Orowan mechanism) are the two general mechanisms that control the strength, when particles hamper the movement of dislocations.

Kim et al (2003) studied the effect of alloy composition on microstructure by varying Ag and Cu composition of SAC alloy from 3.0 to 3.9 wt.% and 0.5 to 0.7 wt.% respectively. They observed a degradation in the mechanical properties of solder joints with the formation of large Ag_3Sn platelets. They also noticed an increase in the formation of Ag_3Sn platelets at the interface, regardless of kind of the substrate used, with the increase of Ag content. Large Ag_3Sn platelets that appeared in Sn–3.5Ag–0.7Cu and Sn–3.9Ag–0.6Cu solders on Cu, Au/Ni/Cu, 42 alloy and stainless steel, induced brittle fracture at an interface and acted as crack initiation sites. They also noticed the formation long needle and hollow shaped Cu_6Sn_5 whiskers in all most all the solder–Cu joints and the high Cu content solder joints. For the high Cu content solder joints with a 42 alloy substrate, long Ni–Cu–Sn whiskers were formed at the interface and in the solder. The fracture surface of the Sn–3Ag–0.5Cu solder–Cu joints exhibited typical ductile fracture, whereas the other two alloys, Sn–3.5Ag–0.7Cu and Sn–3.9Ag– 0.6Cu; showed a mixture of both ductile and brittle fractures. Large Ag_3Sn platelets did not form in alloys with less than 3.2 wt. % Ag content. Large Ag_3Sn plates should be avoided as they provide crack initiation sites under tensile and shear stresses [Kim et al. 2002]. Since there is no way to detect where the Ag_3Sn plates form and in which direction they grow in solder joints, the practical way to subside their detrimental effect on solder joint reliability is to avoid their formation. This can be achieved by reducing the Ag content below its eutectic composition value 3.4 wt.%. When the Ag content is lower than the eutectic composition of 3.4 wt.%, the Ag_3Sn phase forms as the secondary phase in the form of fibers. These Ag_3Sn fibers act as pins to hinder the motion of dislocations in the solder, making the solder more difficult to deform. High Ag content is desired for thermal cycling performance because of the strengthening effect of Ag_3Sn fibers, but it should not be higher than 3.4 wt.%. Consequently, a Sn-Ag-Cu solder joint with lower Ag content can release more stress by plastic deformation of the bulk solder and thus perform better in drop, impact, high-speed bending, shearing, and pulling tests. Ag improves the resistance of the solder to thermal fatigue by forming Ag_3Sn fibers, but it has a negative effect on the interfacial reliability because the Ag_3Sn fibers make it more difficult for the joints to relax the stress.

Lu et al (2006) in their study on impact of Ag (0.0, 1.2, 2.6, 3.0, 3.5 and 3.9) on Sn-xAg-Cu solder, found a similar behaviour by the entire Ag alloy with regard to shear strength. They carried out isothermal aging (150 °C/ 1000 hours) of the test samples and found size reduction and smoothening of sharp edge (spheroidization) of the Ag_3Sn plates. The corresponding mechanical shear performance of the inter connects did not degrade after the aging, regardless of the Ag content. For the first 24 hours of aging there was a decrease in the shear strength and then a stable constant value was maintained throughout the rest of the aging process (Fig.2.4).

Zhang et al (2002) also noticed similar kind of shear force reduction in first 24 hours of isothermal aging at 150° C for Sn-3.5Ag-1.0Cu interconnects due to rapid coarsening of fine Ag_3Sn particles. Lu et al (2006) found a similar decrease in the shear strength during first 24 hours of aging for Sn-0.7Cu. They concluded that, mainly tin is the reason for initial decrease in the shear strength of lead free interconnects. Table 2.4 gives the shear strength of various Sn-Ag-Cu alloy compositions.

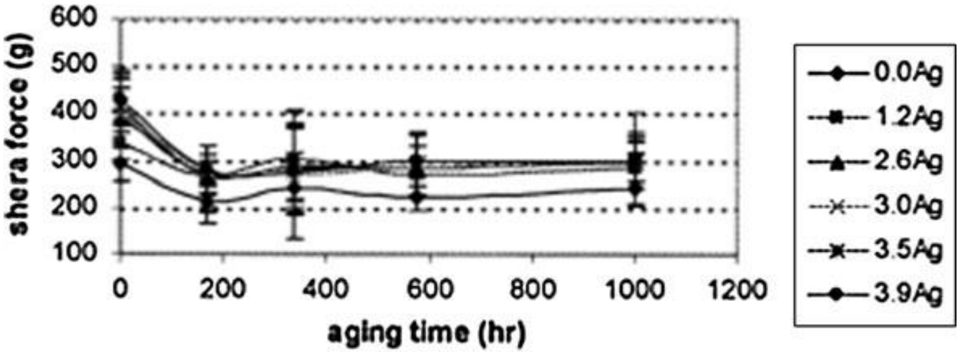

Fig. 2.4 The shear plot of the Sn–xAg–Cu interconnects through the isothermal aging [Lu et al. 2006]

It can be seen from these research works that an increase in Ag content from 3.2 wt. % to any higher level does not offer any enhancement in mechanical properties. When Ag content is around 3-3.2 wt.% the solder shows good temperature cycling reliability. The yield strength, tensile strength, shear strength and hardness show a maximum value. Plasticity suffers with increase of Ag content above 3wt. % but solidification cracks are the major problems in low Ag SAC solders. Solidification cracking occurs during the terminal stage of solidification, when the tensile stresses developed across adjacent grains exceed the strength of the almost completely solidified metal. Lu et al (2010) showed that solidification cracks exist in solder joints when the Ag content is between 1 wt.% to 3.0 wt.%. They found no cracks in Sn-3.8Ag-0.7Cu solder joints. The total crack length of the Sn-Ag-Cu solder joints increased to a maximum and then dropped to zero as Ag content increased from 1.0 wt.% to 3.8 wt.%. Susceptibility to solidification cracking ranged as follows: SAC207> SAC305> SAC107> SAC387. This study is important for an appropriate solder selection for the electronic assemblies.

Table 2.4: Shear strength of various Sn-Ag-Cu solders

Properties	Sn-Ag-Cu	Sn-Pb	References/Notes
Shear strength (MPa)	27(Sn-3.8Ag-0.7Cu) 17(Sn-3.8Ag-0.7Cu)	23 14	At 0.1 mm/min 20 °C 100 °C [John et al. 2003]
	35.1(Sn-3.8Ag-0.7Cu) 18.2(Sn-3.8Ag-0.7Cu)	—	At 0.1 mm/min At room temperature 125 °C [http://www.gullwinguk.com/content/pdf/db_pbfree_solder.pdf]
	<20(Sn-0Ag-0.4Cu) ≈22(Sn-1.0Ag-0.4Cu) ≈28(Sn-2.0Ag-0.4Cu) ≈32.5(Sn-3.0Ag-0.4Cu) ≈31(Sn-3.7Ag-0.4Cu) ≈28.3(Sn-4.5Ag-0.4Cu) ≈27(Sn-5.0Ag-0.4Cu)	For Pb (10 at.%) ≈20 (Soldered at 250 °C)	0.2 mm/s Reflow temperature 340˚C [Keller et al. 2011]
	>24 (Sn-Ag-0.4Cu) For Ag>2 wt.%	—	Reflow temperature 250˚C [Keller et al. 2011]
	9.8(96.5Sn-3Ag-0.5Cu)	—	(On Au/Ni–P/Cu pad) Reflow temperature 220 °C [Chang et al. 2010]

	35(95.5Sn-3.8Ag-0.7Cu) 8(95.5Sn-3.8Ag-0.7Cu)	—	(On FR4 substrate) 25 °C Displacement rate 0.5 mm/min 125 °C Displacement rate 0.005 mm/min [Pang et al. 2004]
	≈55(96.5Sn-3.0Ag-0.5Cu) ≈61(96.5Sn-3.8Ag-0.7Cu) ≈52(95.5Sn-4.0Ag-0.5Cu)	≈51 (Sn63Pb37) Reflowed at 222 °C for 37 s	(On FR4 glass epoxy PCBs with OSP surface finish) Reflowed at 243 °C for 40s. Tested at room temperature. Displacement rate 2mm/min. [Sundelin et al. 2006]
	48(96.5Sn-3.0Ag-0.5Cu) 47(96.5Sn-3.8Ag-0.7Cu) 45(95.5Sn-4.0Ag-0.5Cu)	≈44 (Sn63Pb37) Reflowed at 222 °C for 37 s.	(On FR4 glass epoxy PCBs with OSP surface finish) Reflowed at 243°C for 40 s. Aged at 85 °C for 1000 hours. Tested at room temperature. Displacement rate 2 mm/min. [Sundelin et al. 2006]
	≈46(96.5Sn-3.0Ag-0.5Cu) ≈43(96.5Sn-3.8Ag-0.7Cu) ≈45(95.5Sn-4.0Ag-0.5Cu)	≈46 (Sn63Pb37) Reflowed at 222 °C for 37 s.	(On FR4 glass epoxy PCBs with NiAu surface finish) Reflowed at 243˚C for 40 s. Tested at room temperature. Displacement rate 2mm/min. [Sundelin et al. 2006]

	≈43(96.5Sn-3.0Ag-0.5Cu) ≈44(96.5Sn-3.8Ag-0.7Cu) ≈46(95.5Sn-4.0Ag-0.5Cu)	≈39 (Sn63Pb37) Reflowed at 222 °C for 37 s.	(On FR4 glass epoxy PCBs with NiAu surface finish) Reflowed at 243 °C for 40 s. Aged at 85 °C for 1000 hours. Tested at room temperature. Displacement rate 2 mm/min. [Sundelin et al. 2006]
	32(Sn-0.5Ag-4Cu) 40.5(Sn-4.7Ag-1.7Cu) 17.2(Sn-4.7Ag-1.7Cu)	—	At 0.1 mm/min test speed. At room temperature At room temperature At 125 °C [http://www.gullwinguk.com/content/pdf/db_pbfree_solder.pdf]
	67(Sn-3.6Ag-1.0Cu) 58(Sn-4.7Ag-1.7Cu) 63.8(Sn-3.8Ag-0.7Cu)	36.5(Sn-40Pb)	At 0.1 mm/min tested at 22 °C cooling rate 10 °C/S [John et al. 2003]

2.6.2 Alloying elements

Addition of rare earth elements such as La, Ce, Lu and Y etc. to Sn rich solders was found to improve both the mechanical and physical properties of SAC solder alloys. Rare earth elements can reduce the melting point of the solder, improve the wettability, lower the IMC growth and upgrade the shear strength and creep resistance of SnAgCu solder alloys [Dong et al. 2009]. When small RE concentrations are added to solder alloys, homogenously distributed $RESn_3$ intermetallic phases form in the solders and they allow microscopic voids to nucleate, throughout the solder volume (instead of localized strain at the solder–intermetallic interface), and homogenize the strain in the solder joint thereby increase the ductility of the solder. During loading, force is transferred from the matrix to these slightly stiffer $RESn_3$ particles, which act as second phase. Because they are compliant, it is likely that an appreciable amount of deformation takes place in these phases as well, contributing to the improvement in ductility [Dudek and Chawla 2010]. It is known that the standard Gibbs free energy of formation for Sn–RE IMCs is lower than those for Cu–RE and Ag–RE. So the RE elements have a higher affinity for Sn, and this explains their effectiveness in the refinement of the Sn–rich microstructure [Xie et al. 2012]. Rare earth element addition found to increase the tensile strength of majority of lead free solder alloys atleast by 15% [Wu et al. 2004]. Addition of 0.5Ce to Sn–3.9Ag–0.7Cu improves the joint reliability, ductility, oxidation resistance and also mechanical performance of Sn–3.9Ag–0.7Cu/Cu and Ni–P joints [Xie et al. 2012]. Addition of 0.25 % RE elements of mainly cerium (Ce) and lanthanum (La), to Sn–3.5Ag–0.7Cu refines the coarse β-Sn grains and the IMC particles [Wu et al. 2004].

Lai et al (2007) found that the addition of Ni alters the interfacial intermetallic compound (IMC) structure while Ge enhances the mechanical behaviour of the bulk solder. Although SnAgCu lead free solder provides better mechanical properties, thermal fatigue behaviour than the conventional SnPb solder it faces surface oxidation and shrinkage cracking problem. This problem could be overcome by adding Ni and Ge. Ge is very effective in preventing oxidation of Sn at surface of molten SAC lead free solder. Ni is effective in improving the mechanical properties. The creep behaviour of Sn–3.5Ag–0.5Cu–Ni–0.01Ge was found to be better than SAC solder. Ni suppresses the growth of Cu_3Sn IMC layer. Cu_3Sn is scarcely sensitive to Ni in the range of 0.07–0.25 mass %[Watanabe et al.2006]. The addition of Ni favours the formation of fiber-like IMCs and finer dot-shaped precipitates on the surface of β-Sn matrix rather than needle-like morphology. The addition of 0.06 wt % Ni and 0.5 wt % Sb into SAC105 resulted in improvement of creep resistance of about 210 and 350 % when compared with the SAC105 solder alloy [El-Daly and El-Taher 2013]. Addition of Bi and Ni prominently improved the shear strength of SAC0705 solder joints. This enhancement partially depends on the solid solution strengthening and dispersion strengthening of Bi and Ni in the bulk solder, which significantly increases the integrated intensity of the solder joints [Liu et al. 2012].

[Dong et al (2008) studied the effect of addition of trace amounts of Ni (0.1 wt.%), P (0.01 wt.%) and Ce (0.05 wt.%) to SAC 305 individually. They found a decrease in wettability of SAC305 solder alloy with the addition of Ni and Ce whereas increase in wettability with the addition of P. They could also observe a depression in hot crack formation on the solder surface with the addition of Ni and Ce elements whereas P element additions aggravated the hot cracking of solder. Oxidation resistance of solder was increased with the Ni addition but Ce element addition worsened the anti-oxidation property. However, P significantly improved the anti-oxidation property of SAC305 solder. Addition of Zn to SAC alloys reduces their amount of undercooling during solidification and hence can suppress the formation of large Ag_3Sn plates [Kang et al. 2004]. A delay in the formation of Ag_3Sn was observed by El-Daly (2013) when Ni and Zn element were doped to Sn–2.0Ag–0.5Cu solder. The delay persisted until all the Ni and Zn elements were consumed to form $(Cu,Ni)_6Sn_5$ and Cu_6Zn_5 IMC phases respectively. The addition of 0.05Ni and 0.5Zn to Sn-2Ag-0.5Cu increased YS and UTS as well as the ductility at all temperatures and strain rates. The formations of new $(Cu,Ni)_6Sn_5$ and Cu_6Zn_5 IMCs have been recognized to reinforce the solder matrix and decrease the β-Sn grain size. It was also found that that the strengthening effect of Zn is more than that of Ni. Kotadia et al (2012) found the formation of $(CuNi)_6Sn_5$ IMC at the interface for 0.5–1 wt% Zn. When the Zn concentration was 1.5 wt% a Cu_5Zn_8 IMC layer was observed followed by massive spalling leaving the more thermodynamically stable Cu_6Sn_5 IMC to form at the Cu/solder interface. SAC–Zn solder alloy formed $(CuNiZn)_6Sn_5$ IMC instead of $(CuNi)_6Sn_5$ on Ni–P substrate. The higher Zn concentration solder alloys also showed Ni_5Zn_{21} IMC grains close to the interface. The $(CuNiZn)_6Sn_5$ IMC layer found to grow with aging but the growth rate on Ni–P substrate was significantly lower than on Cu substrate. The lowest growth rate was found in the SAC–1.5Zn/Ni system.

2.6.3 Composite approach

Composite approaches are also given by researchers to improve the reliability of solder joints. Addition molybdenum nano-particles to SAC solder impart their influence on the interfacial IMC as discrete particles. They do not appear to dissolve or react with the solder. They tend to adsorb preferentially at the interface between solder and the IMC scallops and hinder the diffusion flux of the substrate and thereby suppress the IMC growth [Haseeb et al. 2012]. Addition of nano sized Mo particles to Sn–3.8Ag–Cu (SAC387) improves the yield strength of solder alloy [Rao et al. 2011]. Addition of 20 nm moissanite SiC particles to Sn-3.8Ag-0.7Cu solder paste decreases the IMC thickness and size of β-Sn sub grains when compared with solders without SiC nano-particles. This is due to the strong adsorption effect and high surface free energy of the SiC nano-particles. The microhardness of SAC + SiC composite is 44% more than a non composite SAC alloy. Further increase in the addition of SiC (>0.05 wt%) to the matrix results in the entanglement of SiC particles in the bulk solder. Therefore, a significant reduction in the IMC size cannot observed in the composites containing more than 0.05 wt% SiC nano-particles [Liu et al. 2008].

Carbon nanotubes (CNTs) are widely known to have exceptional and attractive physical, thermal, electrical and mechanical properties. CNTs possess almost 100 times the tensile strength (approximately 150 GPa) of high-strength steel alloys. These extraordinary unique qualities make them suitable for making many novel composites to overcome the performance limits of conventional materials [Kumar et al. 2006, Nai et al. 2008]. Nai et al (2006) used 95.8Sn–3.5Ag–0.7Cu with particle size of about 25–45 μm as matrix alloy and multiwall carbon nanotubes (MWCNT) of length 100 μm and 3–20 nm outer diameter as fillers. The composite solder joints showed lower diffusion coefficient when compared to monolithic solder joints indicating the presence of CNTs as reinforcements in solder joints was effective in retarding the growth of the IMC. In order to achieve efficient load transfer during loading, it is essential to have good interfacial bonding between the CNTs and the solder matrix. However, for composite solder materials, the formation of CNT clusters in the solder matrix could hinder effective bonding between the CNTs and the solder particles. Therefore, at higher amount of CNT additions (0.04 and 0.07 wt%), Nai et al (2006) observed only a marginal improvement in the strength value as compared to that of monolithic solder joint. This could also be associated with the higher level of microporosity observed at higher weight percentage of CNTs. Kumar et al. [2006, 2008] added single wall carbon nanotubes (SWCNT) to Sn–3.8Ag–0.7Cu solder and observed an increase in UTS and hardness with the increase of SWCNT up to 1 wt%. The nanotubes were found to be distributed at the edges of grain boundaries of Ag_3Sn intermetallic. The enhanced mechanical properties could be attributed to the effective load-transfer between the solder matrix and the nanotubes. The effect of brittle reinforcement content on strength and ductility of the composite solder can be explained by the strengthening mechanisms such as stress gathering capability of the reinforcing particles, increase in dislocation density, thermally induced matrix work hardening, and significant reduction in the average size/morphology of the secondary phases of the composite solder with the increasing wt% addition of nanotubes. To date, studies by several researchers have shown that, addition of CNTs into conventional solder alloy, convincingly improves the performance. However, researchers are not yet able to take out the full advantage of outstanding properties of CNTs due to few limiting factors, for instance: (1) the difficulty of homogeneously dispersing CNTs in the metal-based matrix, and (2) insufficient bonding at the nanotube– matrix interface. Research has to be carried out to overcome these problems [Han et al. 2012].

It is also found that addition of oxide nano powders such as TiO_2, ZrO_2 etc improves the strength of solder joints. Tsao (2011) noted that addition of 0.5 wt.% nano TiO_2 to Sn-3.5Ag-0.5Cu suppresses the growth of intermetallic compounds. The reduced diffusion coefficient of SAC composite solder/ Cu joints to SAC solder/Cu joints indicated the positive result of nano TiO_2 addition. A stronger affinity of Ag and Sn in the case of nano

TiO_2 addition in to SAC solder, increases the precipitation or adsorption of Ag_3Sn nano particles on Cu_6Sn_5 grain surface and may decrease the activity of Sn atoms effectively suppressing the growth of overall IMC layer. Due to dispersion strengthening the ultimate tensile strength, yield strength and microhardness of the composite solder increases with TiO_2 content from 0.25 to 1 wt.% but the ductility decreases because of the microporosity at the Ag_3Sn grain boundary. Fouzder et al (2011) studied the influence of $SrTiO_3$ nano-particles on the microstructure and shear strength of SAC solder on Au/Ni metallized Cu pads and found that addition of 0.5 wt% $SrTiO_3$ to Sn-3.0Ag-0.5Cu improves the shear strength of the solder joint due to the second phase dispersion strengthening mechanism and refinement of Cu_6Sn_5, Ag_3Sn and $AuSn_4$ IMCs as well. $SrTiO_3$nano-particles are found to be dispersed throughout the β-matrix. The fine IMCs and $SrTiO_3$nano-particles improve the mechanical properties of the solder joint by pinning the grain boundaries. The solder joints containing $SrTiO_3$nano-particles underwent a ductile fracture with a very rough surface due to uniform dispersion of $SnTiO_3$nano-particles. Gain et al (2011) found that addition of ZrO_2 to SAC (Sn-3.0Ag-0.5Cu) solder improves the shear strength of the solder joint. ZrO_2 has few advantages over other nano-particles. For example, density of ZrO_2 is 5.83g/cm^3 which is almost similar to that of SAC, (density of Sn-3.0Ag-0.5Cu is 7.11g/cm^3) when compared to other ceramic particles such as Al_2O_3 (3.97g/cm^3) and SWCNT (1.3g/cm^3). ZrO_2 has higher hardness than Sn-3.0Ag-0.5Cu. The microstructure of Sn-Ag-Cu solder on Au/Ni metalized Cu pad has Ag_3Sn, Cu_6Sn_5 and $AuSn_4$ IMC particles distributed in the β-Sn matrix whereas SAC composite solder containing ZrO_2 nano-particles has uniformly distributed ZrO_2 nano-particles in the β-Sn matrix in addition to the microstructure of unreinforced SAC solder alloy. The thickness of IMCs found to be increased from 2.8μm to 6.7μm for unreinforced SAC solder joints and for the solder joint with 3 wt% ZrO_2 nano-particles it increased from 2μm to 5.2μm after the reflow process. The shear strengths of unreinforced SAC solder and solder joints with 3wt% ZrO_2 nano-particles after one reflow cycle were 38 MPa and 43.4 MPa respectively. The corresponding values after 16 reflow cycles were 31.6 MPa and 40.9 MPa respectively. At any number of reflow cycles the solder joints with high ZrO_2 nano-particles showed a consistently higher strength than that of the one with lower percentage of ZrO_2 nano-particles. So it is confirmed that ZrO_2 nano-particles resist the formation of IMC layers and growth as well. ZrO_2 nano-particles may alter the driving force for the growth of the IMC layer and the diffusivity of the elements involved in its growth. The ZrO_2 nano-particles may get adsorbed at the grain boundary and vary the relative relationship of the growth velocities between crystalline directions of IMC particles, in turn reducing the IMC particles size. Thus composite approach has great potential to improve the microstructure and hence mechanical properties of lead free solders.

2.6.4 Substrate surface finish

The manufactures use various surface finishes for example plating while soldering electronic devices on PCBs [Kim et al. 2003]. Whisker growth is a potential problem for the electronic product reliability. It is a surface relief phenomenon and whiskers relief the compressive stress in the matrix on which they grow. It has mainly arisen on electroplated Tin. Tin whisker growth from vapor deposited tin surfaces has also been reported [Kang et al. 2004, Osenbach et al. 2006, Jiang and Xian 2007]. Tin whisker is a conductive metal wire and it can grow over time with the use of tin plated or pure tin component finishes causing electrical shorts in the lead free solder. Tin whiskers can carry as high as 100 mA of current. Under some electrical/atmospheric conditions, whisker shorts may vaporize into conductive plasma of metal ions. Plasma forms arc capable of carrying hundreds of amps resulting in catastrophic damage [Pan et al. 2004]. There is no specific solution to prevent these whiskers. A thin layer of Ni can be electroplated before the electroplating of Sn, that is by creating a diffusion barrier between Sn and Cu, whisker growth rate can be reduced. This method can be adopted as the room temperature reaction between Sn and Ni is much slower than between Sn and Cu. Another method is to use Cu-Sn compounds as diffusion barrier. Cu_6Sn_5 and Cu_3Sn

compounds are good diffusion barriers to Cu diffusion at room temperature [Zeng and Tu 2002 Osenbach et al. 2006].

Surface finishes influence the wetting properties, interfacial reaction, thickness and composition of IMCs thus reliability of solder joints. Cu is the common metal utilized in contact with solders owing to its good solderability and excellent thermal conductivity. The Cu–Sn IMCs, Cu_6Sn_5 (thicker, adjacent to the bulk solder) and Cu_3Sn (thinner, adjacent to copper pad) between SAC and Cu pad exhibit scallop and layer morphology respectively. The Cu–Sn interdiffusion process continues during solid state reaction. With the increase in aging time Cu_6Sn_5 becomes thicker and more uniform layer. Meanwhile, the thickness of Cu_3Sn layer also grows at the expense of Cu. In addition, some voids form at the Cu–Cu_3Sn interface and in the Cu_3Sn IMC layer after thermal aging for about 500–1,000 h above 100 °C [Kim et al. 2011]. For the two elements Cu and Sn, Cu is the dominant diffusing species through Cu_3Sn and Cu_6Sn_5. In the Cu–SAC solder reaction couple, the diffusing Cu atoms arrive at Cu_3Sn-Cu and Cu_6Sn-solder interfaces and result in the growth of both IMC layers towards the solder. Because of the unbalanced Cu-Sn inter diffusion through interface, atomic-level vacancies left by the migrating Cu atoms on the bare Cu side are not filled by Sn atoms. Theses vacancies coalesce into the so-called Kirkendall voids [Liu et al. 2000, Mei et al. 2005, Xu and Pang 2006]. Voids reduce the mechanical properties of the board level interconnections and affect the conductivity performance and reliability of solder joints. For a bare Cu pad-SnAgCu solder interconnect system, Kirkendall voiding at the Cu and Cu_3Sn IMC interface is main mechanism for degradation of joint strength under thermal aging. The voiding process is activated at temperature as low as 100 °C. Since the interfacial voiding was shown to be detrimental to shock reliability of the system, Cu–SnAgCu solder system is not recommended to use in high temperature application. The growth rate of these voids are exponential with temperature and therefore increases significantly at higher temperatures particularly 125 °C and above, and these Kirkendall voids cause precipitous fall in solder joint reliability [Zeng et al. 2010]. Various surface finishes are applied to overcome these problems. Typical pad metallizations include elecroless nickel immersion gold (ENIG), organic solderability preservative (OSP), Ni–Au, Ni–Pd, immersion Sn (ImSn), immersion Ag (ImAg) lead-free (SAC or Sn-Cu) hot-air solder leveling (HASL) etc [Amore et al. 2008, Choubey et al. 2008, Sona and Prabhu 2015]. Song et al (2006) attached Sn–4.0 %Ag–0.5 %Cu on the package substrates with OSP and ENIG surface finish and found that IMC growth rates in solders on OSP surface finish is higher than that on ENIG. Compared with Sn/Cu system, the apparent activation energy ΔH for Sn/Ni is higher. Hence, Ni is used as a barrier layer to prevent fast consumption of Cu substrate [Xu and Pang 2006]. However, there are situations where rapid diffusion still exists through the breached regions in the nickel layer. To overcome this issue Ni layer is often coated with another layer of Au. In addition, Au layer helps to protect against oxidation [Nai et al. 2009]. Doping Zn into Cu substrates has many advantages for soldering, such as the suppression of large Ag_3Sn compounds, the elimination of Cu_3Sn and Kirkendall voids during thermal aging, and the good drop, creep, and tensile resistances. Therefore, it is expected that Zn containing Cu under bump metallization (UBM) can solve problems encountered in Ni-doped solder joints.

Chen et al (2012) studied the evolution of interfacial phase in Sn–3.0Ag–0.5Cu/Cu (wt%), Sn–3.0Ag–0.5Cu–0.1Ni/Cu, Sn–3.0Ag–0.5Cu/Cu–15Zn, and Sn–3.0Ag–0.5Cu–0.1Ni/Cu–15Zn solder joints. After reflow, scallop-type Cu_6Sn_5 and $Cu_6(Sn,Zn)_5$ was found at the SAC305/Cu and SAC305/Cu–15Zn interfaces respectively. Ni doped in the SAC305–0.1Ni/Cu and SAC305–0.1Ni/Cu–15Zn solder joints changed the morphology of IMCs from scallop-type to layer-type. Moreover, Zn diffused from the Cu–15Zn substrate to suppress the formation of Cu_3Sn at the SAC305/Cu–15Zn and SAC305–0.1Ni/Cu–15Zn interfaces while thin Cu_3Sn layer was present in the solder joints with Cu substrates. During aging at 150 °C, a thick Cu_3Sn layer was observed at the interface between Cu_6Sn_5 and Cu substrate in the SAC305/Cu solder joint and many Kirkendall voids were present in the Cu_3Sn layer while in the SAC305–0.1Ni/Cu solder joint, a thin $(Cu,Ni)_3Sn$ formed at the interface and several Kirkendall voids were found in the

$(Cu,Ni)_3$ Sn layer. SAC305/Cu–15Zn and SAC305–0.1Ni/Cu–15Zn solder joints, neither showed formation of any Cu_3Sn IMC layer nor Kirkendall voids even after aging at 150 °C for 960 h. The SAC305–0.1Ni/Cu–15Zn solder joint exhibited the thinnest and only one $(Cu,Ni)_6(Sn,Zn)_5$ IMC without any voids. The growth of interfacial $(Cu,Ni)_6(Sn,Zn)_5$ was insensitive to the solid state aging, owing to Zn and Ni re-distribution at the joint interface. Kim et al (2012) used electroless nickel/electroless palladium/immersion gold (ENEPIG) surface finish and the mechanical strength of the SAC305/ENEPIG solder joints were investigated at various Pd thicknesses (0–0.5 μm). The $(Cu,Ni)_6Sn_5$ phase formed at the SAC/ENEPIG interface after reflow in all samples. $(Pd,Ni)Sn_4$ phase was found on $(Cu,Ni)_6Sn_5$ when the Pd thickness was almost equal or greater than 0.1 μm. A very thick layer of $(Pd,Ni)Sn_4$ was formed when Pd thickness was 0.3 μm. The interfacial strengths of the SAC/ENEPIG solder joints decreased under high strain rate due to weak interfacial fracture between $(Pd,Ni)Sn_4$ and $(Cu,Ni)_6Sn_5$ interfaces when the Pd thickness was greater than 0.3 μm. The mechanical strength of the SAC/ENEPIG solder joints was enhanced as the Pd thickness increased to 0.1 μm. Berthou et al (2009) studied aging of lead free assembled chip resistors and BGA, with either ENIG or immersion Sn finishes at 80 °C, 125 °C and 150 °C for 1,000 h and found that IMC thickness for a Sn PCB finish was higher than NiAu finish. This was again due to the nickel barrier. Hayes et al (2009) investigated the IMC growth associated with Sn–4.0Ag–0.5Cu solders on Ni–Au, Ni–Pd metallizations. $(Ni,Cu)_3Sn_4$ was present at the Ni interface for both the cases but was coarser and with greater variation in thickness in the case of Ni–Pd. Cu_6Sn_5 and Cu_3Sn were observed for both solder types. Wang et al (2012) used Sn-3.0Ag-0.5Cu solder doped with 0, 100, and 500 ppm Pd in his work and reflowed them on electroless Ni/immersion Au substrate. During reflow process, Ni diffused into the solder alloy from substrate leading to the formation of needle-like $(Cu,Ni)_6Sn_5$ at the interface of the substrate and solder alloy. In comparison with SAC305–0Pd system, the thickness of $(Cu,Ni)_6Sn_5$ was found to be smaller in SAC305–0.05Pd. The Pd additive would trap Cu atoms and precipitated with Cu atoms as $(Cu,Pd)_6Sn_5$. Thus, the growth of interfacial $(Cu,Ni)_6Sn_5$ was restrained. In the Pd doped system, $Cu_4Ni_2Sn_5$ grew continually at the

SAC305–0.05Pd interface. In contrast, $Cu_4Ni_2Sn_5$ grew slowly and Cu_5NiSn_5 formed rapidly in the SnAC305–0Pd joint. This study provides a new SAC305 solder ball design with minor Pd doping, which could reduce the growth of $(Cu,Ni)_6Sn_5$ and promote the formation of stable $Cu_4Ni_2Sn_5$.

Gu et al (2007) employed an electroless Ni–P–carbon nanotubes (Ni–P–CNTs) composite coating as a pad finish for electronic packaging. Electroless Ni–P and electroless Ni–P–CNTs composite coatings with the same P-contents were prepared. A Ni_3Sn_4 IMC layer and a P-rich layer were formed in the solder joints on both coatings after multiple reflows. The IMC layers were compact with chunky-shaped grains in SAC/Ni–P solder joints, whilst porous with needle-shaped grains in the case of SAC/Ni–P–CNTs solder joints. The CNTs dispersed in the Ni–P coating acted as a retardant in the reaction of the Ni with the solder hence growth rates of both the Ni_3Sn_4 IMC layer and the P richer layer in the SAC/Ni–P–CNTs solder joints were slower than those in the SAC/Ni–P solder joints. It was also found that the CNTs in the coating increased the brittleness of solder joints and weakened their shear strength. More brittle fractures occurred in the IMC layer in the Sn–4Ag–0.5Cu/Ni–P–CNTs solder joints during shearing tests. Choubey et al. (2008) used Sn–3.0Ag–0.5Cu solder and ImAg, ImSn, OSP and ENIG pad finishes in their study and found that, after 350 h of aging at 125 °C, the IMC growth in the solder joints of the ImSn, ImAg and OSP were comparable, whereas the ENIG pad finishes showed a lower IMC thickness. After 1,000 h of aging at 100 °C, the IMC thickness was found to be approximately 3 μm, which was 1 μm less than the IMC thickness at 125 °C for the joints aged 1,000 h. In fact, the IMC growth for SAC305 at 350 h and 125 °C was significantly greater than the growth after 1,000 h at 100 °C. IMC thickness on various surface finishes is given in Table 2.5. ENIG is preferable for long term reliability applications to ImSn, ImAg, and OSP finishes. OSP finish can be used for short-term reliability applications since it is economical compared with ImSn, ENIG, and ImAg, also results in comparable IMC thickness but applications prone to tin whisker formation should avoid ImSn finish. Care must be taken while using PCBs with an OSP finish since it is an organic finish and prone to contamination, which can lead to reliability problems. ImAg finish is highly sensitive to plating chemistry and hence is prone to champaign voids, and should be avoided as a primary choice for PCB finish [Choubey et al. 2008].

Though ENIG is suggested for long-term applications, it is prone to black pad, which forms during a plating process and can lead to early failures. Black pad is associated with the phosphorous content in the electroless nickel coating bath. During electroless process, a few atomic percent of phosphorous are co-deposited with Ni. The presence of P with Ni complicates the chemical reactions between Ni and solder. High phosphorous content gives good corrosion resistance but induces solder joint embrittlement with the growth of an intermetallic layer through phosphorus enrichment during soldering. Low phosphorous content in the electroless nickel coating results in poor corrosion resistance [Pan et al. 2004]

Table 2.5: IMC thickness on various surface finishes

IMC thickness on Ni/Au PCB finish	t=0 h ≈1.75 μm	t=500 h (125˚C) ≈2.4 μm	t=1000 h (125˚C) ≈2.5 μm	[Berthou et al. 2009]
	t=0 h ≈1.75 μm	t=500 h (150˚C) ≈3 μm	t=1000 h (150˚C) ≈3.6 μm	
IMC thickness on Sn PCB finish	t=0 h ≈3.9 μm	t=500 h (125˚C) ≈4.4 μm	t=1000 h (125˚C) ≈5.1 μm	[Berthou et al. 2009]
	t=0 h ≈3.9 μm	t=500 h (150˚C) ≈6.4 μm	t=1000 h (150˚C) ≈8 μm	
Sn-4.0Ag-0.5Cu+OSP	t=0 h ≈2μm	t=500 h (150˚C) ≈7μm	t=1000 h (150˚C) ≈9.1μm	[Song et al. 2007]
Sn-4.0Ag-0.5Cu +ENIG	t=0 h ≈1.1 μm	t=500 h (150˚C) ≈2.6 μm	t=1000 h (150˚C) ≈3.3 μm	[Song et al. 2007]

95.5Sn-3.8Ag-0.7Cu+ENIG	t=0 h ≈1.6 μm	t=250 h (150˚C) ≈6.9 μm	t=400h (150˚C) ≈7.4 μm	[Berthou et al. 2009]
	t=0 h ≈1.6 μm	t=250 h (125˚C) ≈2.8 μm	t=400 h (125˚C) ≈3 μm	
Sn-3.0Ag-0.5Cu+ENIG	t=0 h ≈1.5 μm	t=350 h (100˚C) ≈3.1 μm	t=1000 h (100˚C) ≈3.3 μm	[Choubey et al. 2008]
	t=0 h —	t=350 h (125˚C) ≈2.8μm	t=1000 h (125˚C) ≈3.6 μm	
Sn-3.0Ag-0.5Cu+OSP	t=0 h ≈2.5 μm	t=350 h (125˚C) ≈3.4 μm	t=1000 h (125˚C) ≈3.6 μm	[Choubey et al. 2008]
Sn-3.0Ag-0.5Cu+ImSn	t=0 h ≈2 μm	t=350 h (100˚C) ≈2.9 μm	t=1000 h (100˚C) ≈3.1 μm	[Choubey et al. 2008]
	t=0 h ≈2 μm	t=350 h (125˚C) ≈3.5 μm	t=1000 h (125˚C) ≈4.3 μm	
Sn-3.0Ag-0.5Cu+ImAg	t=0 h ≈2.2 μm	t=350h (100˚C) ≈2.7 μm	t=1000 h (100˚C) ≈2.9μm	[Choubey et al. 2008]
	t=0 h ≈2.2 μm	t=350h (125˚C) ≈3.85 μm	t=1000 h (125˚C) ≈3.85 μm	

[t is aging time in hours]

Islam et al (2003) investigated the dissolution kinetics of electrolytic Ni and electroless NiP metallization for Sn-3.5Ag-0.5Cu solder reflowed at 250 °C. After as reflow, all sample were kept again in 250 °C for 5, 10, 30, 120, and 180 min. It was concluded from the experiment that the appearance of P-rich nickel layer acts as a diffusion barrier and decreases the IMC growth rate than that of the electrolytic Ni layer. However, this weakens the interface and reduces the ball shear strength and reliability. You et al (2009) studied the reliability of eutectic Sn–Pb, Sn–1.0Ag–0.5Cu, Sn–3.0Ag–0.5Cu and Sn–4.0Ag–0.5Cu solder alloys on three different pad surface finishes (ENIG, electrolytic

Ni/Au and OSP). The results showed that the electrolytic Ni/Au surface finish ha the highest fracture forces for all three different SAC solder alloys whereas the average fracture force of the Sn–Pb solder joint was independent of the type of surface finish. Among SAC solder alloys Sn–1.0Ag–0.5Cu and Sn–3.0Ag–0.5Cu showed comparable fracture forces on Ni-Au surface finish. Use of gold coating over Electroless Ni or electrolytic Ni to protect Ni from oxidation may hinder the mechanical properties of solder joint. Due to the high dissolution rate and solubility of Au in the molten solder, the entire Au layer disappears from the joint interface after a typical reflow and a large number of the $(Au_xNi_{1-x})Sn_4$ particles are formed inside the bulk solder. During solid state annealing, regrouping of $(Au_xNi_{1-x})Sn_4$ at the solder/substrate interface takes place which in turn reduces the mechanical properties of the joint [Chen and Lin 2006].

2.7 SUMMARY

Solder helps to achieve a durable and reliable electronic connection. Eutectic Sn-37Pb is the conventional solder alloy used in the electronics industry. The awareness of the adverse effects of toxic Pb on both health and the environment, coupled with the implementation of legislation to ban the use of lead based solders, has led to the development of new lead-free solders.

Design and development of new lead free solders require a sound understanding of wetting behaviour of solder alloys, evolution of microstructure, IMC formation at the interface and their interaction. Evolution of microstructure in lead free solders has a significant influence on their mechanical and electrical properties. Formation of IMC is necessary for proper wetting of the solder to the substrate however, massive IMCs present at the interface may decrease the mechanical properties of the entire joint. SAC alloys are the most attractive lead free solders because of their better mechanical properties and thermal fatigue behaviour than the conventional Sn-Pb solder. Sn-xAg-Cu solders with high Ag content (x>3 mass%) are reported to give good temperature cycling reliability but poor drop impact reliability whereas Sn-xAg-Cu solders with low Ag content (x<2 mass%) show poor temperature cycling reliability but good drop impact reliability. Therefore, most semiconductor package assemblers are forced to implement multiple lead free alloys depending on intended performance. Limitations of the SAC solder can be overcome either by alloying or by composite approach. Addition of rare earth elements bring down the rate of formation of the IMC layers by changing the diffusion co-efficient. The addition of second phase nano-particles change the driving force for growth of intermetallic layer as well as the diffusivity of the elements involved in its growth. Nano-particles get adsorbed at the grain boundary and vary the relative relationship of growth velocities between crystalline directions of IMC particles, in turn reducing the IMC particle size. Ni plays a dual role in soldering. It acts as good diffusion barrier and it slows down the growth rate of IMCs which are prone to crack formation.

A better understanding of the effect of soldering process variables on evolution of microstructure and joint strength is essential for accurate prediction of the reliability of solder joints.

2.8 SCOPE AND OBJECTIVES OF THE PRESENT INVESTIGATION

Reliability of the solder joint depends on various parameters such as reflow time, reflow temperature, substrate surface roughness, substrate surface coating, cooling rate, wettability, IMC thickness and morphology [Laurila et al. 2005]. Research work carried out so far on lead free solders were mainly focused on the study of the effect of reflow time on interfacial microstructure. Few researchers have discussed its effect on both the interfacial microstructure and the resulting joint strength. Efforts were made to improve the joint strength by alloying addition, composite approach and so on, but, there is no clear understanding about the effect of reflow time on wettability of solder alloy on the substrate. The wettability was assessed by measuring the equilibrium contact angle in all the previous research work. It is well known that the interfacial reaction takes place immediately once the liquid metal contacts the substrate. Hence, a correlation between the equilibrium contact angle and the joint strength may be misleading particularly in the case of reactive systems. Under such circumstances, spreading kinetics has to be taken in to account. Therefore, a detailed study on effect of reflow time on solder joint reliability is very much desired for correlating the wettability of liquid solder to the microstructure and joint strength.

Following are the objectives of the present investigation.

1. To study the wetting kinetics and joint strength of lead free solder alloys
1. To study and compare the wetting kinetics of lead based and lead free solders
2. To determine the effect of surface coating on wetting kinetics and joint strength of lead free solders.
3. To correlate the kinetics of wetting of lead free solders with microstructure evolution and solder joint reliability.

CHAPTER 3

EXPERIMENTAL WORK

The commercial eutectic Sn-0.7Cu, hypoeutectic Sn-0.3Ag-0.7Cu and Sn-2.5Ag-0.5Cu lead free solder alloys were used in the present study. The composition of lead free solder alloys is given in Table 3.1.

Table 3.1: Composition of lead free solder alloys

Solder alloys	Element in wt. pct.			Remark
	Sn	Ag	Cu	
Sn-0.7Cu	99.3	--	0.7	Multicore Manufacturers, UK
Sn-0.3Ag-0.7Cu	99	0.3	0.7	Alpha Electronics Manufacturers, UK
Sn-2.5Ag-0.5Cu	97	2.5	0.5	Antex Electronics Manufacturers, UK
Sn-3Ag-0.5Cu	96.5	3	0.5	Alpha Electronics Manufacturers, UK

Bare and Ni coated Cu were used as substrate materials. The dimension of both substrates was ϕ12 mm x 8 mm. To investigate the wetting behaviour of lead-free solders on bare and Ni coated Cu substrates, the solder drop spreading experiments were carried out. Initially Cu substrates (Ø12mm X 8mm) were polished using SiC papers of varying grit sizes (1/0–4/0 grade) followed by velvet cloth disk polish using diamond-lapping compound to acquire smooth surface finish. An equal number of Cu substrates were electroplated with Ni. The thickness of electroplated Ni layer on top of Cu substrate was about 15μm.

3.1 Measurement of Surface Roughness

The surface profiles of substrates were measured using Form Talysurf 50 surface profiler. The arithmetic mean roughness (R_a) values were in the range of 0.01±0.006 µm and 0.04±0.008 µm for bare and Ni coated Cu substrates respectively. Each surface profile assessment was carried out at least three times and the mean values of parameters were used in the analysis of the results. A schematic of the surface profiler and the principle of measurement of surface texture are shown in Figure 3.1.

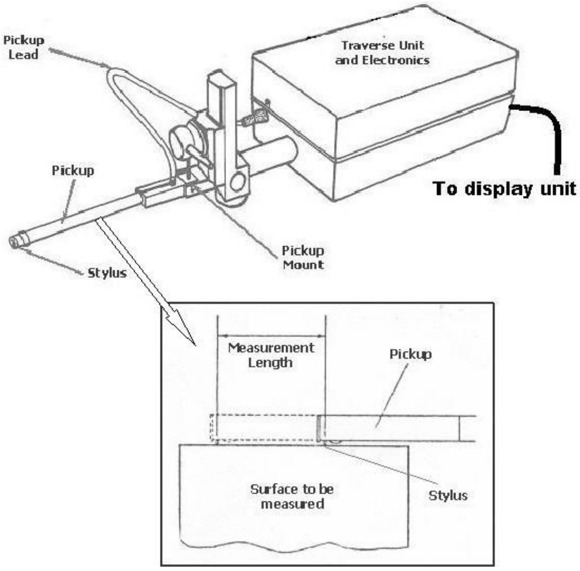

Fig. 3.1: Schematic of surface profiler

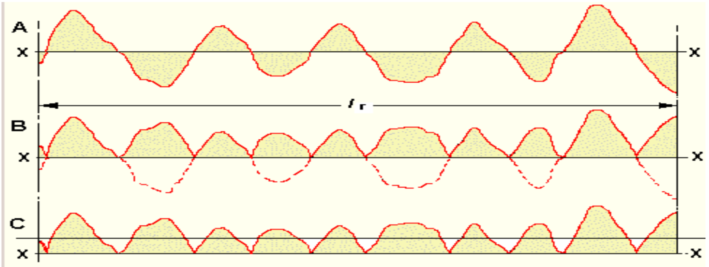

Fig. 3.2: Procedure for the calculation of average roughness index (R_a)

The unit consists of a traversing pickup driven by a motor. The pickup is pulled across the surface for a preset distance. A diamond tip stylus moves on the surface and records the variations of the surface. The Form Talysurf software (Ultra version 5.1.14) measures the roughness parameters of the surface. R_a is the most commonly used parameter in industry for measurement of surface roughness. Mathematically, it is the arithmetic average value of the profile departure from the mean line within a sampling length. A mean line (X-X) is fitted to the measurement profile as shown in Graph A of Figure 3.2. The portions of the profile within the sampling length "l" and below the mean line are then inverted and placed above the line (Graph B of Figure 3.2). R_a is the mean height of the profile above the original mean line.

The equation for calculating the arithmetic mean deviation or R_a is as follows

$$R_a = 1/L \int_0^L | A(X)| dx$$

Usually five consecutive sampling lengths are taken as standard. Figure 3.3 shows the photograph of the Form Talysurf surface profiler.

Fig. 3.3: Photograph of surface profiler (Form Talysurf 50)

3.2 Measurement of contact angle

FTA 200 dynamic contact analyzer was used for the assessment of spreading behaviour of solder alloys on metallic substrates. The equipment has a flexible video system for measuring contact angle, surface and interfacial tensions. An environmental chamber with heating element and temperature controller form the accessory for melting the solder on the substrate for wetting studies. The system can capture both static and dynamic spreading phenomena. The chamber is enclosed in a sheet metal case packed with insulating material (Kaowool) to prevent heat loss to the surrounding. The initial heating rate obtained with the chamber is about 3-4 °C/minute, which eventually reduces as the chamber temperature approaches the set value. Figure 3.4 shows the photograph of the equipment with environmental chamber. Spherical balls of lead free solder alloy weighing approximately 0.08 g (average diameter 2.76±0.035 mm) were prepared from solder wires. A soldering station (ERSA 2000A) was used to prepare solder spheres. Both substrate and solder ball were cleaned using ultrasonic vibrator successively with acetone for about 20 minutes before placing them in the heating chamber. The solder ball was placed on the substrate, after coating the substrate surface with flux (Inorganic acid, Alfa Aesar, USA). The solder/substrate system was then kept inside the environmental chamber. The chamber was heated to a pre-set temperature (above the liquidus of solder alloys) of 270°C and maintained at that temperature throughout the experiment.

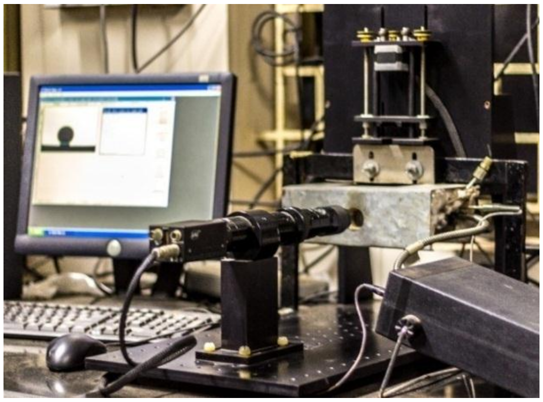

Fig. 3.4: Dynamic contact angle analyzer (FTA 200)

The spreading process was recorded for 10, 100, 300, 500, 1000 and 10000 s individually and the captured images were analyzed using FTA software (FTA 32 Video 2.0) to determine the spreading behaviour of the solder. Spreading behavior of eutectic Sn-Pb solder alloy on bare and Ni coated Cu substrate was also studied to compare the wetting kinetics with lead free solder alloys. The eutectic Sn-Pb solder balls had a diameter of about 2.60 ± 0.04 mm and weight was about 0.08 g. The reflow temperature and reflow time was fixed at 240 °C and 100 s for Sn-Pb solder alloy. Environmental chamber was turned off after the desired reflow time. Solder/substrate system was then allowed to cool to room temperature inside the environmental chamber. Final contact angle (θ_f) was measured as the solder/substrate system achieved room temperature. These samples are named as furnace cooled samples hereafter.

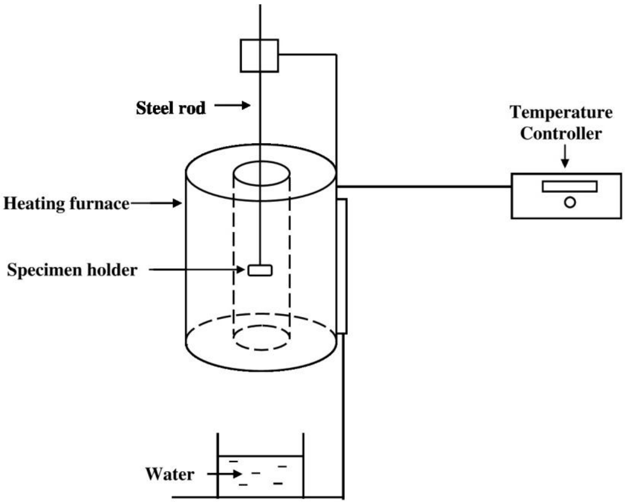

Fig. 3.5: Schematic of quench cooling set up

Another set of similar solder/substrate systems were prepared where quench cooling method was adopted to cool the sample at desired reflow time. This method was adopted to arrest the microstructure at desired reflow time. Figure 3.5 shows the schematic of quench cooling set up. It consists of steel rod with a specimen holder. The specimen holder was loaded with the solder/substrate system and the steel rod was held in position inside the hot zone of the vertical tubular furnace. The vertical tubular furnace was maintained at a reflow temperature of 270 ºC throughout the experiment. Reflow time was counted as the solder started spreading. At the end of reflow time, the steel rod was released and the solder/substrate system was quenched in water kept in a 2 ltr beaker just below the furnace.

3.3 Microexamination

Zeiss stereomicroscope (Stemi 2000-C) was used for obtaining macro images of the solder sessile drop after spreading. The solder drop bonded to the substrate was sectioned along the axis (Figure 3.6) using Isomet low speed precision cutter. The sectioned samples were polished using SiC papers of 1/0, 2/0, 3/0 and 4/0 grades followed by velvet cloth disk polish using colloidal silica polishing suspension. The polished samples were then etched with 5% nital for about 3–5s. The solder/substrate interfacial region was examined under scanning electron microscope (SEM, JEOL JSM 6380LA) combined with energy-dispersive spectroscopy (EDS) in order to study the reaction between the alloy and the solid substrate and the possible formation of different compounds at the interface. X-ray diffraction (XRD) study was carried out to identify and characterize the IMCs at the solder/substrate interfacial region. A JEOL JDX-8P-XRD system was used for this purpose. The matrix of experimental work carried out in the present investigation is presented in Table 3.2

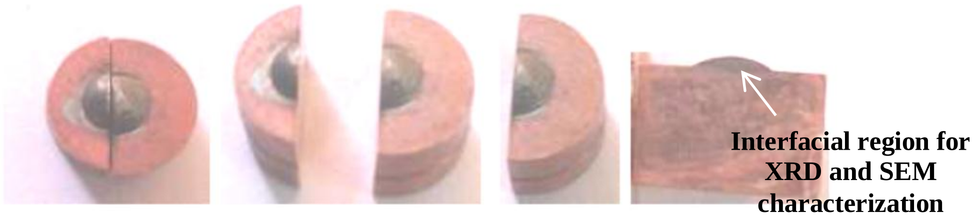

Fig. 3.6: Sectioning of bonded solder drop for micro examination

3.4 Shear test of solder droplet samples

The strength of the solder joint was assessed by performing shear test on solder droplet samples using the Nordson DAGE 4000Plus bond tester. Figure 3.7 shows the photograph of Dage 4000Plus bond tester. The procedure for conducting a shear test on solder droplet samples is shown in Figure 3.8.

Fig. 3.7: Nordson Dage 4000Plus bond tester

Table 3.2: Experimental matrix

Substrate	**Surface texture**	**Cooling method**	**Solder alloys**														
			Sn-0.7Cu					**Sn-0.3Ag-0.7Cu**					**Sn-2.5Ag-0.5Cu**				
			Reflow time (s)														
			10	25	100	300	500	10	40	100	300	500	10	40	100	300	500
Copper	Mirror finished	Furnace cooling	✓	✓	✓	✓	✓	✓	✓	✓	✓	✓	✓	✓	✓	✓	✓
		Quench cooling	✓	✓	✓	✓	✓	✓	✓	✓	✓	✓	✓	✓	✓	✓	✓
Substrate	**Coating**	**Cooling method**	**Reflow time (s)**														
			10	50	100	300	500	10	80	100	300	500	10	80	100	300	500
Copper	Nickel	Quench cooling	✓	✓	✓	✓	✓	✓	✓	✓	✓	✓	✓	✓	✓	✓	✓

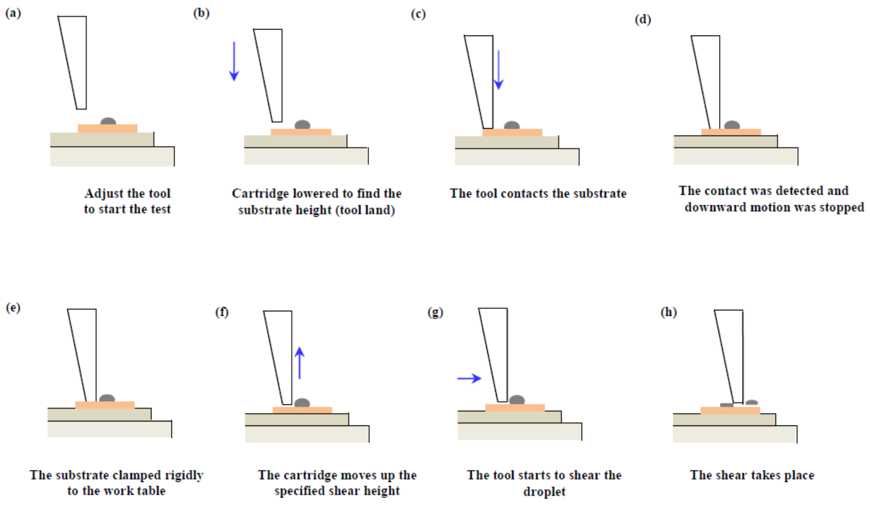

Fig. 3.8 Schematic sketches showing various stages of the shear test

The height of shear tool and the shear speed chosen were 1 μm and 200 μm/s respectively. The force–displacement curves were recorded during the shear test. After the ball shear test, failure mode was assessed by examining the fractured surface under scanning electron microscope.

3.5 Shear test of single lap solder joints

The shear test is designed according to the ‘‘Test method for shear tensile fatigue of spot weld joints’’ (GB/T151n-94). A schematic of the lap-shear geometry is shown in Figure 3.9. Smooth surfaced Cu plate was cut in to small pieces of dimensions of 50 mm x 6 mm x 1 mm. An equal number of Cu plates were metalized with Ni by electroplating method. The thickness of metallic layer was about 15 μm. The R_a value of bare and Ni coated Cu plate was in the range of 0.03±0.008μm and 0.04±0.007 μm respectively. Solder alloys were cut into many small pieces of dimensions 5 mm x 5 mm x 0.5 mm. The lead free solder was placed between two isometallic plates, and placed inside a tubular furnace (Figure 3.5) which is maintained at 270 °C. Similarly lap joint specimens of eutectic Sn-Pb solder alloy were prepared by placing eutectic Sn-Pb between two isometallic plates and keeping inside a tubular furnace which is maintained at 240 °C. Samples were reflowed for 10 s, T_{gz} (time corresponding to the end of gravity regime) and 100 s individually. Reflow time was counted as the solder started spreading. At the end of reflow time, the substrate/solder/substrate system was quenched in water kept below the tubular furnace. The single lap solder joints were tested at room temperature under a strain rate of 0.2×10^{-3} s^{-1} in a pull test carried out using INSTRON 5967 tensile tester (Figure 3.10). Stress-strain graphs were recorded during the test. After the test, failure mode was assessed by examining the fractured surface under the scanning electron microscope.

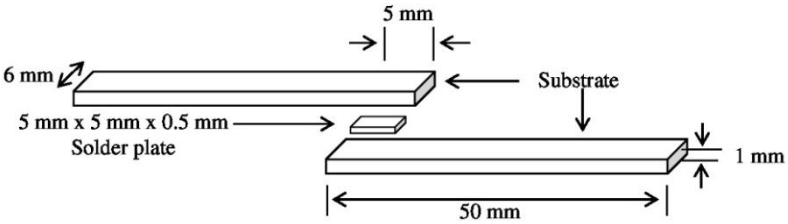

Fig. 3.9 A schematic of the lap-shear geometry

Fig. 3.10. INSTRON 5967 tensile tester

CHAPTER 4

RESULTS

4.1 Substrate surface roughness

Typical surface profiles of bare and Ni coated Cu cylindrical substrates (used for ball shear test) are presented in Figure 4.1a and 4.1b respectively. Corresponding average roughness (R_a) value is also mentioned. Similarly, surface profiles of bare and Ni coated Cu plates (used for lap joint shear test) are given in Figure 4.2a and 4.2b respectively.

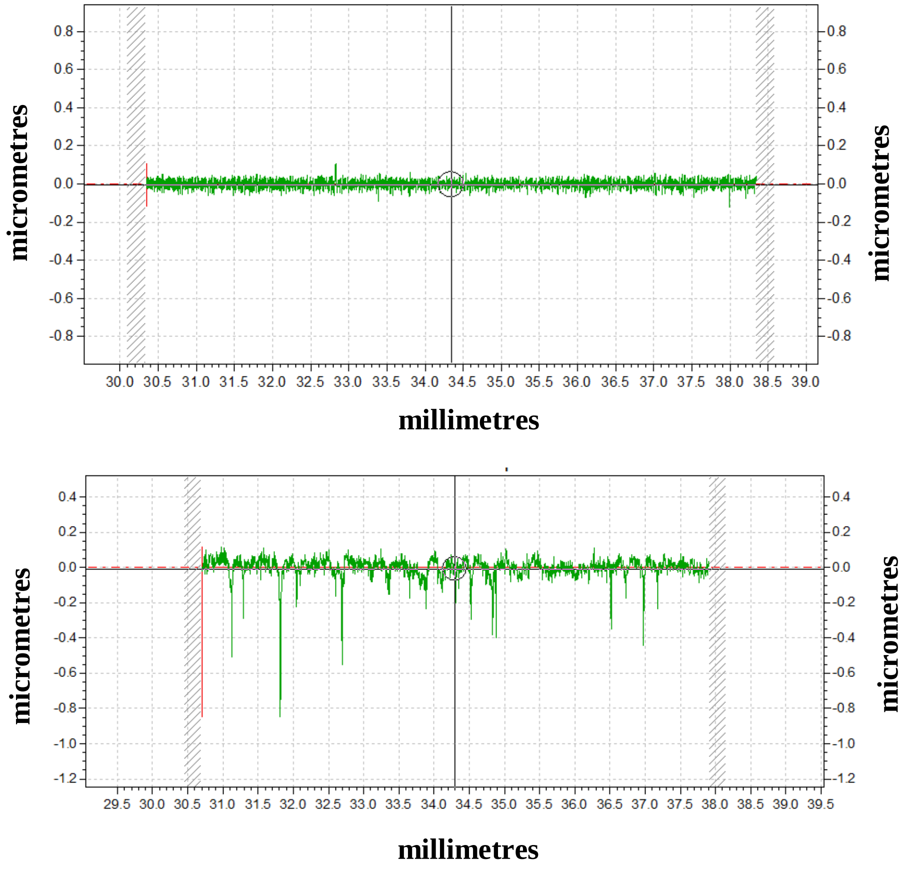

Fig. 4.1: Typical surface roughness profile of (a) bare Cu (R_a = 0.015µm) and (b) Ni coated Cu substrate ((R_a = 0.041µm)

Three reading were taken on each sample in three directions for consistency. The arithmetic mean roughness (R_a) values were in the range of 0.01 ± 0.006 µm and 0.04 ± 0.008 µm for bare and Ni coated Cu cylindrical substrates respectively. R_a values of bare and Ni coated Cu plates were in the range of 0.03 ± 0.008 µm and 0.04 ± 0.007 µm respectively.

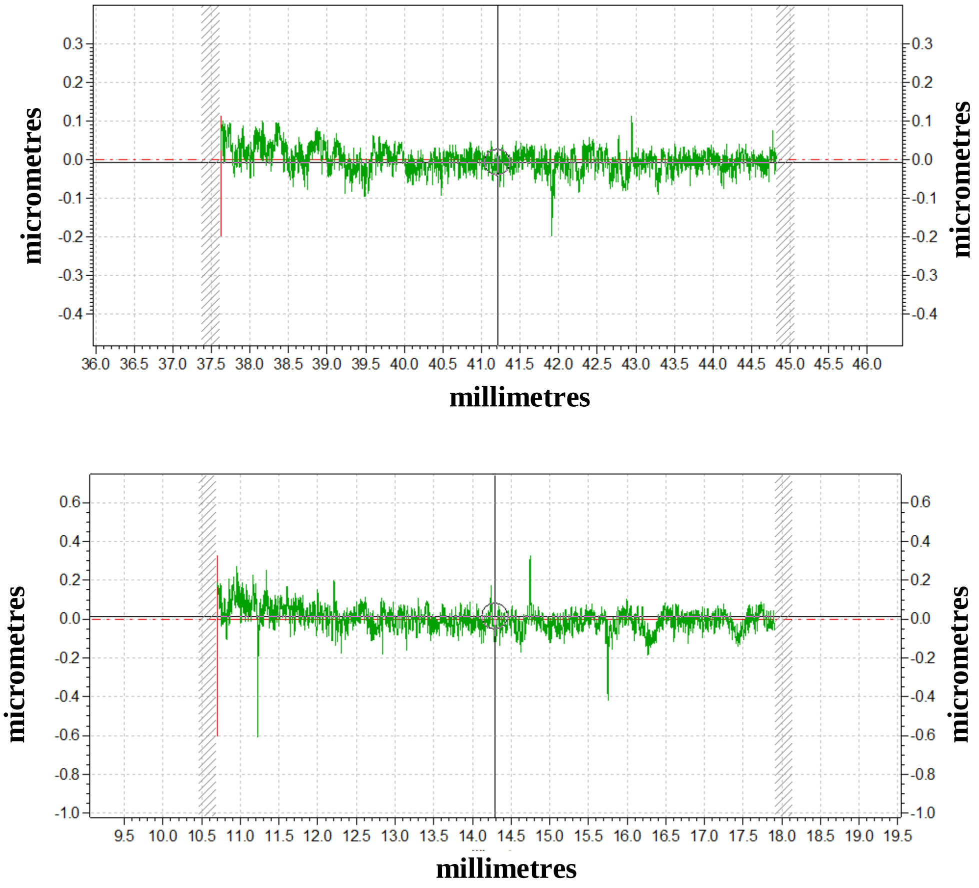

Fig. 4.2: Typical surface roughness profile of (a) bare Cu plate (R_a = 0.031µm) and (b) Ni coated Cu plate

4.2 General wetting behaviour of solder alloys

The time dependence of contact angle, solder drop base radius/drop base area was used as a tool to determine the spreading or relaxation behaviour of solder drop. Contact angle decreases with time as the spreading proceeds while both drop base radius and area increases with time. Similar trend was observed for each solder alloy, characterized by high spreading rate at the beginning followed by slower rate at later stages of spreading. Figure 4.3 and Figure 4.4 shows the typical relaxation behaviour of solder alloy in terms of contact angle versus time and base diameter versus time respectively. Each experiment is repeated thrice for consistency. Figure 4.5 shows the photographic images during successive spreading of solder alloy on the substrate.

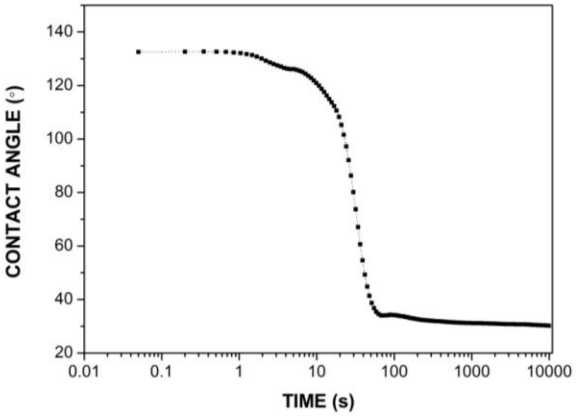

Fig. 4.3: Typical relaxation curve for solder alloy (contact angle versus time)

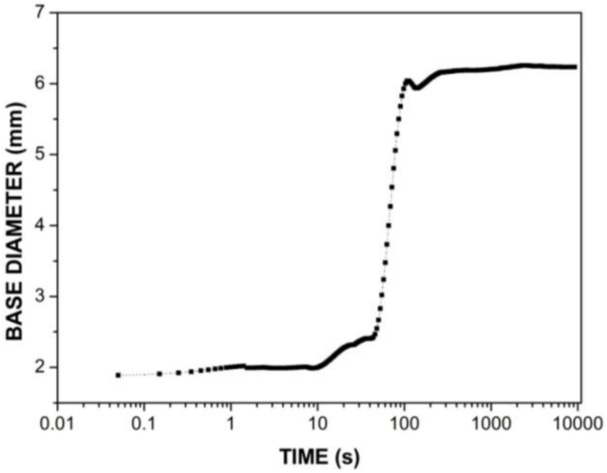

Fig. 4.4: Plot of base diameter versus time

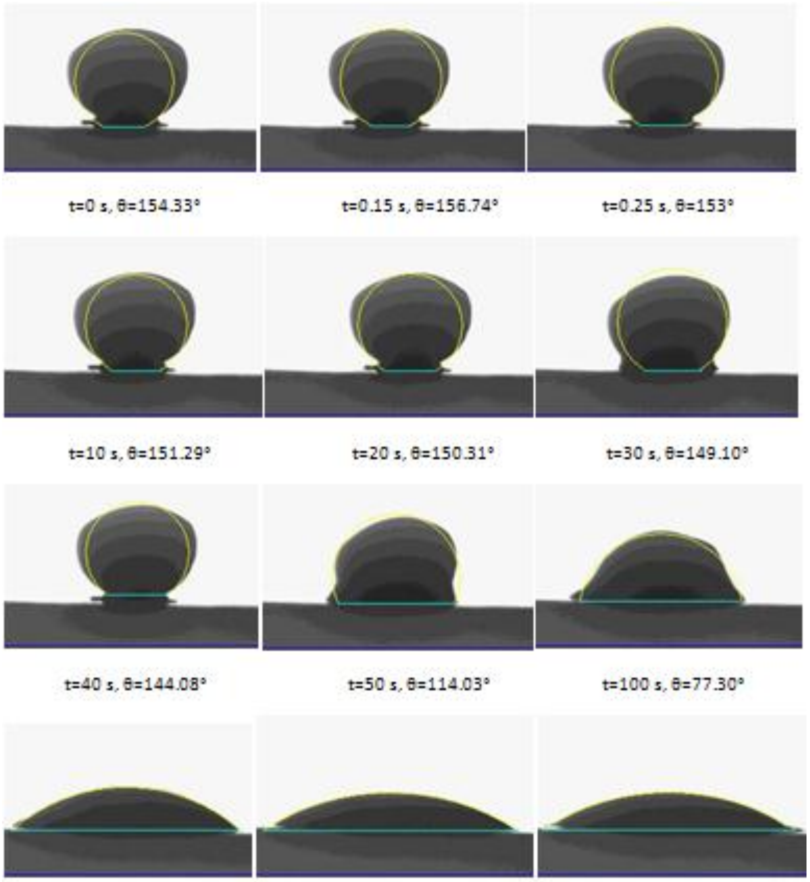

t=0 s, θ=154.33°
t=0.15 s, θ=156.74°
t=0.25 s, θ=153°
t=10 s, θ=151.29°
t=20 s, θ=150.31°
t=30 s, θ=149.10°
t=40 s, θ=144.08°
t=50 s, θ=114.03°
t=100 s, θ=77.30°
t=200 s, θ=41.41°
t=300 s, θ=33.38°
t=500 s, θ=32.44°

Fig. 4.5: Images of spreading droplet of Sn-0.3Ag-0.7Cu solder on Ni coated Cu substrate

4.3 Interfacial reactions between solder/substrate regions

The wetting of a molten solder on metallic surfaces is a complex phenomenon. In addition to physical spreading due to surface tension reduction, diffusion and chemical reactions take place in the solder/substrate interfacial region. Wetting of the liquid solder on a substrate is accompanied by the formation of intermetallic compounds at the interface. These intermetallic compounds act as a binder between solder and substrate. Hence, the microstructures at the solder/substrate interface were studied in order to analyze the nature of interfacial reactions taking place. Figure 4.6 and Figure 4.7 show the typical solder/substrate interface for the spreading of Sn-0.7Cu solder on bare and Ni coated Cu substrates respectively.

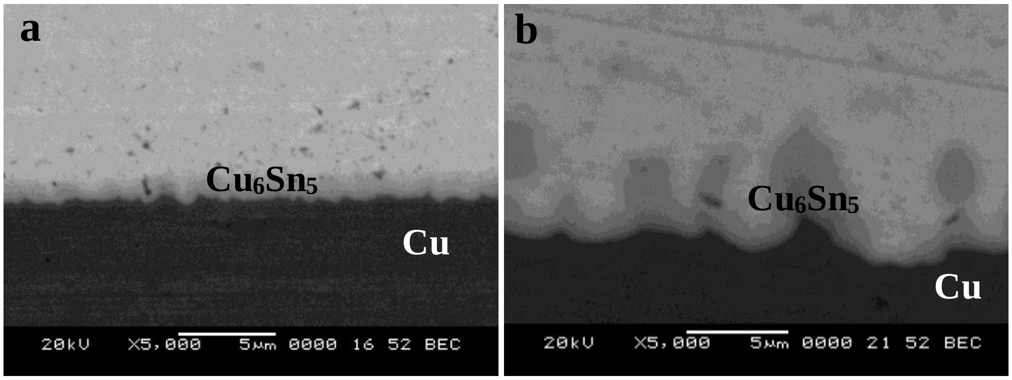

Fig. 4.6: Solder/substrate interface of Sn-0.7Cu/Cu quench cooled system reflowed at 270 °C for (a) 10 s and (b) 500 s

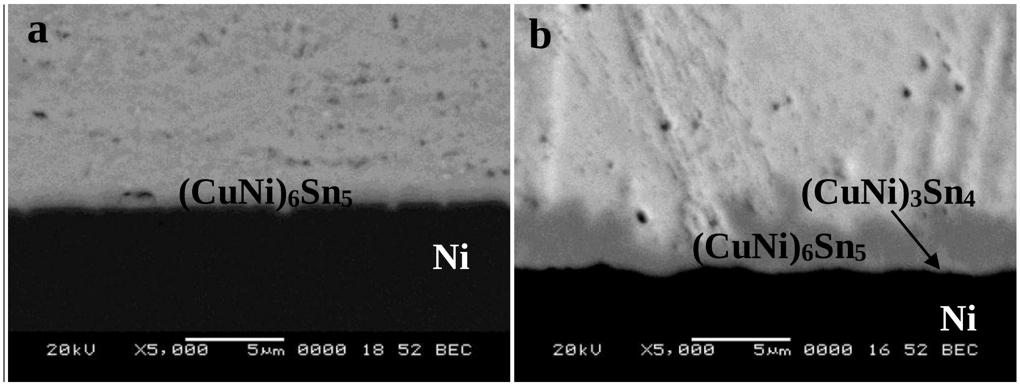

Fig. 4.7: Solder/substrate interface of Sn-0.7Cu/Ni/Cu quench cooled system reflowed at 270 °C for (a) 10 s and (b) 500 s

4.4 Solder joint reliability of solder/substrate bond

The joint reliability (bond strength) of solder/substrate system was assessed by performing the solder ball shear test. The typical force vs. displacement curves corresponding to Sn-0.7Cu alloy obtained during shear test on bare and Ni coated Cu substrate are shown in Figure 4.8

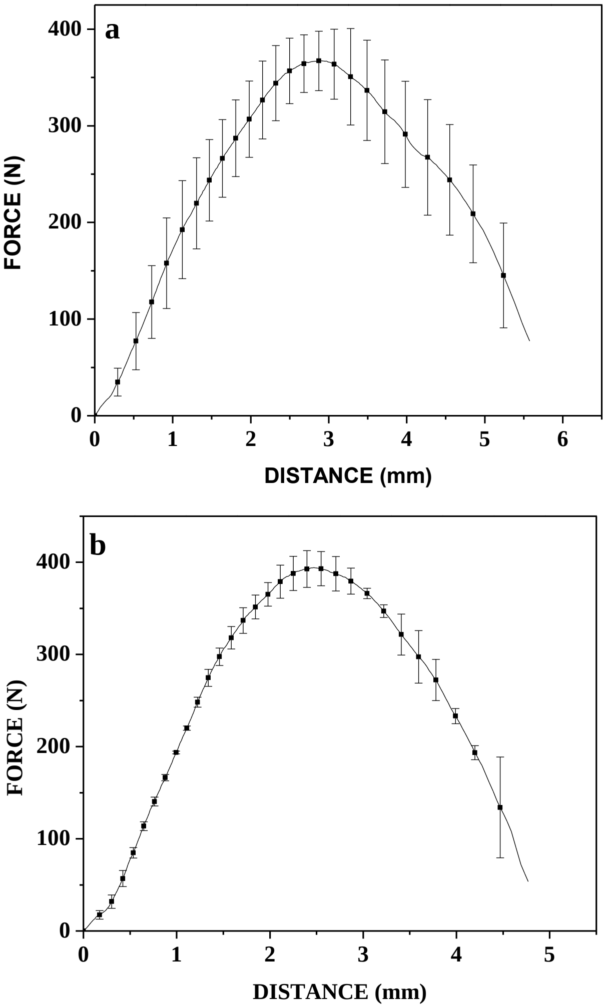

Fig. 4.8: Shear force versus distance curve for the Sn-0.7Cu solder on (a) bare and (b) Ni coated Cu substrate reflowed for 10 s.

4.5 Lap joint shear test of substrate/solder/substrate lap joints

Lap joint shear test was performed to evaluate the effect of the interfacial reactions on bond strength as a function of reflow time. Only three reflow times were selected for reflow purpose namely 10 s, T_{gz} (time corresponding to the end of gravity zone) and 100 s. Figure 4.9 and Figure 4.10 shows the typical stress-strain graphs obtained during the lap joint test on Cu/Sn-0.7Cu/Cu and Ni coated Cu/ Sn-0.7Cu/Ni coated Cu respectively.

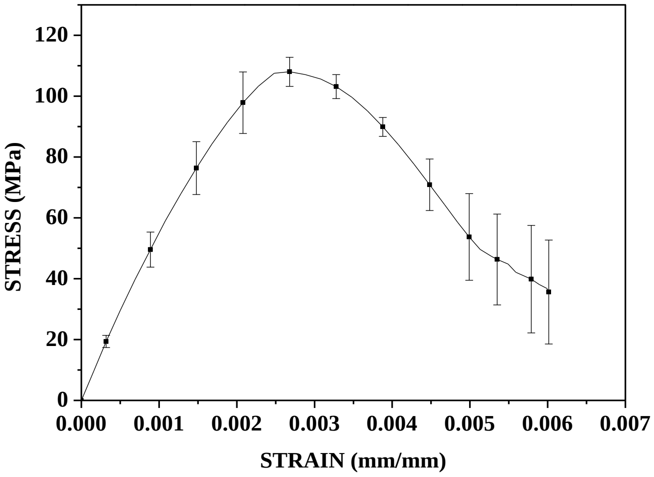

Fig. 4.9: Stress vs strain curve of Cu/Sn-0.7Cu/Cu solder system reflowed for 10 s

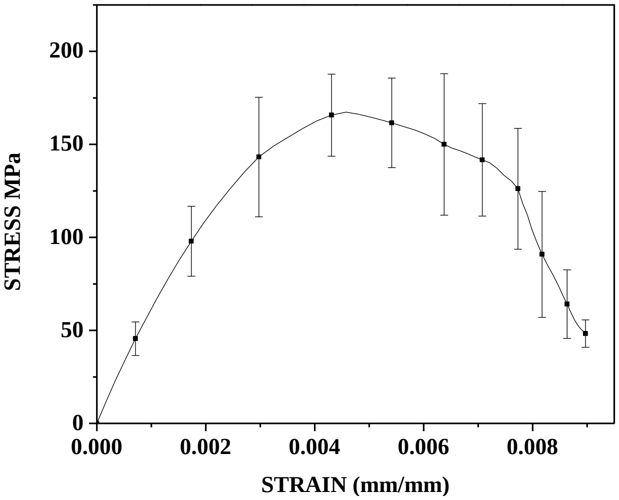

Fig. 4.10: Stress vs strain curve of Ni coated Cu/Sn-0.7Cu/Ni coated Cu system reflowed for 10 s

CHAPTER 5

DISCUSSION

5.1 Spreading behaviour of Sn-0.7Cu, Sn-0.3Ag-0.7Cu and Sn-2.5Ag-0.5Cu solder on bare Cu substrate

The typical relaxation curves for the spreading of Sn-0.7Cu, Sn-0.3Ag-0.7Cu and Sn-2.5Ag-0.5Cu solder alloy on bare Cu substrate as a function of reflow time are presented in Figure 5.1. The wetting or spreading behaviour of solder involves continuous change in the contact angle and drop base diameter with time. Soldering process occurs in three stages namely spreading, base metal dissolution and formation of an IMC layer. The contact angle decreased sharply up to 100 s indicating the start of solder dissolution and precipitation of IMCs during that interval of time. The contact angle stabilized with further increase in time. As the environmental chamber attains the reflow temperature, the lattice distance between atoms increases due to thermal activation. The alloy transforms from solid to liquid state when the activation energy of solder atoms exceeds the force between them in the solid state. Thus, the contact angle of solder suddenly drops in few seconds and the molten solder completely contacts the substrate surface. The wetting of a molten solder on metallic surfaces is a complex phenomenon. Along with the physical spreading of solder alloy on the substrate surface, diffusion and chemical reactions take place in the solder/substrate interfacial region. Wetting of the liquid solder on a substrate is accomplished by the dissolution of the substrate in molten solder and by complex interfacial reactions leading to the formation of IMC layers. The rate of dissolution is very high in the beginning of spreading process. After a short instant the layer of molten solder adjacent to the contacted Cu throughout the interface becomes supersaturated with dissolved Cu. The solid IMC starts to form in this layer at the local equilibrium solubility [Lee et al. 2013].

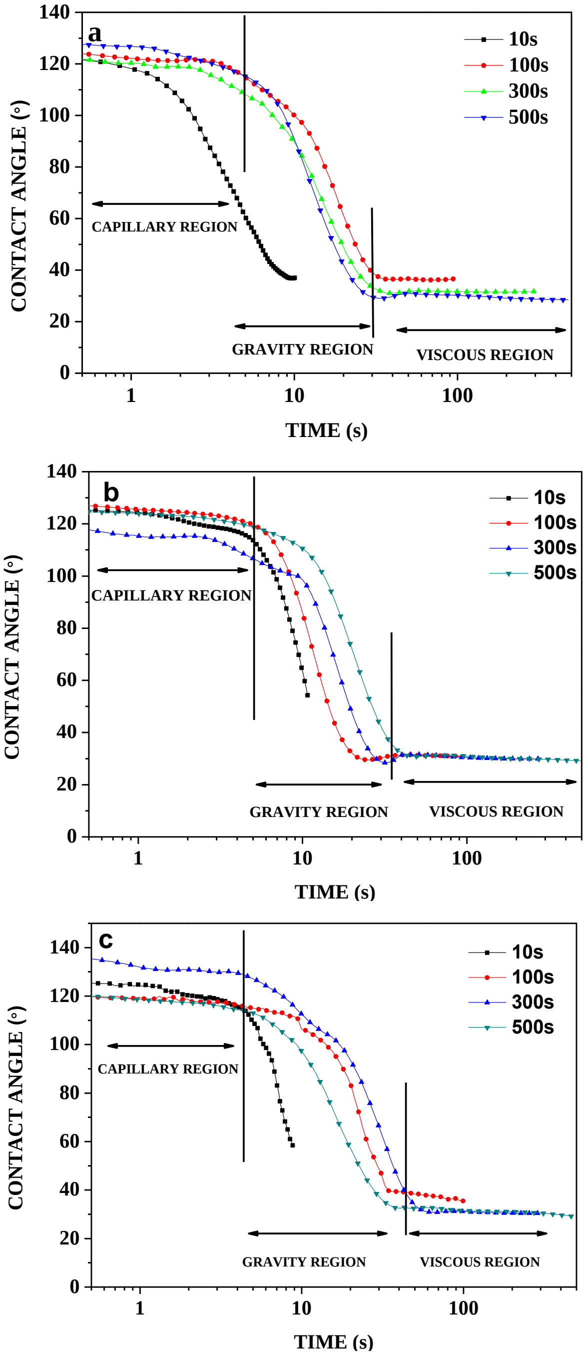

Fig. 5.1: Plots showing relaxation behaviour and various regimes involved during spreading of (a) Sn–0.7Cu, (b) Sn-0.3Ag-0.7Cu and (c) Sn-2.5Ag-0.5Cu solder on bare copper substrate at 270 ºC for various reflow times

The spreading of liquid solder stops as equilibrium state is approached. The contact angle and base radius (drop base area) of the solder alloy exhibited significant variation with time. Figure 5.2 presents the variation of base diameter of the solder on Cu substrate with time. Spreading of the molten solder on Cu substrate occurred uniformly in the radial direction. After solidification, all specimens exhibited spherical cap shape. The values of final contact angle (θ_f) obtained at the end of spreading experiment for Sn-0.7Cu, Sn-0.3Ag-0.7Cu and Sn-2.5Ag-0.5Cu solder alloy on bare Cu substrate are given in Table 5.1 and 5.2. The final contact angle decreased with increase in reflow time showing a better wetting of solder on the substrate. At lower reflow times (≤100 s) furnace cooling resulted in better wetting compared to quench cooled samples. At higher reflow times comparable contact angles were obtained for both quench and furnace cooled samples. The macroscopic images (top view) of the stabilized droplets of Sn-0.7Cu, Sn-0.3Ag-0.7Cu and Sn-2.5Ag-0.5Cu solder on bare Cu substrate (both furnace cooled and quench cooled) are shown in Figure 5.3 to Figure 5.8.

Table 5.1: Final contact angle of Sn-0.7Cu/Cu, Sn-0.3Ag-0.7Cu/Cu and Sn-2.5Ag-0.5Cu/Cu systems reflowed under various time intervals (using furnace-cooling method)

Reflow time (s)	Contact angle θ_f (°)		
	Sn-0.7Cu/Cu	Sn-0.3Ag-0.7Cu/Cu	Sn-2.5Ag-0.5Cu/Cu
10	34.89±0.64	31.54±0.37	33.09±0.70
100	32.73±0.71	30.67±0.12	31.45±0.65
300	31.29±0.52	30.29±0.29	30.34±0.36
500	30.61±0.75	28.7±0.5	29.59±0.39
1000	30.45±0.46	28.02±0.21	28.62±0.54
10000	28.59±0.26	27.81±0.29	27.84±0.32

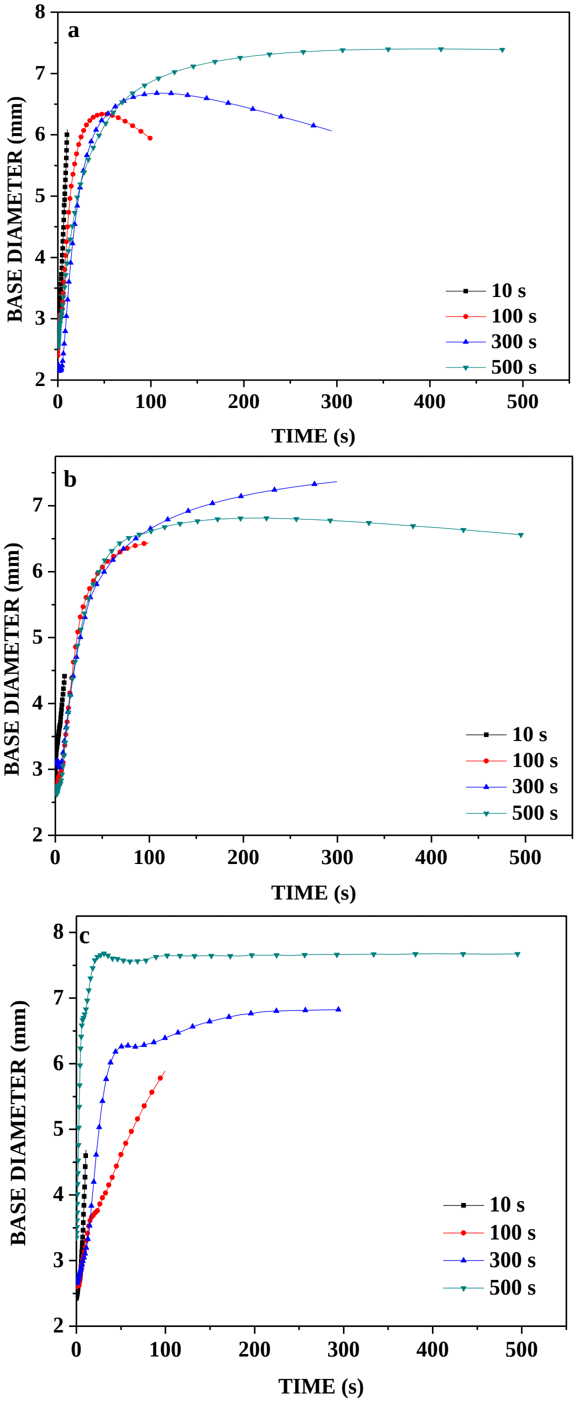

Fig.5.2: Plot showing the variation of the base radius of solder alloy with time of (a) Sn–0.7Cu, (b) Sn-0.3Ag-0.7Cu and (c) Sn-2.5Ag-0.5Cu solder reflowed on bare copper substrate at 270 ºC for various reflow time

Table 5.2: Final contact angle of Sn-0.7Cu/Cu, Sn-0.3Ag-0.7Cu/Cu and Sn-2.5Ag-0.5Cu/Cu systems reflowed under various time intervals (using quench cooling method)

Reflow time (s)	Contact angle θ_f (°)		
	Sn-0.7Cu	Sn-0.3Ag-0.7Cu	Sn-2.5Ag-0.5Cu
10	36.33±1.91	44.98±5.82	43.72±3.48
100	34.4±4.51	30.04±4.47	35.88±1.02
300	31.73±2.67	28.41±0.74	31.25±1.78
500	28.97±0.37	27.2±0.43	29.26±1.35

Furnace cooled samples showed a halo zone that appeared at the solder front Cu substrate and its area increased with the increase in reflow time. It is believed that the formation of the halo region is related to an interfacial reaction and to the formation of intermetallic layer [Satyanarayan and Prabhu 2011]. Very thick IMCs were observed at the solder/substrate interface of the furnace cooled samples when compared to quench cooled systems. Therefore, halo region was prominent in furnace cooled sample than in quench cooled once. The reliability of solder joints in electronic packaging is controlled by the type and morphology of interfacial IMCs formed at the solder and substrate interface. A reflow time of 10 s was sufficient enough to melt the solder alloy but was insufficient for the spreading of solder alloy over Cu substrate, for quench cooled samples. Therefore, a significant difference in the solder quantity for sample reflowed for 10 s on Cu substrate in quench cooled systems when compared to other samples can be observed in Figure 5.6, Figure 5.7 and Figure 5.8 though amount of solder quantity taken was approximately same for all the cases.

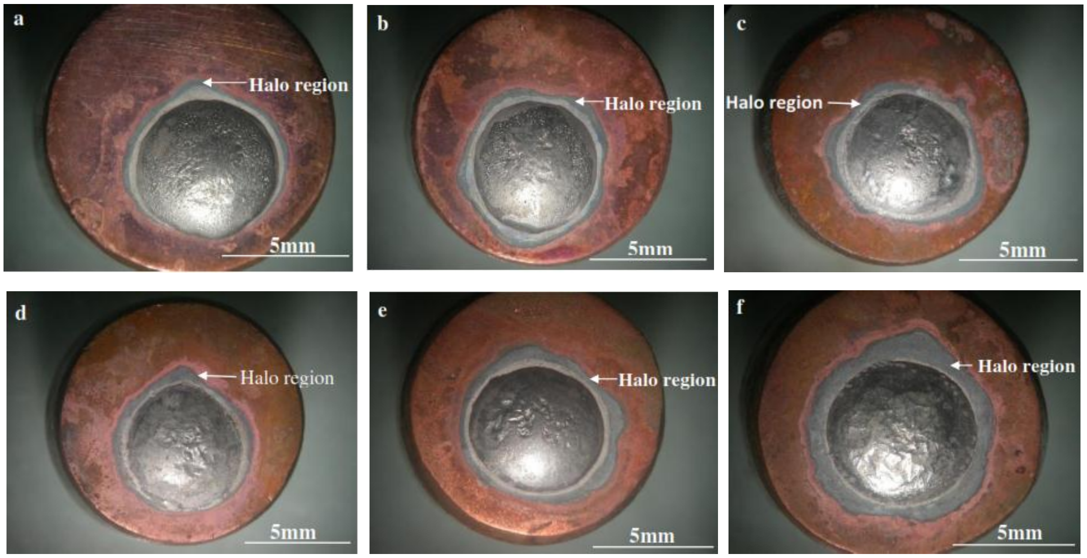

Fig. 5.3: Macroscopic images (top view) of stabilized Sn-0.7Cu solder on bare copper substrate reflowed at 270 °C for various time; (a) 10 s (b) 100 s (c) 300 s (d) 500 s (e) 1000 s and (f) 10000 s (furnace cooled)

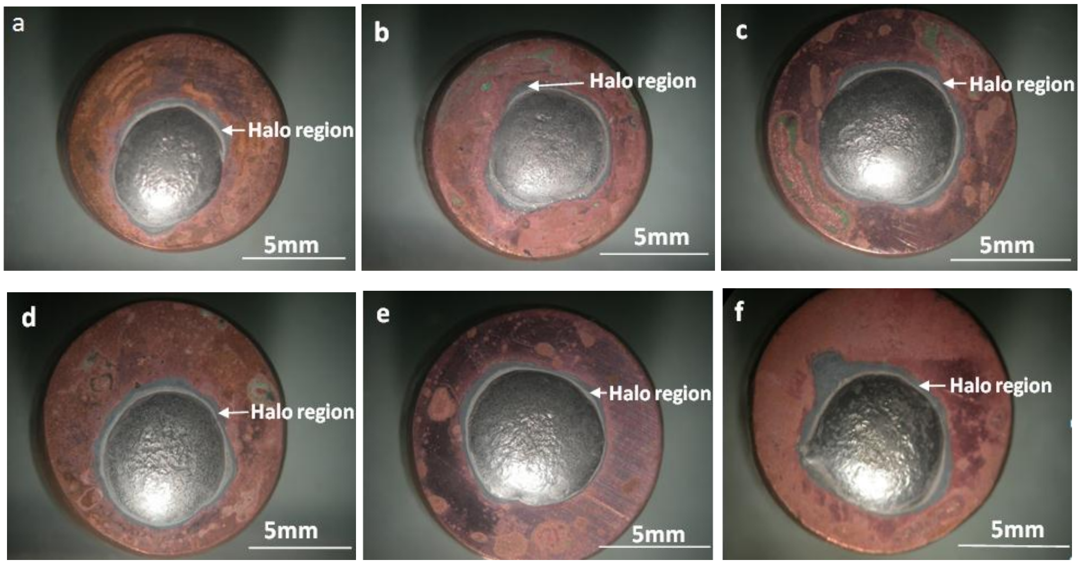

Fig. 5.4: Macroscopic images (top view) of stabilized Sn-0.3Ag-0.7Cu solder on bare copper substrate reflowed at 270 °C for various time; (a) 10 s (b) 100 s (c) 300 s (d) 500 s (e) 1000 s and (f) 10000 s (furnace cooled)

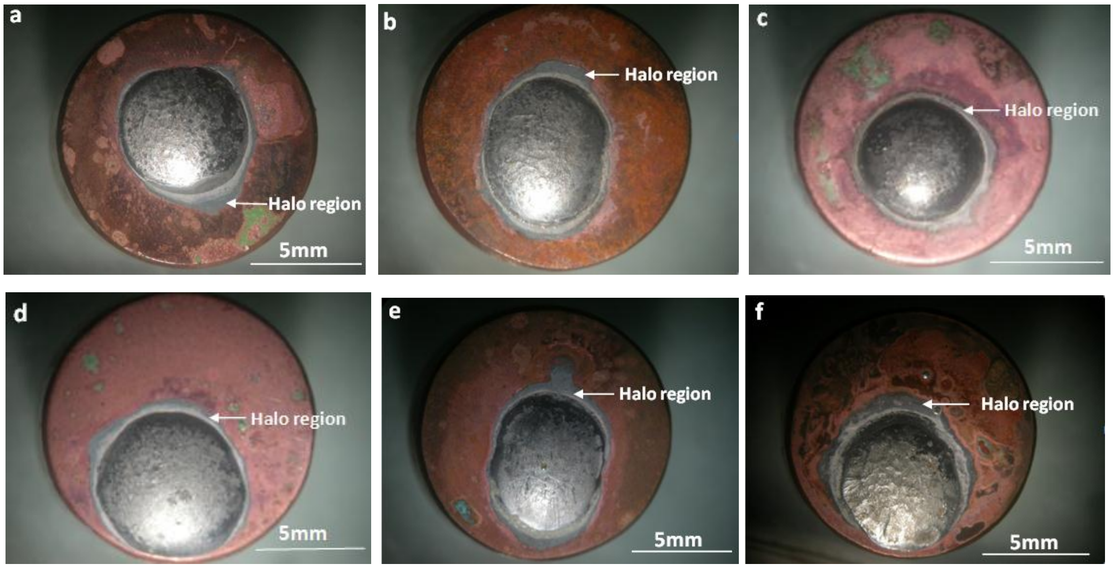

Fig. 5.5: Macroscopic images (top view) of stabilized Sn-2.5Ag-0.5Cu solder on bare copper substrate reflowed at 270 ºC for various time; (a) 10 s (b) 100 s (c) 300 s (d) 500 s (e) 1000 s and (f) 10000 s (furnace cooled)

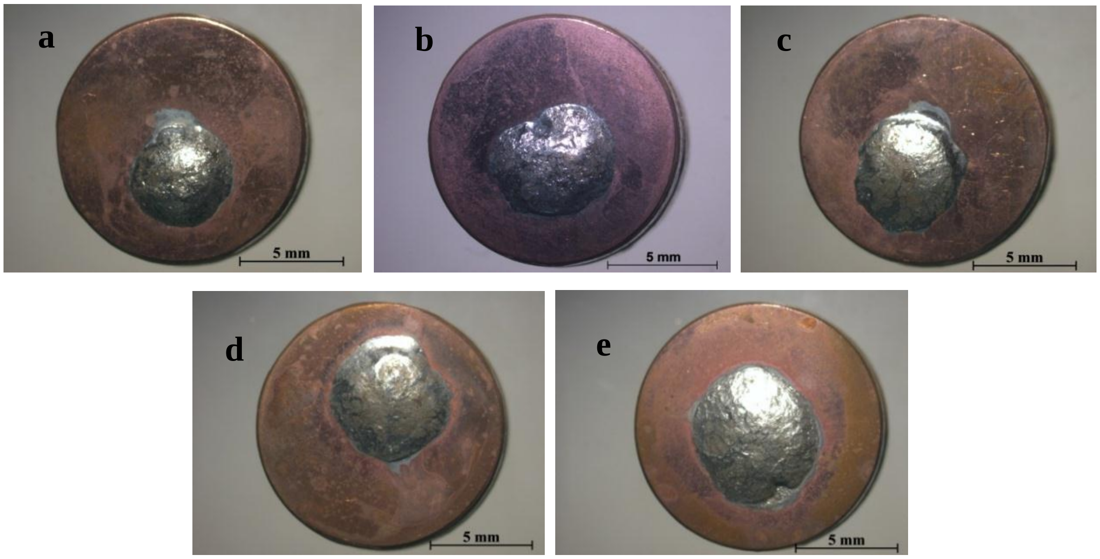

Fig. 5.6: Macroscopic images (top view) of stabilized Sn-0.7Cu solder on bare copper substrate reflowed at 270 ºC for various time; (a) 10 s (b) 25 s (c) 100 s (d) 300 s and (e) 500 s (quench cooled)

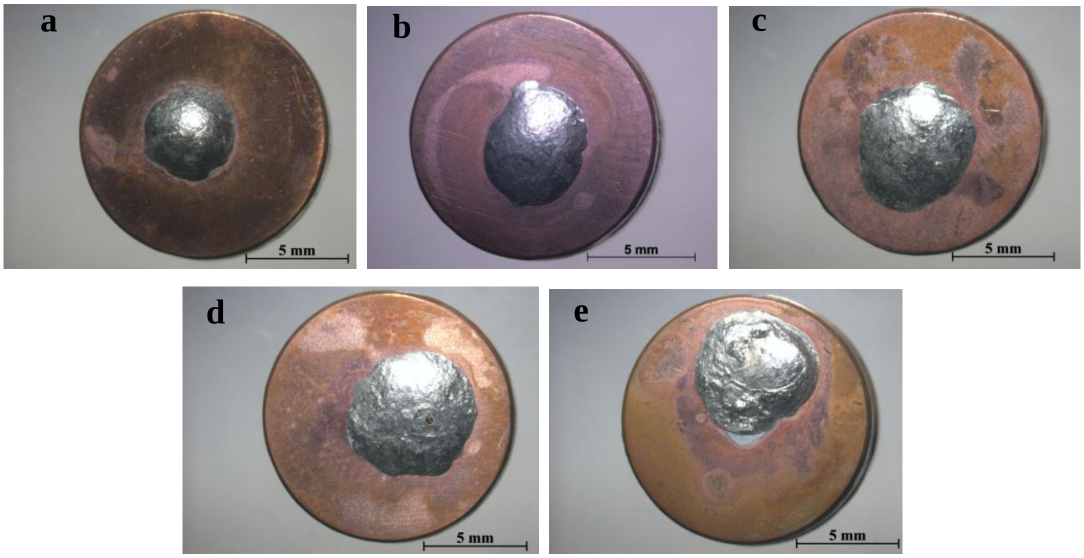

Fig. 5.7: Macroscopic images (top view) of stabilized Sn-0.3Ag-0.7Cu solder on bare copper substrate reflowed at 270 ºC for various time; (a) 10 s (b) 40 s (c) 100 s (d) 300 s and (e) 500 s (quench cooled)

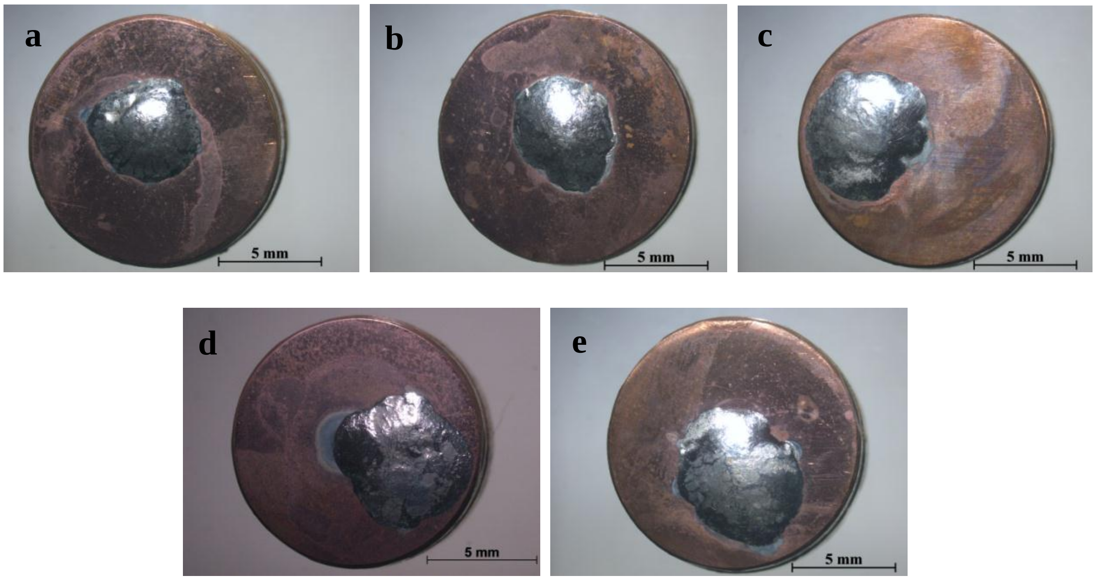

Fig. 5.8: Macroscopic images (top view) of stabilized Sn-2.5Ag-0.7Cu solder on bare copper substrate reflowed at 270 ºC for various time; (a) 10 s (b) 40 s (c) 100 s (d) 300 s and (e) 500 s (quench cooled)

Various regimes were recognized in the relaxation curves by a sharp change in spreading rate. The three regimes involved during spreading of solder alloy on substrate surface were categorised as capillary, gravity (reactive), and viscous zones. Regimes involved during solder spreading were identified by the change of slope in plots of θ versus T, where θ is the contact angle (°) during spreading and T is time (s). In an ideal condition, the entire base diameter versus time as well as contact angle versus time curves should lie on top of each other, however a discrepancy was observed, which can be attributed to slight variation in substrate surface roughness, solder ball mass and diameter due to experimental limitations. The duration of the capillary zone and gravity zone obtained from the relaxation curves during reflow of the solder alloy on bare Cu substrate for various reflow times are presented in Table 5.3. The final contact angle obtained from the experiment for the reflow time corresponding to the end of gravity zone are given in Table 5.4. The contact angle of the solder drops abruptly in the capillary and gravity zones compared with the viscous zone. In the capillary zone, physical spreading of the molten solder takes place by capillary action due to reduction in surface tension. Spreading in this regime is similar to nonreactive spreading of any liquid on a solid substrate surface. Diffusion and chemical reactions take place at the solder–substrate interface in the gravity zone, and the molten solder completely contacts the substrate surface. A metallurgical contact between the solder and substrate forms in the gravity zone due to dissolution of the substrate into the molten solder. Solid IMC starts to form at the interface at the local equilibrium solubility [Laurila et al. 2005]. Therefore, the spreading of molten solder in the gravity region is reactive. Spreading of liquid solder more or less stops in the viscous region. All the solder alloys were therefore reflowed on bare Cu substrate for the average times beyond which the reactive (gravity) zone ends. The average time required for the completion of gravity zone (T_{gz}) for Sn-0.7Cu solder alloy solidified on bare Cu substrate was found to be 25 s. T_{gz} for Sn–0.3Ag-0.7Cu and Sn–2.5Ag-0.5Cu solidified on bare Cu substrates was 40 s. Relaxation rates in capillary, gravity and viscous zones of Sn-0.7Cu/Cu systems are 2.71±0.81 °/s, 3.7±0.2 °/s and

0.01±0.005 °/s respectively. 2.21±0.68 °/s, 2.9±0.18 °/s and 0.01±0.006 °/s are the average relaxation rates in capillary, gravity and viscous zones of Sn-0.3Ag-0.7Cu/Cu systems respectively. Similarly, average relaxation rates in capillary, gravity and viscous zones of Sn-2.5Ag-0.5Cu/Cu systems are 2.01±0.76 °/s, 2.68±0.16 °/s and 0.02±0.006 °/s respectively.

Table 5.3: Time duration of capillary and gravity regimes for the solder alloy on bare Cu substrate surface

Reflow time (s)	Period of capillary regime (s)	Contact angle at the end of capillary regime (θ_{cz}) (°)	Period of gravity regime (s)	Contact angle at the end of gravity regime (θ_{gz}) (°)
	Sn-0.7Cu/Cu			
10			--	--
100	2.95	121.19	2.95-29.32	39.91
300	2.27	118.78	2.27-27.26	35.43
500	2.26	122.45	2.26-24.40	33.52
	Sn-0.3Ag-0.7Cu/Cu			
10	4.86	114.32	--	--
100	5.35	118.69	5.35-36.59	31.25
300	3.83	110.42	3.83-40.35	31.46
500	5.41	118.17	5.41-43.2	31.24
	Sn-2.5Ag-0.5Cu/Cu			
10	4.18	115.11	--	--
100	3.21	117.33	3.21-36.34	39.32
300	3.78	129	3.78-42.79	40.12
500	4.05	114.35	4.05-37.80	32.94

Table 5.4: Final contact angle obtained from the experiment for the reflow time corresponding to the end of gravity zone for Sn-0.7Cu/Cu, Sn-0.3Ag-0.7Cu/Cu and Sn-2.5Ag-0.5Cu/Cu systems [quench cooling method]

Solder system	Reflow time corresponding to (T_{gz}) (s)	Contact angle (θ_f) (°)
Sn-0.7Cu/Cu	25	35.24±0.68
Sn-0.3Ag-0.7Cu/Cu	40	31.95±0.35
Sn-2.5Ag-0.5Cu/Cu	40	36.93±1.17

Sn-0.7Cu/Cu system showed maximum relaxation rate in capillary and gravity zone followed by Sn-0.3Ag-0.7Cu/Cu and Sn–2.5Ag-0.5Cu/Cu systems. All solder/Cu systems showed comparable relaxation rate in viscous zone. A non-uniform relaxation rate was observed in the capillary zone of all the solder/Cu systems. This can be attributed to strive of the molten solder to form the sphere again to maintain the surface tension though the melting process has started. In this zone, solder appears to be in the semi solid condition. With the constant supply of heat, lattice distance between solder atoms further increases and solder attains complete liquid state when the activation energy of solder atoms exceeds the forces between them in the solid state. Therefore, solder attains complete liquid state in gravity zone and spreading becomes easier. Hence, a higher relaxation rate was observed in gravity zone when compared to capillary and viscous zones.

5.2 Spreading behaviour of Sn-0.7Cu, Sn-0.3Ag-0.7Cu and Sn-2.5Ag-0.5Cu solder on Ni coated Cu substrate

The typical relaxation curves for the spreading of Sn-0.7Cu, Sn-0.3Ag-0.7Cu and Sn-2.5Ag-0.5Cu solder alloy on Ni coated Cu substrate as a function of reflow time are presented in Figure 5.9.

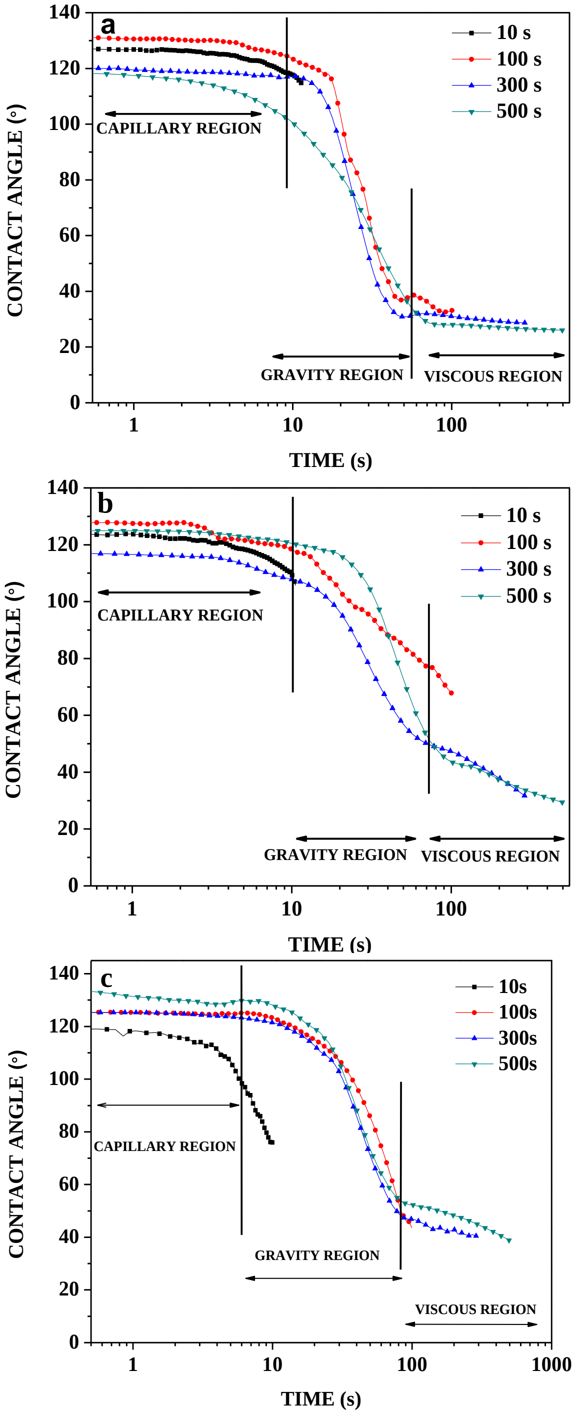

Fig. 5.9: Plots showing relaxation behaviour and various regimes involved during spreading of (a) Sn–0.7Cu, (b) Sn-0.3Ag-0.7Cu and (c) Sn-2.5Ag-0.5Cu solder on nickel coated copper substrate at 270 ºC for various reflow times

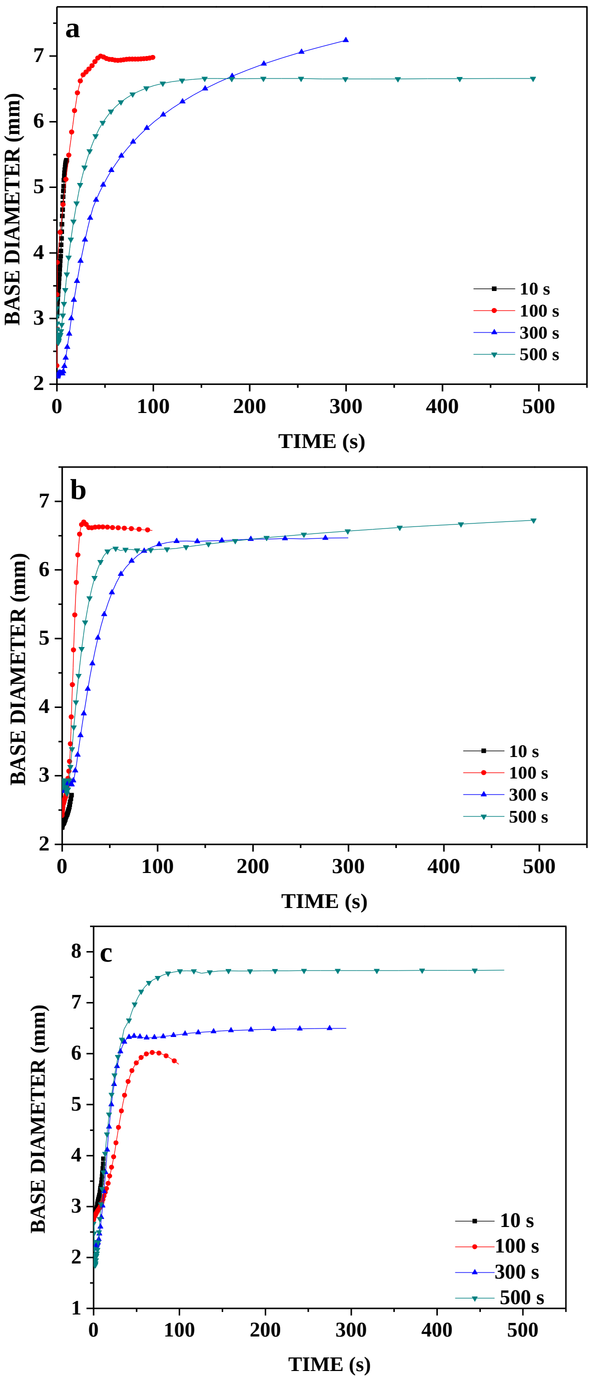

Fig.5.10: Plot showing the variation of the base radius of solder alloy with time of (a) Sn–0.7Cu, (b) Sn-0.3Ag-0.7Cu and (c) Sn-2.5Ag-0.5Cu solder reflowed on nickel coated copper substrate at 270°C for various reflow times

The contact angle and base radius (drop base area) of the solder alloy showed considerable variation with time. Figure 5.10 presents the variation of base diameter of the solder on Cu substrate with time. Spreading of the molten solder on Ni coated Cu substrate occurred uniformly in the radial direction. After solidification, all specimens exhibited spherical cap shape. The values of final contact angle (θ_f) obtained at the end of spreading experiment for Sn-0.7Cu, Sn-0.3Ag-0.7Cu and Sn-2.5Ag-0.5Cu solder alloy on Ni coated Cu substrate are given in Table 5.5. Figure 5.11, Figure 5.12 and Figure 5.13 represents the macroscopic top view of stabilized droplets of Sn-0.7Cu, Sn-03Ag-0.7Cu and Sn-2.5Ag-0.5Cu solder alloys on Ni coated Cu substrate respectively. No halo region was observed around the solder sessile drop on Ni coated Cu substrate. Formation of very thin IMC layer at the solder/substrate interface is the reason for the absence of halo region.

Table 5.5: Contact angle of Sn-0.7Cu/Ni/Cu, Sn-0.3Ag-0.7Cu/Ni/Cu and Sn-2.5Ag-0.5Cu/Ni/Cu systems reflowed under various time intervals (using quench-cooling method)

Reflow time (s)	Contact angle θ_f (°)		
	Sn-0.7Cu	Sn-0.3Ag-0.7Cu	Sn-2.5Ag-0.5Cu
10	36.05±3.15	43.50±2	56.43±2.20
100	29.87±1.69	40.81±0.65	42.69±1.24
300	27.62±2.74	33.31±1.55	40.78±0.52
500	26.64±0.86	28.62±0.76	37.73±0.40

Spreading of solder alloys on Ni coated Cu substrate showed similar trend observed for solder alloys on bare Cu substrate. Three regimes namely capillary, gravity and viscous zones were observed in the relaxation curve during the spreading of solder alloy on Ni coated Cu substrate. The time duration of the capillary zone and gravity zone obtained from the relaxation curve for the solder alloy on Ni coated Cu substrates are given in

Table 5.6. Final contact angle for the reflow time corresponding to the end of gravity zone (T_{gz}) obtained from the experiment are given in Table 5.7. T_{gz} (time required for the end of gravity zone) was found to be about 50 s for Sn-0.7Cu, 70 s for Sn-0.3Ag-0.7Cu and 80 s for Sn-2.5Ag-0.5Cu solder alloy solidified on Ni coated Cu substrate.

Table 5.6: Time duration of capillary and gravity regimes for the solder alloy on Ni coated Cu substrate surface

Reflow time (s)	Period of capillary regime (s)	Contact angle at the end of capillary regime (θ_{cz}) (°)	Period of gravity regime (s)	Contact angle at the end of gravity regime (θ_{gz}) (°)
	Sn-0.7Cu/Ni/Cu			
10	4.53	124.21	--	--
100	4.82	128.41	4.82-55.23	38.3
300	3.13	118.57	3.13-48.68	30.9
500	4.64	111.14	4.64-45.74	42.12
	Sn-0.3Ag-0.7Cu/Ni/Cu			
10	4.68	118.61	--	--
100	4.2	122.04	4.2-69.29	77.30
300	3.58	115.26	3.58-73.32	49.59
500	4.05	123.48	4.05-73.24	51.06
	Sn-2.5Ag-0.5Cu/Ni/Cu			
10	5.25	104.81	--	--
100	6.28	125.10	6.28-75.46	57.48
300	5.99	123.28	5.99-87.61	47.54
500	6.45	129.72	6.45-70.40	58.98

Table 5.7: Final contact angle obtained from the experiment for the reflow time corresponding to the end of gravity zone for Sn-0.7Cu/Ni/Cu, Sn-0.3Ag-0.7Cu/Ni/Cu and Sn-2.5Ag-0.5Cu/Ni/Cu systems.

Solder system	Reflow time corresponding to the end of gravity zone (T_{gz}) (s)	Contact angle (θ_f) (°)
Sn-0.7Cu/Ni/Cu	50	33.53±1.08
Sn-0.3Ag-0.7Cu/Ni/Cu	70	41.12±0.58
Sn-2.5Ag-0.5Cu/Ni/Cu	80	44.52±2.77

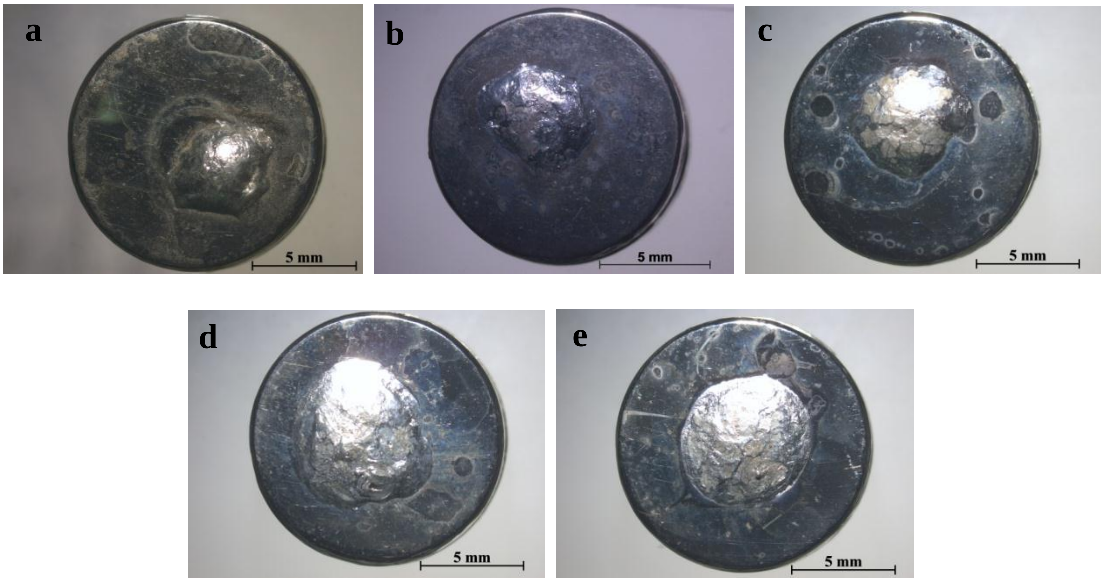

Fig. 5.11: Macroscopic images (top view) of stabilized Sn-0.7Cu solder on Ni coated Cu substrate reflowed at 270 °C for various time; (a) 10 s (b) 50 s (c) 100 s (d) 300 s and (e) 500 s (quench cooled)

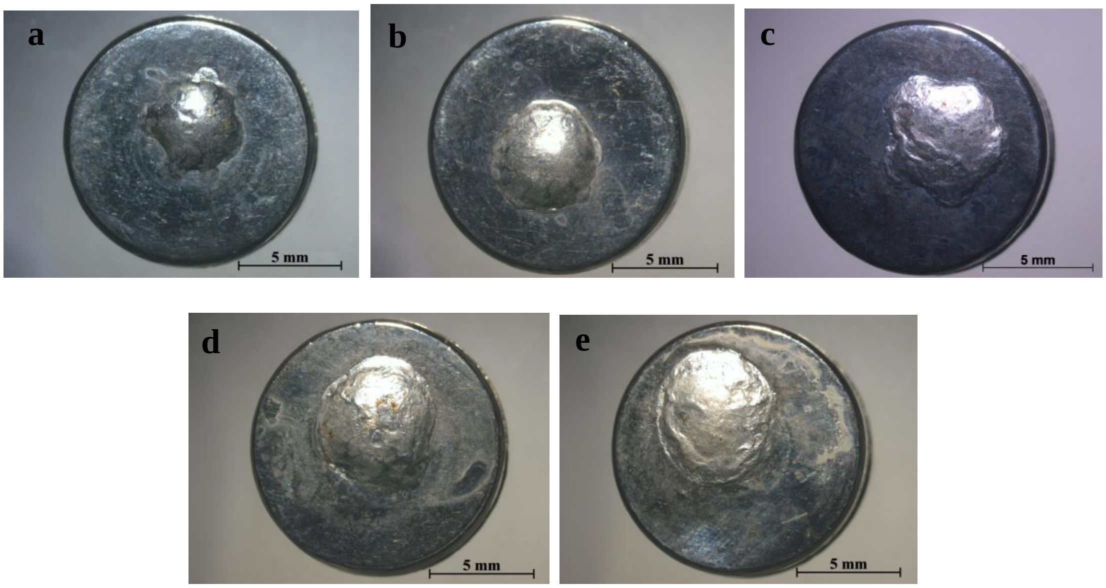

Fig. 5.12: Macroscopic images (top view) of stabilized Sn-0.3Ag-0.7Cu solder on Ni coated Cu substrate reflowed at 270 ºC for various time; (a) 10 s (b) 50 s (c) 100 s (d) 300 s and (e) 500 s (quench cooled)

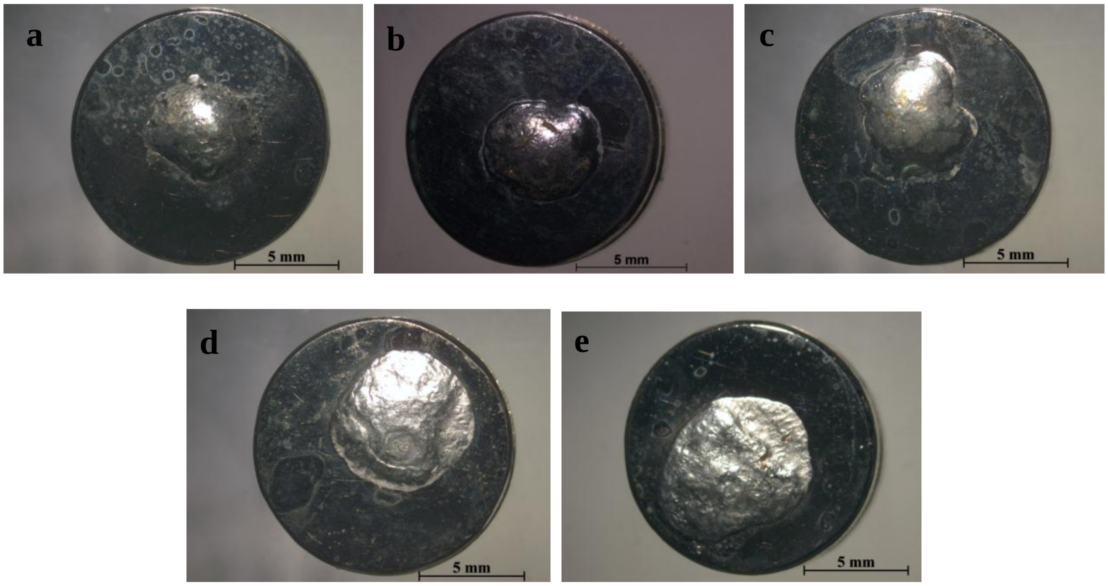

Fig. 5.13: Macroscopic images (top view) of stabilized Sn-2.5Ag-0.5Cu solder on Ni coated Cu substrate reflowed at 270 ºC for various time; (a) 10 s (b) 50 s (c) 100 s (d) 300 s and (e) 500 s (quench cooled)

The period of gravity zone in solder alloy/Ni/Cu system was found be twice than that of solder alloy/Cu system. This shows that Ni acts as a barrier for the solder/substrate interfacial reaction. Spreading of liquid solder more or less stops in the viscous region. Sn-0.7Cu, Sn-0.3Ag-0.7Cu and Sn-2.5Ag-0.5Cu solder alloy were therefore reflowed on Ni coated Cu substrates for 50 s, 70 s and 80 s respectively where 50 s, 70 s and 80 s were the approximate times beyond which the reactive (gravity) zone ends.

Average relaxation rates in capillary, gravity and viscous zones of Sn-0.7Cu/Ni/Cu systems are 0.98±0.57 °/s, 2.15±0.35 °/s and 0.02±0.003 °/s respectively. 0.95±0.52 °/s, 1.21±0.19 °/s and 0.03±0.004 °/s are the average relaxation rates in capillary, gravity and viscous zones of Sn-0.3Ag-0.7Cu/Ni/Cu systems. Similarly, for Sn-2.5Ag-0.5Cu/Ni/Cu system, the average relaxation rates in capillary, gravity and viscous zones are 0.93±1.01 °/s, 1.14±0.18 °/s and 0.03±0.002 °/s respectively. Relaxation rate was higher in capillary and gravity zones of Sn-0.7Cu/Ni/Cu systems followed by Sn-0.3Ag-0.7Cu/Ni/Cu and Sn-2.5Ag-0.5Cu/Ni/Cu systems. The relaxation rate was higher for solder alloys on bare Cu than on Ni coated Cu substrate in capillary and gravity zones where as comparable relaxation rates were observed in viscous zone of both the systems. This clearly shows that the wettability of liquid solder is more on Cu than on Ni coated Cu substrate. The presence of Ag content is also one of the reasons for the decrease in spreading rate, as Ag forms an intermetallic Ag_3Sn with Sn in Ag containing solder alloys. A comparable contact angle was observed for Sn-0.7Cu solder alloy on bare and Nickel coated Cu substrates whereas Sn-0.3Ag-0.7Cu and Sn-2.5Ag-0.5Cu solder alloys showed better wetting (in terms of contact angle) on Cu substrate than on Ni coated Cu substrate.

5.3 Interfacial microstructure of Sn-0.7Cu, Sn-0.3Ag-0.7Cu and Sn-2.5Ag-0.5Cu solder on bare Cu substrate [furnace cooled solder/substrate system]

5.3.1 Interfacial microstructure of Sn-0.7Cu solder alloy on bare Cu substrate

The solder drop bonded to the substrate was sectioned along the axis to study the IMC morphology at the interface. Back-scattered electron images of the interface were captured to show distinctly the boundaries of the interfacial layers.

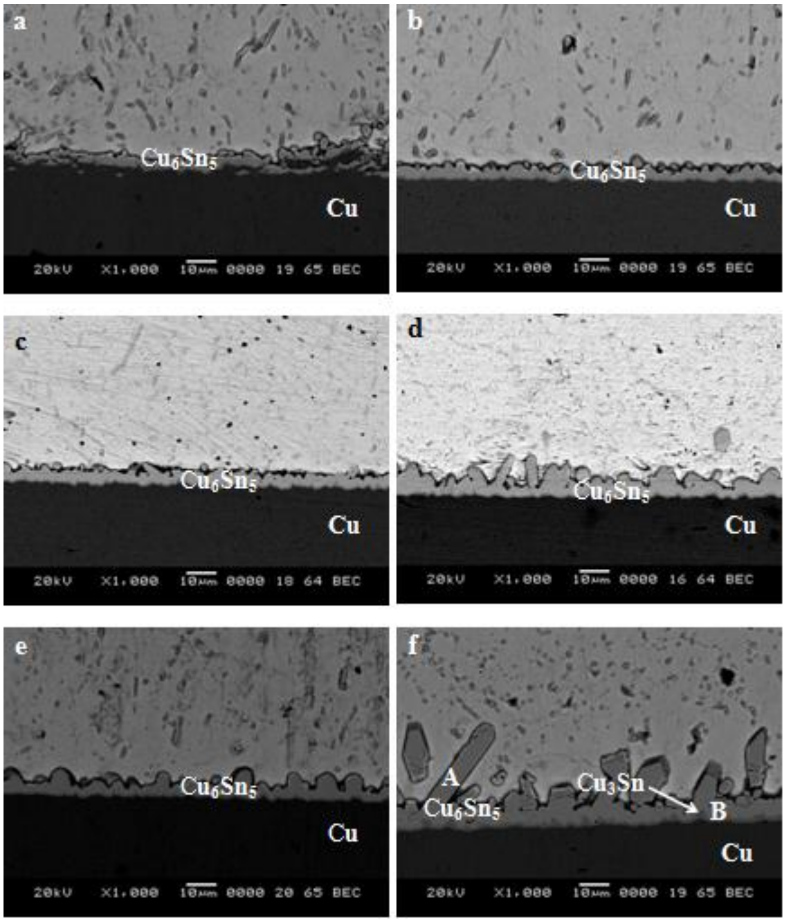

Fig.5.14: The SEM micrographs of furnace cooled Sn–0.7Cu/Cu interface reflowed at 270°C for various times; (a) 10 s, (b) 100s, (c) 300s, (d) 500s (e) 1000, and (f)10000s

Figure 5.14 shows the SEM micrographs of the interface of furnace cooled Sn-0.7Cu/Cu system reflowed at 270 °C for different reaction times. At the initial stages of solder alloy spreading on the substrate, the metallic atoms from the metallic substrate contacting to the molten solder, rapidly dissolve into the molten solder and quickly become supersaturated in the interface regions. Subsequently, the IMC phases start to nucleate and grow at the interface due to the local metastable equilibrium solubility of metallic atoms in the liquid solder alloy [Laurila et al. 2005]. These IMCs grew into the solder field from the interface. The chemical composition of IMCs revealed that the IMCs were composed of Cu and Sn atoms. EDS analysis was carried out to identify the IMCs at the interface. A decrease in the atomic percentage of Cu from the root to the tip of the IMCs was observed. In all the reaction couples, Cu_6Sn_5 IMC was detected between the solder and Cu layer. Cu_3Sn IMC with a layer-type morphology was observed between Cu_6Sn_5 layer and Cu substrate when the reflow time was 10,000 s. Table 5.8 gives the atom % of Cu and Sn present in the position A and B shown in Figure 5.14. The Cu_6Sn_5 IMC formed on the Cu substrate at a reflow time of 10 s had a discontinuous but a well-known morphology of round scallop shape. At a reflow time of 100 and 300 s a continuous layer of IMC with round scallop morphology was formed. With an increase in the reflow time to 500 and 1,000 s, the round morphology of the IMC changed to elongated scallop morphology. At a reflow time of 10,000 s, faceted scallop morphology was formed. The increase in reaction times lead to the increase in the thickness of the Cu_6Sn_5 IMC layer. This is due to the greater dissolution of Cu atoms into the molten solder during longer reflow time intervals. The thickness of the Cu_6Sn_5 IMC layer formed during a reflow time of 10 s was 3.76 μm and its thickness increased to 3.89, 6.2, 6.68, 7.6 and 19.83 μm during 100, 300, 500, 1,000 and 10,000 s reflow time respectively. Thickness of the Cu_3Sn layer formed during 10,000 s of reflow time was about 2 μm. Table 5.9 gives the effect of reflow time on interfacial reaction, morphology of IMCs at Sn-0.7Cu/Cu interface. The growth rate of Cu_3Sn was found to be slower compared to Cu_6Sn_5 since Cu_3Sn intermetallic formation requires higher activation energy and temperature than Cu_6Sn_5 [Ma et al. 2003]. The activation energy for the formation of Cu_6Sn_5 and Cu_3Sn

was found to be 41.4 kJ/mol and 90.4 kJ/mol respectively [Tang et al. 2010]. According to Park et al (2007) Cu_3Sn grows at the expense of Cu_6Sn_5 phase reacting with copper, only in the absence of sufficient supply of Sn. XRD analysis was carried out to confirm the composition of intermetallics formed at the solder/substrate interface. Figure 5.15 shows the XRD pattern of Sn-0.7Cu solder on Cu surface reflowed at 10, 100, 300, 500, 1,000 and 10,000 s. The XRD pattern confirmed the formation of Cu_6Sn_5 IMCs at the interface during all the reflow times and also confirmed the formation of Cu_3Sn IMC exclusively during reflow for 10,000 s.

Table 5.8: EDS analysis results of marked regions in Fig. 5.14 for Sn-0.7Cu solder on Cu substrate

Marks	Cu K (at.%)	Sn L (at.%)	Phase
A	53.13	46.87	Cu_6Sn_5
B	71.39	28.61	Cu_3Sn

Table 5.9: Effect of reflow time on interfacial reaction, morphology of IMCs at Sn-0.7Cu/Cu interface

Reflow time (s)	Interfacial IMC	Morphology of IMC	Thickness of IMC (μm)
10	Cu_6Sn_5	Discontinuous round scallop	3.76
100	Cu_6Sn_5	Round scallop	3.89
300	Cu_6Sn_5	Round scallop	6.2
500	Cu_6Sn_5	Elongated scallop	6.68
1000	Cu_6Sn_5	Elongated scallop	7.6
10000	Cu_6Sn_5 Cu_3Sn	Faceted scallop Layer-type	19.83 2

The growth kinetics of the IMC layer was studied. The obtained thickness values were fitted according to the growth model,

$y = kt^n$ [19]

where y is the intermetallic layer thickness, k is growth constant, t is the reflow time and n is a growth exponent. If growth rate (n) is equal to 1/3, it is assumed that the growth of an IMC layer is dominated by grain boundary (GB) diffusion and limited by the coarsening of the microstructure [Schaefer et al. 2012, Park et al. 2012]. Therefore, the curve was force fitted with a value of the exponent (n) equal to 1/3. The R^2 value obtained was 0.97. This shows that GB diffusion, is the prime transport mechanism that controls the IMC growth rate in Sn-0.7Cu/Cu system. A plot of IMC thickness vs reflow time for Sn-0.7Cu solder alloy on bare Cu substrate is shown in Figure 5.16.

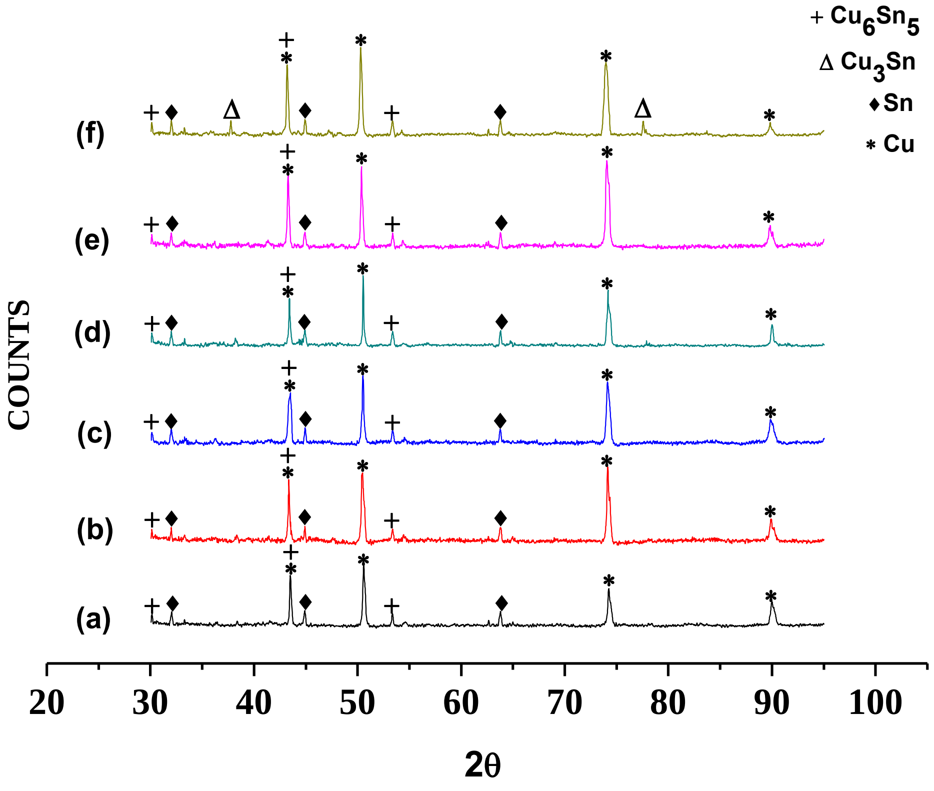

Fig. 5.15: XRD patterns of Sn–0.7Cu/Cu reflowed at 270 °C for (a) 10 s, (b) 100 s, (c) 300 s, (d) 500 s, (e) 1,000 s and (f) 10,000 s

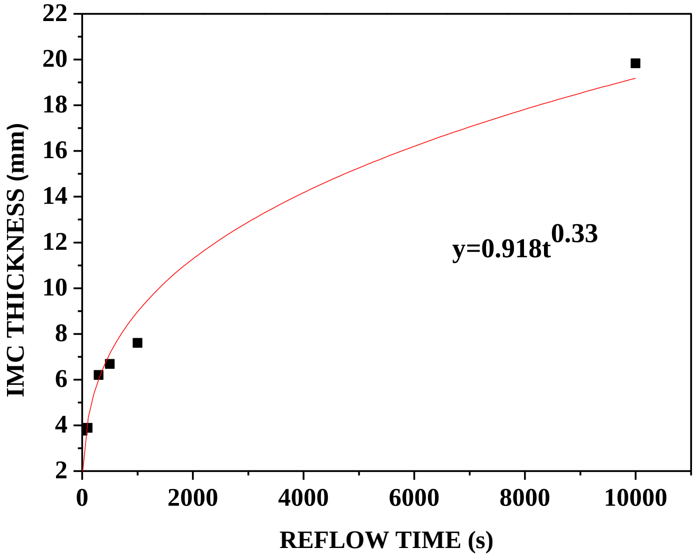

Fig.5.16: Plot of IMC thickness verses reflow time for Sn-0.7Cu solder alloy on bare Cu substrate

5.3.2 Interfacial microstructure of Sn-0.3Ag-0.7Cu solder alloy on bare Cu substrate

Figure 5.17 shows the SEM micrographs of the interface between Sn-0.3Ag-0.7Cu solder and Cu substrate reflowed at 270ºC and furnace cooled for different reaction times. The intermetallic reaction layers are formed in three consecutive stages dissolution, chemical reaction and solidification [Lee et al. 2013]. Cu_6Sn_5 IMC was detected between the solder and Cu layer in all the reaction couples. Cu_6Sn_5 was the initial intermetallic phase found at the interfacial zone after the soldering. Cu_6Sn_5 IMCs are formed because a large driving force for the chemical reaction between Cu and Sn atoms exists at the metastable compositions. Chemical reaction for the formation of Cu_6Sn_5 is given in Equation 20.

$$6Cu+5Sn \rightarrow Cu_6Sn_5 \qquad [20]$$

Since the mass transport mechanism leading to the formation of Cu_6Sn_5 is most efficient at the substrate–IMC–liquid triple points, the nucleated Cu_6Sn_5 grains grow laterally in the initial stages of soldering process. Hence a continuous IMC layer forms, entirely covering the Cu substrate in a fraction of a second [Park et al. 2012]. Once the IMC layer covers the interface the formation of IMC is dominated by Cu diffusion through the phase and grain boundaries [Chung et al. 2010]. As the reaction continues, diffusion of Cu from the substrate leads to the thickening of the Cu_6Sn_5 layer and each grain acquires a scallop-like morphology. This is mainly due to the interplay between interfacial, GB energies and large mass fluxes through GBs [Gagliano et al. 2002, Park et al. 2012]. For a reflow time of 10 s a continuous layer of IMC of 3.43µm thickness was formed. Thickness of IMC increased to 5.43 µm then to 8.32 µm for samples reflowed for 100 and 300s respectively. For a reflow time of 500s IMC thickness was found to be 6.30µm. This drop in thickness can be attributed to the spalling of IMC layer into the bulk solder. Spalling is a consequence of a morphological change of the IMC at the interface[Tu et al. 2003]. Two essential conditions for the spalling to take place are, first is that the inadequate quantity of at least one of the reactive constituents of the solder, and the second is that the soldering reaction has to be very sensitive to the quantity of this component. More and more atoms of this constituent are taken out of the solder and built-in into the intermetallic during the growth of the IMCs. The original intermetallic at the interface becomes a non-equilibrium phase as the concentration of this component decreases and the spalling of the original intermetallic takes place [Yang and Kao 2007]. IMC thickness was found to be 8.30 µm and 9.72 µm for reflow time of 1000 and 10000 s respectively. Ag_3Sn precipitates were also detected in the bulk matrix of Sn-0.3Ag-0.7Cu solder solidified on Cu substrate. However, Ag_3Sn IMCs precipitated only at some locations and not distributed uniformly in the solder. Cu_3Sn IMC with layer-type morphology was observed between Cu_6Sn_5 layer and Cu substrate when the reflow time was 10000s and its thickness was found to be 2.55µm. The formation of Cu_3Sn is affected by the phase stability of Cu according to the following reaction [Gao et al. 2006]

$$Cu_6Sn_5+9Cu \rightarrow 5Cu_3Sn \qquad [21]$$

With an increase in reflow time a change in the morphology of Cu_6Sn_5 IMCs was observed. At a reflow time for 10s IMC had scallop morphology. A long needle morphology was observed in the samples reflowed for 100, 300, 500 and 1000s and it became more coarsened when the samples were reflowed for 10000s.

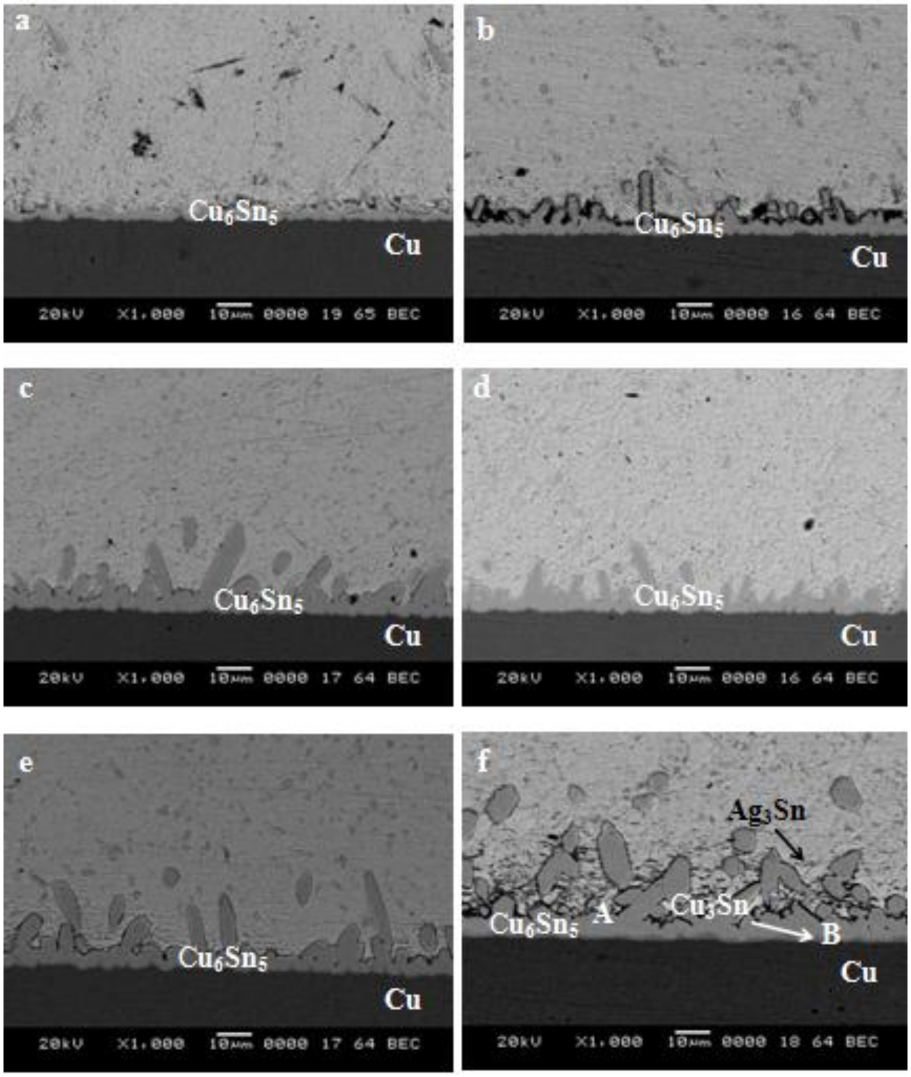

Fig.5.17: The SEM micrographs of the interface between Sn-0.3Ag-0.7Cu solder and Cu substrate reflowed at 270 ºC for different reaction times, (a) 10 s, (b) 100 s, (c) 300 s, (d) 500 s, (e) 1,000 s and (f) 10,000 s

Table 5.10 gives the EDS analysis of marked regions in Figure 5.17. Fig.5.18 shows the XRD pattern of Sn-0.3Ag-0.7Cu solder on Cu surface reflowed at 10, 100, 300, 500, 1000 and 10000 s. The XRD pattern confirmed the formation of Cu_6Sn_5 IMCs at the interface during all the reflow times and also confirmed the formation of Cu_3Sn IMC exclusively during reflow for 10000 s. Table 5.11 shows the effect of reflow time on interfacial reaction, morphology of IMCs of Sn-0.3Ag-0.7Cu/Cu solder joint.

Table 5.10: EDS analysis results of marked regions in Fig. 5.17 for Sn-0.3Ag-0.7Cu solder on Cu substrate

Marks	Cu K (at.%)	Sn L (at.%)	Ag (at.%)	Phase
A	57.02	42.81	0.17	Cu_6Sn_5
B	73.22	26.5	0.28	Cu_3Sn
C	2.33	26.42	71.25	Ag_3Sn

Table 5.11. Effect of reflow time on interfacial reaction, morphology of IMCs and the failure mode of Sn-0.3Ag-0.7Cu/Cu solder joint

Reflow time (s)	Interfacial IMC	Morphology of IMC	Thickness of IMC (μm)
10	Cu_6Sn_5	Continuous round scallop	3.43
100	Cu_6Sn_5	Long needle shape	5.43
300	Cu_6Sn_5	Long needle shape	8.32
500	Cu_6Sn_5	Long needle shape	6.30
1000	Cu_6Sn_5	Long needle shape	8.30
10000	Cu_6Sn_5 Cu_3Sn	Coarse needle shape Layer-type	9.72 2.55

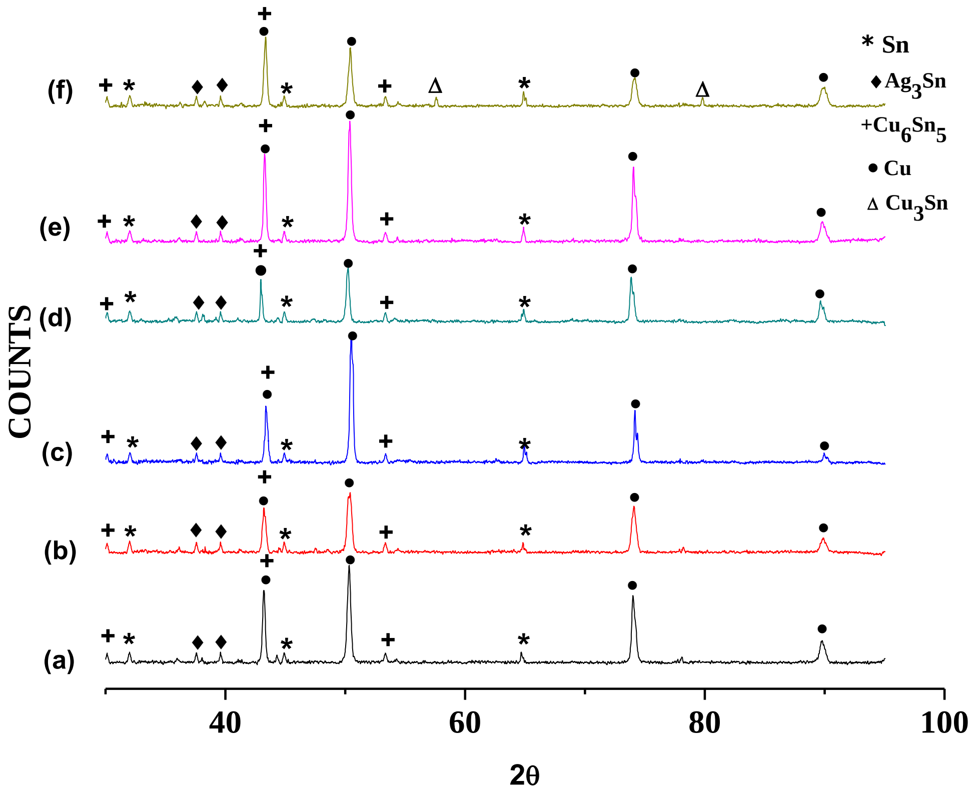

Fig 5.18: **XRD patterns of Sn-0.3Ag-0.7Cu/Cu reflowed at 270 °C for (a) 10 s, (b) 100 s, (c) 300 s, (d) 500 s, (e) 1,000 s and (f) 10,000 s**

The IMC thickness values obtained from the experiment were fitted to equation 19. The plot of IMC thickness vs. reflow time in given in Figure 5.19. The curve could be force fitted with a value of the exponent (n) equal to 1/3 only up to a reflow time of 300 s. The R^2 value obtained was 0.94. Force fitting the curve with n=1/3 for higher value of reflow time yielded a very low R^2 value. This shows that grain boundary diffusion is the governing mechanism for mass transport across the IMC layer during the early stages of the soldering reaction [Park et al. 2012]. The role of grain boundary diffusion diminishes, as the IMC layer grows thicker. The latter part of the growth curve would flatten during the change-over to a slower transport mechanism [Schaefer et al. 2012].

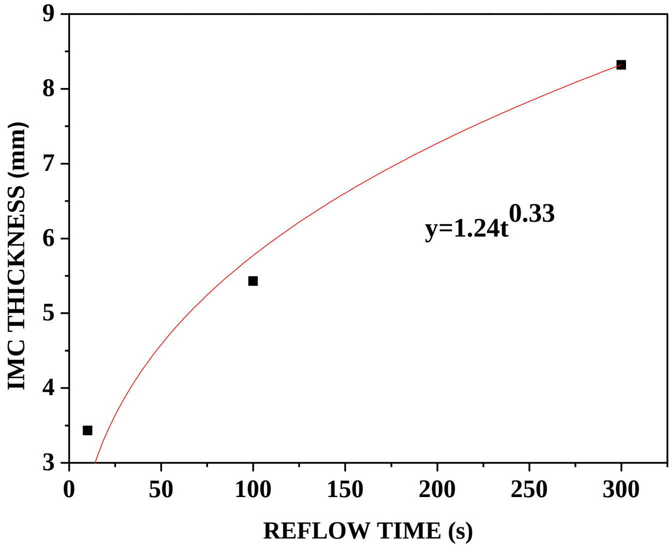

Fig. 5.19: Plot of IMC thickness verses reflow time for Sn-0.3Ag-0.7Cu solder alloy on bare Cu substrate

5.3.3 Interfacial microstructure of Sn-2.5Ag-0.5Cu solder alloy on bare Cu substrate

Figure 5.20 shows the SEM micrographs of the interface between Sn-2.5Ag-0.5Cu solder and Cu substrate reflowed at 270 °C for different reaction times. Cu atoms from the substrate quickly diffuse in to molten solder and get dissolved during initial stages of soldering. Dissolution is a non-equilibrium process[Lee et al. 2013]. Thermodynamically, at the local equilibrium solubility, the solid IMCs begin to form at the solder/substrate interface. Metal solutes were taken out of the saturated liquid solder for the formation of IMCs resulting in further dissolution of the contacted metal, particularly if the intermetallic layer is not uniform on top of the substrate [Laurila et al. 2005]. Hence a change in morphology of IMCs were observed with the reflow time. The primary IMC found at the interface was Cu_6Sn_5. EDS analysis confirmed the formation of Cu_6Sn_5 at the interface of all Sn-2.5Ag-0.5Cu/Cu system in the present study. Sn-2.5Ag-0.5Cu/Cu exhibited both Cu_6Sn_5 and Ag_3Sn IMCs in the bulk of the solder alloy and at the interface, Cu_6Sn_5 IMCs protruded into the solder matrix with few precipitates of Ag_3Sn.

A thin layer of Cu_3Sn IMC was found underneath the Cu_6Sn_5 IMCs at the interface during reflow for 10000 s. The presence of Ag_3Sn IMCs is due to the presence of Ag in solder alloy.

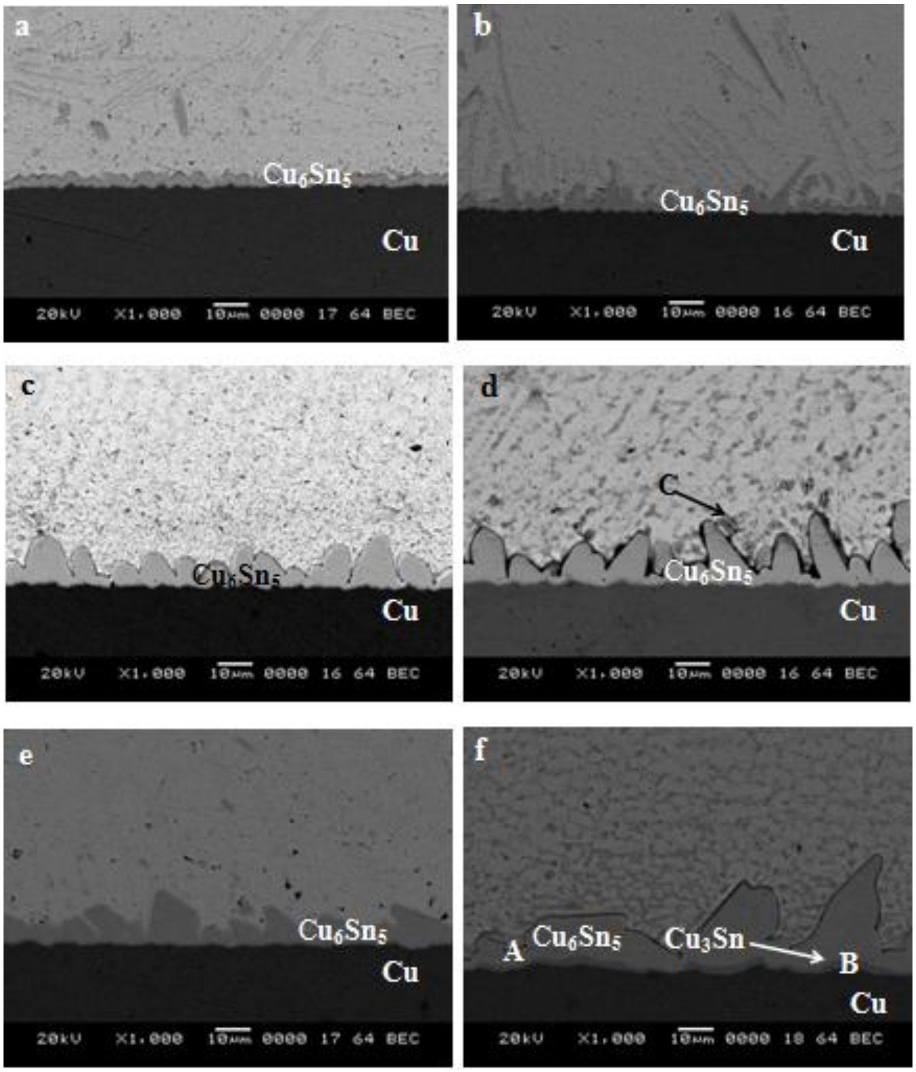

Fig. 5.20: The SEM micrographs of the interface between Sn-2.5Ag-0.5Cu solder and Cu substrate reflowed at 270°C for different reaction times: (a) 10 s, (b) 100 s, (c) 300 s, (d) 500 s, (e) 1,000 s and (f) 10,000 s

Cu_6Sn_5 IMC exhibited scallop shape morphology at the interface during a reflow for 10 s. With an increase in reflow time to 100 s, the morphology of the IMC changed from continuous scallop to long needle morphology and then to coarse needle morphology for the samples reflowed for 300 and 500 s. The interfacial IMCs had highly coarse needle morphology for samples reflowed for 1000 and 1000 s. The increase in reaction times lead to the increase in the thickness of the Cu_6Sn_5 IMC layer. The thickness of the Cu_6Sn_5 IMC layer formed during a reflow time of 10 s was 3.09 µm and its thickness increased to 4.40 µm, 8.21 µm, 10.96 µm, 6.62 µm and 14.66 µm during 100s, 300, 500, 1000 s and 10000 s reflow time respectively. The thickness of Cu_3Sn IMC was measured and it was found to be 2.53 µm. The thickness of Cu_6Sn_5 decreases at the beginning of formation of Cu_3Sn at the interface. This is because at the initial stages of Cu_3Sn formation, it grows at the expense of Cu_6Sn_5 as described by Eq. (19). On formation of the Cu_3Sn layer, Cu_6Sn_5 layer starts to grow again, due to the reaction between Cu atoms diffusing through the intermetallic layers and Sn atoms from the solder [Mookam et al. 2012]. In Sn-2.5Ag-0.5Cu/Cu system a drop in Cu_6Sn_5 IMC thickness was noticed for the samples reflowed for 1000 s and later an increase in thickness in the same layer was observed for samples reflowed for 10000 s. Table 5.12 gives the EDS analysis of marked regions in Figure 5.20. Table 5.13 gives the effect of reflow time on interfacial reaction and morphology of Sn-2.5Ag-0.5Cu/Cu solder joint.

Table 5.12: EDS analysis results of marked regions in Fig. 5.20 for Sn-2.5Ag-0.5Cu solder on bare Cu substrate

Marks	Cu K (at.%)	Sn L (at.%)	Ag L (at.%)	Phase
A	55.54	44.2	0.25	Cu_6Sn_5
B	62.67	37.33	--	Cu_3Sn
C	1.85	29.61	68.59	Ag_3Sn

Table 5.13. Effect of reflow time on interfacial reaction and morphology of Sn-2.5Ag-0.5Cu/Cu solder joint

Reflow time (s)	Interfacial IMC	Morphology of IMC	Thickness of IMC (μm)
10	Cu_6Sn_5	Continuous round scallop	3.09
100	Cu_6Sn_5	Long needle shape	4.40
300	Cu_6Sn_5	Coarse needle shape	8.21
500	Cu_6Sn_5	Coarse needle shape	10.96
1000	Cu_6Sn_5	Highly coarse needle shape	6.62
10000	Cu_6Sn_5 Cu_3Sn	Highly coarse needle shape Layer-type	14.66 2.53

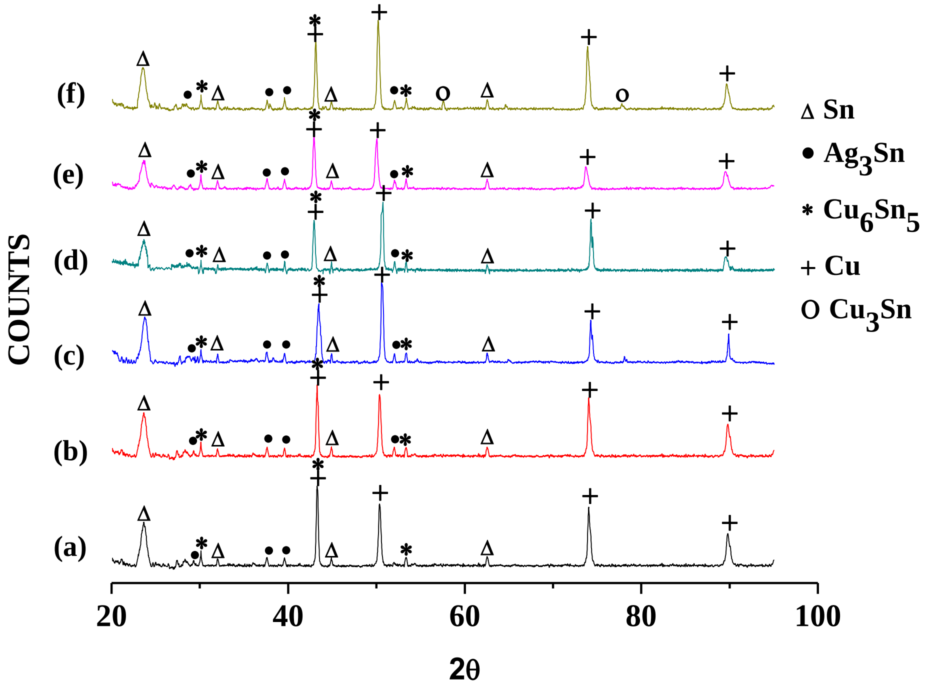

Fig. 5.21: XRD patterns of Sn-2.5Ag-0.5Cu/Cu reflowed at 270 °C for (a) 10 s, (b) 100 s, (c) 300 s, (d) 500 s, (e) 1,000 s and (f) 10,000 s

Figure 5.21 shows the XRD pattern of Sn-2.5Ag-0.5Cu solder on Cu surface reflowed at 10, 100, 300, 500, 1000 and 10000 s. The XRD pattern confirmed the formation of Cu_6Sn_5 IMCs at the interface during all the reflow times and the formation of Cu_3Sn IMC only during reflow for 10000 s.

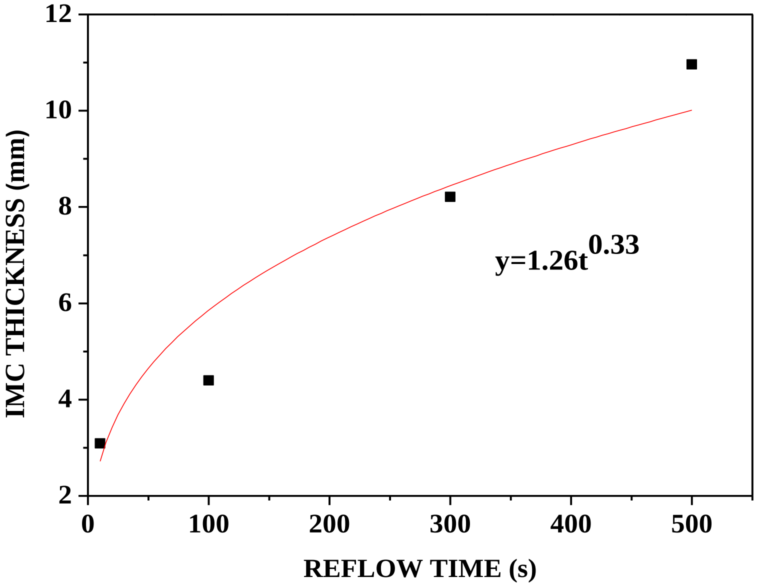

Fig. 5.22: Plot of IMC thickness verses reflow time for Sn-2.5Ag-0.5Cu solder alloy on bare Cu substrate

The obtained IMC thickness values were fitted to a growth model given in equation 19. Plot of IMC thickness verses reflow time in given in Figure 5.22. The curve could force fitted with a value of the exponent (n) equal to 1/3 only up to a reflow time of 500 s. The R^2 value obtained was 0.92. Force fitting the curve with n=1/3 for higher value of reflow time yielded a very low R^2 value. This clearly confirms that grain boundary diffusion is the governing mechanism for mass transport across the IMC layer during the early stages of the soldering reaction. The role of grain boundary diffusion diminishes, as the IMC layer grows thicker and volume boundary diffusion governs the mass transport during later stages of soldering reaction

5.4 Interfacial microstructure of Sn-0.7Cu, Sn-0.3Ag-0.7Cu and Sn-2.5Ag-0.5Cu solder on bare Cu substrate [quench cooled solder/substrate system]

5.4.1 Interfacial microstructure of Sn-0.7Cu on bare Cu substrate

Figure 5.23 shows the SEM micrographs of the interface of quench cooled Sn–0.7Cu/Cu system reflowed at 270 °C for different reaction times. The various reflow times were 10, 25, 100, 300 and 500 s.

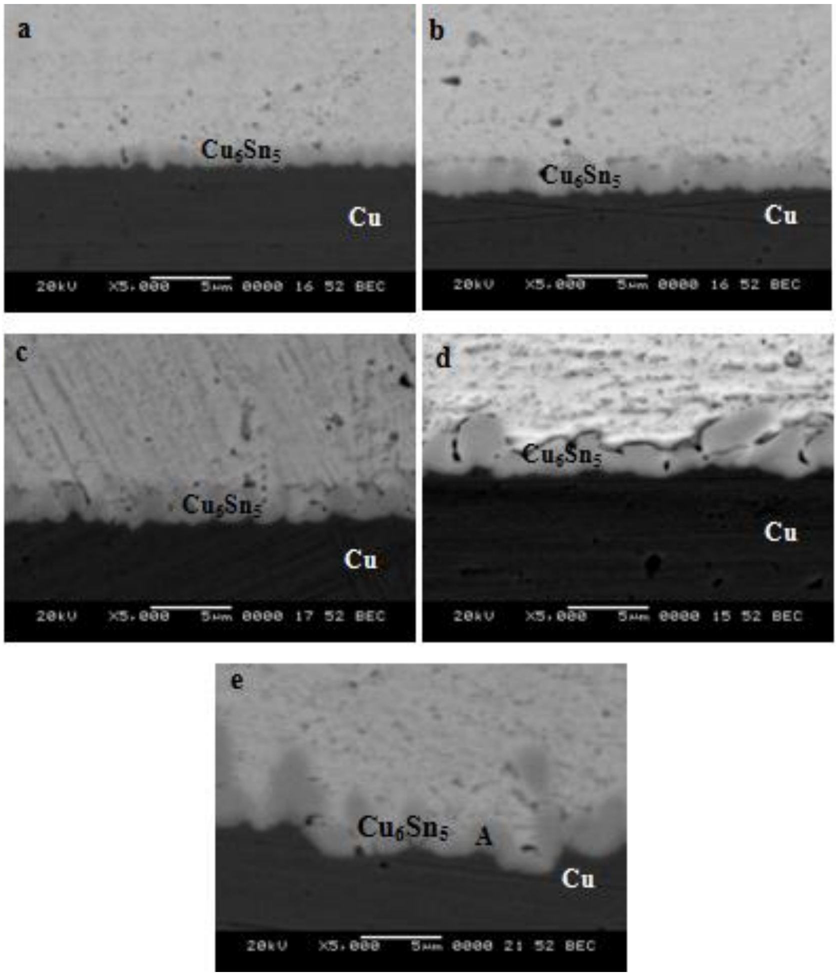

Fig.5.23: The SEM micrographs of the Sn-0.7Cu/Cu interface reflowed at 270 °C for various times; (a) 10 s, (b) 25 s, (c) 100 s, (d) 300 s and (e) 500 s

Quench cooling method was opted as furnace cooling had no effective control on the reflow time, also which would hinder the examination of microstructure at desired reflow time. EDS analysis revealed that the IMCs were composed of Cu and Sn atoms. IMC thickness was lower than those obtained for furnace cooled solder/substrate system as it was quenched at the desired reflow time. Atomic percentage of Cu decreased from the root to the tip of the IMC. In all the reaction couples, only Cu_6Sn_5 IMC was detected between the solder and Cu layer. No Cu_3Sn was found at the interface of any Sn-0.7Cu/Cu system. EDS analysis of marked regions in Figure 5.23 are given in Table 5.14. Table 5.15 gives the effect of reflow time on interfacial IMC thickness and morphology. The Cu_6Sn_5 IMC formed on the Cu substrate had round scallop shape morphology. With an increase in reflow time above 100 s, the morphology of the IMC changed from a round scallop shape to elongated scallop shape.

Table 5.14: EDS analysis results of marked regions in Fig. 5.17 for Sn--0.7Cu solder on Cu substrate

Marks	Cu K (at.%)	Sn L (at.%)	Phase
A	53.41	46.59	Cu_6Sn_5

Table 5.15: Effect of reflow time on interfacial reaction, morphology of IMCs at Sn-0.7Cu/Cu interface.

Reflow time (s)	Interfacial IMC	Morphology of IMC	Thickness of IMC (μm)
10	Cu_6Sn_5	Round scallop	0.93
25	Cu_6Sn_5	Round scallop	1.15
100	Cu_6Sn_5	Round scallop	1.62
300	Cu_6Sn_5	Elongated scallop	2.29
500	Cu_6Sn_5	Elongated scallop	3.25

The obtained IMC thickness values were force fitted with a growth rate equal to 1/3, to a growth model given by equation 19. Plot of IMC thickness verses reflow time is given in Figure 5.24. Force fitting the curve with n=1/3 yielded an R^2 value of 0.96. This clearly confirms that grain boundary diffusion is the prime transport mechanism in rate-controlling process for the IMC growth in Sn-0.7Cu/Cu systems.

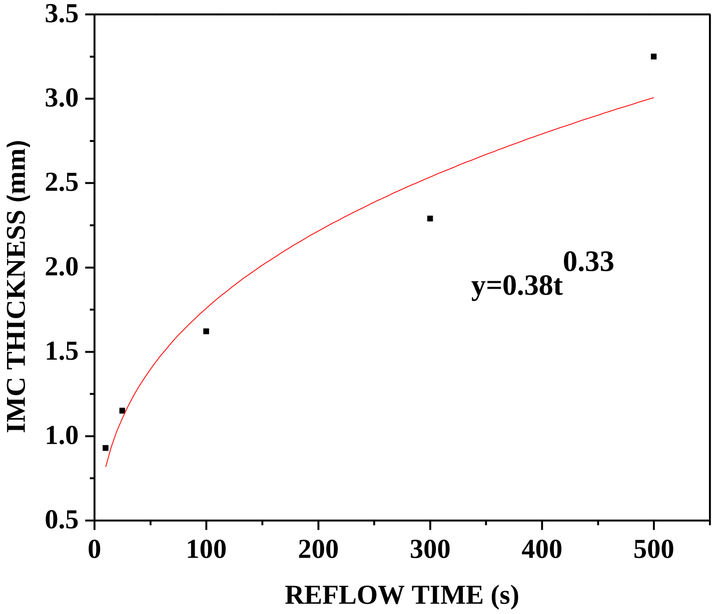

Fig. 5.24: Plot of IMC thickness verses reflow time for Sn-0.7Cu solder alloy on bare Cu substrate

5.4.2 Interfacial microstructure of Sn-0.3Ag-0.7Cu on bare Cu substrate

Figure 5.25 shows the SEM micrographs of the Sn-0.3Ag0.7Cu/Cu interface reflowed at 270 °C for various times. EDS analysis showed the presence of only Cu_6Sn_5 in all the solder/substrate interface reflowed for 10, 40, 100, 300 and 500 s. At lower reflow times say 10, 40 and 100 Cu_6Sn_5 showed round scallop morphology. For the reflow times above 100 s morphology of the IMC changed from a round scallop shape to elongated needle shape.

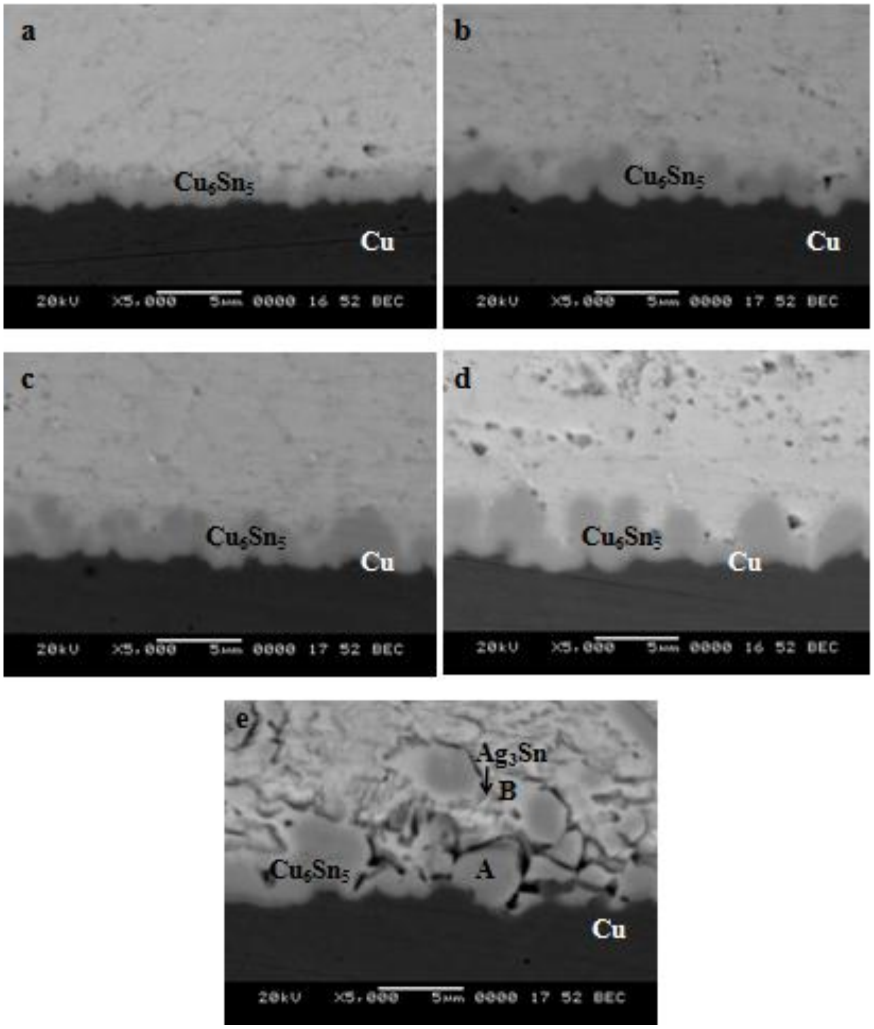

Fig.5.25: The SEM micrographs of the Sn-0.3Ag-0.7Cu/Cu interface reflowed at 270 °C for various times; (a) 10 s, (b) 40 s, (c) 100 s, (d) 300 s and (e) 500 s

Table 5.16 gives the EDS analysis results of marked regions in Figure 5.25. IMC thickness found to increase with increase in reflow time. Table 5.17 gives the effect of reflow time on thickness and morphology of interfacial IMC. Figure 5.26 shows the plot of IMC thickness verses reflow time for Sn-0.3Ag-0.7Cu solidified on bare copper substrate. The graph was force fitted to a growth exponent, n=1/3 in the growth model given by equation 19. However, a lower R^2 (0.4) was obtained compared to other solder/substrate systems.

Table 5.16: EDS analysis results of marked regions in Fig. 5.25 for Sn-0.3Ag-0.7Cu solder on bare Cu substrate

Marks	Cu K (at.%)	Sn L (at.%)	Ag L (at.%)	Phase
A	53.10	46.77	0.13	Cu_6Sn_5
B	1.20	32.85	65.95	Ag_3Sn

Table 5.17: Effect of reflow time on thickness and morphology of interfacial IMC formed between Sn-0.3Ag-0.7Cu and bare Cu substrate.

Reflow time (s)	Interfacial reaction product	Morphology of IMC	IMC thickness (µm)
10	Cu_6Sn_5	Round scallop	1.67
40	Cu_6Sn_5	Round scallop	1.74
100	Cu_6Sn_5	Round scallop	2.20
300	Cu_6Sn_5	Elongated needle	2.85
500	Cu_6Sn_5	Elongated needle	2.91

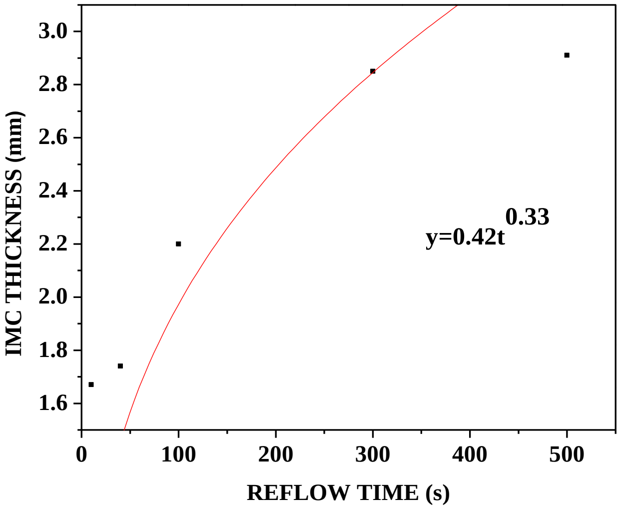

5.26: Plot of IMC thickness verses reflow time for Sn-0.3Ag-0.7Cu solder alloy on bare Cu substrate

5.4.3 Interfacial microstructure of Sn-2.5Ag-0.5Cu on bare Cu substrate

Figure 5.27 shows the SEM micrographs of the interface of quench cooled Sn-2.5Ag-0.5Cu /Cu system reflowed at 270 °C for different reaction times. The various reflow times were 10, 40, 100, 300 and 500 s. EDS analysis revealed that the IMCs were composed of Cu and Sn atoms. In all the reaction couples, only Cu_6Sn_5 IMC was detected between the solder and Cu layer. EDS analysis of marked regions in Figure 5.27 are given in Table 5.18. Table 5.19 shows the effect of reflow time on interfacial IMC thickness and morphology. The Cu_6Sn_5 IMC formed on the Cu substrate had round scallop shape morphology. With an increase in reflow time above 100 s, the morphology of the IMC changed from a round scallop shape to elongated needle shape.

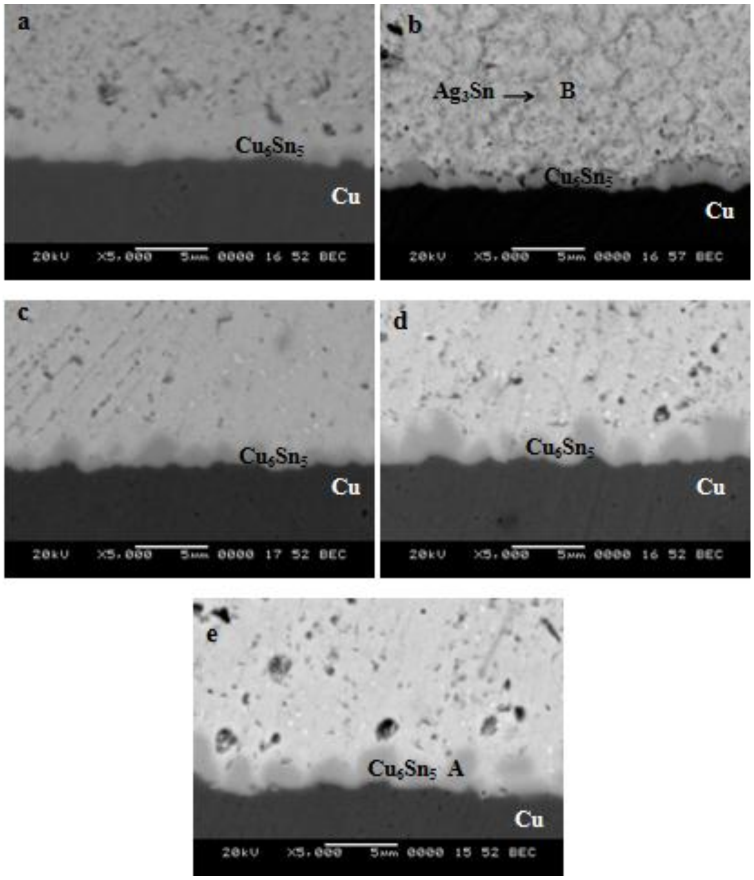

Fig.5.27: The SEM micrographs of the Sn-2.5Ag-0.5Cu/Cu interface reflowed at 270°C for various times; (a) 10 s, (b) 40 s, (c) 100 s, (d) 300 s and (e) 500 s

Table 5.18: EDS analysis results of marked regions in Fig. 5.14 for Sn-2.5Ag-0.5Cu solder on bare Cu substrate

Marks	Cu K (at.%)	Sn L (at.%)	Ag L (at.%)	Phase
A	51.40	48.16	0.44	Cu_6Sn_5
B	1.03	25.71	73.26	Ag_3Sn

Figure 5.28 shows the plot of IMC thickness verses reflow time for Sn-2.5Ag-0.5Cu solidified on bare copper substrate. Growth kinetics showed that grain boundary diffusion is the prime transport mechanism in rate-controlling process for the IMC growth in Sn-2.5Ag-0.5Cu /Cu systems. The obtained IMC thickness was fitted to growth model given by equation 19. The R^2 value obtained by force fitting the graph to a growth exponent, n=1/3 was about 0.93.

Table 5.19: Effect of reflow time on thickness and morphology of interfacial IMC formed between Sn-2.5Ag-0.5Cu and bare Cu substrate.

Reflow time (s)	Interfacial reaction product	Morphology of IMC	IMC thickness (μm)
10	Cu_6Sn_5	Round scallop	0.75
40	Cu_6Sn_5	Round scallop	1.04
100	Cu_6Sn_5	Round scallop	1.197
300	Cu_6Sn_5	Elongated needle	1.81
500	Cu_6Sn_5	Elongated needle	1.95

Among the three solder alloys reflowed on Cu substrate [quench cooled], Sn-0.3Ag-0.7Cu/Cu showed highest IMC thickness whereas Sn-2.5Ag-0.5Cu/Cu showed lowest thickness up to a reflow time of 100 s. At higher reflow times Sn-0.7Cu /Cu showed maximum IMC thickness. A similar trend was seen in furnace cooled solder/Cu systems.

Up to a reflow time of 300 s, maximum IMC thickness was observed in Sn-0.3Ag-0.7Cu/Cu system and Sn-0.7Cu/Cu showed lowest IMC thickness.

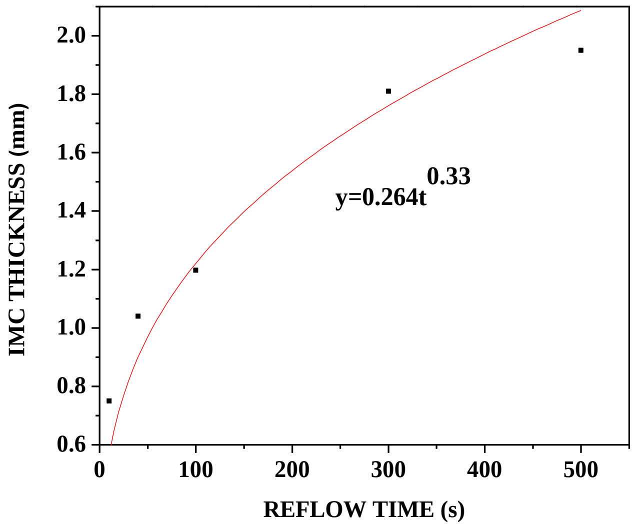

5.28: Plot of IMC thickness verses reflow time for Sn-2.5Ag-0.5Cu solder alloy on bare Cu substrate

5.5 Interfacial microstructure of Sn-0.7Cu, Sn-0.3Ag-0.7Cu and Sn-2.5Ag-0.5Cu solder on Ni coated substrate [quench cooled solder/substrate system]

5.5.1 Interfacial microstructure of Sn-0.7Cu on Ni coated Cu substrate

Figure 5.29 shows the SEM (Back-scattered electron mode) micrographs of the interface between Sn-0.7Cu solder and Ni coated Cu substrate reflowed at 270°C for various reaction times. Two reaction products, $(CuNi)_6Sn_5$ and $(CuNi)_3Sn_4$ were identified at the solder/substrate interface by EDS analysis. Table 5.20 gives the atom % of Cu, Ni and Sn present in the interfacial region. $(CuNi)_6Sn_5$ was the only IMC existed at the interface up to a reflow time of 300 s. Samples reflowed for 500 s showed both $(CuNi)_6$ Sn_5 and $(CuNi)_3Sn_4$ IMCs at the interface. $(CuNi)_3Sn_4$ was found underneath $(CuNi)_6Sn_5$ and its thickness was very small to be measured. Thickness of $(CuNi)_6Sn_5$ IMC increased with increase in reflow time. IMC thickness was 0.89 μm, 0.98 μm, 1.12 μm, 1.61 μm and 1.89 μm for a reflow time of 10, 50, 100, 300 and 500 s respectively.

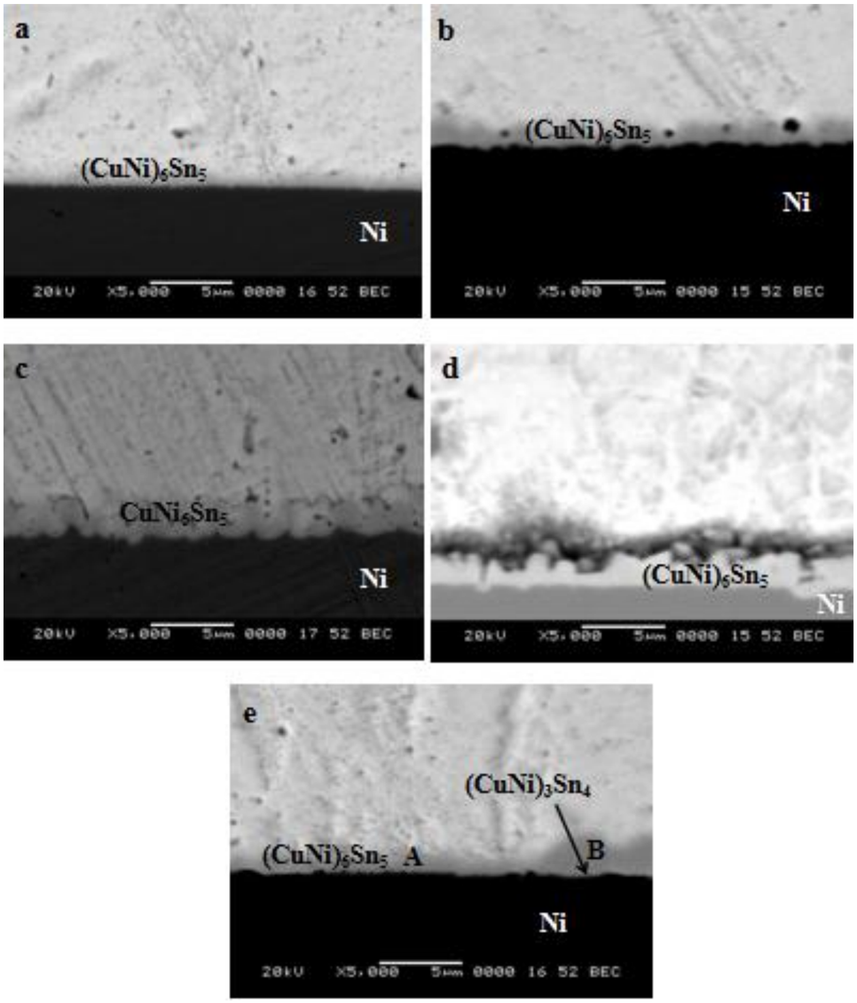

Fig.5.29: The SEM micrographs of the Sn-0.7Cu/Ni/Cu interface reflowed at 270°C for various times; (a) 10 s, (b) 50 s, (c) 100 s, (d) 300 s and (e) 500 s

The thickness of IMCs formed at the interface was lower on Ni coated Cu substrate when compared to that of the same solder alloy on bare Cu substrate. This clearly indicates that Ni acts as a diffusion barrier to prevent the rapid reaction of the molten solder with Cu substrate. The thickness and morphology of IMCs at various reflow times are summarized in Table 5.21. The growth kinetics of the IMC layer was studied. The obtained thickness values were fitted according to the growth model given by equation [19]. Figure 5.30 shows the plot of IMC thickness verses reflow time. The R^2 value was found to be 0.81 when the IMC thickness was force fitted to growth exponent value, n =1/3. Therefore, it was concluded that grain boundary diffusion is the growth controlling process in Sn-0.7Cu/Ni/Cu system.

Table 5.20: EDS analysis results of marked regions in Fig. 5.21 for Sn-0.7Cu solder on Ni coated Cu substrate

Marks	Cu K (at.%)	Sn L (at.%)	Ni K (at.%)	Phase
A	31.77	47.15	21.08	$(CuNi)_6Sn_5$
B	11.58	56.21	32.21	$(CuNi)_3Sn_4$

Table 5.21: Effect of reflow time on IMC thickness and morphology of interfacial IMC formed between Sn-0.7Cu and Ni coated Cu substrate.

Reflow time (s)	Interfacial reaction product	Morphology of IMC	IMC thickness (μm)
10	$(CuNi)_6Sn_5$	Scallop	0.89
50	$(CuNi)_6Sn_5$	Scallop	0.98
100	$(CuNi)_6Sn_5$	Scallop	1.12
300	$(CuNi)_6Sn_5$	scallop	1.61
500	$(CuNi)_6Sn_5$ $(CuNi)_3Sn_4$	Coarse scallop	1.89

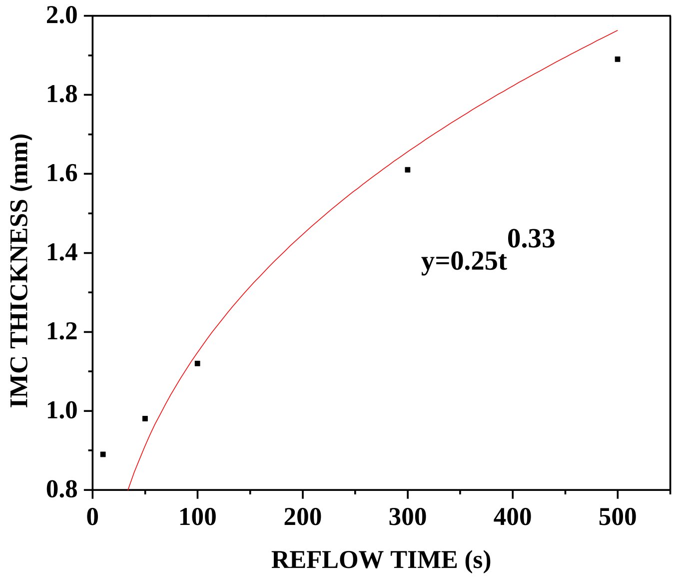

Fig. 5.30: Plot of IMC thickness verses reflow time for Sn-0.7Cu solder alloy on Ni coated Cu substrate

5.5.2 Interfacial microstructure of Sn-0.3Ag-0.7Cu on Ni coated Cu substrate

Figure 5.31 shows the SEM (Back-scattered electron mode) micrographs of the interface between Sn-0.3Ag-0.7Cu solder and Ni coated Cu substrate reflowed at 270°C for various reaction times. $(CuNi)_6Sn_5$ and $(CuNi)_3Sn_4$ IMCs were identified at the solder/substrate interface by EDS analysis. Table 5.22 gives the atom % of Cu, Ni and Sn present in the interfacial region marked in Figure 5.31. Only $(CuNi)_6Sn_5$ IMC was observed at the interface up to a reflow time of 300 s. Samples reflowed for 500 s showed both $(CuNi)_6Sn_5$ and $(CuNi)_3Sn_4$ IMCs at the interface. IMC thickness increased with increase in reflow time up to 300 s. IMC thickness was 0.3 µm, 1.15 µm and 2.03 µm for a reflow time of 10, 100 and 300 s respectively. IMC thickness dropped to 1.94 µm for a reflow time of 500s. As long as sufficient Cu was available, it combines with Ni and Sn to form $(CuNi)_6Sn_5$. Eventually, this growing phase consumes essentially all the available Cu in the solder. This consumption can alter the mechanical properties of Pb-free solder joints as the mechanical properties of Sn–Ag–Cu alloys depend upon the Cu content. After consumption of the Cu from the solder, further reflow gradually transforms the

$(CuNi)_6Sn_5$ phase into a $(CuNi)_3Sn_4$ [Zribi et al. 2001, Wong et al. 2008] Therefore, spalling of $(CuNi)_6Sn_5$ observed for samples reflowed for 500 s can be attributed to the decrease of the available Cu in the solders. More and more atoms of this constituent are taken out of the solder and built-in into the intermetallic during the growth of the IMCs. The original intermetallic at the interface becomes a non-equilibrium phase as the concentration of this component decreases and the spalling of the original intermetallic takes place [Sona and Prabhu 2015].

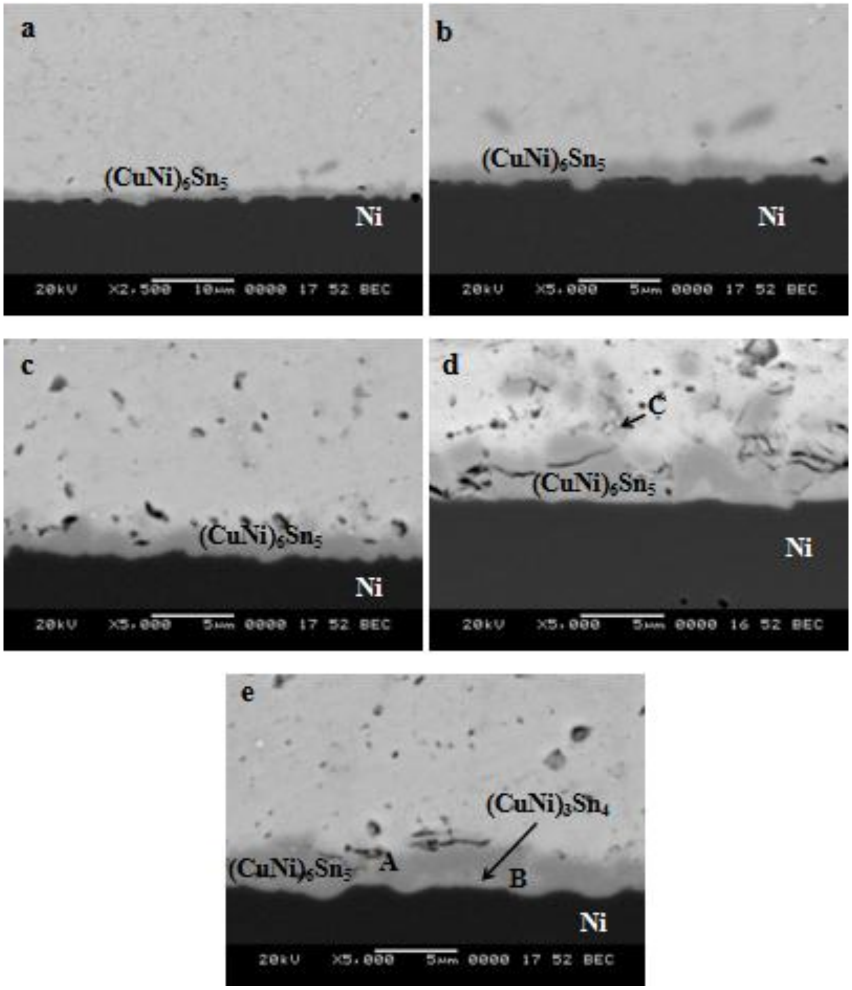

Fig.5.31: The SEM micrographs of the Sn-0.3Ag-0.7Cu/Ni/Cu interface reflowed at 270°C for various times; (a) 10 s, (b) 70 s, (c) 100 s, (d) 300 s and (e) 500 s

The effect of reflow time on IMC formation and thickness of IMCs given in Table 5.23. IMC thickness was plotted against reflow time and the graph was force fitted to a growth exponent, n =1/3 in the growth model given by equation [19]. The R^2 value was found to be 0.91 which indicated that the grain boundary diffusion was the growth rate controlling process in Sn-0.3Ag-0.7Cu/Ni/Cu system. Figure 5.32 shows the plot of IMC thickness verses reflow time. Thickness of IMCs at the interface of Sn-0.3Ag-0.7Cu/Ni/Cu system was found be lower than Sn-0.3Ag-0.7Cu/Cu indicating Ni act as a barrier for the formation of intermetallics at the solder/substrate interface.

Table 5.22: EDS analysis results of marked regions in Fig. 5.31 for Sn-0.3Ag-0.7Cu solder on Ni coated Cu substrate

Marks	Cu K (at.%)	Ag L (at.%)	Ni K (at.%)	Sn L (at.%)	Phase
A	29.19	0.20	24.74	45.86	$(CuNi)_6Sn_5$
B	13.58	0.31	29.71	56.4	$(CuNi)_3Sn_4$
C	1.28	71.28	2.16	25.28	Ag_3Sn

Table 5.23: Effect of reflow time on IMC thickness and morphology of interfacial IMC formed between Sn-0.3Ag-0.7Cu and Ni coated Cu substrate.

Reflow time (s)	Interfacial reaction product	Morphology of IMC	IMC thickness (μm)
10	$(CuNi)_6Sn_5$	Scallop	0.3
70	$(CuNi)_6Sn_5$	Scallop	0.95
100	$(CuNi)_6Sn_5$	Scallop	1.15
300	$(CuNi)_6Sn_5$	Highly coarse scallop	2.03
500	$(CuNi)_6Sn_5$ $(CuNi)_3Sn_4$	Coarse scallop	1.94

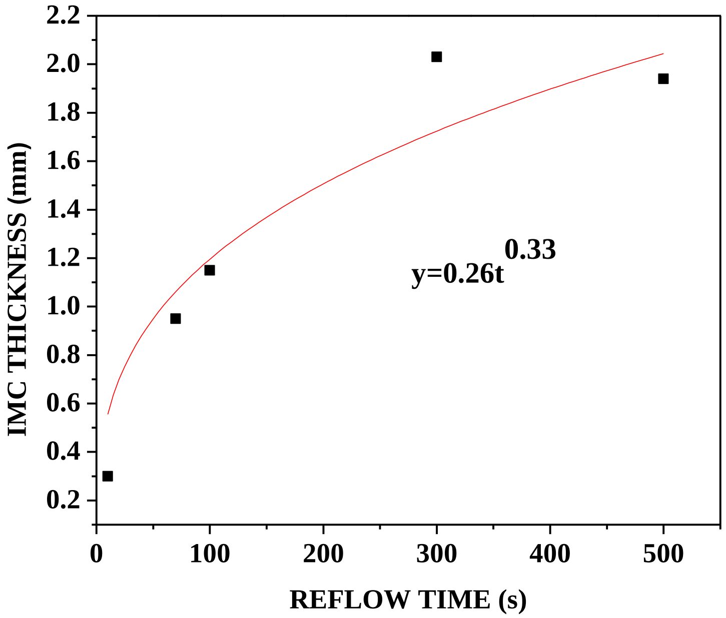

Fig. 5.32: Plot of IMC thickness verses reflow time for Sn-0.3Ag-0.7Cu solder alloy on Ni coated Cu substrate

5.5.3 Interfacial microstructure of Sn-2.5Ag-0.5Cu on Ni coated Cu substrate

Figure 5.33 shows the SEM micrographs (back-scattered electron mode) of the interface between Sn-2.5Ag-0.5Cu solder and Ni coated Cu substrate reflowed at 270°C for various reaction times. The chemical composition of IMCs revealed that the IMCs were composed of Cu, Ni and Sn atoms. $(CuNi)_6Sn_5$ and $(CuNi)_3Sn_4$ were the two kinds of reaction products identified at the interface. Table 5.24 gives the atom % of Cu, Ni and Sn present in the interfacial region. $(CuNi)_6Sn_5$ IMC was the only IMC found at the solder/substrate interface up to a reflow time of 300s and has a scallop morphology. Cu from the solder combines with Ni and Sn to form $(CuNi)_6Sn_5$ IMC. Thickness of $(CuNi)_6Sn_5$ IMC was found to increase up to a reflow time of 300 s. IMC thickness was 0.69 μm, 0.84 μm, 1.81 μm and 2.86 μm for a reflow time of 10, 80, 100 and 300s respectively. Eventually, this growing phase consumes essentially all the available Cu in the solder. After Cu has been completely consumed from the Sn-Ag-Cu bulk solder $(CuNi)_6Sn_5$ gets eventually replaced by $(CuNi)_3Sn_4$ [Zribi et al. 2001, Wong et al. 2008].

Both $(CuNi)_6Sn_5$ and $(CuNi)_3Sn_4$ IMCs were found in samples reflowed for 500 s. Thickness of $(CuNi)_6Sn_5$ IMC dropped to 1.99 µm for a reflow time of 500 s. The reduction in thickness of $(CuNi)_6Sn_5$ observed for samples reflowed for 500s was attributed to the decrease of the available Cu in the solder bulk matrix. The thickness of IMCs formed at the interface was lower on Ni coated Cu substrate when compared to the same alloy on bare Cu substrate up to a reflow time of 100 s. This clearly indicates that Ni acts as a diffusion barrier to prevent the rapid reaction of the molten solder with Cu substrate. The effect of reflow time on IMC formation and thickness of IMCs given in Table 5.25.

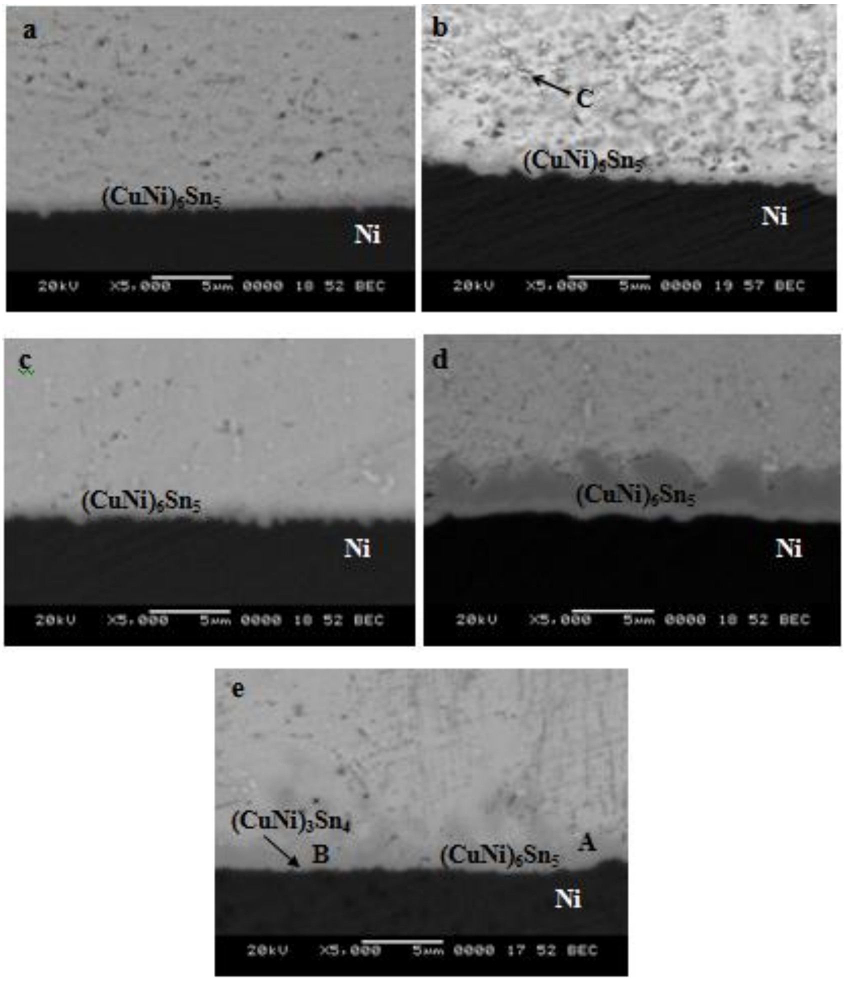

Fig.5.33: The SEM micrographs of the Sn-2.5Ag-0.5Cu/Ni/Cu interface reflowed at 270°C for various times; (a) 10 s, (b) 80 s, (c) 100 s, (d) 300 s and (e) 500

Table 5.24: EDS analysis results of marked regions in Fig. 5.33 for Sn-2.5Ag-0.5Cu solder on Ni coated Cu substrate

Marks	Cu K (at.%)	Ag L (at.%)	Ni K (at.%)	Sn L (at.%)	Phase
A	30.43	0.34	20.44	48.79	$(CuNi)_6Sn_5$
B	12	0.28	30.62	57.1	$(CuNi)_3Sn_4$
C	1.05	72.57	2.45	23.93	Ag_3Sn

Table 5.25: Effect of reflow time on IMC thickness and morphology of interfacial IMC formed between Sn-2.5Ag-0.5Cu and Ni coated Cu substrate.

Reflow time (s)	Interfacial reaction product	Morphology of IMC	IMC thickness (μm)
10	$(CuNi)_6Sn_5$	Scallop	0.69
80	$(CuNi)_6Sn_5$	Scallop	1.54
100	$(CuNi)_6Sn_5$	Scallop	1.81
300	$(CuNi)_6Sn_5$	Highly coarse scallop	2.86
500	$(CuNi)_6Sn_5$ $(CuNi)_3Sn_4$	Coarse scallop	1.99

The thickness of IMC was found to be greater at the interface of Sn-2.5Ag-0.5Cu solder and Ni coated Cu substrate for longer reflow times. The growth kinetics of the IMC layer was studied. The obtained thickness values were fitted according to the growth model given by equation [19]. Since it is assumed that the growth of an IMC layer is dominated by grain boundary (GB) diffusion and limited by the coarsening of the microstructure when growth rate (n) is equal to 1/3, the curve was force fitted with a value of the exponent (n) equal to 1/3. The R^2 value obtained was 0.62 for Sn-2.5Ag-0.5Cu/Ni/Cu system. This shows that GB diffusion, is the prime transport mechanism in the rate-controlling process for the IMC growth in Sn-2.5Ag-0.5Cu/Ni/Cu systems. A plot of

IMC thickness verses reflow time for Sn-2.5Ag-0.5Cu solder alloy on Ni coated Cu substrate is shown in Figure 5.34.

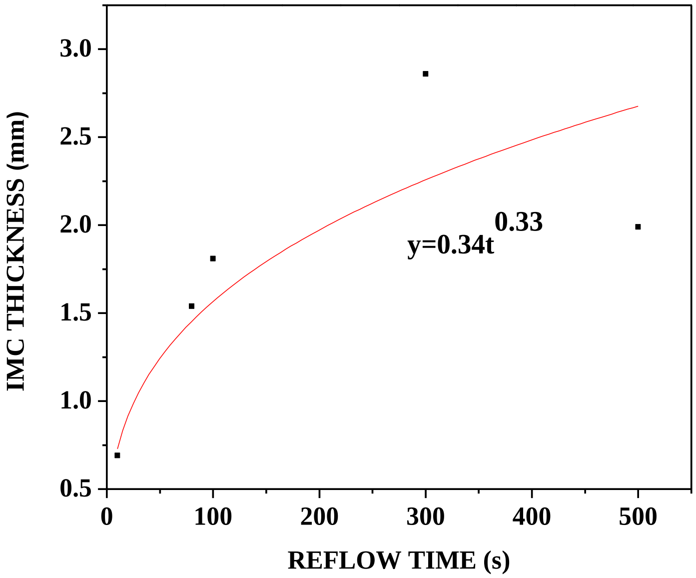

Fig. 5.34: Plot of IMC thickness verses reflow time for Sn-2.5Ag-0.5Cu solder alloy on Ni coated Cu substrate

5.6 Ball shear test results

5.6.1. Shear strength of Sn-0.7Cu, Sn-0.3Ag-0.7Cu and Sn-2.5Ag-0.5Cu solder on bare Cu substrate [furnace cooled samples]

During service, due to temperature variation thermal stresses are generated in the solder. The prime reason behind this is the difference in coefficient of thermal expansion between the solder and the substrate. These stresses, whether in creep or thermal fatigue, have a predominantly shear component. Thus, adequate mechanical characterization of solder joints requires shear testing. Several shear testing techniques have been used so far for solder joints. These include the Iosipescu technique, ring-and-plug, single lap-shear, double lap-shear and ball shear. The Iosipescu technique, for example, has typically been used to test the in-plane and inter laminar shear strength of composite materials using an asymmetric bending moment to induce a state of predominant shear loading. Yet, this technique is quite cumbersome in terms of gripping and specimen preparation. The ring-and-plug technique, which has also been used in solder joints, consists of placing a solder preform in a hollow ring, and dipping the “plug” to form a circular joint. The shortcomings of this technique are that uniform wetting of the solder throughout the joint is difficult to achieve, and that the shear stresses vary from the inside diameter to the outside diameter of the joint [Chawla et al. 2004].

Ball shear testing is the most widely accepted method for evaluating quality of Ball grid array (BGA) solder joints. Ball shear tests were performed to evaluate the effect of the interfacial reactions on the reliability of solder joints as a function of reflow time. During the shear test, the solder joint fractures along the weak point which indicates the failure mode of the solder joint. It was reported that, if the applied stress by the shear tool on the interface is higher than the solder strength, although the net interfacial stress during the shear test is lower than the interfacial adhesion strength, the solder ball will fail inside the solder. On the other hand, if the adhesion strength between the IMC layer and the substrate metallisation layer (or any other layer) is lower than the net interfacial stress during the shear test, the solder ball will fail through the interface [Yoon and Jung 2009]. Figure 5.35, Figure 5.36 and Figure 5.37 show the force-distance curves obtained during the shear test on Sn-0.7Cu/Cu, Sn-0.3Ag-0.7Cu/Cu and Sn-2.5Ag-0.5Cu/Cu furnace cooled solder/substrate surfaces respectively. Three sets of experiments were carried out to obtain consistent results, and the error bars on the force-distance curves indicate the standard deviation in the shear strength values in these three sets of tests. The variation in the spread area of the sessile drop resulted in slight scatter in the force-distance curves. The shear energy was calculated by measuring the area under the force-displacement curve. The shear energy values of Sn-0.7Cu/Cu, Sn-0.3Ag-0.7Cu/Cu and Sn-2.5Ag-0.5Cu/Cu furnace cooled systems obtained from the bond testing experiment are given in Table 5.26.

Table 5.26. Shear energy of Sn-0.7Cu/Cu, Sn-0.3Ag-0.7Cu/Cu and Sn-2.5Ag-0.5Cu/Cu systems (furnace cooling method)

Reflow time (s)	Shear energy (kJ/m^2)		
	Sn-0.7Cu	SAC0307	SAC2505
10	37.54±0.48	42.71±1.52	35.66±1.92
100	40.84±0.60	43.20±2.89	44.75±0.97
300	39.10±0.28	39.61±3.65	45.99±1.98
500	34.89±1.31	37.73±1.82	49.87±1.17
1000	31.03±0.21	36.89±0.59	45.83±2.55
10000	26.14±0.38	30.76±2.71	39.81±1.09

Force versus distance curves exhibited a gradual decrease after reaching a peak value. Sn-0.7Cu/Cu and Sn-0.3Ag-0.7Cu/Cu systems showed maximum shear energy for the reflow time of 100 s. Sn-2.5Ag-0.5Cu/Cu systems reflowed for 500 s gave maximum shear energy value among Sn-2.5Ag-0.5Cu/Cu systems reflowed for various reflow times. A drop in shear energy values was observed for samples reflowed for higher time intervals in the later stages. In addition, a reduction in the shear force for all the solder joints was recorded with increasing thickness of interfacial Cu–Sn IMC layer after the critical thickness or reflow time corresponding to the maximum strength. This is mainly due to the continuous depletion of Sn from the bulk Sn–Cu solder during the growth of interfacial Cu-Sn IMC at the solder joint. This will lead to a lower tin content and hence lower the joint strength as long as the fracture crack is confined in the bulk solder [Chan et al. 1998]. SAC2505/Cu system showed a better strength when compared with Sn-0.7Cu/Cu and SAC0307/Cu systems. The increase in shear energy for the Ag bearing solder is mainly due to the presence of minor Ag content.

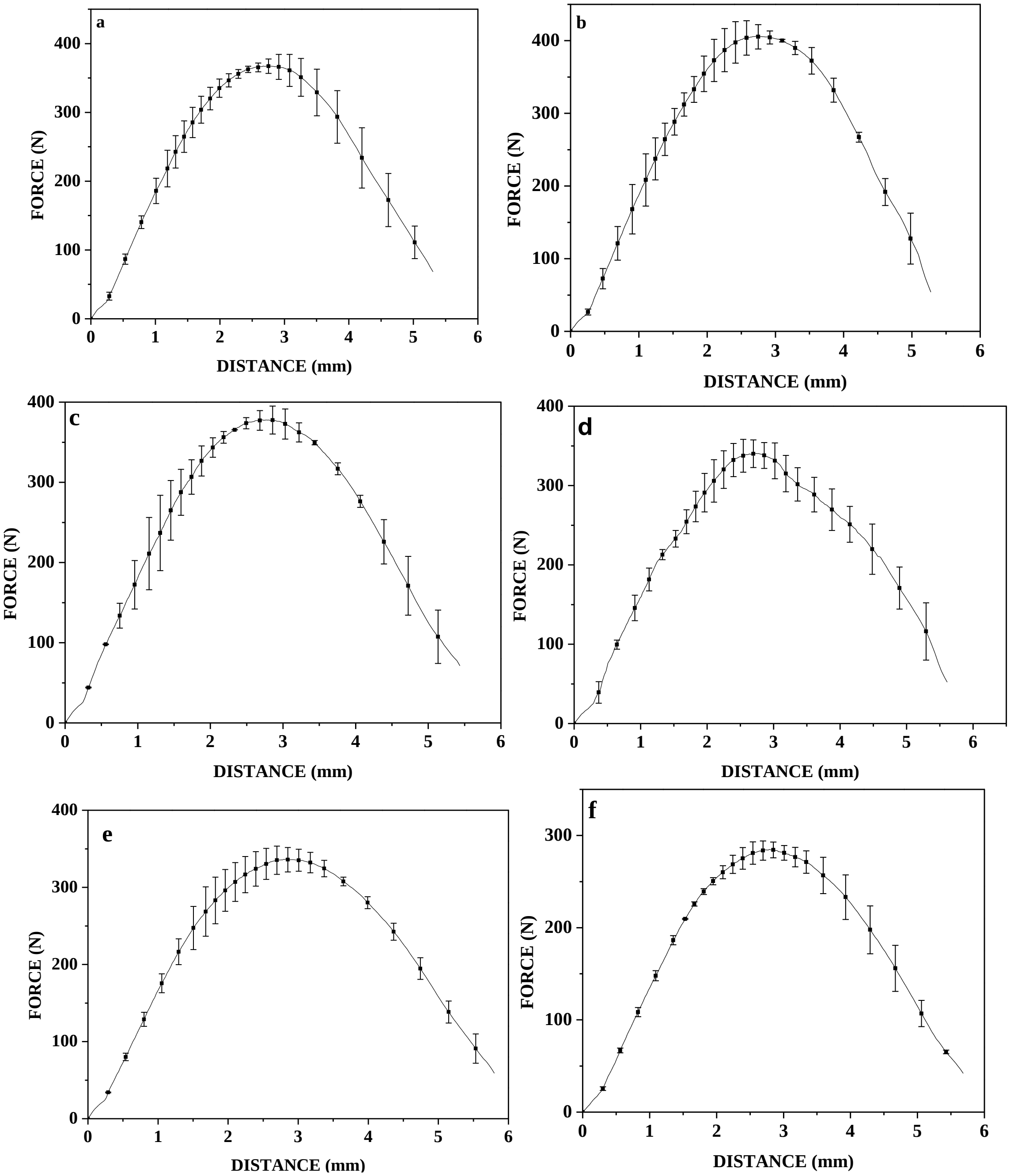

Fig. 5.35: Shear force versus distance curve for the Sn-0.7Cu solder on bare copper substrate surface reflowed for various time; (a) 10 s (b) 100 s (c) 300 s (d) 500 s (e) 1000 s and (f) 10000 s

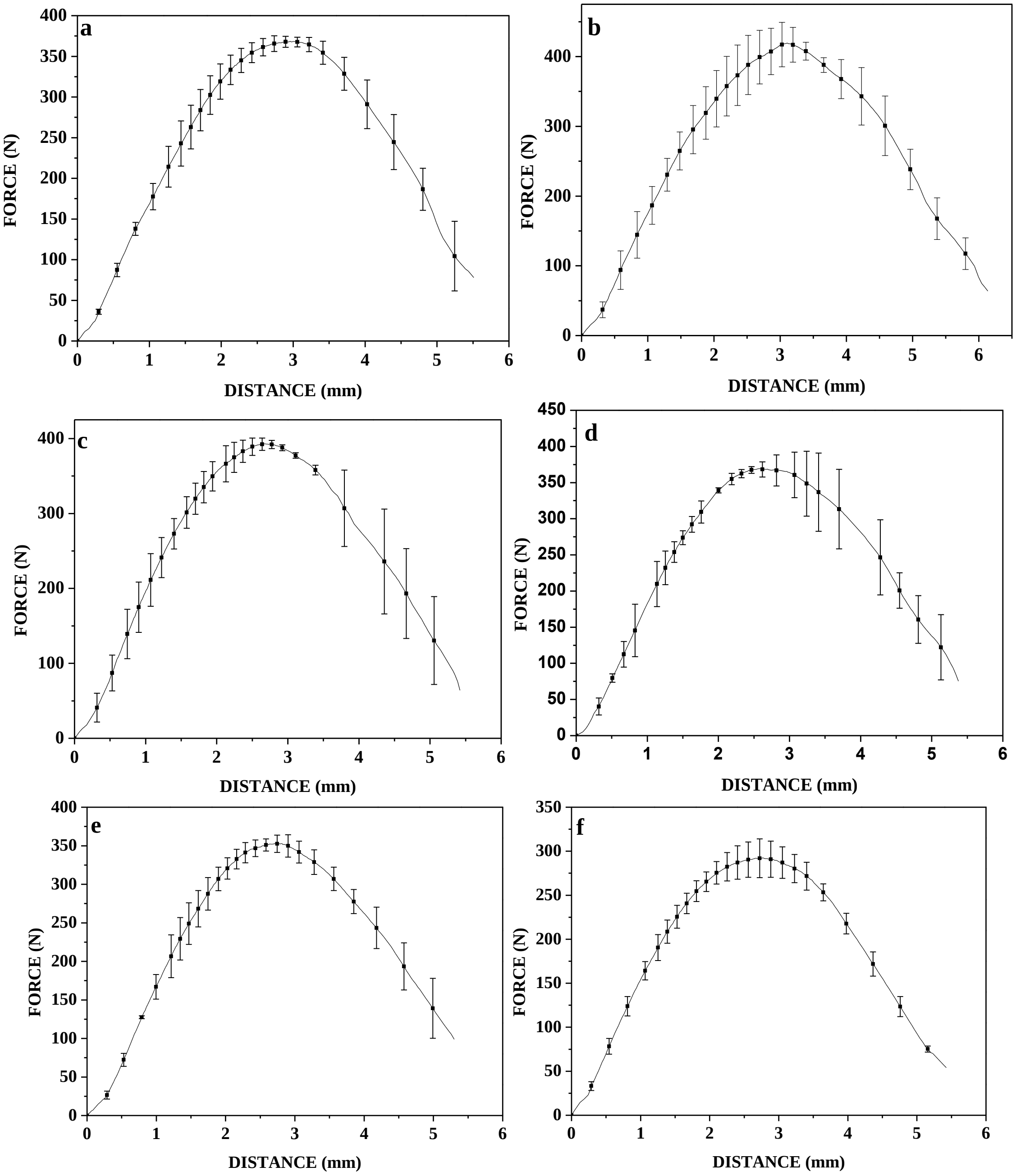

Fig. 5.36: Shear force versus distance curve for the Sn-0.3Ag-0.7Cu solder on bare copper substrate surface reflowed for various time; (a) 10 s (b) 100 s (c) 300 s (d) 500 s (e) 1000 s and (f) 10000 s

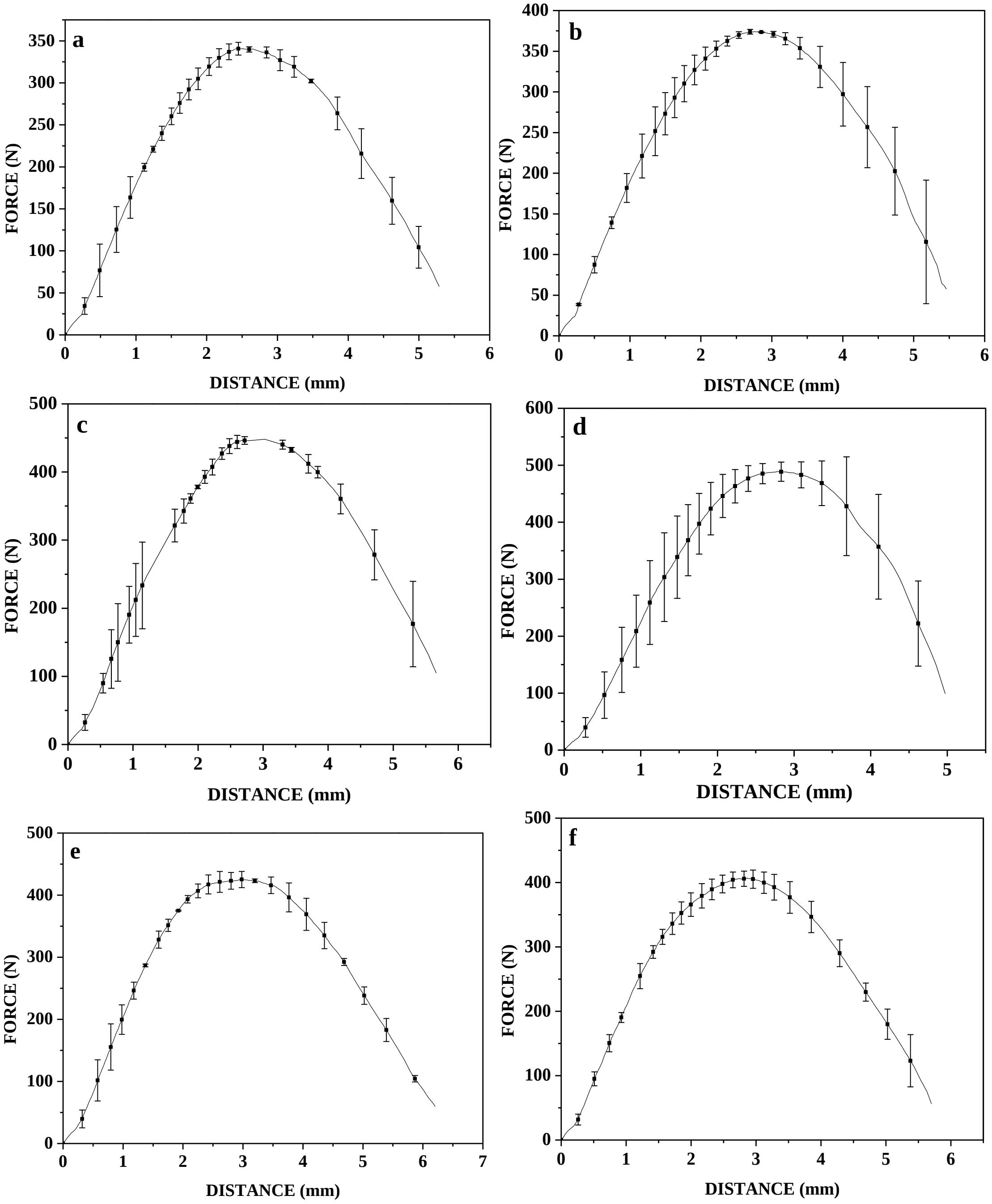

Fig. 5.37: Shear force versus distance curve for the Sn-2.5Ag-0.5Cu solder on bare copper substrate surface reflowed for various time; (a) 10 s (b) 100 s (c) 300 s (d) 500 s (e) 1000 s and (f) 10000 s

All the samples exhibited ductile failure. A gradual decrease observed in the force versus distance curve, instead of a sudden failure signifies ductile failure. Shear marks on the fractured surfaces indicated the occurrence of failure predominantly in the bulk solder regardless of the reflow time. EDAX analysis showed only tin in the fractured area thus confirming fracture has occurred in the bulk solder. Each test was performed three times. Figures 5.38-5.40 show the SEM images of fractured surfaces. Shear marks indicate the direction of the shear action.

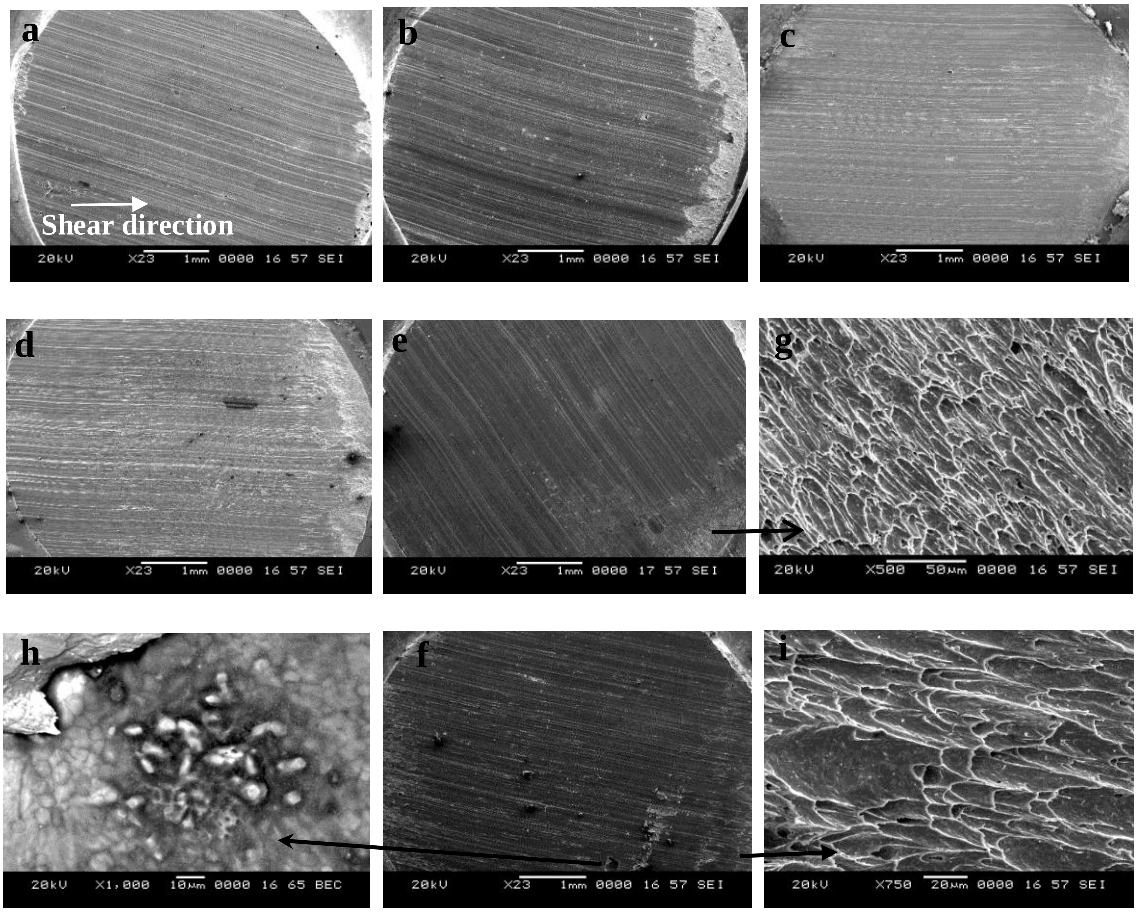

Fig. 5.38 SEM micrographs of fractured surfaces of Sn–0.7Cu /Cu reflowed at (a) 10s (b)100s (c)300 (d) 500s (e) 1000s (f) 10000s and (g), (h), (i) show the enlarged view of the parts indicated by the arrow mark.

For the Sn-0.3Ag-0.7Cu/Cu samples reflowed for 10,000 s, (Fig. 5.39h) the needle shaped IMCs that were intact with shear loading were found inside the dimple. These needle shape intermetallics were confirmed to be Cu_6Sn_5 by EDS analysis. It clearly indicates that, the IMCs that are formed at the interface are not completely exposed to the shear. The results of the fracture analysis showed that the shear strength could not be explicitly related to the thickness of the IMC layer.

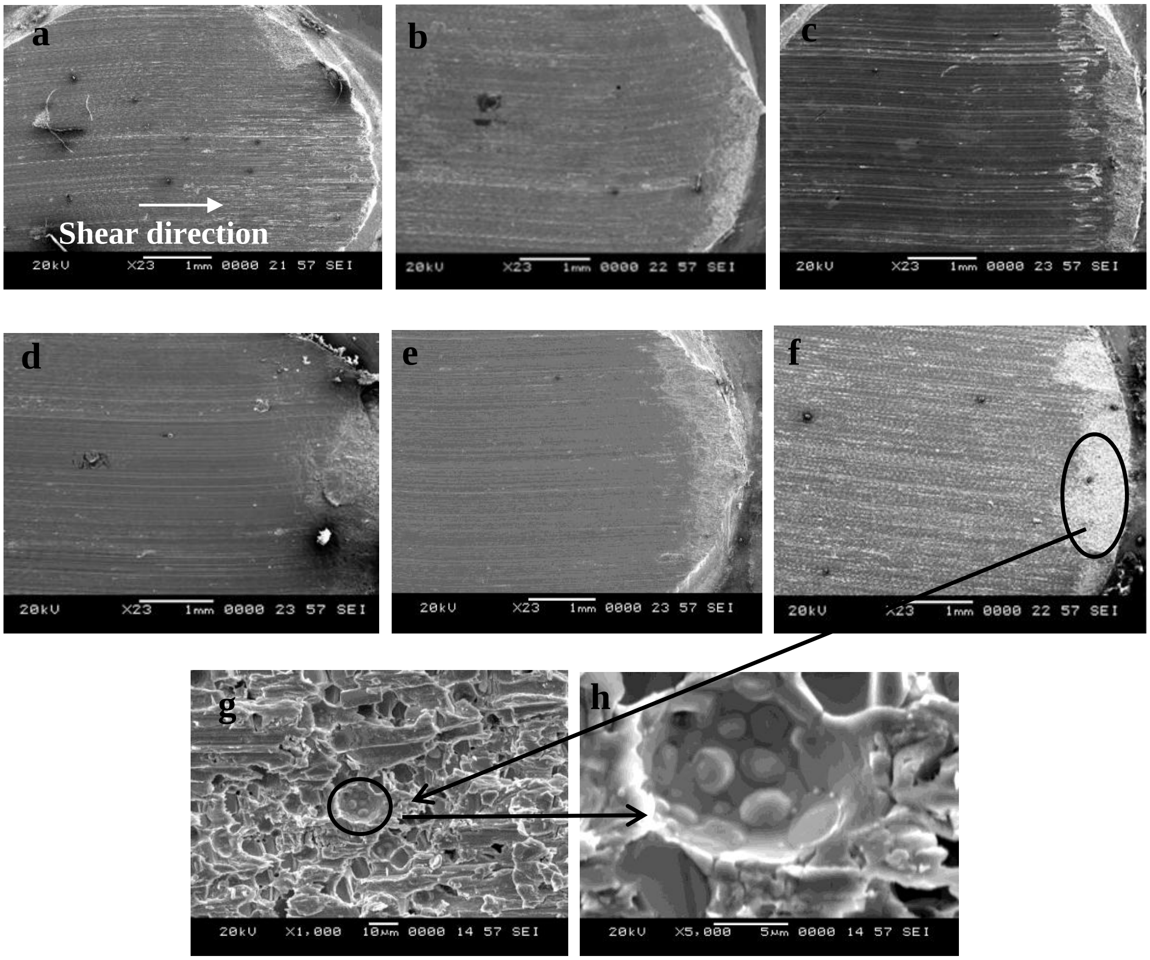

Fig. 5.39 SEM micrographs of fractured surfaces of Sn-03Ag-0.7Cu /Cu reflowed at (a) 10s (b)100s (c)300 (d) 500s (e) 1000s (f) 10000s and (g), (h) show the enlarged view of the parts indicated by the arrow mark.

During the shear test, higher stresses are concentrated on the right side of the solder alloy (at the edge where shear tool stops after the shear test). This is due to the increasing back stress evolved by the work hardening of the solder alloy during the shear test. Therefore, the deformation can be clearly seen at one of the edges of fractured surfaces where shear tool has stopped after the test.

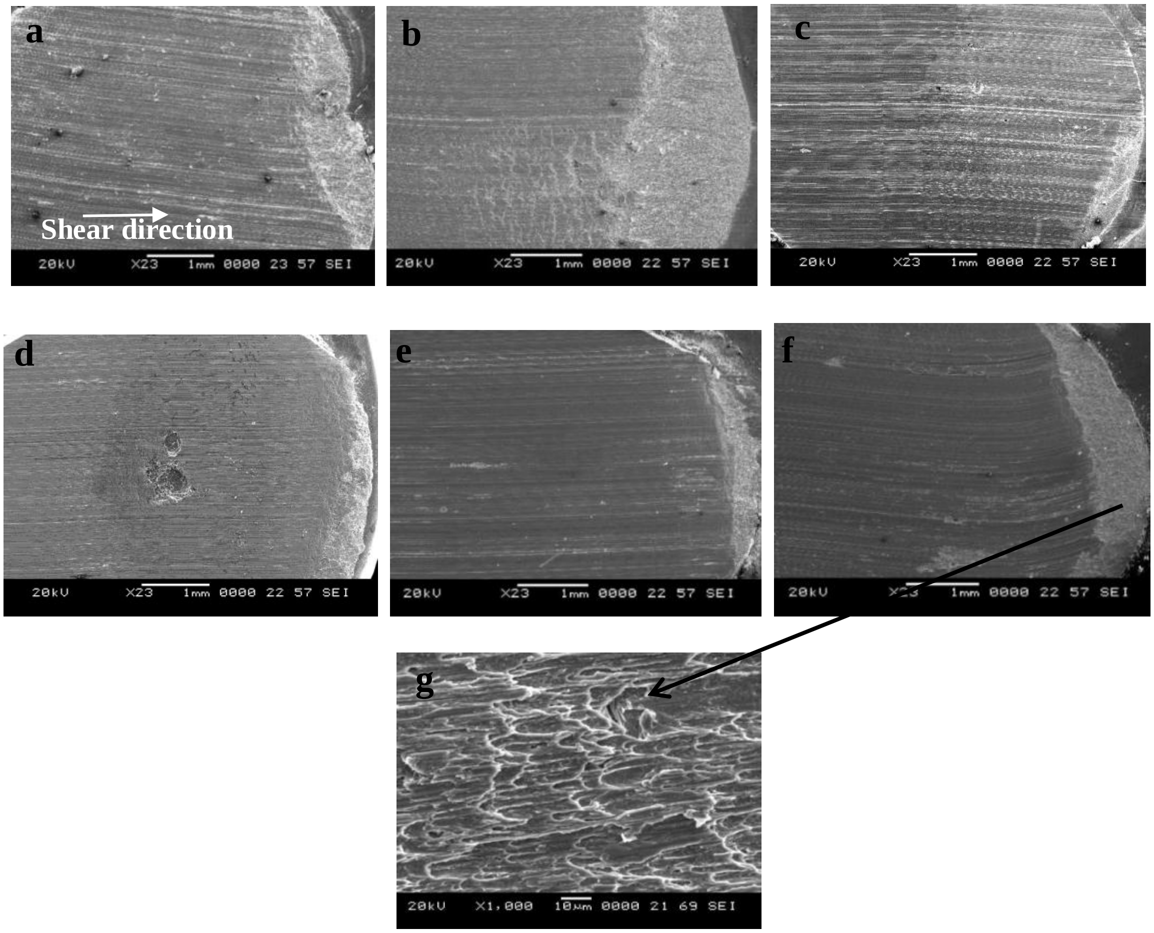

Fig 5.40 SEM micrographs of fractured surfaces of Sn–2.5Ag-0.5Cu /Cu reflowed for (a) 10s (b)100s (c)300 (d) 500s (e) 1000s (f) 10000s and (g) show the enlarged view of the region indicated by the arrow mark.

5.6.2 Shear strength of Sn-0.7Cu, Sn-0.3Ag-0.7Cu and Sn-2.5Ag-0.5Cu solder on bare Cu substrate [quench cooled samples]

Ball shear test was performed on quench cooled solder/substrate system to evaluate the effect of the interfacial reactions on bond strength as a function of reflow time. Figure 5.41, Figure 5.42 and Figure 5.43 show the force-distance curves obtained during the shear test on Sn-0.7Cu/Cu, Sn-0.3Ag-0.7Cu/Cu and Sn-2.5Ag-0.5Cu/Cu quench cooled solder/substrate surfaces respectively. Three sets of experiments were carried out to for consistency. The error bars in force-distance curves indicate the standard deviation in the shear strength values while carrying out three sets of tests. The variation in the spread area of the sessile drop resulted in slight scatter in the force Vs distance curve. The shear energy values are given in Table 5.27.

Table 5.27. Shear energy of Sn-0.7Cu/Cu, Sn-0.3Ag-0.7Cu/Cu and Sn-2.5Ag-0.5Cu/Cu systems (quench cooling method)

Sn-0.7Cu/Cu		Sn-0.3Ag-0.7Cu/Cu		Sn-2.5Ag-0.5Cu/Cu	
Reflow Time (s)	Shear energy (kJ/m^2)	Reflow Time (s)	Shear energy (kJ/m^2)	Reflow Time (s)	Shear energy (kJ/m^2)
10	54.35±5.99	10	60.79±0.23	10	67±1.58
25	63.26±8.01	40	87.76±4.33	40	91.39±3.41
100	58.35±6.08	100	63.30±2.76	100	74.98±0.37
300	55.85±8.03	300	74.38±0.21	300	77.67±2.01
500	48.76±4.44	500	58.77±1.54	500	67.01±2.14

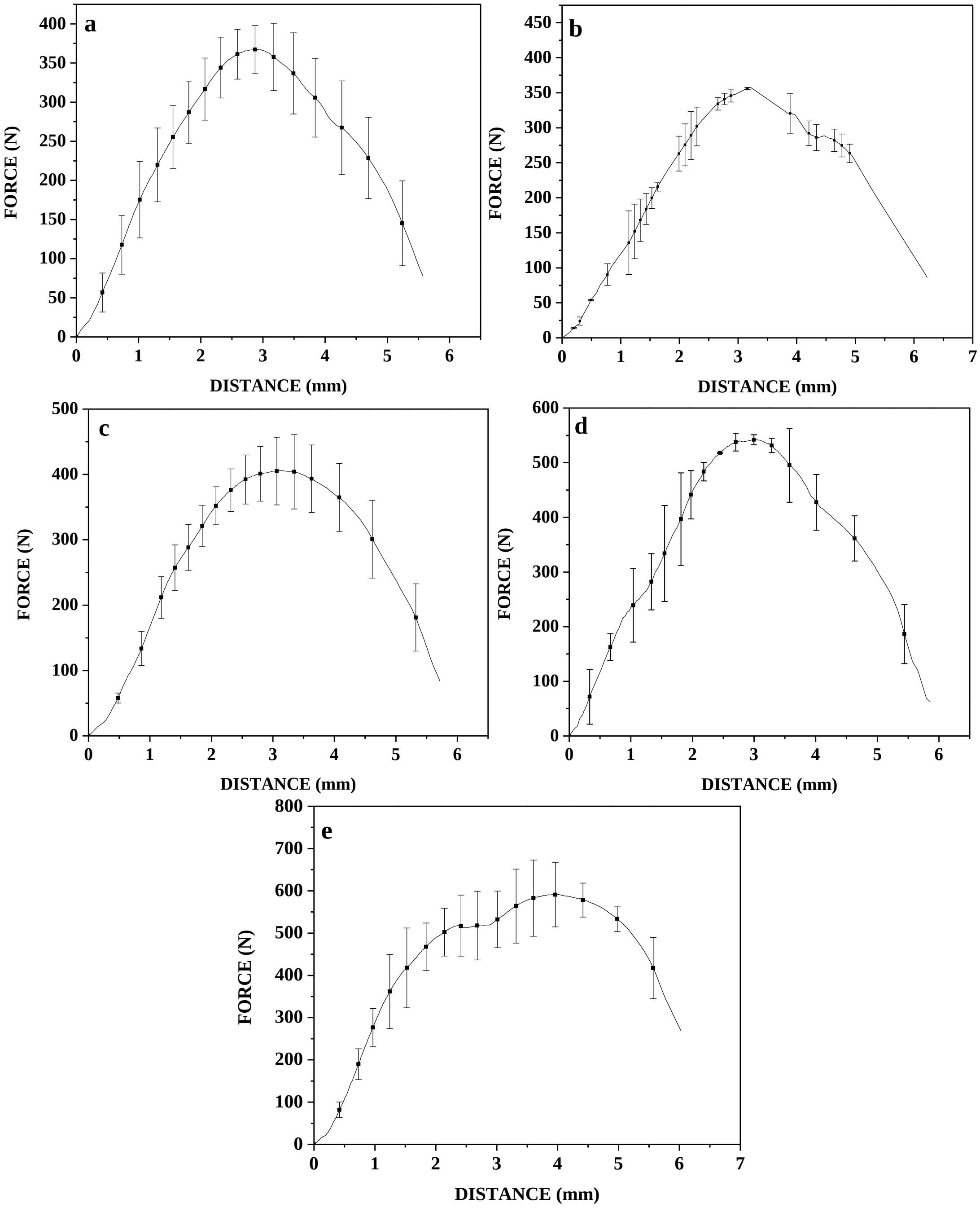

Fig.5.41: Shear force versus distance curve for the Sn-0.7Cu solder on bare copper substrate surface reflowed for various time; (a) 10 s (b) 25 s (c) 100 s (d) 300 s and (e) 500 s

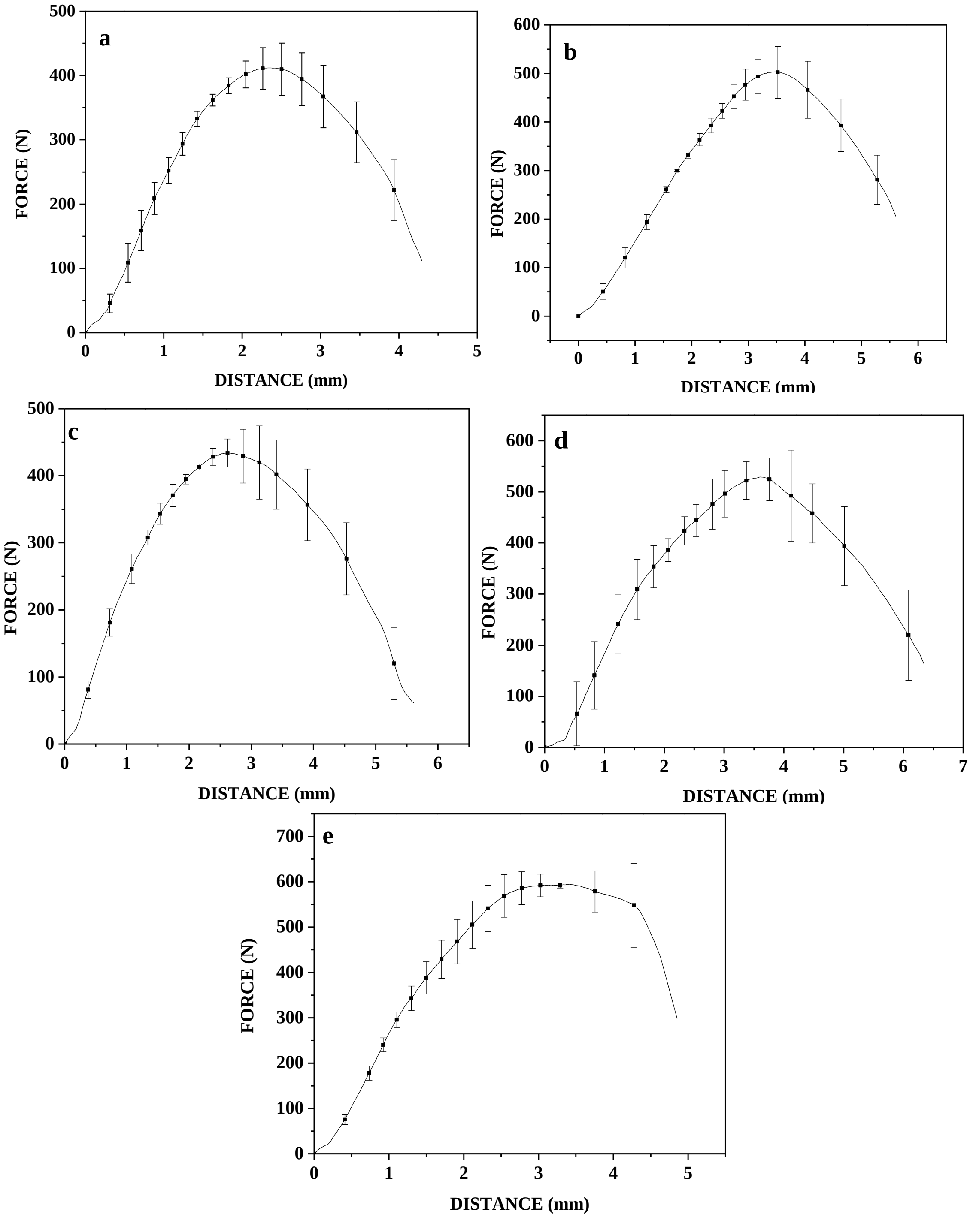

Fig.5.42: Shear force versus distance curve for the Sn-0.3Ag-0.7Cu solder on bare copper substrate surface reflowed for various time; (a) 10 s (b) 40 s (c) 100 s (d) 300 s and (e) 500 s

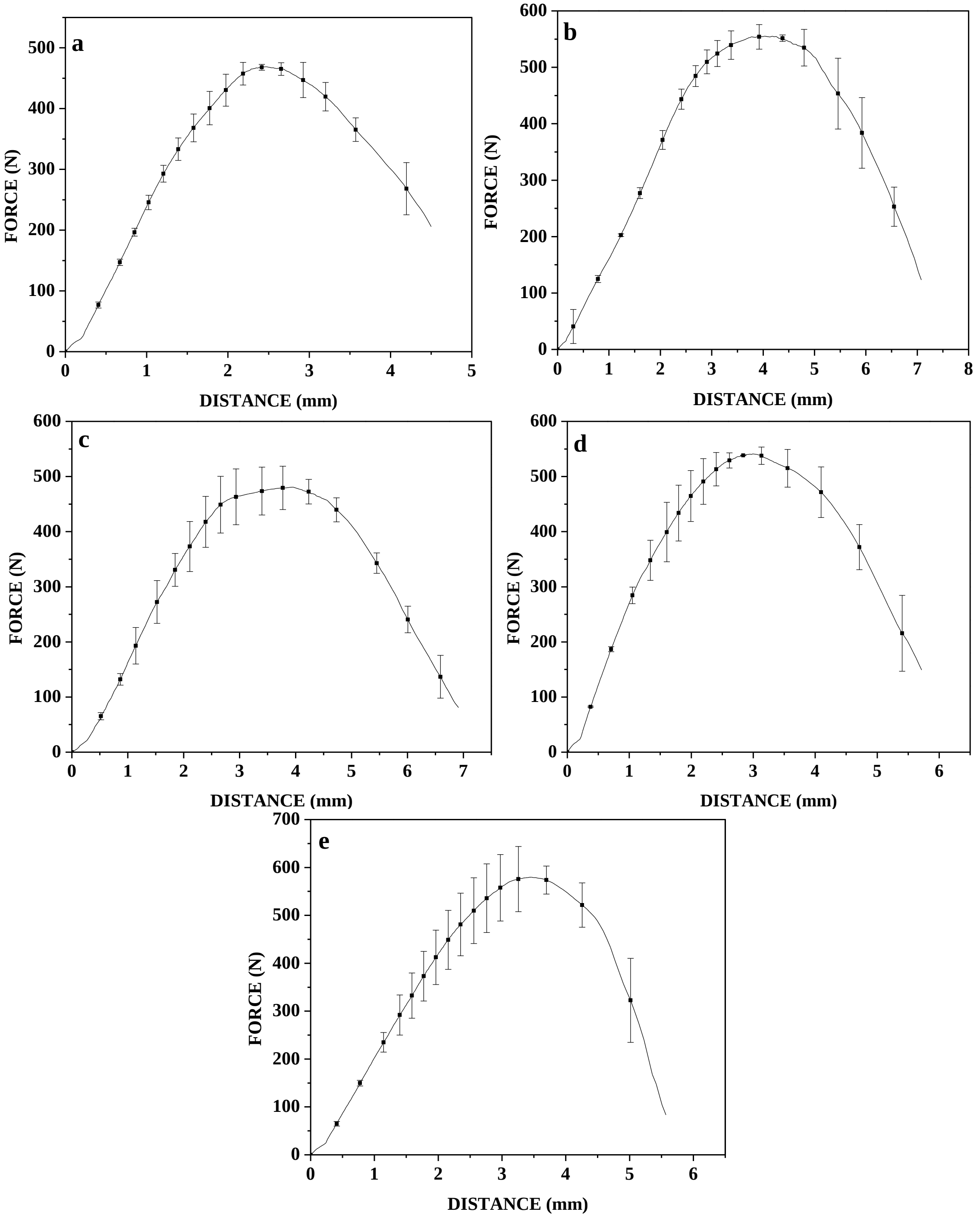

Fig.5.43: Shear force versus distance curve for the Sn-2.5Ag-0.5Cu solder on bare copper substrate surface reflowed for various time; (a) 10 s (b) 40 s (c) 100 s (d) 300 s and (e) 500 s

Quench cooled solder/Cu systems yielded 30-40 % increase in shear energy values compared to furnace cooled samples. This can be attributed to fine tin grains formed during quench cooling. Furnace cooling results in bigger tin grains at the bulk solder hence the lower shear energy. The presence of higher Ag in the alloy increases the shear strength of the solder alloy because with increasing Ag content, the primary β-Sn grain size and eutectic network size becomes finer [Huh et al. 2001].

Force Vs distance curve exhibited a gradual decrease reaching a peak value. Sn-0.7Cu/Cu system showed maximum bond strength for reflow time of 25 s whereas Sn-0.3Ag-0.7Cu/Cu and Sn-2.5Ag-0.5Cu/Cu systems showed maximum bond strength for reflow time of 40 s. Since 25 s is the approximate time at which gravity zone comes to an end in Sn-0.7Cu/Cu system and 40 s is the time at which gravity zone comes to an end in both Sn-0.3Ag-0.7Cu/Cu and Sn-2.5Ag-0.5Cu/Cu systems, it was concluded that the dynamic contact angle at the end of gravity zone (θ_{gz}) is responsible for the maximum bond strength. Bond strength decreased with further increase in reflow time and IMC thickness in the later stages. This also suggests that the solder reflow should not extend beyond the gravity regime.

SEM images of Sn-0.7Cu/Cu Sn-0.3Ag-0.7Cu/Cu and Sn-2.5Ag-0.5Cu/Cu fractured surfaces are shown in Figure 5.44, Figure 5.45 and Figure 5.46 respectively. EDS analysis showed 99 % tin on the fractured surface, indicating fracture has taken place in bulk solder rather than at the interface. Deformed area on the fractured surface, where shear tool has stopped after the test was observed in all the solder/Cu combinations. This is due to the increasing back stress evolved by the work hardening of the solder alloy during the shear test. Presence of dimples indicate that the ductile failure has taken place.

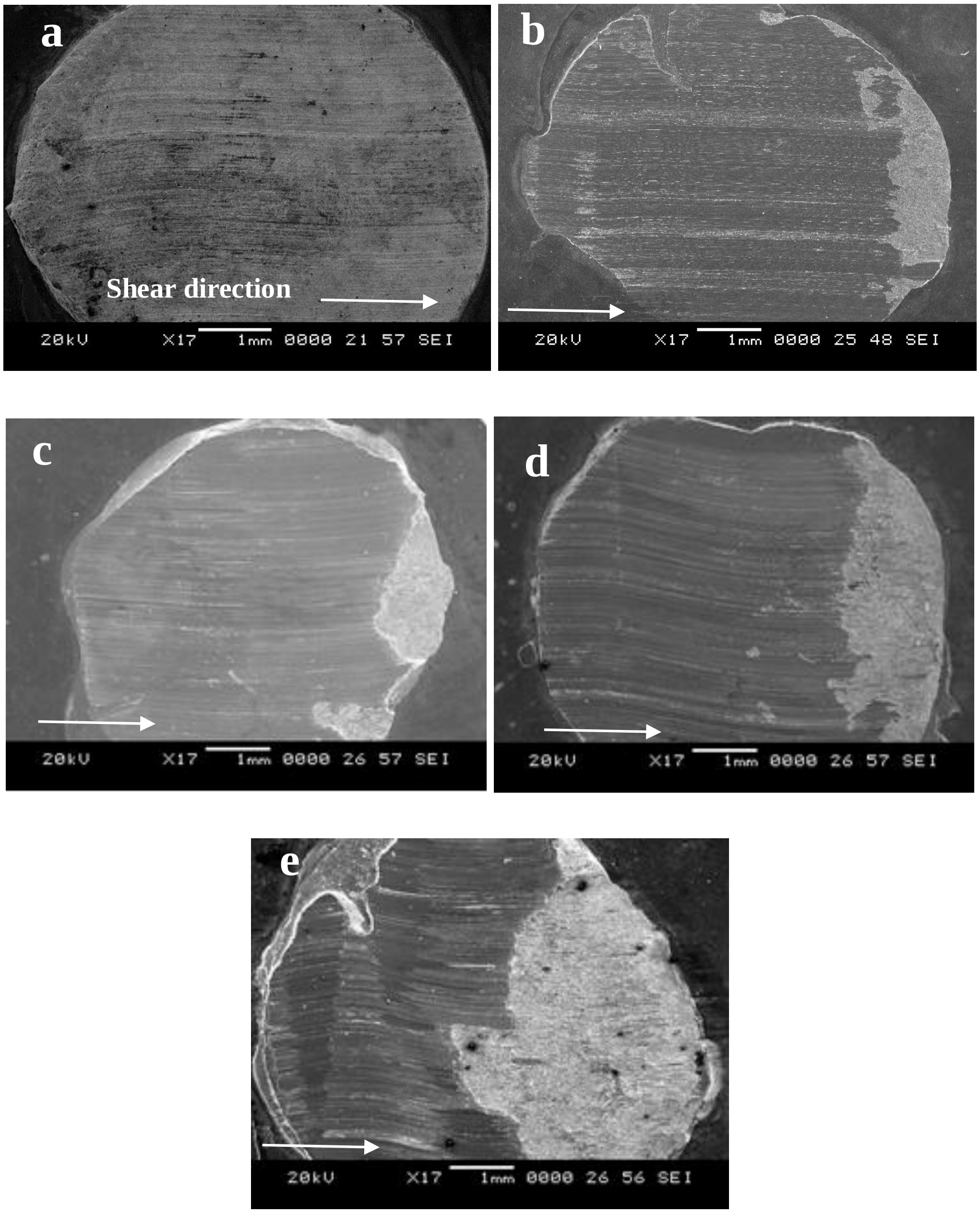

Fig. 5.44. SEM micrographs of fractured surfaces of Sn-0.7Cu /Cu reflowed at (a) 10 s (b) 25 s (c) 100 s (d) 300 s and (e) 500 s

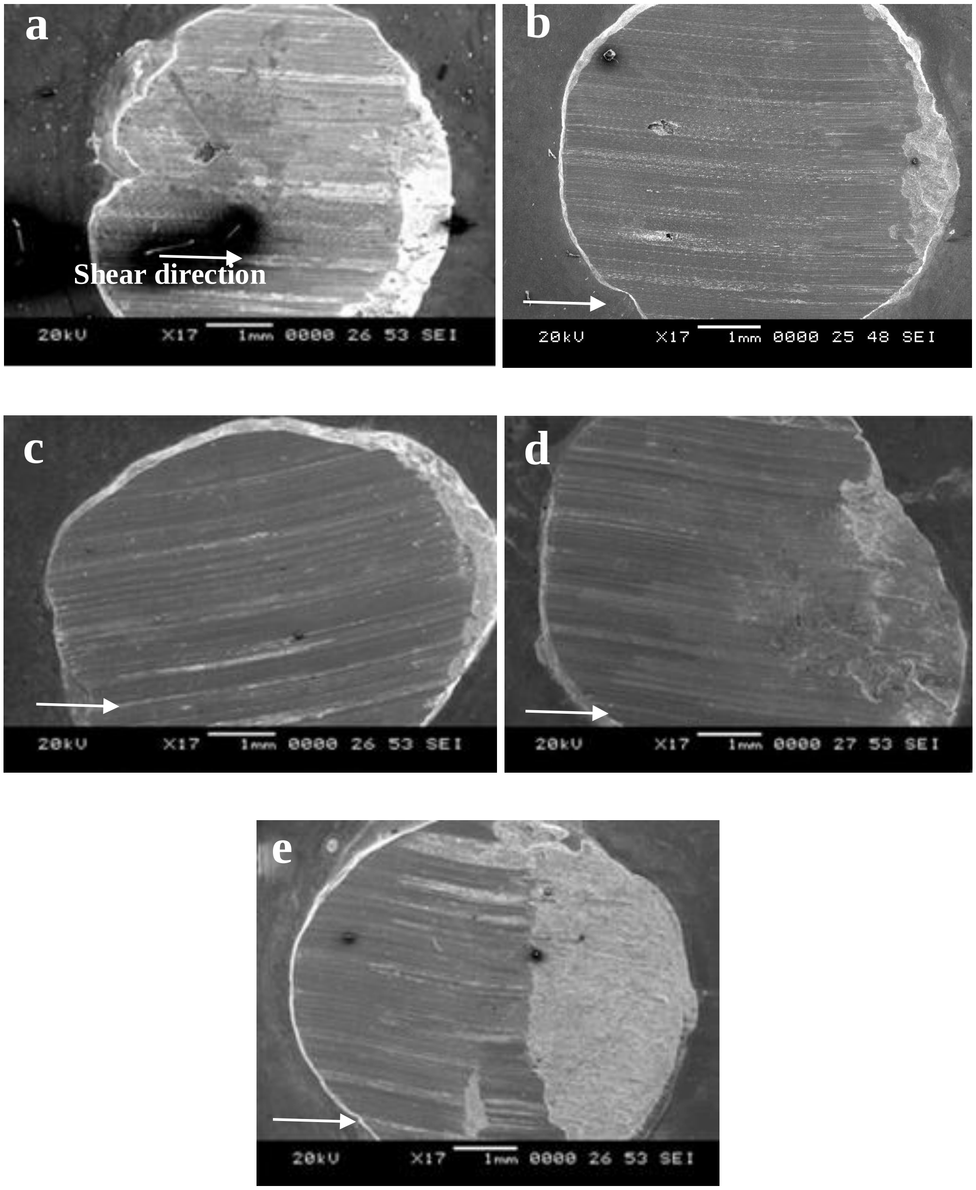

Fig. 5.45. SEM micrographs of fractured surfaces of Sn-0.3Ag-0.7Cu /Cu reflowed at (a) 10 s (b) 40 s (c)100 s (d) 300 s and (e)500 s

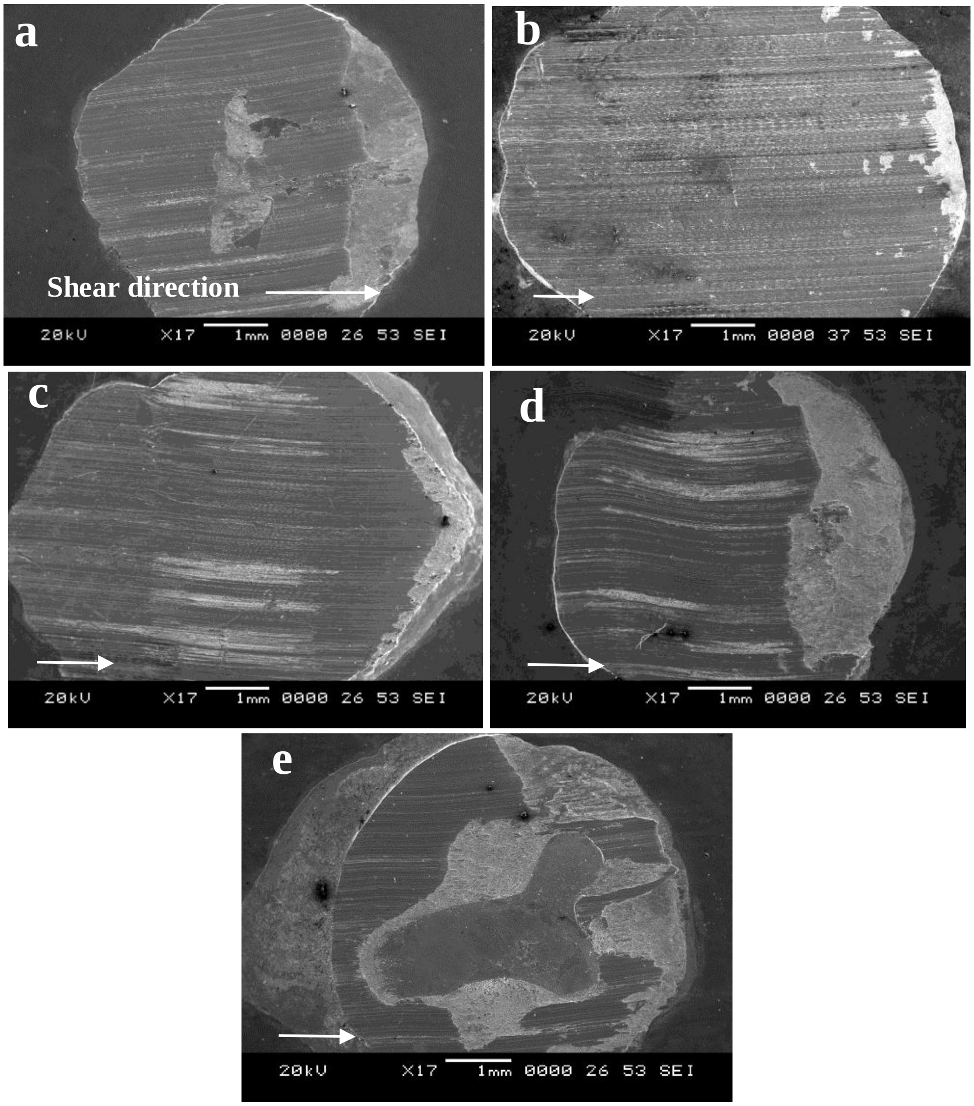

Fig. 5.46. SEM micrographs of fractured surfaces of Sn-2.5Ag-0.5Cu /Cu reflowed at (a) 10 s (b) 40 s (c)100 s (d)300 s and (e)500 s

5.6.3 Shear strength of Sn-0.7Cu, Sn-0.3Ag-0.7Cu and Sn-2.5Ag-0.5Cu solder on Ni coated Cu substrate [quench cooled samples]

Evaluation of the effect of the interfacial reactions on bond strength of quench cooled solder/Ni coated Cu substrate system was carried out by performing ball shear test on solder/substrate surfaces. Figure 5.47, Figure 5.48 and Figure 5.49 show the force-distance curves obtained during the shear test on Sn-0.7Cu/Ni/Cu, Sn-0.3Ag-0.7Cu/Ni/Cu and Sn-2.5Ag-0.5Cu/Ni/Cu quench cooled solder/substrate surfaces respectively.

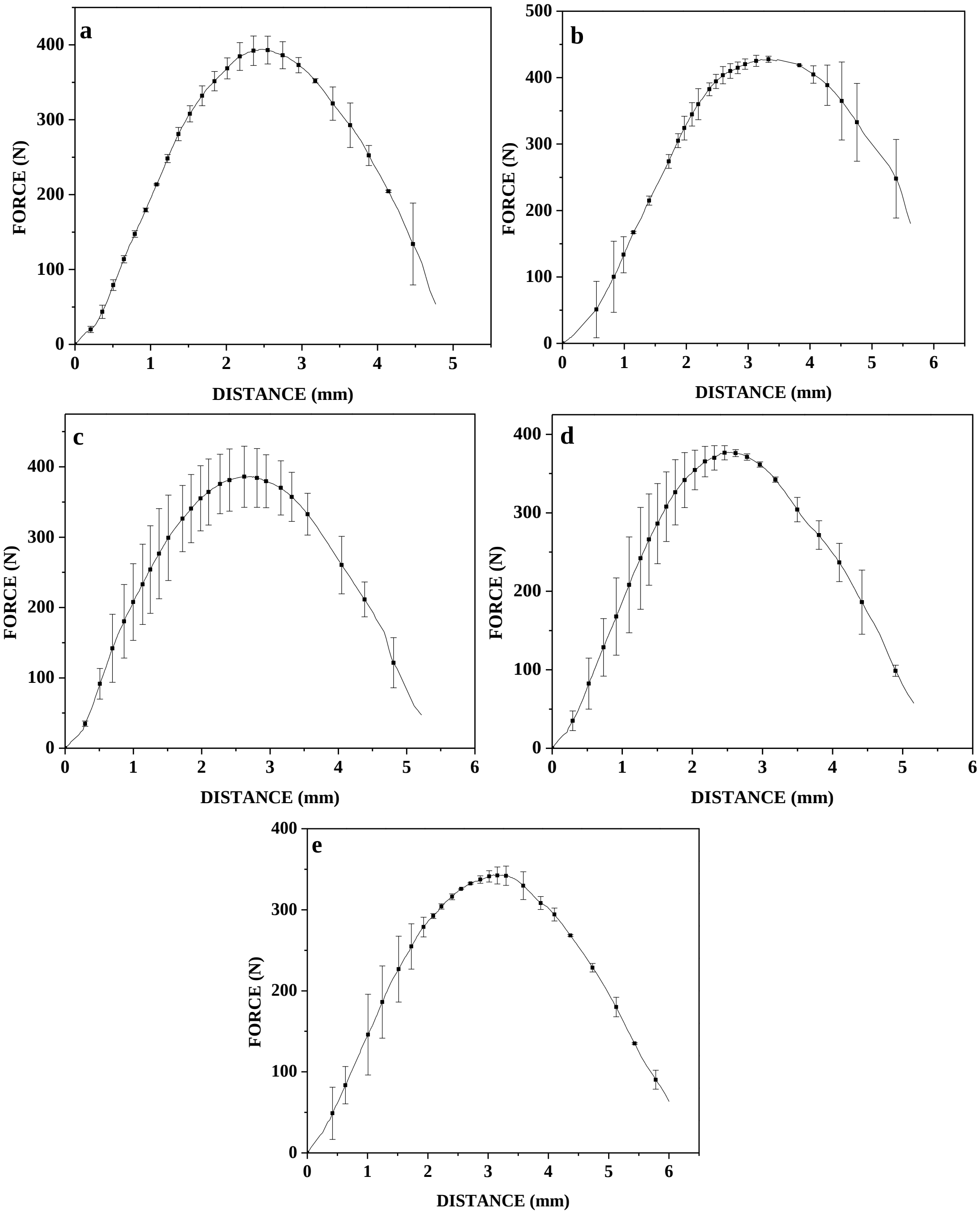

Fig.5.47: Shear force versus distance curve for the Sn-0.7Cu solder on Ni coated copper substrate surface reflowed for various time; (a) 10 s (b) 50 s (c) 100 s (d) 300 s and (e) 500 s

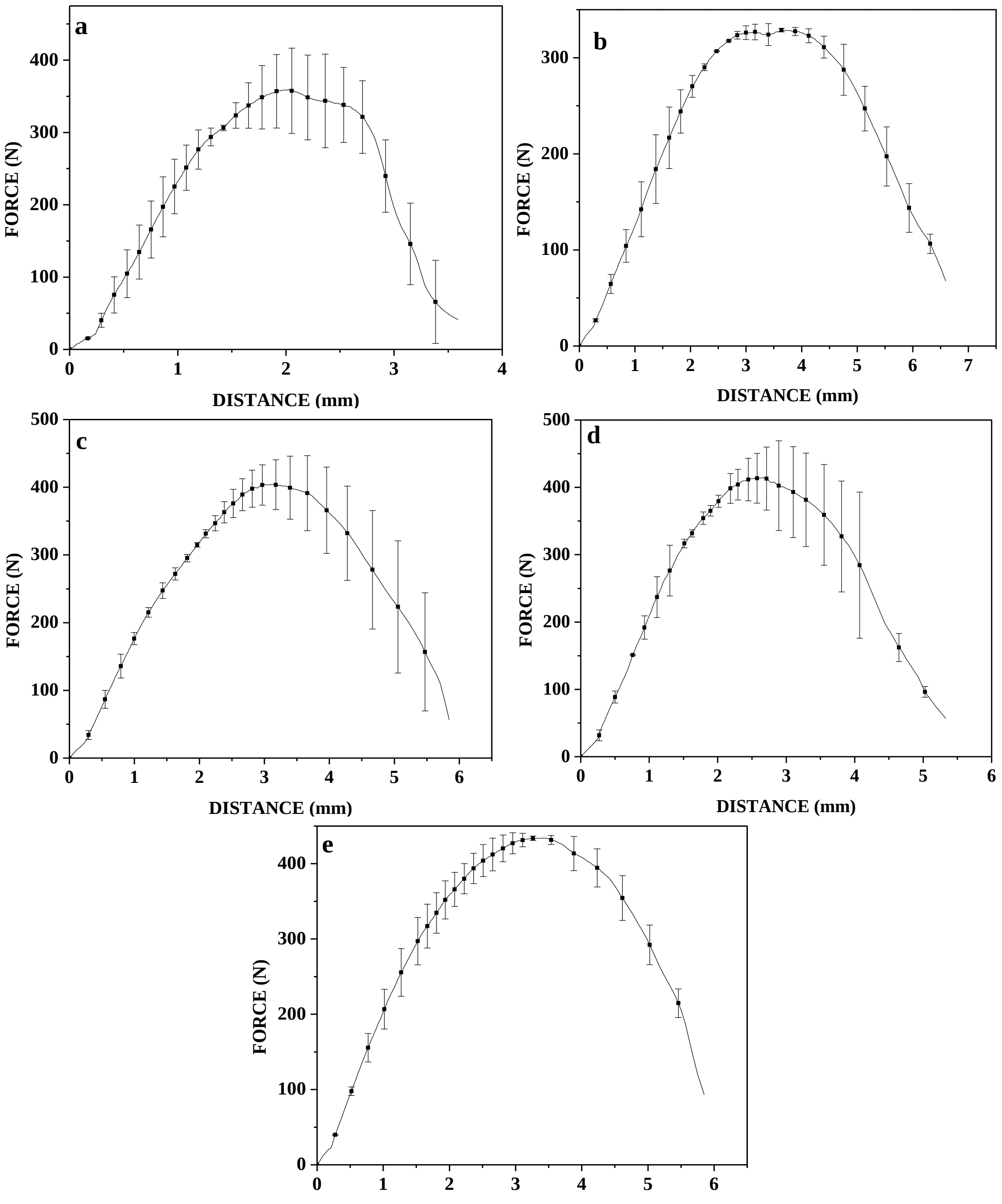

Fig.5.48: Shear force versus distance curve for the Sn-0.3Ag-0.7Cu solder on Ni coated copper substrate surface reflowed for various time; (a) 10 s (b) 70 s (c) 100 s (d) 300 s and (e) 500 s

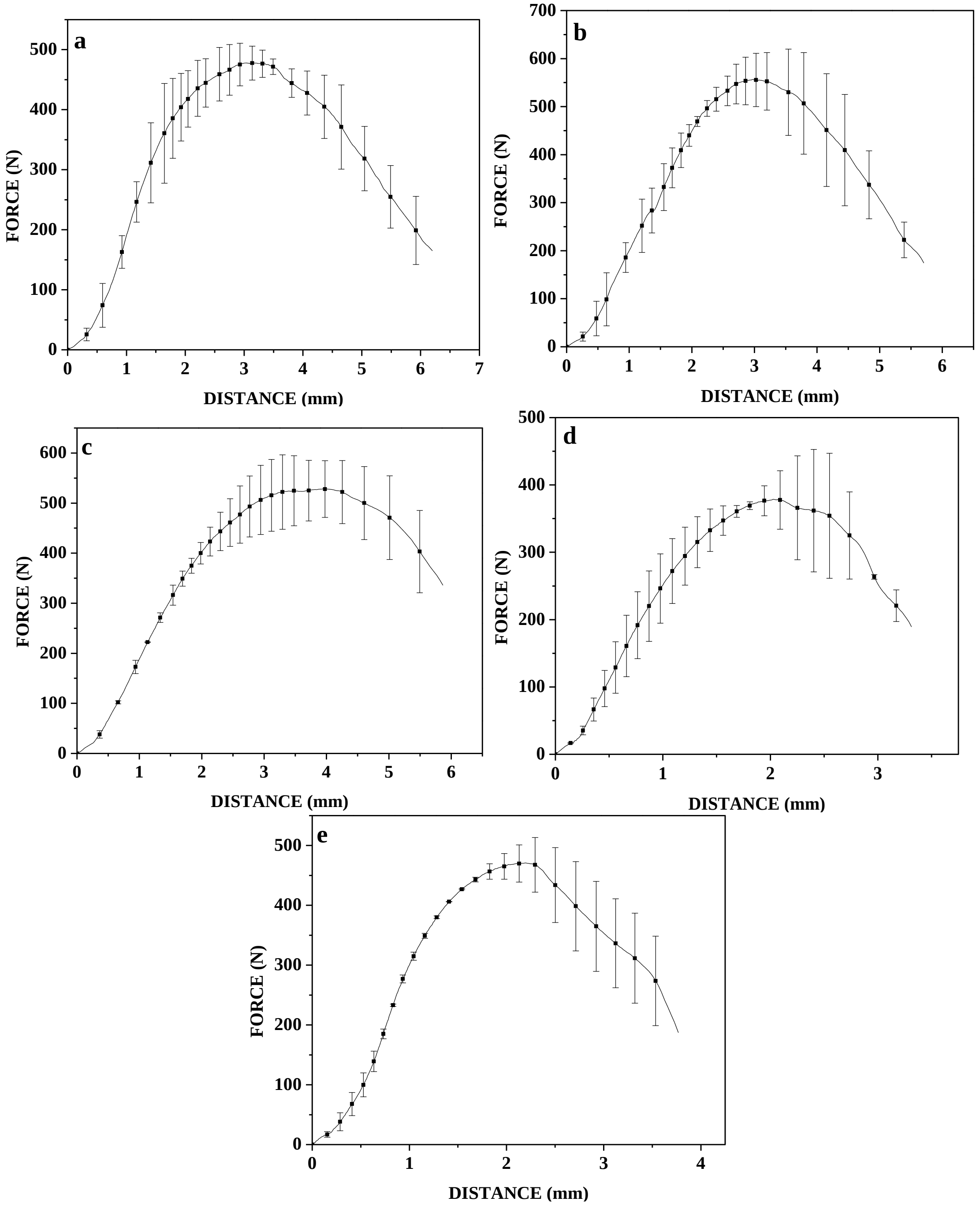

Fig.5.49: Shear force versus distance curve for the Sn-2.5Ag-0.5Cu solder on Ni coated copper substrate surface reflowed for various time; (a) 10 s (b) 80 s (c) 100 s (d) 300 s and (e) 500 s

Three sets of experiments were carried out to for consistency. The error bars in force-distance curves indicate the standard deviation in the shear strength values while carrying out three sets of tests. Scatter in the force verses distance curve is attributed to a slight variation in the spread area of solder sessile drop. The shear energy values are given in Table 5.28.

Table 5.28. Shear energy of Sn-0.7Cu/Ni/Cu, Sn-0.3Ag-0.7Cu/Ni/Cu and Sn-2.5Ag-0.5Cu/Ni/Cu systems (quench cooling method)

Sn-0.7Cu		Sn-0.3Ag-0.7Cu		Sn-2.5Ag-0.5Cu	
Reflow Time (s)	Shear energy (kJ/m^2)	Reflow Time (s)	Shear energy (kJ/m^2)	Reflow Time (s)	Shear energy (kJ/m^2)
10	54.72±0.08	10	52.40±1.35	10	69.71±0.41
50	69.24±3.43	70	88.35±2.75	80	94.75±2.82
100	56.54±0.49	100	63.76±0.92	100	79.38±0.99
300	52.57±0.64	300	51.25±1.46	300	56.91±0.59
500	42.18±2.09	500	53.10±1.14	500	63.74±2.05

Force Vs distance curve showed a peak followed by a decrease in the value thereafter. Sn-0.7Cu/Ni/Cu system showed maximum bond strength for reflow time of 50 s whereas Sn-0.3Ag-0.7Cu/Cu and Sn-2.5Ag-0.5Cu/Cu systems showed maximum bond strength for reflow time of 70 s and 80 s respectively. Since 50 s, 70 s and 80 s are the approximate times at which gravity zone come to an end in Sn-0.7Cu/Ni/Cu, Sn-0.3Ag-0.7Cu/Ni/Cu and Sn-2.5Ag-0.5Cu/Ni/Cu systems respectively, we concluded that the dynamic contact angle at the end of gravity zone (θ_{gz}) is responsible for the maximum bond strength. Solder reflow beyond the gravity regime resulted in lower bond strength. Figure 5.50, Figure 5.51 and Figure 5.52 show the fractured surfaces of Sn-0.7Cu, Sn-0.3Ag-0.7Cu and Sn-2.5Ag-0.5Cu solidified on Ni coated Cu substrate. Deformed area due to back stress was more prominent for Sn-2.5Ag-0.5Cu solder on Ni coated Cu substrate. As Sn-2.5Ag-0.5Cu has more Ag content, needle shaped Ag_3Sn IMCs form in more number at the bulk solder. They act as stress concentrators. It also adds to the back stress due to work hardening, and hence more stress deformed area was observed in Sn-2.5Ag-0.5Cu/Ni/Cu than that in Sn-0.3Ag-0.7Cu/Ni/Cu and Sn-0.7Cu/Ni/Cu systems.

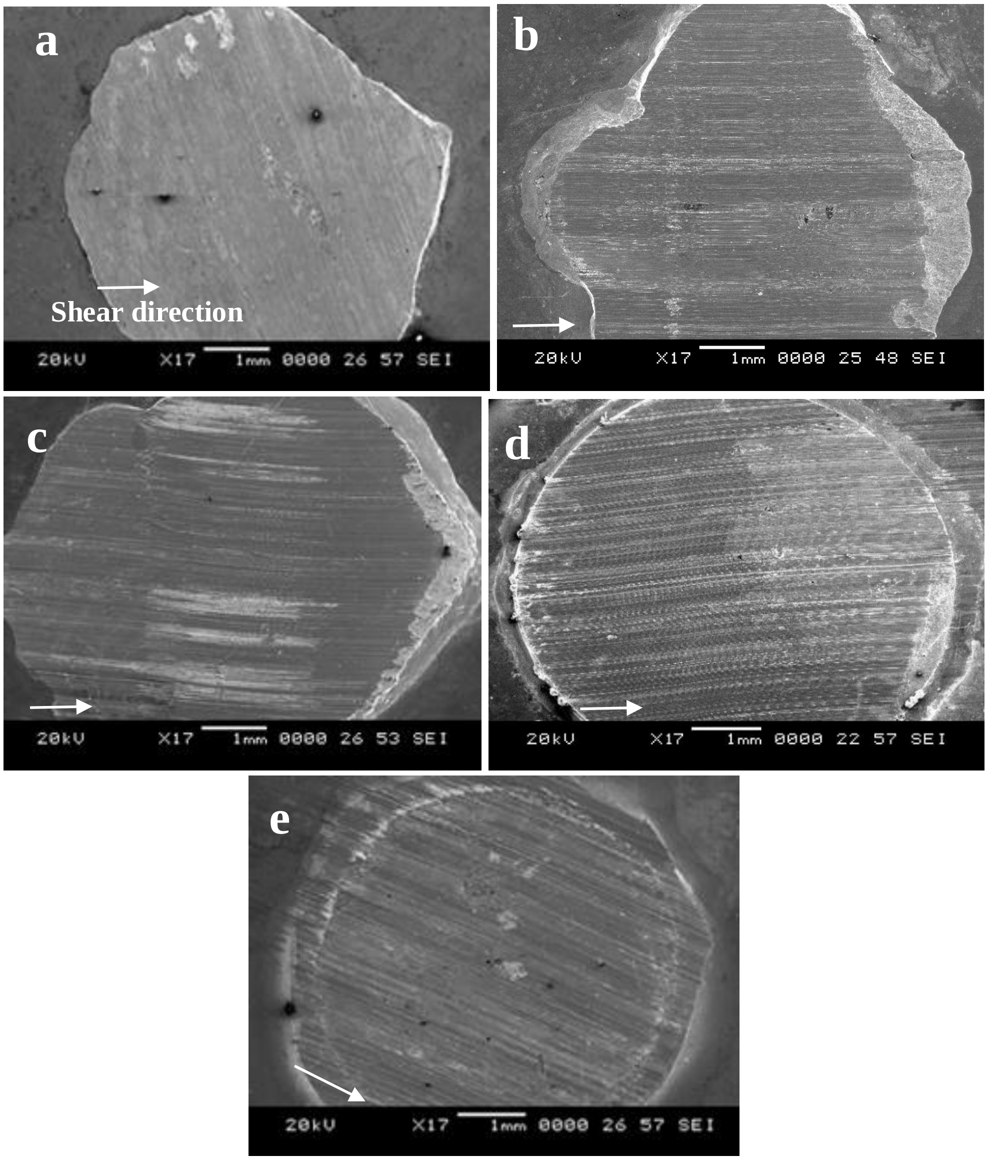

Fig. 5.50: SEM micrographs of fractured surfaces of Sn-0.7Cu /Ni/Cu reflowed at (a) 10 s (b) 70 s (c)100 s (d)300 s and (e)500 s

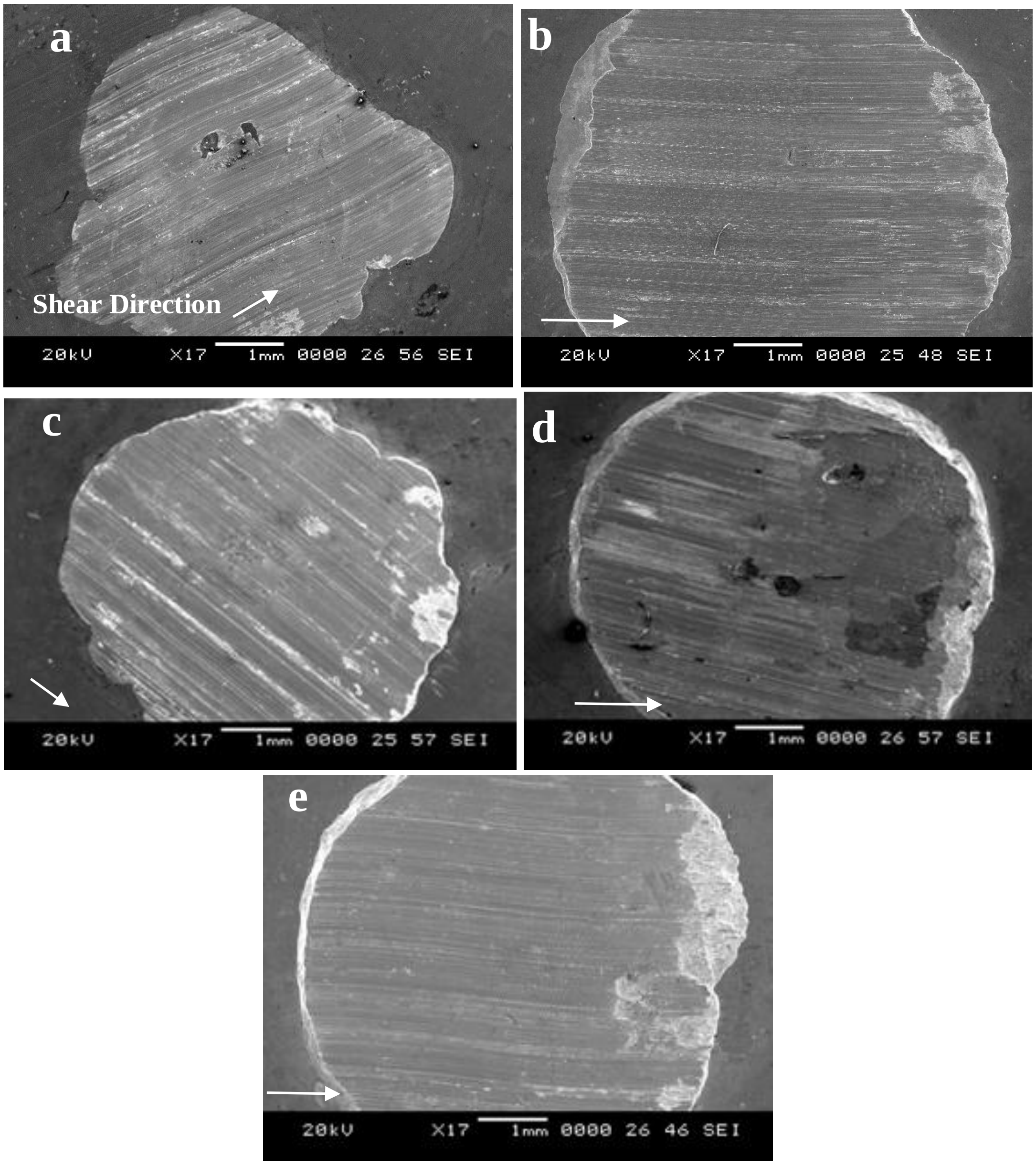

Fig. 5.51: SEM micrographs of fractured surfaces of Sn-0.3Ag-0.7Cu /Ni/Cu reflowed at (a) 10 s (b) 70 s (c)100 s (d)300 s and (e)500 s

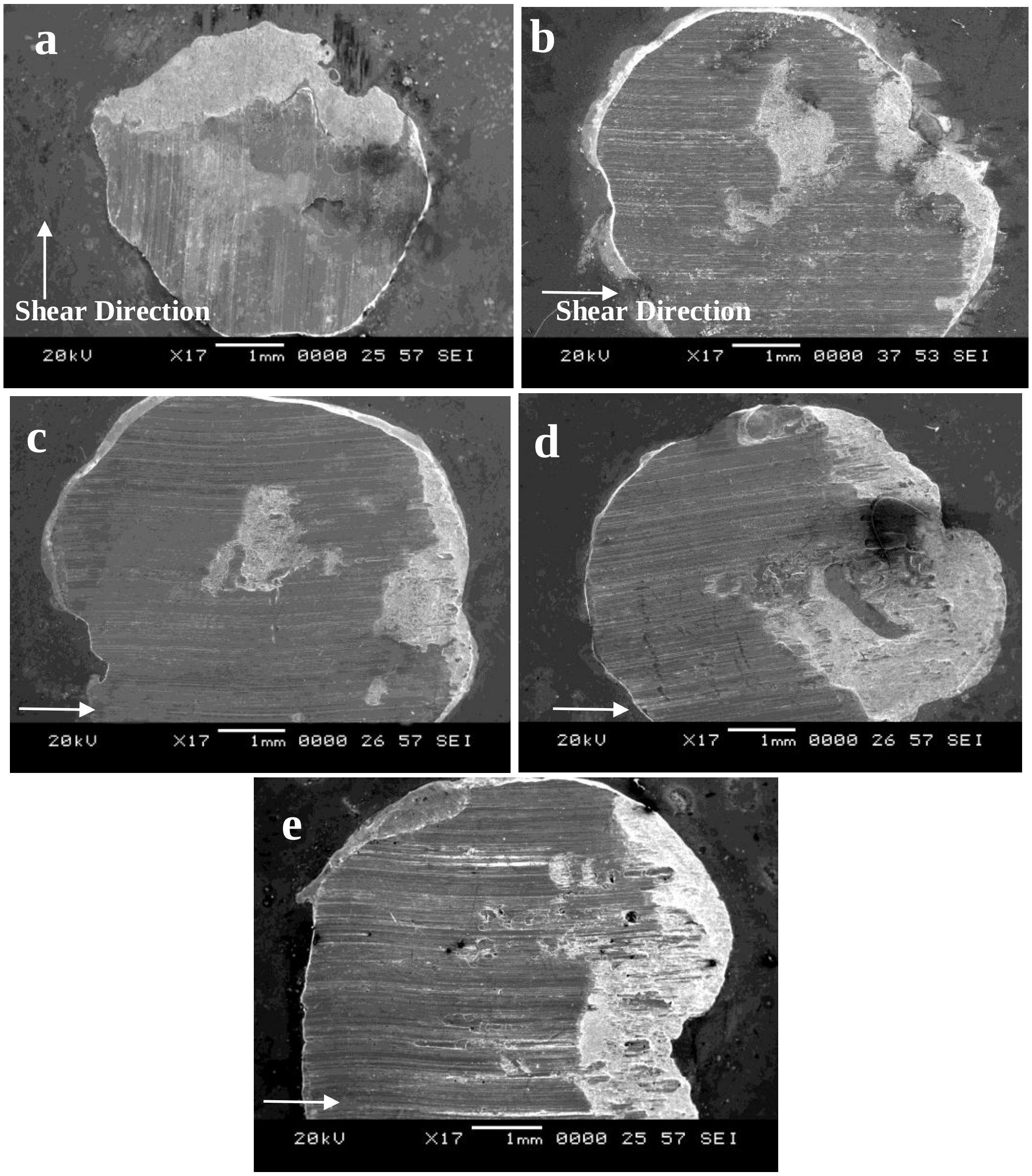

Fig. 5.52: SEM micrographs of fractured surfaces of Sn-2.5Ag-0.5Cu /Ni/Cu reflowed at (a) 10 s (b) 80 s (c)100 s (d)300 s and (e)500 s

Shear strength of Sn-Pb eutectic alloy solidified on bare and Ni coated cu substrate was also measured to compare the results obtained with lead free solder alloys. Sn-Pb solder alloy was initially reflowed at 240 °C for 100 s. From that T_{gz} was found to be 7 s for 63Sn-37Pb on bare and 14 s on Ni coated Cu substrate. Then the eutectic Sn-Pb/Cu system was quench cooled for reflow times of 7 s, 10 s and 100 s whereas Sn-Pb/Ni/Cu system for 10 s, 14 s and 100 s respectively. Final contact angle θ_f for Sn-Pb solidified on bare Cu substrate for reflow times of 7 s, 10 s and 100 s was found to be 23.44°, 23.5 ° and 22.46° respectively. Similarly, for the same alloy on Ni coated Cu substrate for the reflow time of 10 s, 14 s and 100 s, θ_f was found to be 41.29°, 37.88° and 35.54° respectively. This clearly shows that the time to attain equilibrium contact angle is significantly lower for lead based solder alloy as compared to lead free solder alloys. Relaxation curve obtained during the spreading of eutectic Sn-Pb alloy on bare and Ni coated Cu substrate are given in Figure 5.53.

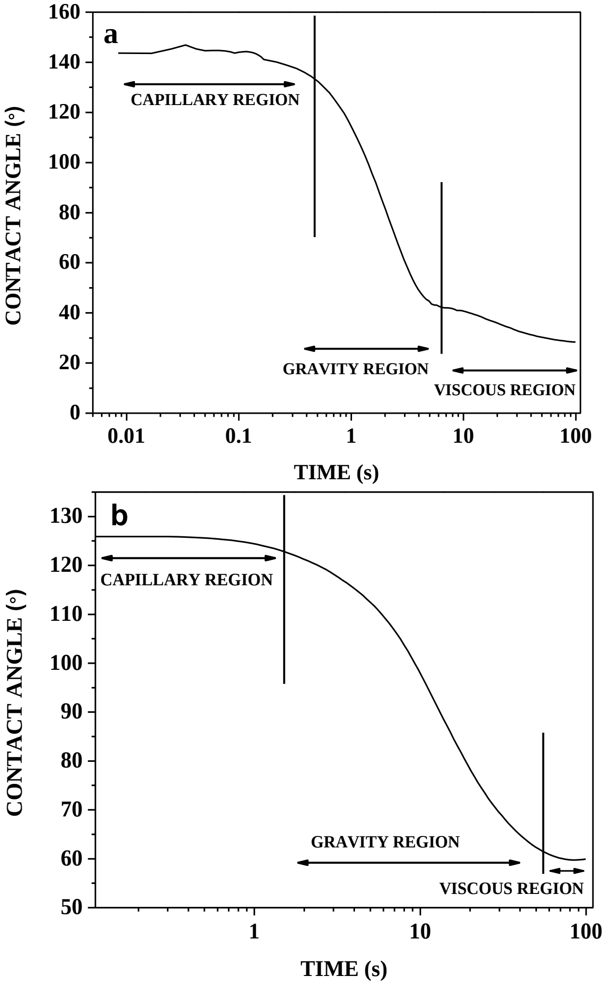

Fig. 5.53: Typical relaxation curves for the spreading of eutectic Sn-Pb on (a) bare and (b) Ni coated Cu substrates

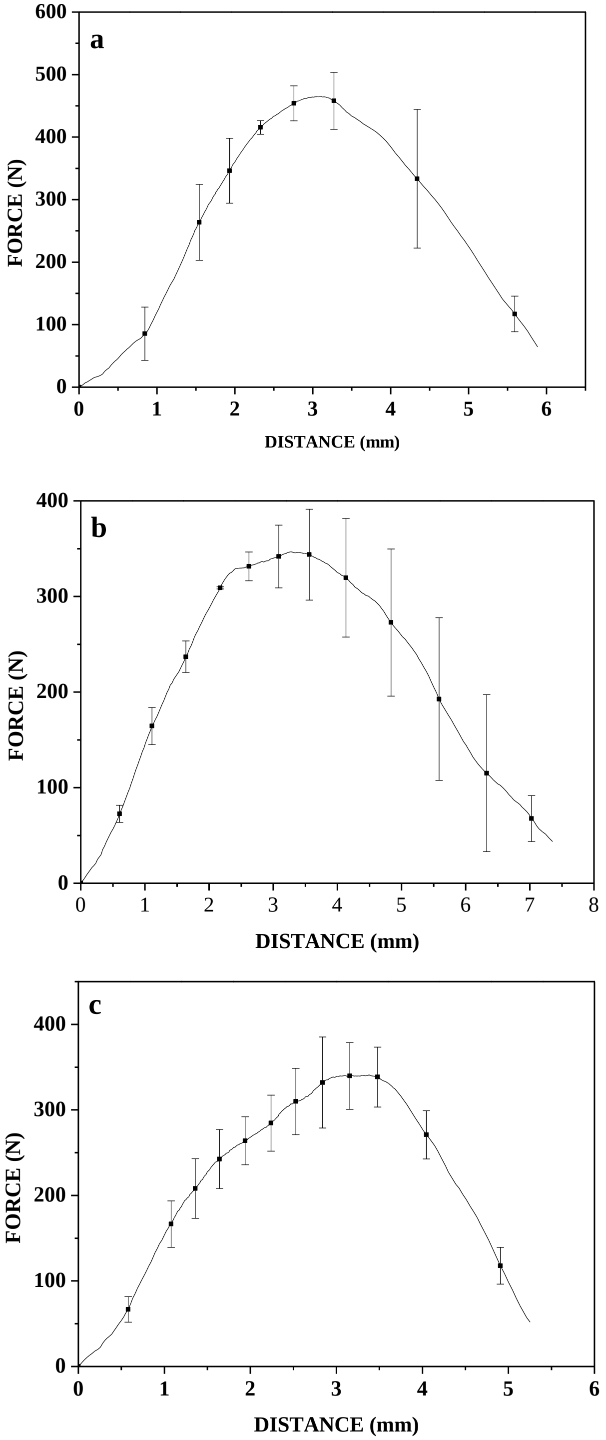

Fig.5.54: Shear force versus distance curve for the eutectic Sn-Pb solder on bare copper substrate surface reflowed for various time; (a) 7 s (b) 10 s and (c) 100 s

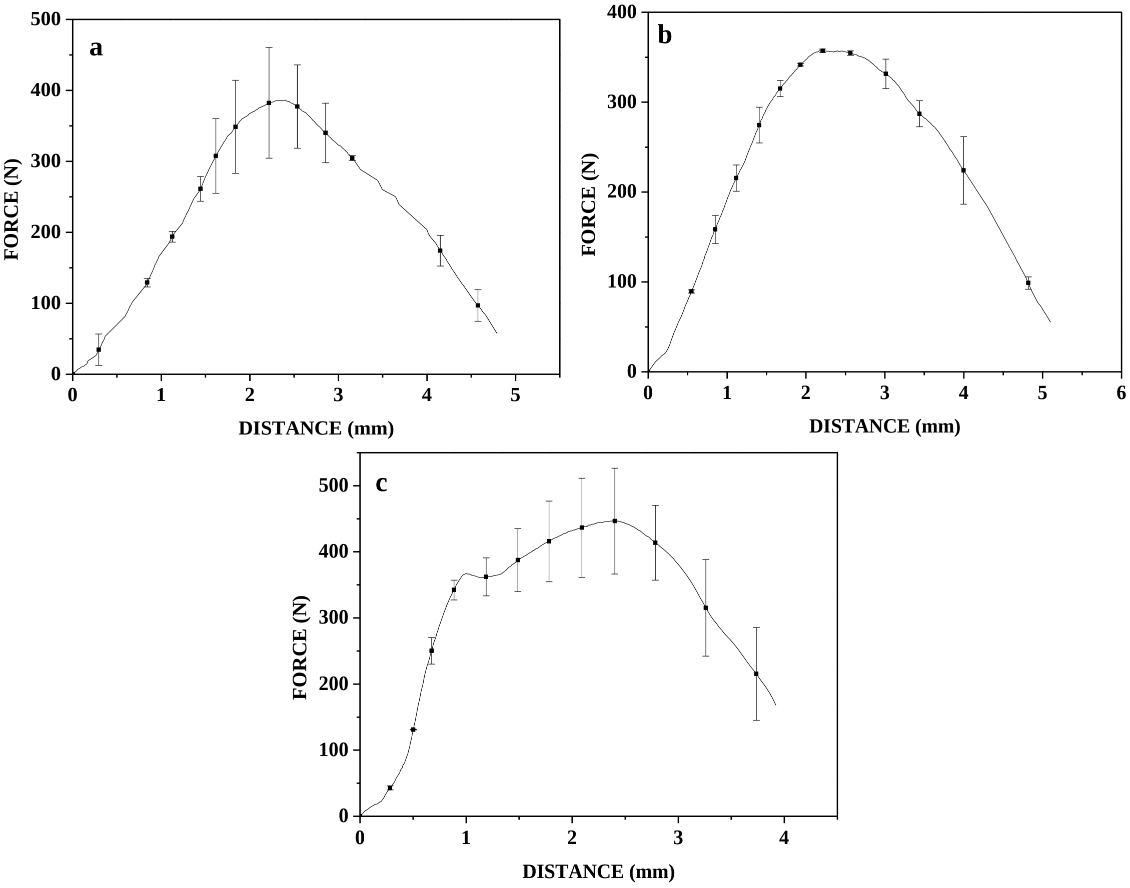

Fig.5.55: Shear force versus distance curve for the eutectic Sn-Pb solder on Ni coated copper substrate surface reflowed for various time; (a) 10 s (b) 14 s and (c) 100 s

A similar trend shown by Sn-0.7Cu, Sn-0.3Ag-0.7Cu and Sn-2.5Ag-0.5Cu alloy during their spreading on bare and Ni coated Cu substrates was observed for Sn-Pb solder alloy as well. The time taken for the spreading of Sn-Pb on Ni coated Cu substrate was twice than that on bare Cu substrate. This once again strengthens the fact that Ni acts as a barrier at the solder/Cu interface. The results obtained from ball shear test are given in Table 5.29. Samples reflowed for T_{gz} gave maximum shear strength for both Sn-Pb/Cu and Sn-Pb/Ni coated Cu systems. Sn-Pb on Ni coated Cu substrate showed a lower value than on bare Cu substrate. Figure 5.54 and Figure 5.55 show the Force Vs Distance curves for Sn-Pb reflowed on both bare and Ni coated Cu substrate respectively. Sn-Pb solidified on Cu substrate showed a comparable strength with Sn-0.7Cu alloy on bare and Ni coated Cu substrate. SAC alloys exhibited better strength than Sn-Pb alloys. The strength of eutectic Sn-Pb solder primarily depends on the morphological distribution of Sn-Pb eutectic and the primary phases. Further, the system does not exhibit any IMC phase. On the other hand, the higher strength of the lead free solders can be attributed to the formation of IMC. The lower strength obtained for higher reflow times in the case of lead free solders is attributed to the unfavourable IMC leading to high stress intensity.

Table 5.29: Shear energy of the eutectic Sn-Pb/Cu and Sn-Pb/Ni/Cu systems (quench cooling method)

Sn-Pb/Cu		Sn-Pb/Ni/Cu	
Reflow time (s)	Shear energy (kJ/m^2)	Reflow time (s)	Shear energy (kJ/m^2)
7	69.14±1.39	10	29.48±1.88
10	65.29±3.78	14	46.33±4.79
100	44.95±4.26	100	29.15±0.99

5.7 Single lap shear test results

5.7.1 Single lap shear test of Cu/solder/Cu systems

The most widely used technique for shear testing of solders is the lap-shear technique. The lap-shear technique is commonly used to evaluate the shear, creep, and thermal fatigue behaviour of solder joints. Here, the solder is placed between two substrate blocks, which are pulled in opposing directions to provide shear loading [Chawla et al. 2004]. Single lap joint tests were performed to evaluate the effect of reflow time on the interfacial reactions and reliability of solder joints. Only three reflow times were selected for reflow purpose namely 10 s, T_{gz} (time corresponding to the end of gravity zone) and

100 s. The photographs showing the top and bottom views of the joint shear sample are shown in Figure 5.56 and 5.57 respectively.

Fig. 5.56: Top view of Cu/solder/Cu and single lap solder joint (top view).

Fig. 5.57: Side view of Cu/solder/Cu lap solder joint

Table 5.30: Lap shear strength of Sn-0.7Cu/Cu, Sn-0.3Ag-0.7Cu/Cu and Sn-2.5Ag-0.5Cu/Cu systems

Sn-0.7Cu		Sn-0.3Ag-0.7Cu		Sn-2.5Ag-0.5Cu	
Reflow Time (s)	Yield strength (0.2% proof strength) (MPa)	Reflow Time (s)	Yield strength (0.2% proof strength) (MPa)	Reflow Time (s)	Yield strength (0.2% proof strength) (MPa)
10	88.76±6.62	10	105.03±2.66	10	112.25±4.58
25	107.67±6.35	40	125.45±4.68	40	169.32±3.02
100	61.77±6.31	100	78.85±4.56	100	73.91±3.59

The typical stress-strain graphs obtained during the lap joint test on Cu/Sn-0.7Cu/Cu, Cu/Sn-0.3Ag-0.7Cu/Cu and Cu/Sn-2.5Ag-0.5Cu/Cu lap joints are shown in Figure 5.58,

Figure 5.59 and Figure 5.60 respectively. The yield strength values obtained from the experiments are tabulated in Table 5.30. Cu/Sn-0.7Cu/Cu showed maximum yield strength for a reflow time of 25 s whereas Cu/Sn-0.3Ag-0.7Cu/Cu and Cu/Sn-2.5Ag-0.5Cu/Cu lap joints showed maximum for 40 s. Yield strength values were found to be maximum for samples reflowed for time corresponding to the end of gravity zone. This strongly supports that reflow time should not extend beyond the gravity regime.

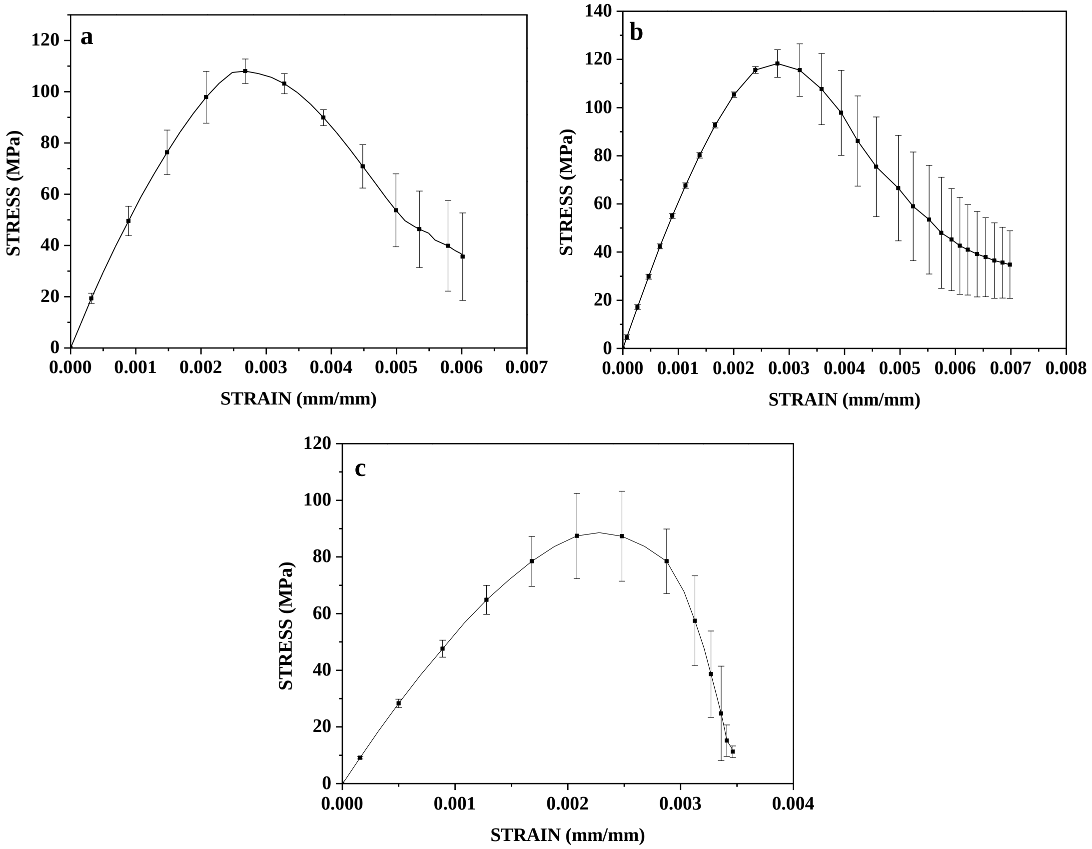

Fig. 5.58: Stress versus strain graphs for single lap Sn-0.7Cu/Cu joint reflowed for (a) 10 s (b) 25 s and (c) 100 s

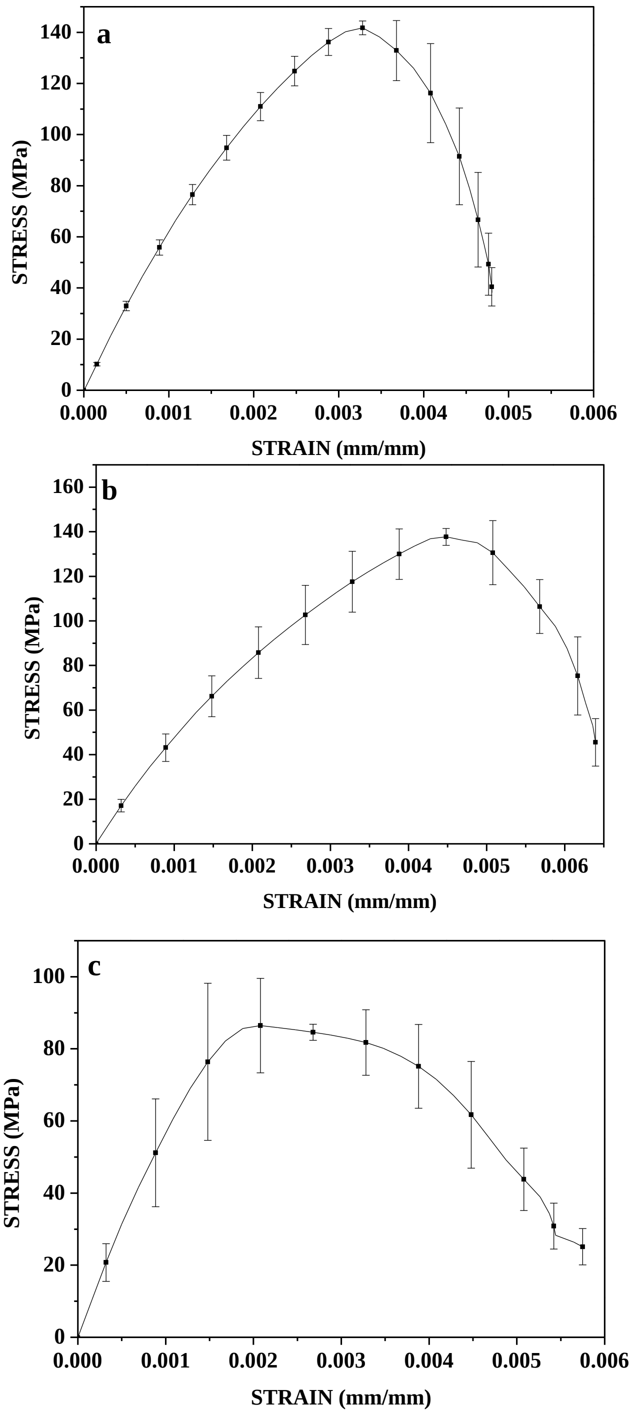

Fig. 5.59: Stress versus strain graphs for single lap Sn-0.3Ag-0.7Cu/Cu joint reflowed for (a) 10 s (b) 40 s and (c) 100 s

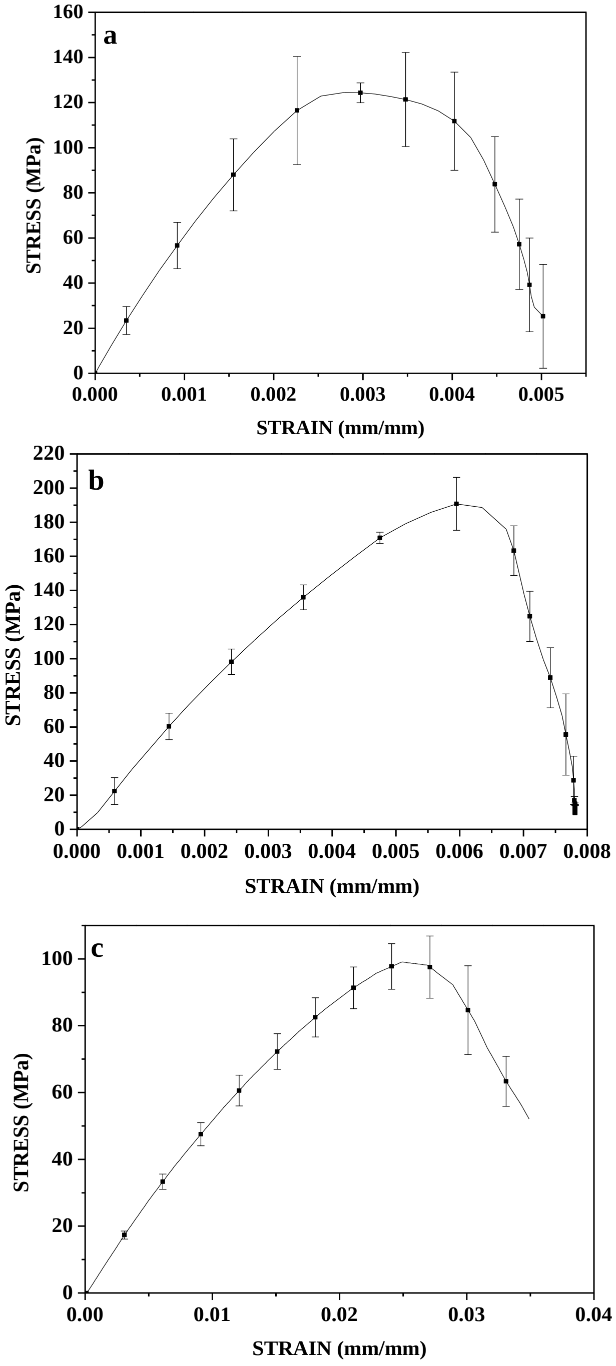

Fig. 5.60: Stress versus strain graphs for single lap Sn-2.5Ag-0.5Cu/Cu joint reflowed for (a) 10 s (b) 40 s and (c) 100 s

The sheared samples were observed under SEM. In general, failure of the lap solder happens in three different ways.

1. Failure takes place at the bulk solder.
2. Fracture starts across the solder bulk region then diverts its path toward the solder/Cu interface.
3. Total failure of lap joint takes place across the solder/Cu interface.

Figure 5.61 shows the schematic illustration of cross-section of substrate/solder/substrate lap joint.

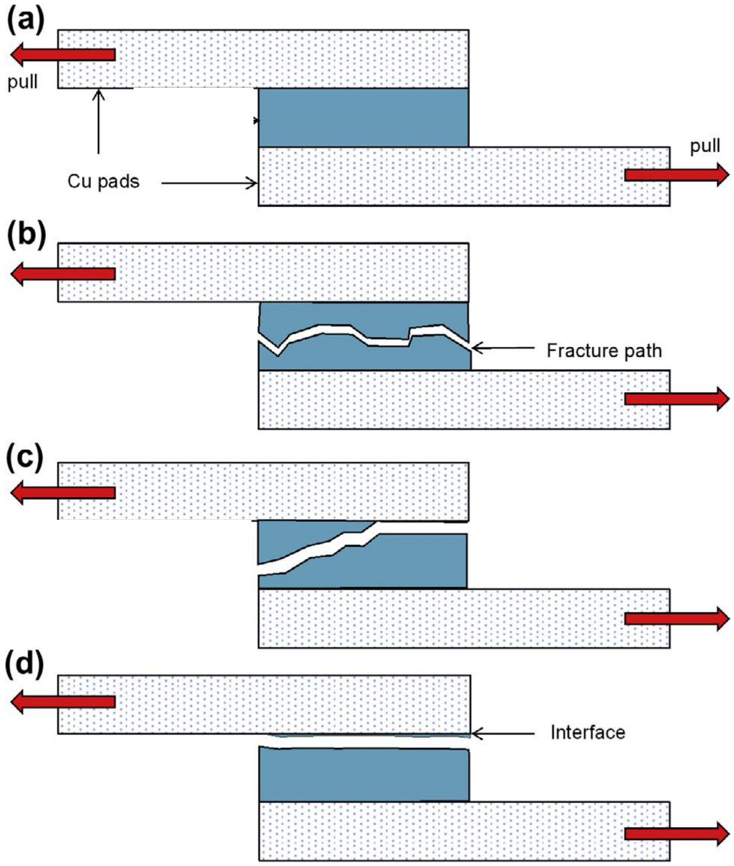

Fig. 5.61: A schematic illustration of cross-section of substrate/solder/substrate lap joint [Affendy and Mohamad 2015]

Affendy and Mohamad [2015] observed a failure in the bulk solder at lower crosshead speed (0.5 to 1 mm/min). At medium crosshead speed (1.5 to 2 mm/min), second type of fracture was observed whereas at higher crosshead speeds (2.5 to 3mm/min) third type of fracture took place.

In the present study, single lap solder joints were tested at room temperature under a strain rate of 0.2 x 10^{-3} s^{-1}. Figure 5.62- 5.64 show the SEM images of fractured surfaces. In all cases, it was observed that the Cu/Sn-0.7Cu/Cu and Cu/Sn-0.3Ag-0.7Cu/Cu specimens fractured within the solder matrix. This suggests that the solder matrix is weaker than the IMC layer between the solder and the Cu substrate. Furthermore, the fracture surfaces in Figure 5.62 and Figure 5.63 contain elongated dimple like structures. Hence, it is apparent that Cu/Sn-0.7Cu/Cu and Cu/Sn-0.3Ag-0.7Cu/Cu fail with a ductile fracture mode, irrespective of their reflow time conditions. Cu/Sn-2.5Ag-0.5Cu/Cu specimens reflowed for 10 s and T_{gz} (time corresponding to the end of gravity regime) fractured within the solder matrix where as in samples reflowed for 100 s, fracture started at the bulk region and then diverted its path toward the solder/Cu interface medium. Figure 5.64 shows the fractured surface of Cu/Sn-2.5Ag-0.5Cu/Cu specimen. Solder bulk region suffered a ductile failure whereas fracture at the solder/IMC layer exhibited brittle failure. Figure shows the partial debonding failure that occurred at the interface between the solder matrix and the Cu_6Sn_5 IMC layer. The faceted appearance of the fracture surfaces is caused by the cleavage fracture of the Cu_6Sn_5 IMC layer.

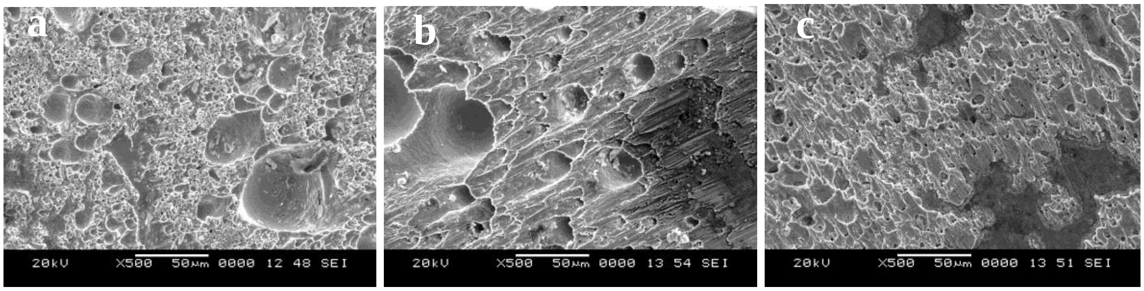

Fig. 5.62: SEM micrographs of fractured surfaces of single lap Sn-0.7Cu/Cu joint reflowed at (a) 10 s (b) 25 s and (c) 100 s

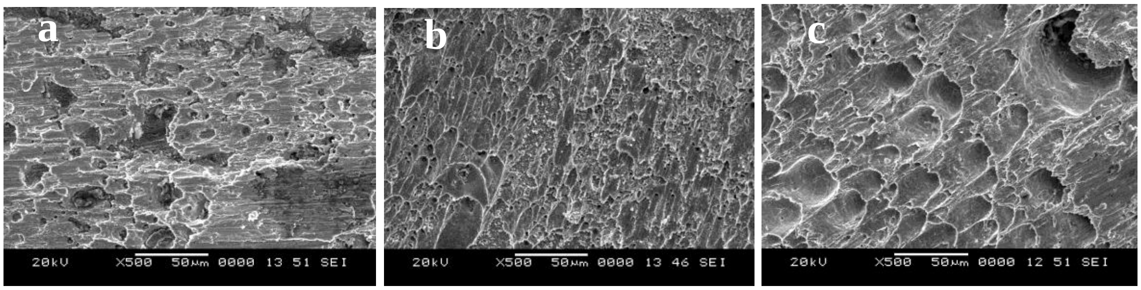

Fig. 5.63: SEM micrographs of fractured surfaces of single lap Sn-0.3Ag-0.7Cu/Cu joint reflowed at (a) 10 s (b) 40 s and (c) 100 s

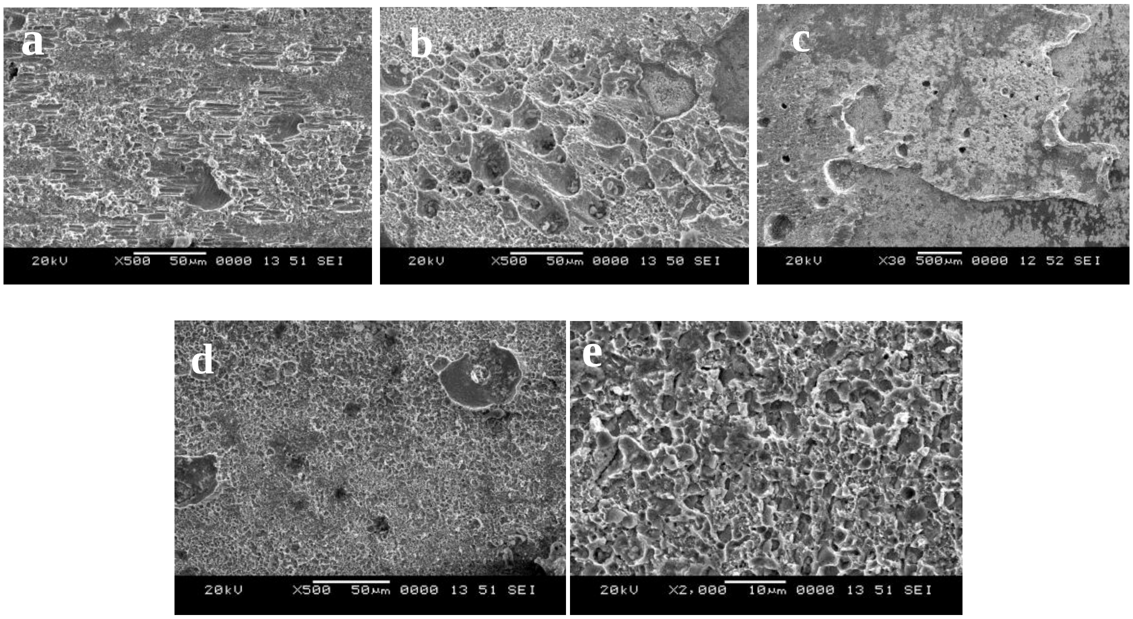

Fig. 5.64: SEM micrographs of fractured surfaces of single lap Sn-2.5Ag-0.5Cu/Cu joint reflowed at (a) 10 s (b) 40 s (c) 100 s and (d), (e) show the enlarged view of the parts indicated by the arrow mark

5.7.2 Single lap shear test of Ni coated Cu/solder/Ni coated Cu systems

The typical stress-strain graphs obtained during the lap joint test on Ni coated Cu/Sn-0.7Cu/Ni coated Cu, Ni coated Cu/Sn-0.3Ag-0.7Cu/ Ni coated Cu and Ni coated Cu/Sn-2.5Ag-0.5Cu/ Ni coated Cu lap joints are shown in Figure 5.65, Figure 5.66 and Figure 5.67 respectively. The yield strength values obtained from the experiments are tabulated in Table 5.31. Single lap solder joints of Sn-0.7Cu solder reflowed on Ni coated Cu substrates showed maximum yield strength for a reflow time of 50 s whereas Sn-0.3Ag-0.7Cu solder reflowed on Ni coated Cu substrates showed maximum yield strength for a reflow time of 70 s, similarly Sn-2.5Ag-0.5Cu showed maximum yield strength at 80 s. Yield strength values were found to be maximum for samples reflowed for time corresponding to the end of gravity zone.

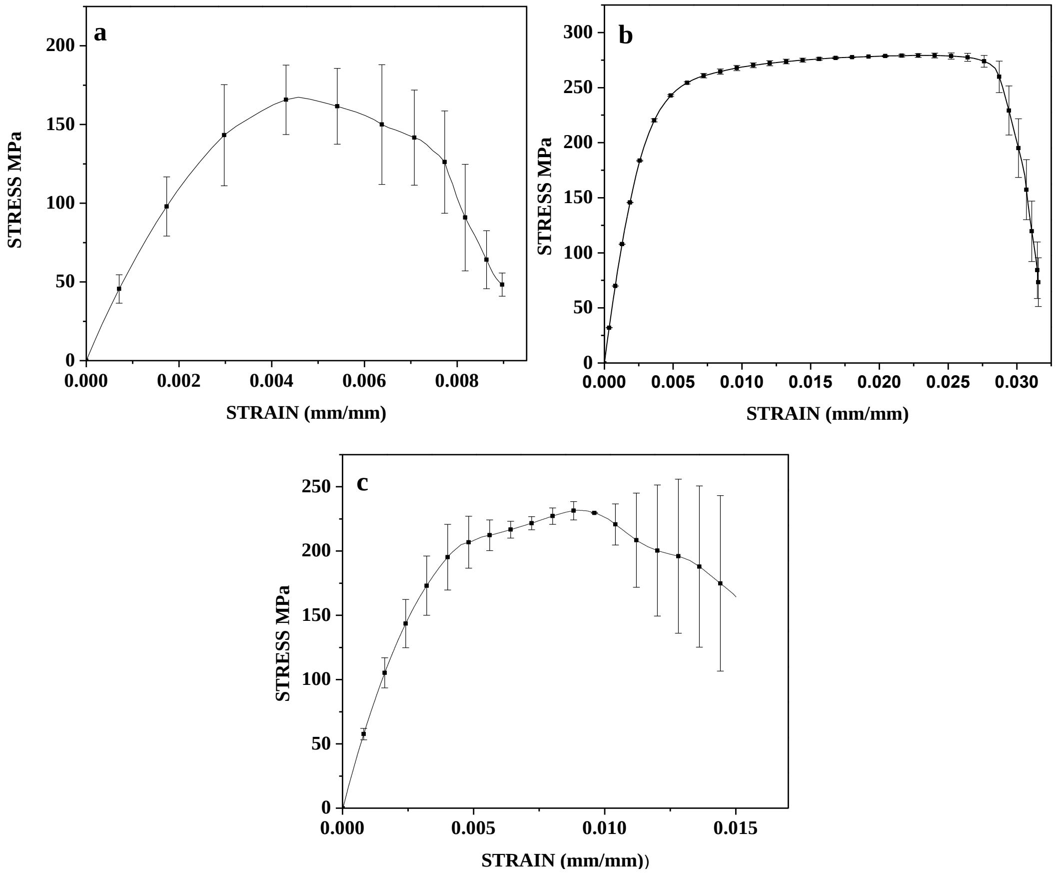

Fig. 5.65: Stress versus strain graphs for single lap Sn-0.7Cu/Ni coated Cu joint reflowed for (a) 10 s (b) 50 s and (c) 100 s

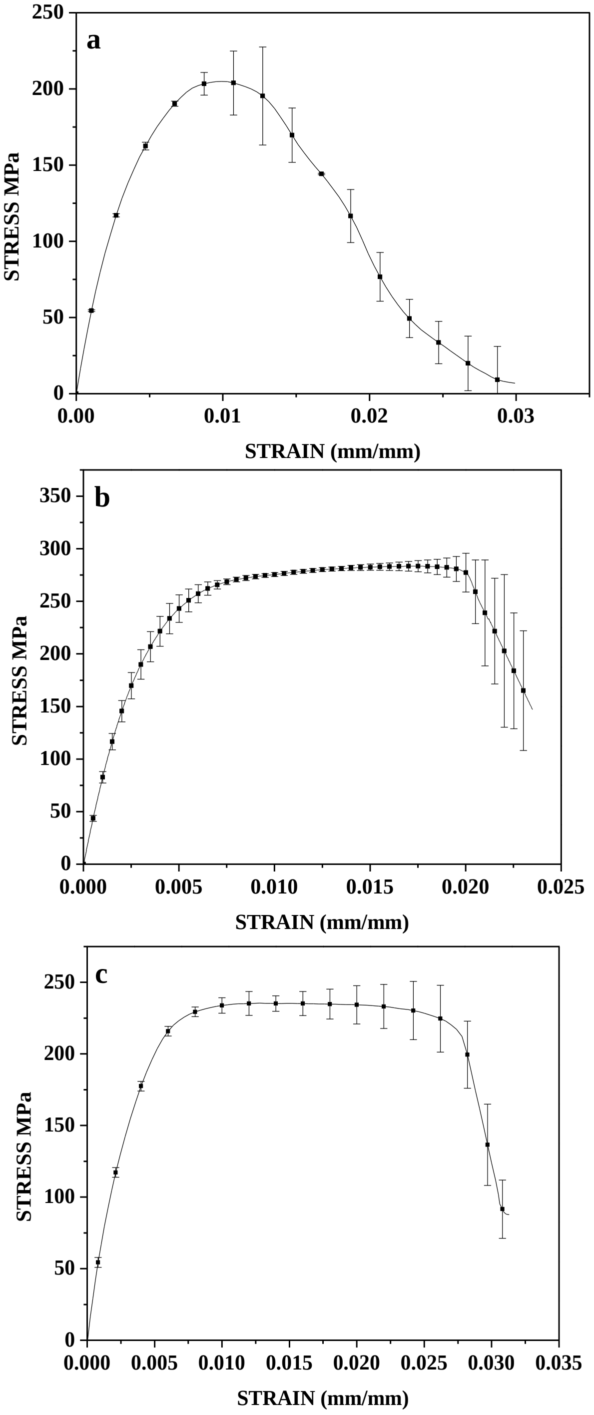

Fig. 5.66: Stress versus strain graphs for single lap Sn-0.3Ag-0.7Cu/Ni coated Cu joint reflowed for (a) 10 s (b) 70 s and (c) 100 s

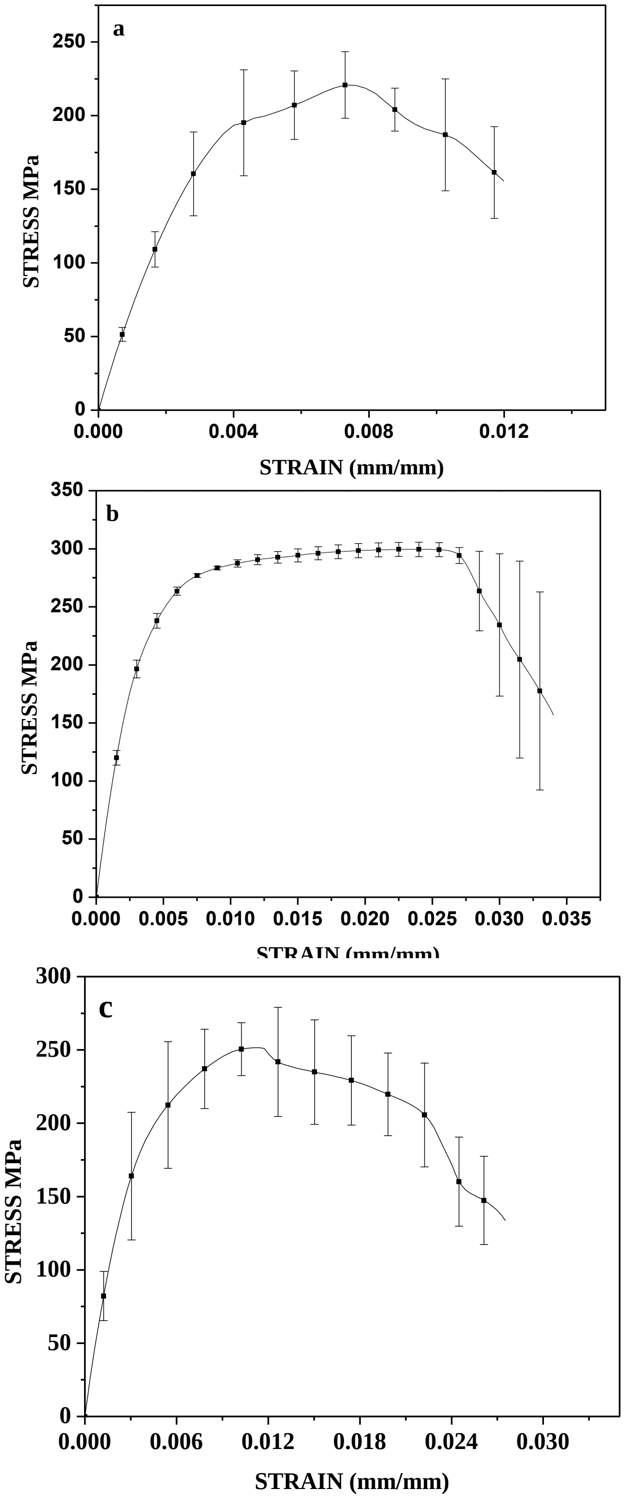

Fig. 5.67: Stress versus strain graphs for single lap Sn-2.5Ag-0.5Cu/ Ni coated Cu joint reflowed for (a) 10 s (b) 80 s and (c) 100 s

Table 5.31 Lap shear strength of Sn-0.7Cu/Ni/Cu, Sn-0.3Ag-0.7Cu/Ni/Cu and Sn-2.5Ag-0.5Cu/Ni/Cu systems

Sn-0.7Cu		Sn-0.3Ag-0.7Cu		Sn-2.5Ag-0.5Cu	
Reflow Time (s)	Yield strength (0.2% proof strength) (MPa)	Reflow Time (s)	Yield strength (0.2% proof strength) (MPa)	Reflow Time (s)	Yield strength (0.2% proof strength) (MPa)
10	191.39±2.82	10	199.04±0.71	10	245.6±2.33
50	265.37±1.47	70	272.05±1.21	80	274.98±2.94
100	251.74±6.08	100	264.18±0.14	100	261.22±1.76

It is observed that single lap solder joint specimen of Sn-0.7Cu reflowed on Ni coated Cu fractured within the solder matrix irrespective of reflow time. Single lap solder joint specimen of Sn-0.3Ag-0.7Cu on Ni coated Cu substrate and Sn-2.5Ag-0.5Cu on Ni coated Cu substrate reflowed for 10 s and T_{gz} failed at the bulk solder whereas specimens reflowed for 100 s showed partial debonding failure at the interface between the solder matrix and the $(CuNi)_6Sn_5$ IMC layer. Due to the combined effect of the brittle $(CuNi)_6Sn_5$ IMC layer and the stress concentration at the solder/intermetallic interface, $(CuNi)_6Sn_5$ nodular tips protrude into the fracture surface. Under shear conditions, these nodular tips cause a large shear strain localization effect, and hence the IMC interface becomes the preferred site for crack formation and propagation. Therefore, as shown in Figures 5.69 and 5.70, partial debonding failures occur at the interface between the solder matrix and the $(CuNi)_6Sn_5$ IMC layer. The faceted appearance of the fracture surfaces in Figure 5.69 (d) and Figure 5.70 (d) is due to cleavage fractures of the $(CuNi)_6Sn_5$ layer. When the cleavage planes in neighbouring $(CuNi)_6Sn_5$ grains are approximately parallel, the fracture propagates easily through the inside of the IMC layer or along the interface of the $(CuNi)_6Sn_5$ layer and the solder matrix [Lee and Lee 2007]. It appears that the probability of debonding shear failure depends on the relative balance between the strength of the solder matrix and the strength of the $(CuNi)_6Sn_5$/solder interface.

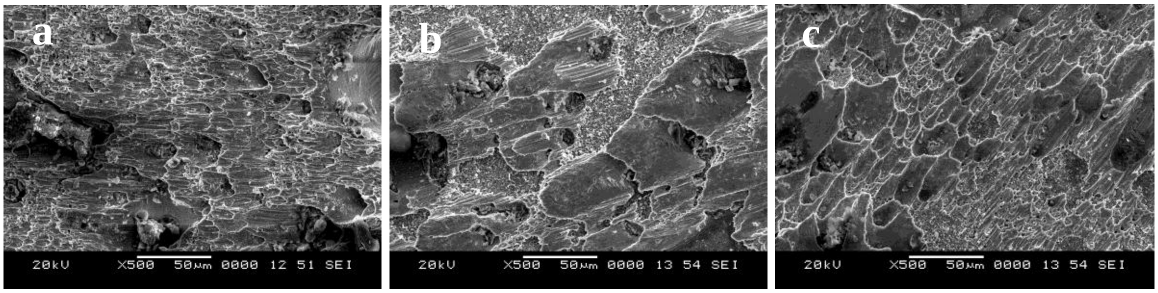

Fig. 5.68: SEM micrographs of fractured surfaces of single lap Sn-0.7Cu/Ni/Cu joint reflowed at (a) 10 s (b) 50 s and (c) 100 s

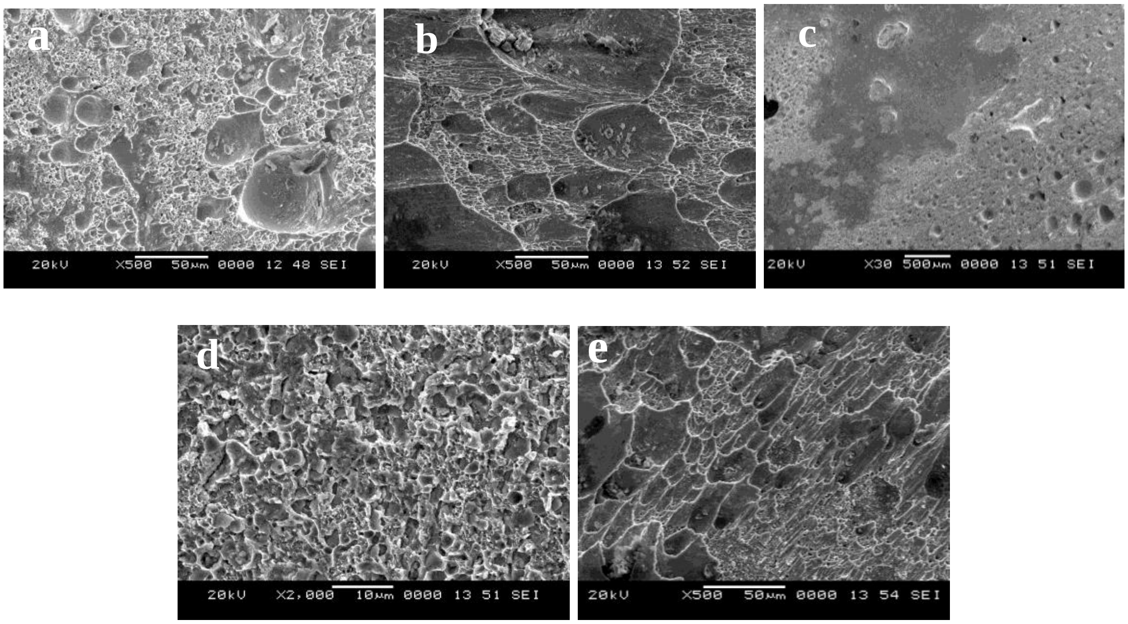

Fig. 5.69: SEM micrographs of fractured surfaces of single lap Sn-0.3Ag-0.7Cu/Ni/Cu joint reflowed at (a) 10 s (b) 70 s (c) 100 s and (d), (e) show the enlarged view of the parts indicated by the arrow mark

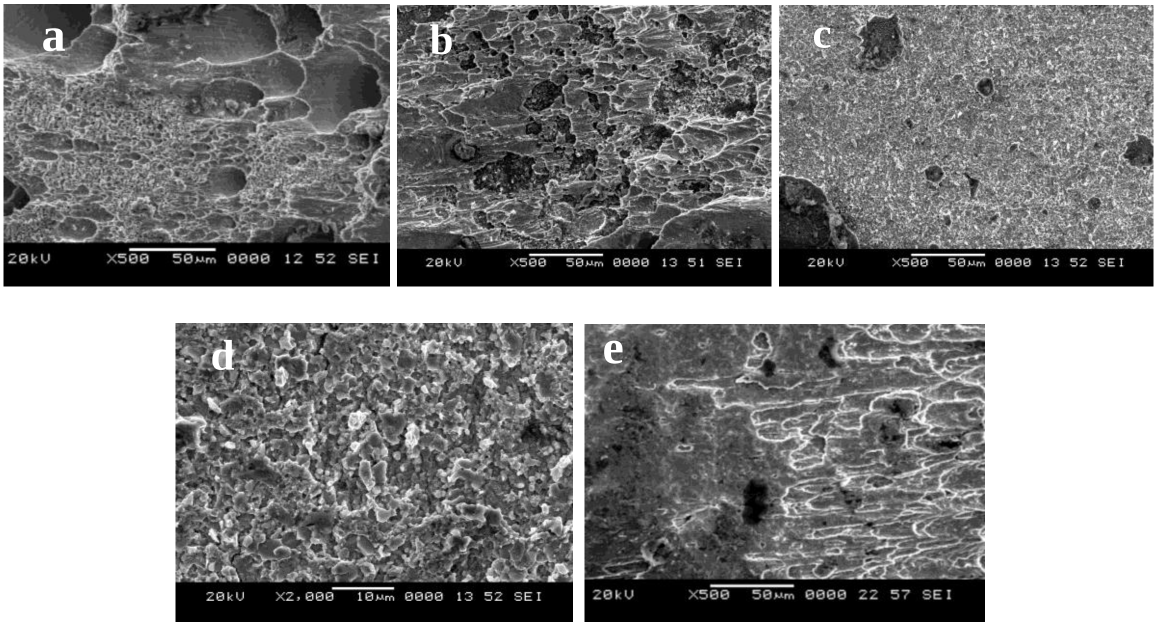

Fig. 5.70: SEM micrographs of fractured surfaces of single lap Sn-2.5Ag-0.5Cu/Ni/Cu joint reflowed at (a) 10 s (b) 80 s (c) 100 s and (d), (e) show the enlarged view of the parts indicated by the arrow mark

Lap joint tests of Cu/Sn-Pb/Cu and Ni coated Cu/Sn-Pb/Ni coated Cu single lap solder joints were carried out to compare the results obtained with lead free solder alloys. Three reflow times were choosen. 10, 100 and T_{gz}.. Samples were quench cooled after corresponding reflow time. Figure 5.71 shows the stress versus strain graphs for Sn-Pb solidified between Cu plates for 7 s, 10 s and 100 s respectively. Table 5.32 gives the yield strength values obtained for the test. Samples reflowed for 7 s gave maximum strength. Figure 5.72 shows the stress versus strain graphs for Sn-Pb solidified between Ni coated Cu plates for 10 s, 14 s and 100 s respectively. Samples reflowed for 14 s gave the maximum strength among Sn-Pb solidified between Ni coated Cu substrates for various reflow times. This confirmed the prominent role T_{gz} in the determination of optimum reflow time for any solder alloy. Sn-Pb showed maximum stength on bare Cu rather than on Ni coated Cu substrate. Sn-Pb showed higher strength than Sn-0.7Cu, Sn-0.3Ag-0.7Cu and Sn-2.5Ag-0.5Cu solder alloy solidified on Cu substrate.

Table 5.32 Lap shear strength of Sn-Pb/Cu and Sn-Pb/Ni/Cu systems

Sn-Pb/Cu		Sn-Pb/Ni/Cu	
Reflow Time (s)	Yield strength (0.2% proof strength) (MPa)	Reflow Time (s)	Yield strength (0.2% proof strength) (MPa)
7	261.35±2.59	10	171.68±8.77
10	155.47±3.42	14	233.38±3.89
100	45.48±3.26	100	226.64±2.43

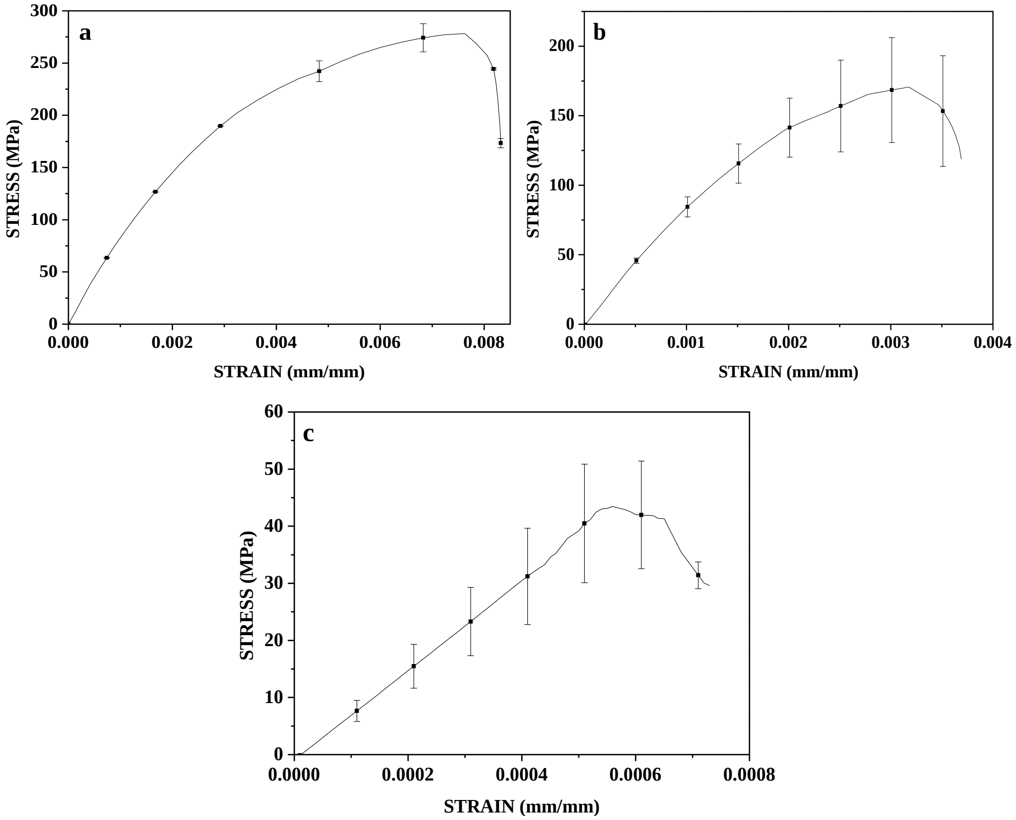

Fig. 5.71: Stress versus strain graphs for single lap Sn-Pb/Cu joint reflowed for (a) 7 s (b) 10 s and (c) 100 s

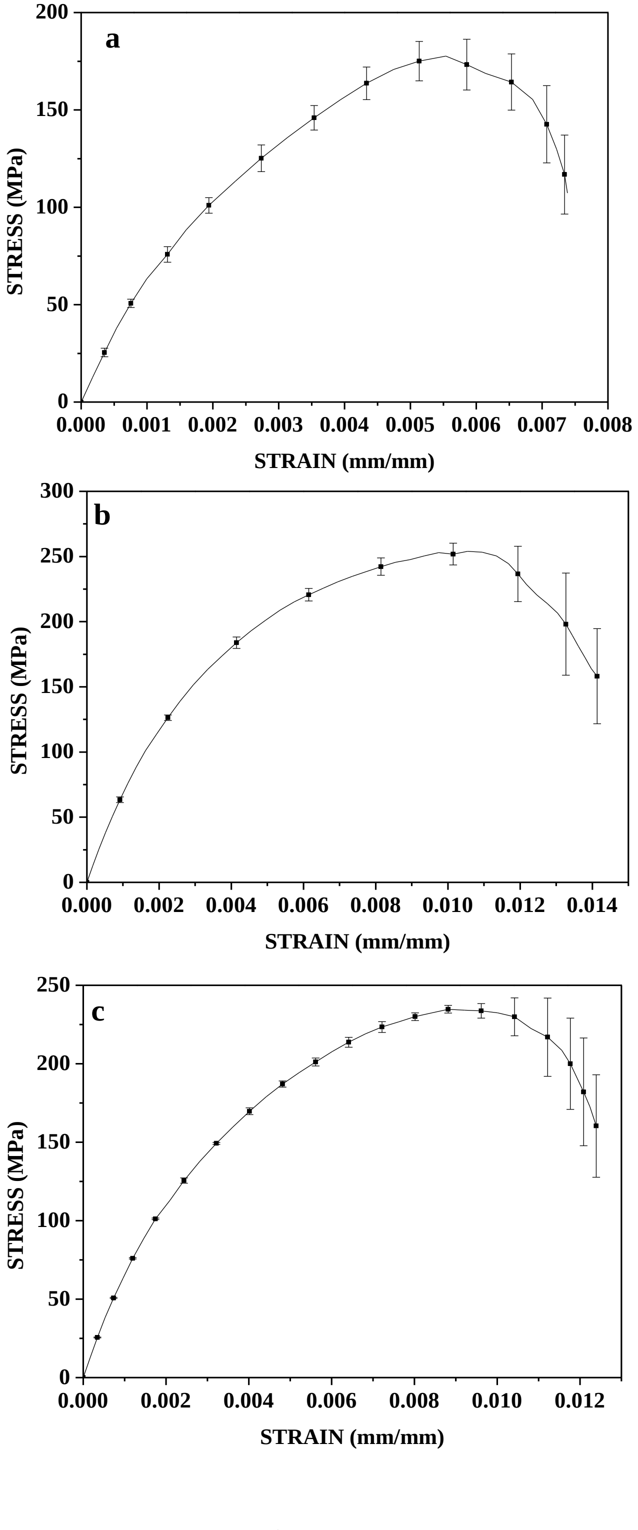

Fig. 5.72: Stress versus strain graphs for single lap Sn-Pb/Ni/Cu joint reflowed for (a) 10 s (b) 14 s and (c) 100 s

CHAPTER 6

CONCLUSION

Based on the study of the effect of reflow time on wettability, microstructure and joint strength of Sn–0.7Cu, Sn–0.3Ag-0.7Cu and Sn–2.5Ag-0.5Cu reflowed on bare and Ni coated Cu substrates, the following conclusions were drawn.

- The final contact angle decreased with the increase in the reflow time for all of the solder/substrate systems.
- Final contact angle (θ_f) obtained at the end of the reflow time was comparable for Sn-0.7Cu/Cu and Sn-0.7Cu/Ni/Cu systems. Sn–0.3Ag-0.7Cu, Sn–2.5Ag-0.5Cu alloys showed lower contact angles on bare Cu when compared to that obtained on Ni coated Cu substrates.
- The spreading behaviour of the solder alloy was categorized into capillary, gravity (diffusion), and viscous zones.
- The time required for the completion of gravity zone (T_{gz}) for Sn-0.7Cu solder alloy solidified on bare Cu substrate was found to be 25 s. T_{gz} for Sn–0.3Ag-0.7Cu and Sn–2.5Ag-0.5Cu solidified on bare Cu substrates was 40 s.
- T_{gz} value for Sn–0.7Cu, Sn–0.3Ag-0.7Cu and Sn–2.5Ag-0.5Cu alloys solidified on Ni coated Cu substrate were 50, 70 and 80 s respectively.
- Furnace cooling resulted in maximum growth of IMCs compared to quench cooling. Cu_6Sn_5 IMC thickness increased from 3.76 μm to 6.68 μm with the increase in reflow time from 10 s to 500 s in furnace cooled Sn-0.7Cu/Cu system. The corresponding values varied from 3.43 μm to 6.30 μm in Sn-0.3Ag-0.7Cu/Cu system and 3.09 μm to 10.96 μm in Sn-2.5Ag-0.5Cu/Cu system respectively.
- The Cu_6Sn_5 IMC thickness varied from 0.7 μm to 3.25 μm for all the solder/Cu systems, cooled by quench cooling method.

- Furnace cooling had no effective control on the reflow time and hence quench cooling is more reliable in assessing the effect of reflow time on microstructure and joint strength.
- Thickness of IMCs at the solder/substrate interface region of Sn–0.7Cu, Sn–0.3Ag-0.7Cu alloys and Ni coated Cu substrate was lower than at the interface of same alloys on bare Cu substrates. Thickness of IMCs at the interface of Sn–2.5Ag-0.5Cu alloy and Ni coated Cu substrate was found to be slightly higher for longer reflow times (above 100 s) than for the same alloy on bare Cu substrate.
- Quench cooled solder/Cu systems showed an increase in shear strength by about 40 %.
- Grain boundary diffusion was found to be the rate-controlling process for the IMC growth in all solder/substrate combinations.
- From the study of growth kinetics of furnace cooled solder/Cu systems, it was observed that the role of grain boundary diffusion diminishes, as the IMC layer grows thicker (≈ > 8 μm) and volume diffusion controls the growth rate thereafter.
- Solder alloys reflowed till the end of gravity zone (T_{gz}) yielded maximum joint strength under ball shear test compared to that obtained for reflow times required to achieve the stabilized contact angle (θ_f).
- Shear strength of single lap solder joints (Cu/solder/Cu, and Ni coated Cu/solder/ Ni coated Cu systems) were also measured for 10 s, 100 s and the time (T_{gz}) at the end of gravity zone. Single lap solder joints showed maximum joint strength for samples reflowed till the end of gravity zone time (T_{gz}) validating the results obtained from ball shear tests.
- Shear energy increased with the increase of Ag content in solder alloys. The increase in shear energy for the Ag bearing solder was mainly due to the presence of Ag_3Sn intermetallics in the bulk solder.
- Sn-2.5Ag-0.5Cu showed maximum shear energy on both Cu and Ni coated Cu substrates when compared to Sn-0.7Cu and Sn-0.3Ag-0.7Cu solder alloys. Sn-

2.5Ag-0.5Cu/Ni/Cu systems reflowed for 80 s showed maximum bond strength among all other solder/substrate systems reflowed for T_{gz}.

- A thickness of IMCs between 1-2 μm on bare Cu and 1-1.5 μm on Ni coated Cu substrate yielded a good joint strength and hence found to be optimum.
- Only Cu_6Sn_5 intermetallics were found at the interface in samples reflowed for various reflow times on bare Cu substrates.
- $(CuNi)_6Sn_5$ intermetallics were found at the interface in samples reflowed for 10, 100 and 300 s on Ni coated Cu substrates. In addition, a very small amount of $(CuNi)_3Sn_4$ intermetallics were also found between $(CuNi)_6Sn_5$ and Ni coating for the samples reflowed for 500s. The IMC thickness increased initially up to a reflow time of 300 s followed by a drop in the thickness for Sn-0.3Ag-0.7Cu/Ni/Cu and Sn-2.5Ag-0.5Cu/Ni/Cu systems for 500 s. The samples reflowed for 500 s showed spalling leading to the decrease in the joint strength.
- Ball and single lap shear strengths of eutectic Sn-Pb on bare and Ni coated Cu substrates were determined to compare the results obtained with lead free solder alloys. T_{gz} was found to be 7 s and 14 s for eutectic Sn-Pb on bare and Nickel coated Cu substrates respectively. Ball shear strength of Sn-Pb on Cu was comparable for samples reflowed for T_{gz} (7s) and 10 s and sample reflowed for 100 s showed a lower value. Samples reflowed for 7 s on Cu substrate gave maximum value under lap joint test. Ball shear as well as lap shear strengths showed a maximum value for systems reflowed for T_{gz} (14 s) in case of Sn-Pb on Ni coated Cu substrate.
- A dynamic contact angle (θ_{gz}) was found to be more reliable compared to the stabilized contact angle (θ_f) and the time to reach this value was used to correlate the wettability of liquid solder to the microstructure and joint strength. The present work suggests that the solder reflow should end before the start of viscous regime. The study clearly brings out the importance of gravity zone in determining the optimum reflow time for lead free solder alloys at particular reflow temperature.

REFERENCES

Abtew, M. and Selvaduray, G. (2000). "Lead-free Solders in Microelectronics." *Mater. Sci. Eng. R Rep.*, 27(5–6), 95–141.

Affendy, M.G. and Mohamad, A.A. (2015). "Effects of crosshead speeds on solder strength of Cu/Sn–9Zn/Cu lap joints." *J. King Saud Univ. - Eng. Sci.*, 27(2), 225–231.

Amore, S., Ricci, E., Borzone, G. and Novakovic, R. (2008). "Wetting behaviour of lead-free Sn-based alloys on Cu and Ni substrates." *Mater. Sci. Eng. A*, 495(1–2), 108–112.

Arenas, M.F. and Acoff, V.L. (2004). "Contact angle measurements of Sn-Ag and Sn-Cu lead-free solders on copper substrates." *J. Electron. Mater.*, 33(12), 1452–1458.

Arenas, M.F., He, M. and Acoff, V.L. (2006). "Effect of flux on the wetting characteristics of SnAg, SnCu, SnAgBi, and SnAgCu lead-free solders on copper substrates." *J. Electron. Mater.*, 35(7), 1530–1536.

Awasthi, A., Bhatt, Y.J. and Garg, S.P. (1996). "Measurement of contact angle in systems involving liquid metals." *Meas. Sci. Technol.*, 7(5), 753.

Berthou, M., Retailleau, P., Frémont, H., Guédon-Gracia, A. and Jéphos-Davennel, C. (2009). "Microstructure evolution observation for SAC solder joint: Comparison between thermal cycling and thermal storage." *Microelectron. Reliab.*, 49(9–11), 1267–1272.

Chan, Y.C., So, A.C.K. and Lai, J.K.L. (1998). "Growth kinetic studies of Cu–Sn intermetallic compound and its effect on shear strength of LCCC SMT solder joints." *Mater. Sci. Eng. B*, 55(1–2), 5–13.

Chang, S.Y., Huang, Y.C. and Lin, Y.-M. (2010). "Mechanical property and fracture behaviour characterizations of 96.5 Sn–3.0 Ag–0.5 Cu solder joints." *J. Alloys Compd.*, 490(1–2), 508–514.

Chawla, N., Shen, Y.L., Deng, X. and Ege, E.S. (2004). "An evaluation of the lap-shear test for Sn-rich solder/Cu couples: Experiments and simulation." *J. Electron. Mater.*, 33(12), 1589–1595.

Chen, C.M. and Lin, H.C. "Interfacial reactions and mechanical properties of ball-grid-array solder joints using Cu-cored solder balls." *J. Electron. Mater.*, 35(11), 1937–1947.

Chen, W.Y., Yu, C.Y. and Duh, J.G. (2012). "Suppressing the growth of interfacial Cu–Sn intermetallic compounds in the Sn–3.0Ag–0.5Cu–0.1Ni/Cu–15Zn solder joint during thermal aging." *J. Mater. Sci.*, 47(9), 4012–4018.

Choubey, A., Yu, H., Osterman, M., Pecht, M., Yun, F., Yonghong, L. and Ming, X. (2008). "Intermetallics Characterization of Lead-Free Solder Joints under Isothermal Aging." *J. Electron. Mater., 37*(8), 1130–1138.

Chung, C.K., Duh, J.G. and Kao, C.R. (2010). "Direct evidence for a Cu-enriched region at the boundary between Cu6Sn5 and Cu3Sn during Cu/Sn reaction." *Scr. Mater.*, 63(2), 258–260.

"Database for properties of lead-free solder alloys." http://www.gullwinguk.com/content/pdf/db_pbfree_solder.pdf (Dec. 10, 2015).

Dong, W., Shi, Y., Lei, Y., Xia, Z. and Guo, F. (2008). "Effects of small amounts of Ni/P/Ce element additions on the microstructure and properties of Sn3.0Ag0.5Cu solder alloy." *J. Mater. Sci. Mater. Electron.*, 20(10), 1008–1017.

Dudek, M.A. and Chawla, N. (2010). "Nanoindentation of rare earth–Sn intermetallics in Pb-free solders." *Intermetallics,* 18(5), 1016–1020.

El-Daly, A.A. and El-Taher, A.M. (2013). "Improved strength of Ni and Zn-doped Sn–2.0Ag–0.5Cu lead-free solder alloys under controlled processing parameters." *Mater. Des.*, 47, 607–614.

Ervina Efzan, M.N. and Aisyah Marini, A. (2012). "A review of solder evolution in electronic application." *Int. J Eng. App. Sci*, 1, 1-10.

Gagliano, R.A., Ghosh, G. and Fine, M.E. (2002). "Nucleation kinetics of Cu6Sn5 by reaction of molten tin with a copper substrate." *J. Electron. Mater.*, 31(11), 1195–1202.

Gao, F., Takemoto, T. and Nishikawa, H. (2006). "Effects of Co and Ni addition on reactive diffusion between Sn–3.5Ag solder and Cu during soldering and annealing." *Mater. Sci. Eng. A*, 420(1–2), 39–46.

Gu, X., Chan, Y.C., Wu, B.Y. and Yang, D. (2007). "Effect of Carbon Inclusion in the Ni-P Coating on Shearing Behaviour of Sn4Ag0.5Cu Ball Grid Array Solder Joints." *Proc., 8th Int. Conf. on Electronic Packaging Technology,* ICEPT. Shanghai, China., 1-5.

Han, Y.D., Jing, H.Y., Nai, S.M.L., Xu, L.Y., Tan, C.M. and Wei, J. (2012). "Interfacial reaction and shear strength of Ni-coated carbon nanotubes reinforced Sn–Ag–Cu solder joints during thermal cycling." *Intermetallics*, 31,72–78.

Hansen, K.S., Jellesen, M.S., Moller, P., Westermann, P.J.S. and Ambat, R. (2009). "Effect of solder flux residues on corrosion of electronics." *Proc., Int. Symp. on Reliability and Maintainability,* RAMS, TX, USA., 502–508.

Haseeb, A.S.M.A., Arafat, M.M. and Johan, M.R. (2012). "Stability of molybdenum nanoparticles in Sn–3.8Ag–0.7Cu solder during multiple reflow and their influence on interfacial intermetallic compounds." *Mater. Charact.*, 64, 27–35.

Hayes, S.M., Chawla, N. and Frear, D.R. (2009). "Interfacial fracture toughness of Pb-free solders." *Microelectron. Reliab.*, 49(3), 269–287.

Ho, C.E., Yang, S.C. and Kao, C.R. (2006). "Interfacial reaction issues for lead-free electronic solders." *Lead-Free Electronic Solders*, 155–174.

Huang, Z., Conway, P.P. and Thomson, R.C. (2006). "Microstructural Considerations for Ultrafine Lead Free Solder Joints." *Microelectron. Reliab.*, 47(12), 1997-2006.

Huh, S.-H., Kim, K.-S. and Suganuma, K. (2001). "Effect of Ag Addition on the Microstructural and Mechanical Properties of Sn-Cu Eutectic Solder." *Mater. Trans.*, 42(5), 739–744.

Islam, M.N., Chan, Y.C., Sharif, A. and Alam, M.O. (2003). "Comparative study of the dissolution kinetics of electrolytic Ni and electroless Ni–P by the molten Sn3.5Ag0.5Cu solder alloy." *Microelectron. Reliab.*, 43(12), 2031–2037.

Jiang, B. and Xian, A.-P. (2007). "Observations of ribbon-like whiskers on tin finish surface." *J. Mater. Sci. Mater. Electron.*, 18(5), 513–518.

John, H., Lau, C.P., Wong, Ning, C.L., Shi-Wei, R.L. (2003) "Prevailing lead free solder." www.digitalengineeringlibrary.com (Jan. 5, 2016).

Kang, S.K., Shih, D.-Y., Leonard, D., Henderson, D.W., Gosselin, T., Cho, S., Yu, J. and Choi, W.K. (2004). "Controlling Ag3Sn plate formation in near-ternary-eutectic Sn-Ag-Cu solder by minor Zn alloying." *JOM*, 56(6), 34–38.

Kariya, Y., Hosoi, T., Terashima, S., Tanaka, M. and Otsuka, M. (2004). "Effect of silver content on the shear fatigue properties of Sn-Ag-Cu flip-chip interconnects." *J. Electron. Mater.*, 33(4), 321–328.

Kattner, U.R. (2002). "Phase diagrams for lead-free solder alloys." *JOM*, 54(12), 45–51.

Keller, J., Baither, D., Wilke, U. and Schmitz, G. (2011). "Mechanical properties of Pb-free SnAg solder joints." *Acta Mater.*, 59(7), 2731–2741.

Kim, K.S., Huh, S.H. and Suganuma, K. (2002). "Effects of cooling speed on microstructure and tensile properties of Sn–Ag–Cu alloys." *Mater. Sci. Eng. A*, 333(1–2), 106–114.

Kim, K.S., Huh, S.H. and Suganuma, K. (2003). "Effects of intermetallic compounds on properties of Sn–Ag–Cu lead-free soldered joints." *J. Alloys Compd.*, 352(1–2), 226–236.

Kim, Y.M., Park, J.-Y. and Kim, Y.-H. (2012). "Effect of Pd Thickness on the Interfacial Reaction and Shear Strength in Solder Joints Between Sn-3.0Ag-0.5Cu Solder and Electroless Nickel/Electroless Palladium/Immersion Gold (ENEPIG) Surface Finish." *J. Electron. Mater.*, 41(4), 763–773.

Kotadia, H.R., Mokhtari, O., Clode, M.P., Green, M.A. and Mannan, S.H. (2012). "Intermetallic compound growth suppression at high temperature in SAC solders with Zn addition on Cu and Ni–P substrates." *J. Alloys Compd.*, 511(1), 176–188.

Kumar, G., Prabhu, K.N., Prabhu, N. and Dean, S.W. (2010). "Wetting Behaviour of Solders." *J. ASTM Int.*, 7(5), 103-115.

Kumar, K.M., Kripesh, V. and Tay, A.A.O. (2006). "Sn-Ag-Cu lead-free composite solders for ultra-fine-pitch wafer-level packaging." *Proc. of 56th Int. Conf. on Electronic Components and Technology*, ECTC, San Diego, USA. 7-11.

Kumar, K.M., Kripesh, V. and Tay, A.A.O. (2008). "Single-wall carbon nanotube (SWCNT) functionalized Sn–Ag–Cu lead-free composite solders." *J. Alloys Compd.*, 450(1–2), 229–237.

Lai, Y.-S., Song, J.-M., Chang, H.-C. and Chiu, Y.-T. (2007). "Ball Impact Responses of Ni- or Ge-Doped Sn-Ag-Cu Solder Joints." *J. Electron. Mater.*, 37(2), 201–209.

LaLonde, A., Emelander, D., Jeannette, J., Larson, C., Rietz, W., Swenson, D. and Henderson, D.W. (2004). "Quantitative metallography of β-Sn dendrites in Sn-3.8Ag-0.7Cu ball grid array solder balls via electron backscatter diffraction and polarized light microscopy." *J. Electron. Mater.*, 33(12), 1545–1549.

Laurila, T., Vuorinen, V. and Kivilahti, J.K. (2005). "Interfacial reactions between lead-free solders and common base materials." *Mater. Sci. Eng. R Rep.*, 49(1–2), 1–60.

Law, C.M.T., Wu, C.M.L., Yu, D.Q., Wang, L. and Lai, J.K.L. (2006). "Microstructure, solderability, and growth of intermetallic compounds of Sn-Ag-Cu-RE lead-free solder alloys." *J. Electron. Mater.*, 35(1), 89–93.

Lee, L.M., Mohamad, A.A., Lee, L.M. and Mohamad, A.A. (2013). "Interfacial Reaction of Sn-Ag-Cu Lead-Free Solder Alloy on Cu: A Review, Interfacial Reaction of Sn-Ag-Cu Lead-Free Solder Alloy on Cu: A Review." *Adv. Mater. Sci. Eng.*, 2013, 1-11

Lee, N.C. (1997). "Getting Ready for Lead-free Solders*." *Solder. Surf. Mt. Technol.*, 9(2), 65–69.

Lee, Y.-H. and Lee, H.-T. (2007). "Shear strength and interfacial microstructure of Sn–Ag–xNi/Cu single shear lap solder joints." *Mater. Sci. Eng. A*, 444(1–2), 75–83.

Lewis, D., Allen, S., Notis, M. and Scotch, A. (2002). "Determination of the eutectic structure in the Ag-Cu-Sn system." *J. Electron. Mater.*, 31(2), 161–167.

Liu, C.-Y., Lai, C.-H., Wang, M.-C. and Hon, M.-H. (2006). "Thermal behaviour and microstructure of the intermetallic compounds formed at the Sn–3Ag–0.5Cu/Cu interface after soldering and isothermal aging." *J. Cryst. Growth*, 290(1), 103–110.

Liu, C.Y., Tu, K.N., Sheng, T.T., Tung, C.H., Frear, D.R. and Elenius, P. (2000). "Electron microscopy study of interfacial reaction between eutectic SnPb and Cu/Ni(V)/Al thin film metallization." *J. Appl. Phys.*, 87(2), 750–754.

Liu, Y., Sun, F., Zhang, H. and Zou, P. (2012). "Solderability, IMC evolution, and shear behaviour of low-Ag Sn0.7Ag0.5Cu-BiNi/Cu solder joint." *J. Mater. Sci. Mater. Electron.*, 23(9), 1705–1710.

Lu, H.Y., Balkan, H. and Ng, K.Y.S. (2006). "Effect of Ag content on the microstructure development of Sn-Ag-Cu interconnects." *J. Mater. Sci. Mater. Electron.*, 17(3), 171–178.

Lu, W., Shi, Y. and Lei, Y. (2010). "Effect of Ag Content on Solidification Cracking Susceptibility of Sn-Ag-Cu Solder Joints." *J. Electron. Mater.*, 39(8), 1298–1302.

Ma, H. and Suhling, J.C. (2009). "A review of mechanical properties of lead-free solders for electronic packaging." *J. Mater. Sci.*, 44(5), 1141–1158.

Ma, X., Wang, F., Qian, Y. and Yoshida, F. (2003). "Development of Cu–Sn intermetallic compound at Pb-free solder/Cu joint interface." *Mater. Lett.*, 57(22–23), 3361–3365.

M. Reid, J. Punch, M. Collins and C. Ryan (2008). "Effect of Ag content on the microstructure of Sn-Ag-Cu based solder alloys." *Solder. Surf. Mt. Technol.*, 20(4), 3–8.

Manko, H. H. (1964). "Solder and Soldering", 3rd ed., McGraw-Hill, Inc., New York, 1-153.

Matsumoto, T. and Nogi, K. (2008). "Wetting in Soldering and Microelectronics." *Annu. Rev. Mater. Res.*, 38(1), 251–273.

McCormack, M. and Jin, S. (1994). "New, lead-free solders." *J. Electron. Mater.*, 23(7), 635–640.

Mei, Z., Ahmad, M., Hu, M. and Ramakrishna, G. (2005). Kirkendall voids at Cu/solder interface and their effects on solder joint reliability. *Proc. Int. Conf. Electronic Components and Technology*, ECTC, FL, USA., 415–420.

Minna Arra, Dongkai Shangguan, Eero Ristolainen and Toivo Lepistö (2002). "Effect of reflow profile on wetting and intermetallic formation between Sn/Ag/Cu solder components and printed circuit boards." *Solder. Surf. Mt. Technol.*, 14(2), 18–25.

Moon, K.-W., Boettinger, W.J., Kattner, U.R., Biancaniello, F.S. and Handwerker, C.A. (2000). "Experimental and thermodynamic assessment of Sn-Ag-Cu solder alloys." *J. Electron. Mater.*, 29(10), 1122–1136.

Nai, S.M.L., Wei, J. and Gupta, M. (2006). "Lead-free solder reinforced with multiwalled carbon nanotubes." *J. Electron. Mater.*, 35(7), 1518–1522.

Nai, S.M.L., Wei, J. and Gupta, M. (2008). "Effect of Carbon Nanotubes on the Shear Strength and Electrical Resistivity of a Lead-Free Solder." *J. Electron. Mater.*, 37(4), 515–522.

Nai, S.M.L., Wei, J. and Gupta, M. (2009). "Interfacial intermetallic growth and shear strength of lead-free composite solder joints." *J. Alloys Compd.*, 473(1–2), 100–106.

Osenbach, J.W., DeLucca, J.M., Potteiger, B.D., Amin, A. and Baiocchi, F.A. (2006). "Sn-whiskers: truths and myths." *J. Mater. Sci. Mater. Electron.*, 18(1–3), 283–305.

Pan, J., Wang, J. and Shaddock, D. (2004). "Lead-free Solder Joint Reliability – State of the Art and Perspectives." *Proc. 37th Int. Symp. Microelectron.* Long Beach CA., 72-83.

Pang, J.H.L., Xiong, B.S., Neo, C.C., Mang, X.R. and Low, T.H. (2003). "Bulk solder and solder joint properties for lead free 95.5Sn-3.8Ag-0.7Cu solder alloy." *Proc. 53rd Int. Conf. on Electronic Components and Technology,* ECTC, New Orleans, Louisiana., 673–679.

Pang, J.H.L., Xu, L., Shi, X.Q., Zhou, W. and Ngoh, S.L. (2004). "Intermetallic growth studies on Sn-Ag-Cu lead-free solder joints." *J. Electron. Mater.*, 33(10), 1219–1226.

Park, M.S., Stephenson, M.K., Shannon, C., Cáceres Díaz, L.A., Hudspeth, K.A., Gibbons, S.L., Muñoz-Saldaña, J. and Arróyave, R. (2012). "Experimental and computational study of the morphological evolution of intermetallic compound (Cu_6Sn_5) layers at the Cu/Sn interface under isothermal soldering conditions." *Acta Mater.*, 60(13–14), 5125–5134.

Park, Y.W., Narayanan, T.S.N.S. and Lee, K.Y. (2007). "Effect of temperature on the fretting corrosion of tin plated copper alloy contacts." *Wear,* 262 (3–4), 320–330.

Rao, B.S.S.C., Kumar, K.M., Kripesh, V. and Zeng, K.Y. (2011). "Tensile deformation behaviour of nano-sized Mo particles reinforced SnAgCu solders." *Mater. Sci. Eng. A*, 528(12), 4166–4172.

Satyanarayan and Prabhu, K.N. (2011). "Reactive wetting, evolution of interfacial and bulk IMCs and their effect on mechanical properties of eutectic Sn–Cu solder alloy." *Adv. Colloid Interface Sci.*, 166(1–2), 87–118.

Satyanarayan and Prabhu, K.N. (2013). "Solder joint reliability of Sn–0·7Cu and Sn–0·3Ag–0·7Cu lead-free solder alloys solidified on copper substrates with different surface roughnesses." *Mater. Sci. Technol.*, 29(12), 1430–1440.

Schaefer, M., Fournelle, R.A. and Liang, J. "Theory for intermetallic phase growth between cu and liquid Sn-Pb solder based on grain boundary diffusion control." *J. Electron. Mater.*, 27(11), 1167–1176.

Sharma, A., Das, S. and Das, K. (2016). "Pulse Electrodeposition of Lead-Free Tin-Based Composites for Microelectronic Packaging." In Electrodeposition of Composite Materials, A.M.A. Mohamed, and T.D. Golden, eds. Intech., 253-272.

Shnawah, D.A., Sabri, M.F.M. and Badruddin, I.A. (2012a). "A review on thermal cycling and drop impact reliability of SAC solder joint in portable electronic products." *Microelectron. Reliab.*, 52(1), 90–99.

Shnawah, D.A., Said, S.B.M., Sabri, M.F.M., Badruddin, I.A. and Che, F.X. (2012b). "High-Reliability Low-Ag-Content Sn-Ag-Cu Solder Joints for Electronics Applications." *J. Electron. Mater.*, 41(9), 2631–2658.

Silva, B.L., Cheung, N., Garcia, A. and Spinelli, J.E. (2015). "Evaluation of solder/substrate thermal conductance and wetting angle of Sn–0.7wt%Cu (0–0.1 wt%Ni) solder alloys." *Mater. Lett.*, 142, 163–167.

Sona, M. and Prabhu, K.N. (2013). "Review on microstructure evolution in Sn–Ag–Cu solders and its effect on mechanical integrity of solder joints." *J. Mater. Sci. Mater. Electron.*, 24(9), 3149–3169.

Sona, M. and Prabhu, K.N. (2015). "Assessment of Joint Reliability of Sn–2.5Ag–0.5Cu Solder/Cu as a Function of Reflow Time." *Trans. Indian Inst. Met.*, 69(4), 941–947.

Song, F., Lee, S.W.R., Newman, K., Sykes, B. and Clark, S. (2007). "High-Speed Solder Ball Shear and Pull Tests vs. Board Level Mechanical Drop Tests: Correlation of Failure Mode and Loading Speed." *Proc. 57th Int. Conf. on Electronic Components and Technology*, ECTC, Sparks, Nevada., 1504–1513.

Sundelin, J.J., Nurmi, S.T., Lepistö, T.K. and Ristolainen, E.O. (2006). "Mechanical and microstructural properties of SnAgCu solder joints." *Mater. Sci. Eng. A*, 420(1–2), 55–62.

Tang, W., He, A., Liu, Q. and Ivey, D.G. (2010). "Solid state interfacial reactions in electrodeposited Cu/Sn couples." *Trans. Nonferrous Met. Soc. China*, 20(1), 90–96.

Tsao, L.C. (2011). "Suppressing effect of 0.5 wt.% nano-TiO2 addition into Sn–3.5Ag–0.5Cu solder alloy on the intermetallic growth with Cu substrate during isothermal aging." *J. Alloys Compd.*, 509(33), 8441–8448.

Tu, K.N., Gusak, A.M. and Li, M. (2003). "Physics and materials challenges for lead-free solders." *J. Appl. Phys.*, 93(3), 1335–1353.

Turbini, L.J., Munie, G.C., Bernier, D., Gamalski, J. and Bergman, D.W. (2001). "Examining the environmental impact of lead-free soldering alternatives." *IEEE Trans. Electron. Packag. Manuf.*, 24(1), 4–9.

Vianco, P.T. (2000). "Lead (pb)-Free Solder Applications (Sandia National Labs., Albuquerque, NM (US); Sandia National Labs., Livermore, CA (US)

Vianco, P.T., Rejent, J.A. and Hlava, P.F. (2004). "Solid-state intermetallic compound layer growth between copper and 95.5Sn-3.9Ag-0.6Cu solder." *J. Electron. Mater.*, 33(9), 991–1004.

Wang, I.-T., Duh, J.-G., Cheng, C.-Y. and Wang, J. (2012). "Interfacial reaction and elemental redistribution in Sn3.0Ag0.5Cu–xPd/immersion Au/electroless Ni solder joints after aging." *Mater. Sci. Eng. B*, 177(2), 278–282.

Watanabe, H., Hidaka, N., Shohji, I. and Ito, M. (2006) "Effect of Ni and Ag on Interfacial Reaction and Microstructure of Sn-Ag-Cu-Ni-Ge Lead-Free Solder." MS & T.,135-146

Wenzel, R.N. (1936). “Resistance of solid surfaces to wetting by water.” *Ind. Eng. Chem.*, 28(8), 988-994.

Wong, C.K., Pang, J.H.L., Tew, J.W., Lok, B.K., Lu, H.J., Ng, F.L. and Sun, Y.F. (2008). "The influence of solder volume and pad area on Sn–3.8Ag–0.7Cu and Ni UBM reaction in reflow soldering and isothermal aging." *Microelectron. Reliab.*, *48*(4), 611–621.

Wu, C.M.L., Yu, D.Q., Law, C.M.T. and Wang, L. (2004). "Properties of lead-free solder alloys with rare earth element additions." *Mater. Sci. Eng. R Rep.*, 44(1), 1–44.

Xie, H., Chawla, N. and Mirpuri, K. (2012). "Thermal and Mechanical Stability of Ce-Containing Sn-3.9Ag-0.7Cu Lead-Free Solder on Cu and Electroless Ni-P Metallizations." *J. Electron. Mater.*, 41(12), 3249–3258.

Xu, L. and Pang, J.H.L. (2006). "Effect of intermetallic and Kirkendall voids growth on board level drop reliability for SnAgCu lead-free BGA solder joint." *Proc. 56th Int. Conf. on Electronic Components and Technology*, ECTC, San Diego, USA. 8-12.

Xu, L., Pang, J.H.L. and Che, F.X. (2005). "Intermetallic Growth and Failure Study for Sn-Ag-Cu/ENIG PBGA Solder Joints Subject to Thermal Cycling." *Proc. Int. Conf. on Electronic Components and Technology*, ECTC, FL, USA., 682–686.

Yang, S.C. and Kao, C.R. (2007). Massive Spalling of Intermetallics in Solder Joints: a General Phenomenon that Can Occur in Multiple Solder-Substrate Systems. *Proc. 57th Int. Conf. on Electronic Components and Technology*, ECTC, Las Vegas, USA., 1825–1830.

Yin, L., Wentlent, L., Yang, L., Arfaei, B., Oasaimeh, A. and Borgesen, P. (2011). "Recrystallization and Precipitate Coarsening in Pb-Free Solder Joints During Thermomechanical Fatigue." *J. Electron. Mater.*, 41(2), 241–252.

Yoon, J.W. and Jung, S.-B. (2004). "Effect of isothermal aging on intermetallic compound layer growth at the interface between Sn-3.5Ag-0.75Cu solder and Cu substrate." *J. Mater. Sci.*, 39(13), 4211–4217.

Yoon, J.W. and Jung, S.-B. (2009). "Interfacial reaction and mechanical reliability of eutectic Sn–0·7Cu/immersion Ag-plated Cu solder joint." *Mater. Sci. Technol.*, 25(12), 1478–1484.

You, T., Kim, Y., Jung, W., Moon, J. and Choe, H. (2009). "Effect of surface finish on the fracture behaviour of Sn–Ag–Cu solder joints during high-strain rate loading." *J. Alloys Compd.*, 486(1–2), 242–245.

Yu, D.Q. and Wang, L. (2008). "The growth and roughness evolution of intermetallic compounds of Sn–Ag–Cu/Cu interface during soldering reaction." *J. Alloys Compd.*, 458(1–2), 542–547.

Yuan, Y. and Lee, T.R. (2013). "Contact Angle and Wetting Properties." In Surface Science Techniques, G. Bracco, and B. Holst, eds. (Springer Berlin Heidelberg), 3–34.

Zeng, G., Xue, S., Zhang, L., Gao, L., Dai, W. and Luo, J. (2010). "A review on the interfacial intermetallic compounds between Sn–Ag–Cu based solders and substrates." *J. Mater. Sci. Mater. Electron.*, 21(5), 421–440.

Zeng, K. and Tu, K.N. (2002). "Six cases of reliability study of Pb-free solder joints in electronic packaging technology." *Mater. Sci. Eng. R Rep.*, 38(2), 55–105.

Zhang, F., Li, M., Balakrisnan, B. and Chen, W.T. (2002). "Failure mechanism of lead-free solder joints in flip chip packages." *J. Electron. Mater.*, 31(11), 1256–1263.

Zribi, A., Clark, A., Zavalij, L., Borgesen, P. and Cotts, E.J. (2001). "The growth of intermetallic compounds at Sn-Ag-Cu solder/Cu and Sn-Ag-Cu solder/Ni interfaces and the associated evolution of the solder microstructure." *J. Electron. Mater.*, 30(9), 1157–1164.

LIST OF PUBLICATIONS (Based on Ph.D research work)

Peer Reviewed Journals

1. Sona, M. and Prabhu, K.N. (2013). "Review on microstructure evolution in Sn–Ag–Cu solders and its effect on mechanical integrity of solder joints." *J. Mater. Sci. Mater. Electron.*, 24(9), 3149–3169.
2. Sona, M. and Prabhu, K.N. (2014). "The effect of reflow time on reactive wetting, evolution of interfacial IMCs and shear strength of eutectic Sn–Cu solder alloy." *J. Mater. Sci. Mater. Electron.*, 25(3), 1446–1455.
3. Sona, M. and Prabhu, K.N. (2015). "Spreading Behaviour and Joint Reliability of Sn–0.3Ag–0.7Cu Lead-Free Solder Alloy on Nickel Coated Copper Substrate as a Function of Reflow Time." *Trans. Indian Inst. Met.*, 68(6), 1027–1031.
4. Sona, M. and Prabhu, K.N. (2015). "The effect of reflow time on wetting behaviour, interfacial reaction and shear strength of Sn–0.3Ag-0.7Cu solder/Cu joint." Journal of Surface Mount Technology, 28(2), 36-42.
5. Sona, M. and Narayan Prabhu, K. (2015). "Wetting Kinetics and Joint Strength of Sn-0.3Ag-0.7Cu Lead-Free Solder Alloy on Copper Substrate as a Function of Reflow Time." *Mater. Sci. Forum*, 830–831, 286–289.
6. Sona, M. and Prabhu, K.N. (2015). "Assessment of Joint Reliability of Sn–2.5Ag–0.5Cu Solder/Cu as a Function of Reflow Time." *Trans. Indian Inst. Met.*, 69(4), 941–947.
7. Sona, M. and Prabhu, K.N. (2016). "Effect of Reflow Time on Wetting Behaviour, Microstructure Evolution, and Joint Strength of Sn-2.5Ag-0.5Cu Solder on Bare and Nickel-Coated Copper Substrates." *J. Electron. Mater.*, 45(7), 3744–3758.

Conference Proceedings

1. Sona, M. and Prabhu, K.N. (2015). “Wettability and bond strength of Sn0.7Cu lead-free solder alloy reflowed on copper substrate” *Proc. of Int. Engineering Symposium*, (IES-2015), Kumamoto University, Japan, March 4-5, 2015

BIO DATA

Name : Mrunali Sona
Date of birth : 20-05-1986
Permanent Address : Sonangeri Nadumane, Sullia (D.K.)
Karnataka-574239
Email : mrunalisona@gmail.com

Academic qualification

BSc (Physics, Chemistry, Maths) : St. Philomena College Puttur
M.Sc (Materials Science) : Mangalore University
M.Tech (Materials Engineering) : National Institute of Technology Karnataka
Surathkal, Mangalore
Work Experience : Eighteen months of teaching experience